SECTION III: RESULTS & DISCUSSIONS

9. ALGINATE BEADS

9.1. Alginate-Amylase Beads

9.1.1. EFFECT OF THE FACTORS ON RESPONSES

9.1.1.1. % Entrapment

Contour plots of response surface for % entrapment are shown in Figure 9.1A from which it can be concluded that more than 85% entrapment value was obtained at the high level of the sodium alginate concentration especially when it was followed by the low levels of the other two factors. Whilst, the calcium chloride concentration and hardening time were affecting negatively (negative coefficient; Table 9.2; i.e. response decreases with increase in factor level) in significant amount.

On addition of sodium alginate solution to a calcium chloride solution, instantaneous interfacial crosslinking takes place with precipitation of calcium alginate followed by a more gradual gelation of the interior which causes loss of enzyme from the surface of the beads. This can be noticed from the pores on the bead surface (Figure 9.2) created due to the water-soluble macromolecules both because it affected the calcium alginate network formation during the unit preparation and because it was leached from the membrane into the medium. (Iannuccelli et al., 1998) Loss of surface enzyme was found to be proportional to the degree of crosslinking. Increase in viscosity with increase in sodium alginate concentration retarded penetration of calcium to the interior of the bead, resulted in decreased crosslinking (also decreased surface roughness and porosity; Figure 9.2A-C) and increased entrapment efficiency. Degree of crosslinking increases with increase in

calcium concentration and contact time, (Wang and He, 2002) hence entrapment efficiency decreased. Calcium chloride concentration was the most influencing (Table 9.2) factor, while no interaction terms were significant.

Table 9.1: Distribution of Doehlert shell design experiments in the space of three process variables and results for the measured responses.

Factors/ levels				Responses					
ES[a]	Na. alginate (% w/v)	Calcium chloride (M)	Hardening time (min)	% Entrapment	T_{50}	T_{90}	Particle size (μm)	Angle of repose	Overall desirability[b]
11	0	0	0	83.43	15.65	80.43	264.505	20.57	0.502
9	1	0	0	84.22	18.39	96.95	673.059	17.52	0.252
8	0.5	0.866	0	74.40	18.60	95.54	422.886	19.66	0.111
2	-0.5	0.866	0	71.00	14.30	65.28	167.623	23.35	0.000
16	-1	0	0	78.28	9.01	37.13	182.603	24.11	0.648
7	-0.5	-0.866	0	87.01	11.55	50.14	205.206	21.32	0.833
14	0.5	-0.866	0	88.34	16.83	80.00	457.498	18.02	0.485
10	0.5	0.289	0.816	78.63	19.24	94.11	413.634	19.65	0.000
3	-0.5	0.289	0.816	76.70	14.09	68.40	173.296	23.30	0.407
13	0	-0.577	0.816	84.54	16.60	75.74	274.498	20.25	0.449
5	0.5	-0.289	-0.816	88.19	15.81	86.01	434.691	18.71	0.576
4	**-0.5**	**-0.289**	**-0.816**	**86.09**	**10.78**	**51.86**	**185.973**	**21.75**	**0.848**
15	0	0.577	-0.816	78.38	15.69	78.58	261.218	20.69	0.384
12	0	0	0	82.73	15.67	77.53	258.405	20.49	0.486
6	0	0	0	83.01	15.39	78.03	264.705	20.43	0.511
1	0	0	0	82.23	15.72	80.53	258.205	20.75	0.472

[a] ES, experimental sequence.
[b] Overall desirability was calculated using the individual desirability of % entrapment and T_{50}

9.1.1.2. T_{50}

As shown in Figure 9.1B and Table 9.2, all three factors had significant positive (i.e. response increases with increase in factor level) effect on response value. However, immediate release of enzyme for quicker on set of action and hence shorter T_{50} was the desirable criteria for the optimum formulation, hence low value of all three variables

resulted the beads with T_{50} as low as 10.78 min (experiment 4, Table 9.1). T_{50} was found to be proportional to the particle size and degree of crosslinking. As the concentration and hence the viscosity of alginate solutions incereases, larger beads (discussed under 'Particle size') with less surface porosity (Figure 9.2A-C) were obtained which took long time for complete dissolution and resulted in higher T_{50}. Higher calcium concentration and hardening time caused penetration of calcium to the interior of the bead, resulted in increased crosslinking, (Wang and He, 2002) increased surface roughness and porosity (Figure 9.2D-F), delayed dissolution and hence higher T_{50}.

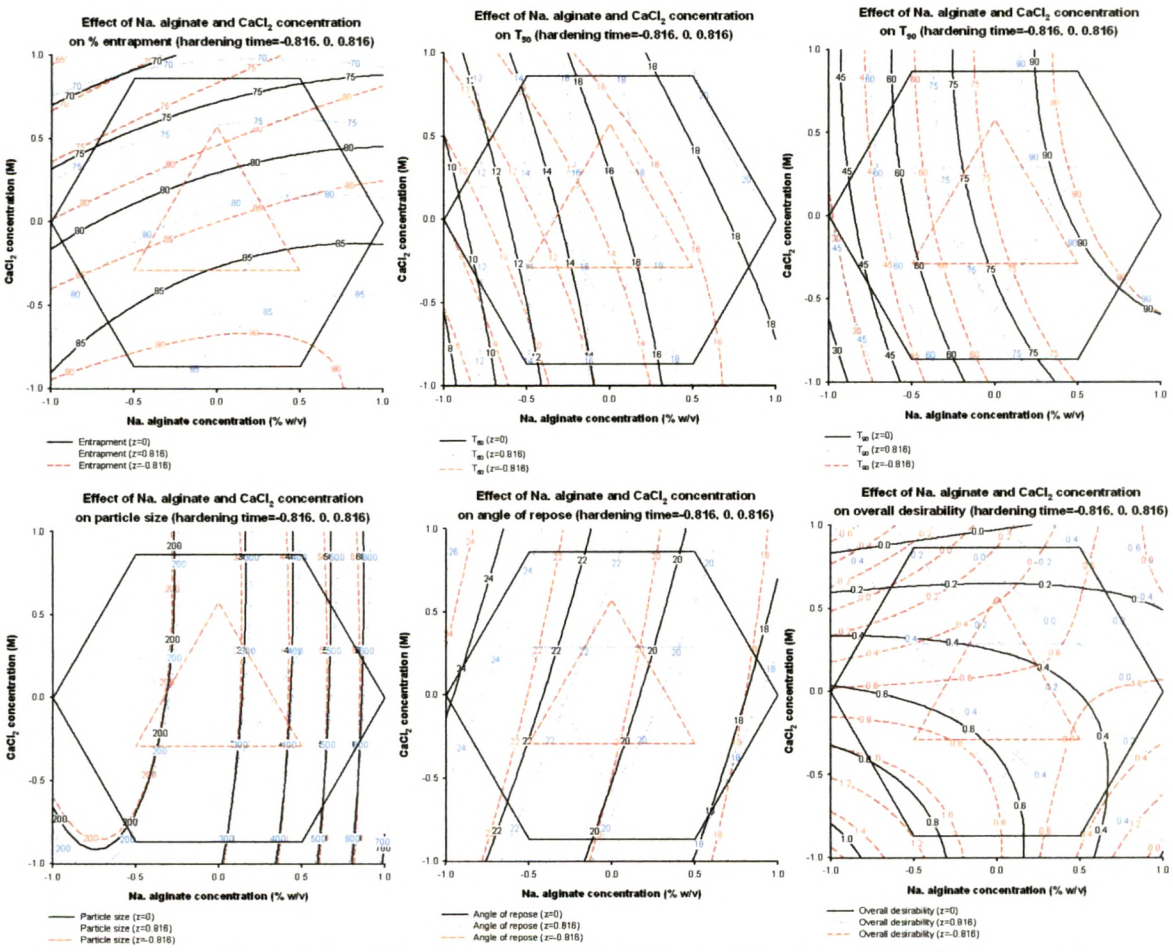

Figure 9.1: Contour plots of % entrapment, T50, T90, particle size, angle of repose, and overall desirability as a function of sodium alginate concentration and calcium chloride concentration at different hardening time (20.9, 25, 29.1 min i.e. at z=-0.816, 0, 0.816).

Table 9.2: ANOVA results (P values): effect of the variables on % entrapment, T50, T90, particle size and angle of repose.

Factors	% Entrapment		T_{50}		T_{90}		Particle size		Angle of repose	
	Coefficient	*P*	Coefficient	*P*	Coefficient	*P*	Coefficient	*P*	Coefficient	*P*
Intercept	82.85	-	15.61	-	79.13	-	261.46	-	20.56	-
A	2.77	0.0002*	4.72	<0.0001*	29.96	<0.0001*	248.08	<0.0001*	-3.36	<0.0001*
B	-8.74	<0.0001*	1.33	<0.0001*	8.83	<0.0001*	-19.98	0.0003*	1.04	<0.0001*
C	-2.61	0.0001*	1.56	<0.0001*	4.45	0.0008*	-4.17	0.1175	0.42	0.0016*
A^2	-1.60	0.0112*	-1.91	<0.0001*	-12.09	0.0001*	166.38	<0.0001*	0.26	0.0800
B^2	-3.02	0.0007*	0.25	0.0723	-4.49	0.0081*	13.67	0.0159*	-0.05	0.6951
C^2	0.01	0.9749	0.06	0.6201	-0.87	0.4211	-1.37	0.7191	0.20	0.1346
AB	1.20	0.0798	-0.57	0.0124*	0.23	0.8762	1.72	0.7500	-0.23	0.2065
AC	-0.53	0.4255	0.27	0.1587	-5.25	0.0207*	-5.74	0.3599	-0.29	0.1515
BC	0.84	0.2282	-0.88	0.0031*	-0.23	0.8910	-5.87	0.3500	0.43	0.0544
ABC	-3.19	0.2254	1.55	0.0562	-0.13	0.9838	-15.05	0.5170	0.07	0.9186
$r^2_{adj.}$	0.9912	-	0.9979	-	0.9947	-	0.9990	-	0.9947	-

Regression coefficients are in coded values.
* Statistically significant (P <0.05)

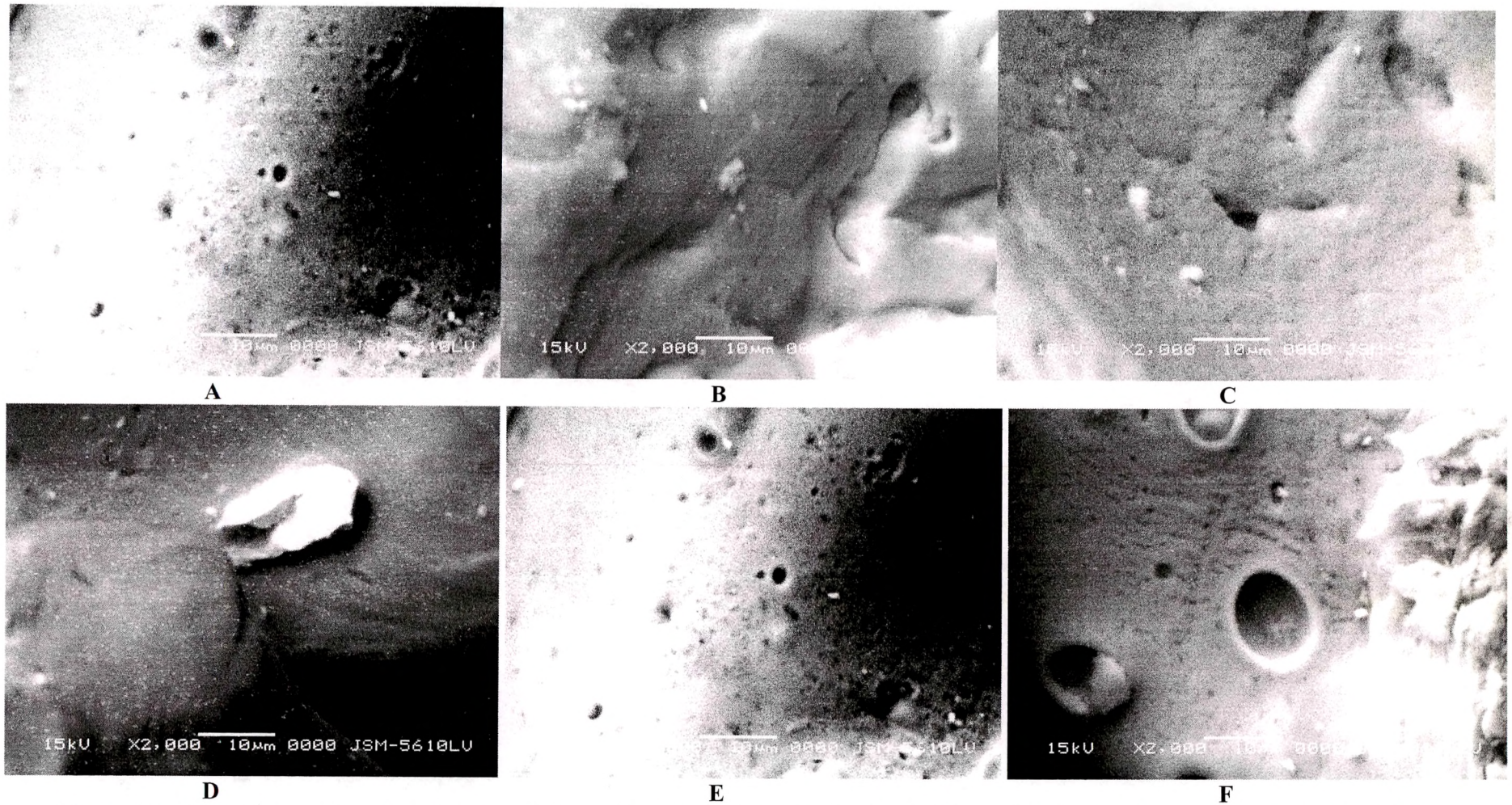

Figure 9.2: SEM micrographs and surface morphology of calcium alginate beads: (A–C) Effect of sodium alginate concentration on surface morphology (calcium chloride concentration 0.15 M) (A) 1.0% w/v, (B) 1.5% w/v and (C) 2.0% w/v sodium alginate concentration. (D– F) Effect of calcium chloride concentration on surface morphology (sodium alginate concentration 1.5 % w/v) (D) 0.10 M, (E) 0.15 M and (F) 0.20 M calcium chloride concentration.

9.1.1.3. T_{90}

Same as the T_{50}, all three factors had positive effect on this response which can be observed in Figure 9.1C. Similar to T_{50}, complete release of enzyme for complete and quick action and hence shorter T_{90} was the desired criteria. T_{90} was also found to be proportional to the particle size and degree of crosslinking. For further explanation, see '*T_{50}*' above.

9.1.1.4. Particle Size

As shown in Figure 9.1D and Table 9.2, the sodium alginate concentration was the factor affecting the most. The bead size is influenced by the opening through which the alginate solution is allowed to pass (which was kept constant) and the viscosity of the alginate solution. Increased viscosity at higher concentration of sodium alginate resulted in larger particles. Calcium chloride concentration and hardening time had the negative effect on the particle size. High calcium chloride concentration and hardening time caused shrinkage of beads and resulted in smaller particle size due to high degree of crosslinking. (Wang and He, 2002) Though the negative effect of calcium chloride concentration and hardening time was of less magnitude, they contribute to the morphology of the beads and surface became rougher and porous (Figure 9.2D-F).

9.1.1.5. Angle of Repose

Here the sodium alginate concentration had significant negative effect on angle of repose. However, calcium chloride concentration and hardening time had synergistic positive

effect at higher levels, their individual effect were negligible. Particle size increased with increase in sodium alginate concentration and resulted in decreased angle (lowest angle of 17.52; experiment 9; Table 9.1). Higher calcium chloride concentration and hardening time resulted in smaller beads with irregular surface due to shrinkage and showed increased angle.

9.1.2. INTERACTIONS BETWEEN THE FACTORS

An interaction is the failure of a factor to produce the same effect on the response at the different levels of the other factor. (Montgomery, 2001) The ANOVA results (Table 9.2) showed that the interaction AB and BC had significant influence on T_{50} while interaction AC had significant influence on T_{90}.

The analysis of the results shown in Table 9.1 by multiple regression leads to equations that adequately describe the influence of the selected factors on % entrapment, T_{50}, T_{90}, particle size and angle of repose. In Table 9.2 regression coefficients of these equations are presented.

9.1.3. OPTIMIZATION OF THE PROCESS USING THE DESIRABILITY FUNCTION

Generally the aim of the optimization of pharmaceutical formulations is to find the optimum levels of the variables, which affect a process, where a product of good characteristics could be produced. Using the desirability function, all the selected responses were combined in one overall response, the overall desirability. As it has been already discussed, the overall desirability response was calculated from the individual

desirability of each of the responses using the Eqs. (10)–(11). The equation found out using multiple regression was as follow (coded factors):

Eq. 9.1

$$D = 0.49 - 0.17A - 0.34B - 0.19C - 0.04A^2 - 0.17B^2 - 0.02C^2 + 0.27AB - 0.18AC + 0.01BC - 0.71ABC \; (r^2_{adj.} = 0.9828, P < 0.0001)$$

In Figure 9.1F the contour plots that describe the influence of the independent factors on the overall desirability is presented. The study of these plots showed that the highest values of the desirability could be obtained at low values of all three process variables (experiment 4). Especially the analysis of the Eq. 9.1 resulted to the optimum combination of the independent variables where a product of desired characteristics may occur and results of this analysis are shown in Table 9.3.

Table 9.3: Optimum levels of the independent process variables.

Independent variables	Optimum values
Sodium alginate concentration	1.3% w/v
Calcium chloride concentration	0.0856 M
Hardening time	20.9 min
Overall desirability	0.848

9.1.4. EVALUATION OF MODEL USING CROSS-VALIDATION

In order to assess the reliability of the model, five experiments were conducted by varying the process variables at values other than that of the model. For each of these test experiments the responses were estimated by using the equations and experimental procedure. In Table 9.4 the comparison between the experimental and predicted values of the response for these additional experiments is presented. Bios was calculated by the following equation:

Eq. 9.2

$$\text{Bias} = \left[\frac{(\text{predicted value} - \text{edperimental value})}{\text{predicted value}} \right] \times 100$$

It can be seen that in all cases there was a reasonable agreement between the predicted and the experimental value, since low value of the bias were found. For this reason it can be concluded that the equations describe adequately the influence of the selected process variables on the responses under study.

Table 9.4: Comparison of responses between predicted and experimental values for the cross-validation set.

Responses	Test	Factors/levels			Experimental values	Predicted values	Bias%
		A	B	C			
% Entrapment	1	-0.3	0.2	0.4	79.10	76.17	3.7
	2	0.3	-0.2	-0.4	86.19	88.09	-2.2
	3	0.3	0.2	0.4	80.62	83.04	-3.0
	4	-0.3	-0.2	-0.4	84.70	82.02	3.2
	5	0	-0.4	0.4	84.69	87.74	-3.6
T_{50}	1	-0.3	0.2	0.4	14.82	14.26	3.8
	2	0.3	-0.2	-0.4	15.95	16.28	-2.1
	3	0.3	0.2	0.4	17.73	18.11	-2.1
	4	-0.3	-0.2	-0.4	13.04	12.54	3.8
	5	0	-0.4	0.4	15.89	16.54	-4.1
T_{90}	1	-0.3	0.2	0.4	72.88	71.94	1.3
	2	0.3	-0.2	-0.4	83.76	85.54	-2.1
	3	0.3	0.2	0.4	89.62	92.57	-3.3
	4	-0.3	-0.2	-0.4	64.56	63.47	1.7
	5	0	-0.4	0.4	76.56	75.61	1.2
Particle size	1	-0.3	0.2	0.4	197.15	183.74	6.8
	2	0.3	-0.2	-0.4	356.60	341.27	4.3
	3	0.3	0.2	0.4	344.10	364.06	-5.8
	4	-0.3	-0.2	-0.4	207.30	222.02	-7.1
	5	0	-0.4	0.4	270.69	289.36	-6.9
Angle of repose	1	-0.3	0.2	0.4	22.08	21.30	3.5
	2	0.3	-0.2	-0.4	19.31	19.87	-2.9
	3	0.3	0.2	0.4	19.97	20.84	-4.4
	4	-0.3	-0.2	-0.4	21.23	20.64	2.8
	5	0	-0.4	0.4	20.27	20.98	-3.5
Overall desirability	1	-0.3	0.2	0.4	0.41	0.38	6.4
	2	0.3	-0.2	-0.4	0.56	0.53	5.3
	3	0.3	0.2	0.4	0.26	0.28	-6.9
	4	-0.3	-0.2	-0.4	0.69	0.65	6.5
	5	0	-0.4	0.4	0.52	0.50	3.0

9.1.5. CURVE FITTING AND RELEASE MECHANISM

Values of release exponent (n) and kinetic constant (K) were derived using zero-order kinetics, first-order kinetics, Higuchi's square root of time equation, Korsmeyer-Peppas' power law equation and Hixson-Crowell's cube root of time equation for α-amylase release and presented in Table 9.5. The enzyme release data show a good fit to the first-order release kinetics (Eq. 6.5) which can further be confirmed by comparing the values of correlation coefficient (r) with that of the other models.

Table 9.5: Comparison of different dissolution kinetics models.

ES[a]	Release model										
	Zero-order		First-Order		Higuchi matrix		Korsmeyer-Peppas			Hixson-Crowell	
	K_o	r_0	K_1	r_1	K_H	r_H	n	K_k	r_k	K_s	r_s
11	1.15	0.53	-0.03	0.95	10.63	0.92	0.73	4.49	0.85	-0.01	0.88
9	1.06	0.70	-0.03	0.96	9.90	0.93	0.90	2.09	0.87	-0.01	0.91
8	1.07	0.69	-0.03	0.96	9.96	0.93	0.91	2.02	0.86	-0.01	0.91
2	1.19	0.43	-0.03	0.95	10.97	0.91	0.66	6.09	0.86	-0.01	0.84
16	1.28	*	-0.04	0.88	12.16	0.78	0.46	15.26	0.78	-0.01	0.61
7	1.24	*	-0.04	0.86	11.63	0.85	0.48	13.39	0.86	-0.01	0.67
14	1.15	0.60	-0.03	0.96	10.56	0.92	0.75	4.17	0.88	-0.01	0.89
10	1.08	0.73	-0.03	0.96	9.93	0.93	0.96	1.66	0.87	-0.01	0.93
3	1.20	0.37	-0.04	0.94	11.08	0.91	0.59	8.30	0.87	-0.01	0.90
13	1.17	0.59	-0.03	0.96	10.70	0.92	0.79	3.53	0.86	-0.01	0.88
5	1.13	0.52	-0.03	0.92	10.53	0.91	0.66	5.89	0.88	-0.01	0.84
4	1.24	*	-0.04	0.85	11.69	0.83	0.43	16.39	0.86	-0.01	0.64
15	1.16	0.55	-0.03	0.95	10.66	0.91	0.79	3.61	0.84	-0.01	0.86

[a] ES, experimental sequence.
* Not possible.

Finally, in order to know weather the enzyme release was due to erosion of diffusion, the release data of the optimized batch (experiment 4) was fitted into Kopcha model and parameters like A, B, and A/B at different time intervals are shown graphically in Figure 9.3. The Kopcha model (Eq. 6.9) monitored the diffusion to erosion ratio A/B. Initially A/B was <1 and expressed the predominance of erosion relative to diffusion inside the

matrices (Figure 9.3). However, diffusion term *A* increased in the course of time as diffusion appeared latter. The corresponding Kopcha profile showed that after 23.62 min drug release was subsequent to predominant matrix diffusion. This explains the biphasic nature (erosional first and diffusional latter) of the '*in vitro*' release profile of the optimized batch (Figure 9.4), plateau of which was attained when *A/B*=1. The diffusion term *A* increases with time because diffusion though the hydrated eroded particles or the layer in process of erosion is easier. (Ratsimbazafy et al., 1999)

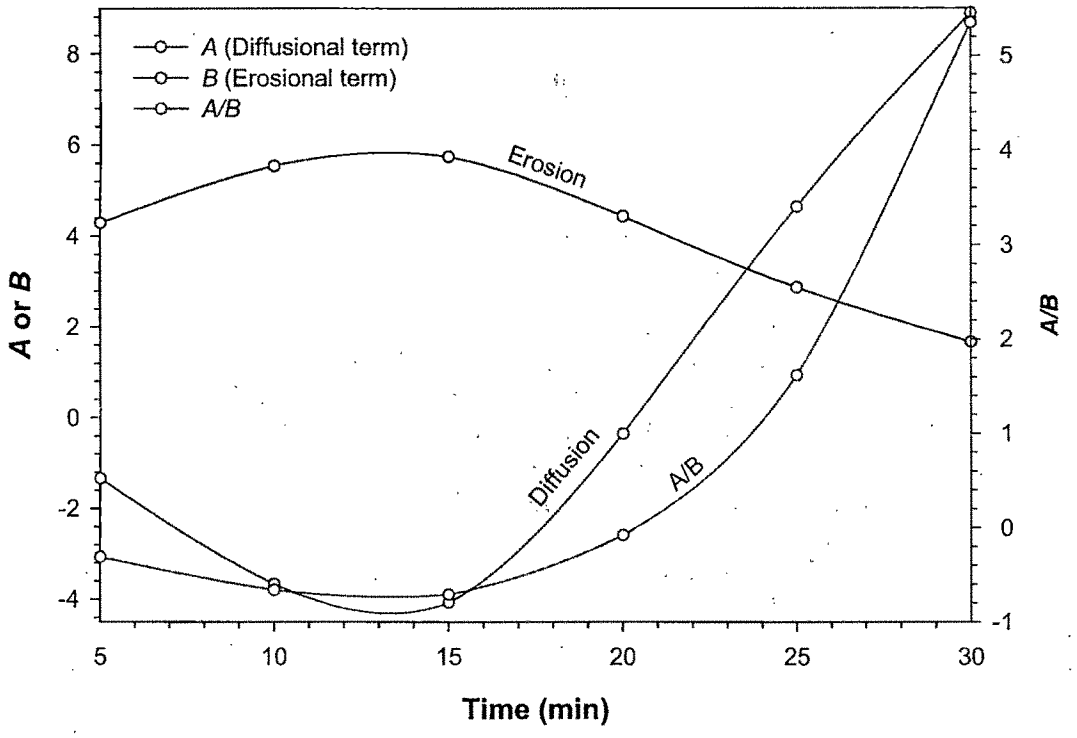

Figure 9.3: Kopcha model parameters (A, B and A/B) versus time profile for optimized batch (experiment 4).

9.1.6. CHARACTERIZATION OF OPTIMAL FORMULATION

9.1.6.1. Effect of pH on Release Profile

The effect of pH on the release of α-amylase from calcium alginate beads in different pH (1.2, 4.0, 5.4, 6.8, 7.4, and 8.0) buffers simulating the human gastrointestinal tract is given in Figure 9.4A. Release profile of optimized batch (experiment 4) in simulated intestinal fluid without enzyme is shown in Figure 9.4B. Generally, higher molecular weight and poorly water-soluble drugs are not released from calcium alginate beads due to stability and non swelling property in acidic environment while swell and disintegrate in intestinal fluid. (Yotsuyanagi et al., 1987; Kim and Lee, 1992) This was further confirmed by very low amount of α-amylase release in the acidic media (pH 1.2, 4.0, and 5.4) due to higher molecular weight. The swelling and disintegration of calcium alginate beads are dependent on compositions of dissolution medium, e.g. sodium and phosphate, and solubility of drug entrapped into alginate beads. (Ostberg et al., 1994) The swelling and disintegration of alginate beads in intestinal fluid (pH 6.8) were due to the affinity of calcium to phosphate and sodium/calcium exchange. However, the complete release profile was delayed up to 6 hr as the pH increased (7.4 and 8.0) despite the presence of sodium and phosphate. This study confirms the site specific α-amylase delivery to the intestine rather than the stomach.

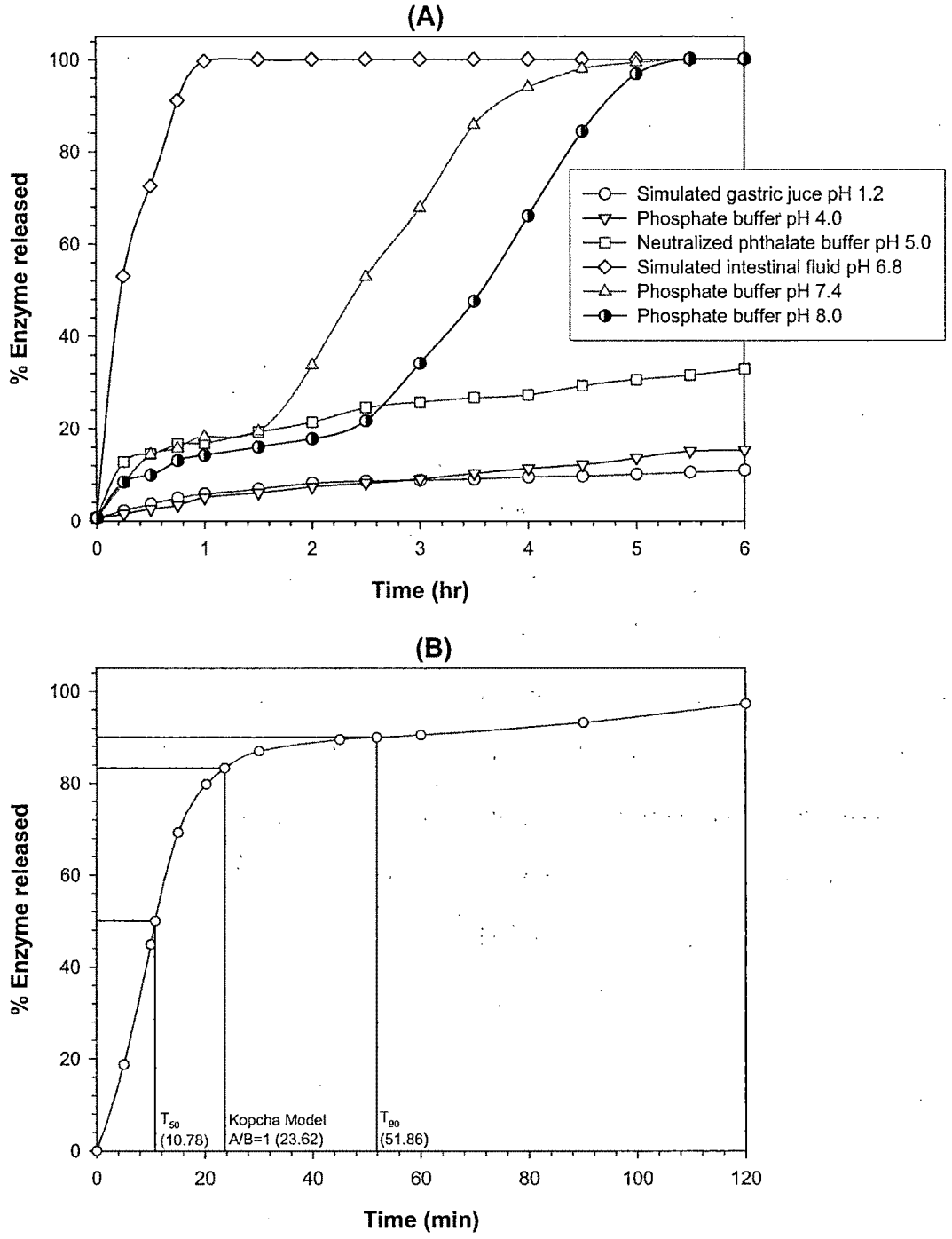

Figure 9.4: The effect of pH on the release profile of α-amylase in different buffers simulating the human gastrointestinal tract (B) *'In vitro'* release profile of optimized batch (experiment 4) in simulated intestinal fluid without enzyme.

9.1.6.2. Fourier Transform Infra-red Spectroscopy (FTIR)

FTIR spectra of α-amylase, sodium alginate, calcium alginate blank beads, enzyme loaded optimized batch, and physical mixture of α-amylase and blank beads are shown in Figure 9.5. FTIR spectrum of sodium alginate powder showed various distinct peaks of alginate: hydroxyl at 3263.33 cm^{-1}, carbonyl at 1600.81 cm^{-1}, and carboxyl and

Figure 9.5: The FTIR spectra of α-amylase, sodium alginate, blank calcium alginate beads, α-amylase-loaded alginate beads, and physical mixture of α-amylase and blank calcium alginate beads.

carboxylate at about 1000–1400 cm^{-1}. Crosslinking of alginate by Ca^{2+} was shown by a decrease in the wavenumber of carbonyl peak from 1600.81 to 1579.32 cm^{-1}. The hydroxyl peak of calcium alginate had a higher value of wavenumber than that of the sodium alginate (Figure 9.5). This was probably due to a negative effect on bond formation involving adjacent hydroxyl groups as a result of conformational changes of alginate after reacting with Ca^{2+}. (Wong et al., 2002) With incorporation of α-amylase, the spectrum of beads was similar to that of the calcium alginate blank beads. However, the physical mixture of α-amylase and calcium alginate blank beads showed the peaks due to both α-amylase and calcium alginate. This confirms the amylase entrapment into the alginate beads at molecular level.

9.1.6.3. Differential Scanning Calorimetry (DSC)

The DSC thermograms of α-amylase, sodium alginate, blank calcium alginate beads and α-amylase-loaded beads are shown in Figure 9.6. The degradation exotherm of sodium alginate at 251.2°C was absent in blank calcium alginate bead and an additional endothermic peak at 221°C corresponding to alginate-calcium interaction was observed. Similar results were reported by Fernandez-Hervas et al. (Fernandez-Hervas et al., 1998) The α-amylase exhibits endothermic peaks at 148.5, 215.5, and 226.8°C while the melting peak shape of α-amylase-loaded alginate beads was similar to the blank beads and did not show any peak at 148.5, 215.5, or 226.8°C. This confirms that the most of the enzyme was uniformly dispersed at the molecular level in the beads.

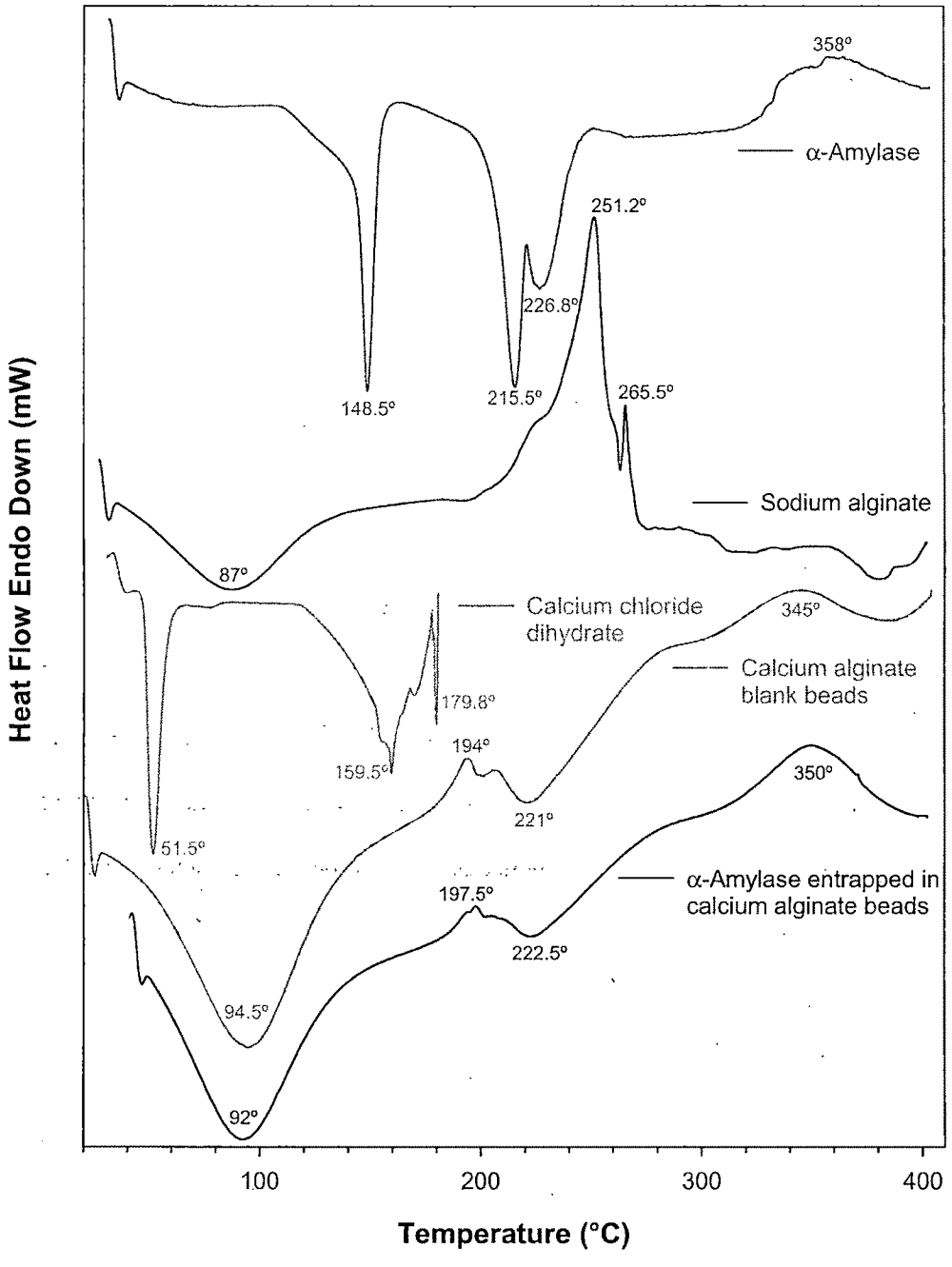

Figure 9.6: The DSC thermograms of α-amylase, sodium alginate, blank calcium alginate beads, and α-amylase-loaded alginate beads made at the same analytical conditions.

9.1.6.4. Morphology of the Beads

The spherical shape of beads in wet state was usually lost after drying especially for beads prepared with low alginate concentration. In 1.0% (w/v) alginate, the dried beads were very irregular and tend to agglomerate due to low mechanical strength. With the increasing of alginate concentration (2.0% w/v), the shape of beads changed to a spherical disc with a collapsed center (Figure 9.7). Normally the spherical shape was retained when the alginate concentration was as high as 5.0% (w/v), but viscosity of 5.0% w/v solution was too high for bead preparation under present experimental conditions so it was not studied. These results indicated that the shape of calcium alginate beads was seriously destroyed in the drying process, and the spherical shape of dried beads improved with the increase of alginate concentration. It was reported by Skjåk-Bræk et al. (Skjak-Brae et al., 1989) that calcium alginate beads usually have a heterogeneous structure with dense surface layer and loose core due to the heterogeneous gelation mechanism, which resulted in the collapse of beads during the drying process.

Figure 9.7: The scanning electron micrograph of dried alginate beads at 100X magnification.

9.1.7. STABILITY STUDY

For the developed formulation, the similarity factor (f_2) was calculated by a comparison of the dissolution profiles at each storage condition with the control at the initial condition. Results of f_2 factors ranged from 76 to 98 with 2 to 5% average difference. Overall, results from the stability studies indicated that capsules were physically and chemically stable for at least 12 months at 40±2°C/75±5% relative humidity and for more than 12 months (approximately for double time period) at 30±2°C/65±5% relative humidity.

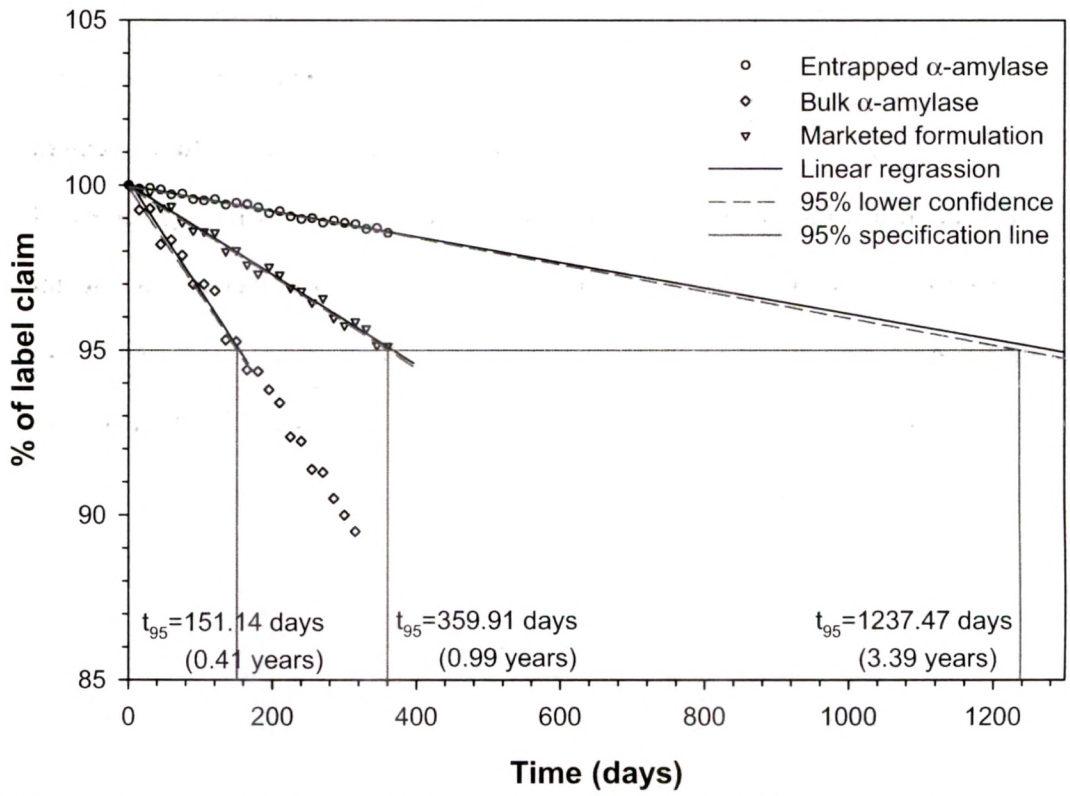

Figure 9.8: Extrapolation of accelerated stability data for shelf-life calculation.

An approach for analyzing the data on a quantitative attribute that is expected to change with time is to determine the time at which the 95% one-sided confidence limit for the mean curve intersects the acceptance criterion (not more than 5% change in assay from its

initial value). The accelerated stability data for prepared formulation, marketed formulation and the bulk α-amylase were extrapolated to calculate the shelf-life (Figure 9.8) and were found be 3.39 years, 0.99 year, and 0.41 year respectively. Hence, the stability of the entrapped α-amylase was significantly improved than the conventional dosage forms.

9.1.8. CONCLUSIONS

The optimization of the process using the desirability function resulted in more than 85% entrapment and les than 15 min of T_{50} at low levels of all three process variables (1.3% sodium alginate, 0.0856 M calcium chloride, and 20.9 min hardening time). Entrapment of α-amylase in alginate beads was confirmed using FTIR and DSC study. Texture analysis of the beads formulations illustrated that the degree of crosslinking decreased with increase in sodium alginate concentration while increased with increase in calcium chloride concentration and hardening time. Dissolution studies over a pH range similar to the human gastrointestinal tract demonstrated that alginate beads can be used for site specific intestinal delivery of α-amylase. Accelerated and long term stability study illustrated considerably improved shelf-life of α-amylase entrapped in alginate beads than the conventional dosage form. Based on the provided methodologies and depending on the site of action for α-amylase within the gastrointestinal tract, desirable beads can be easily manufactured. The results of this study may be of value to those pharmaceutical scientists who are engaged in site-specific delivery, as well as the oral delivery of enzymes, peptides, proteins and ulcerogenic agents.

9.2. Alginate-Papain Beads

9.2.1. pH DEPENDENT RELEASE PROFILE

Generally, higher molecular weight and poorly water-soluble drugs are not released from calcium alginate beads due to stability and non swelling property in acidic environment while swell and disintegrate in intestinal pH(Yotsuyanagi et al., 1987; Kim and Lee, 1992; Lee and Min, 1995). The swelling and disintegration of calcium alginate beads are dependent on compositions of dissolution medium, e.g. sodium and phosphate, and solubility of drug entrapped into alginate beads. Papain was not released from alginate beads due to higher molecular weight. The swelling and disintegration of alginate beads in intestinal fluid were due to the affinity of calcium to phosphate and sodium/calcium

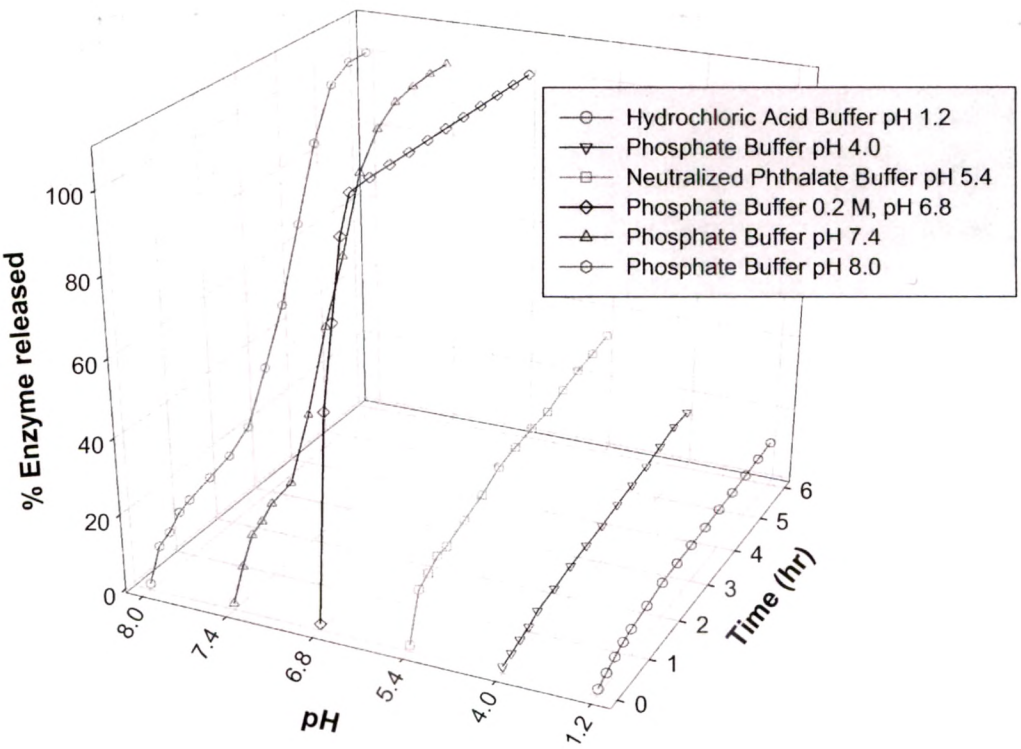

Figure 9.9: Determination of pH dependent release profile by 'In vitro' dissolution study.

exchange(Ostberg et al., 1993; Ostberg et al., 1994). The effect of pH on the release of papain from calcium alginate beads in different pH buffers simulating the human gastrointestinal tract is given in Figure 9.9. Release profile of optimized batch in simulated intestinal fluid without enzyme is shown in Figure 9.10.

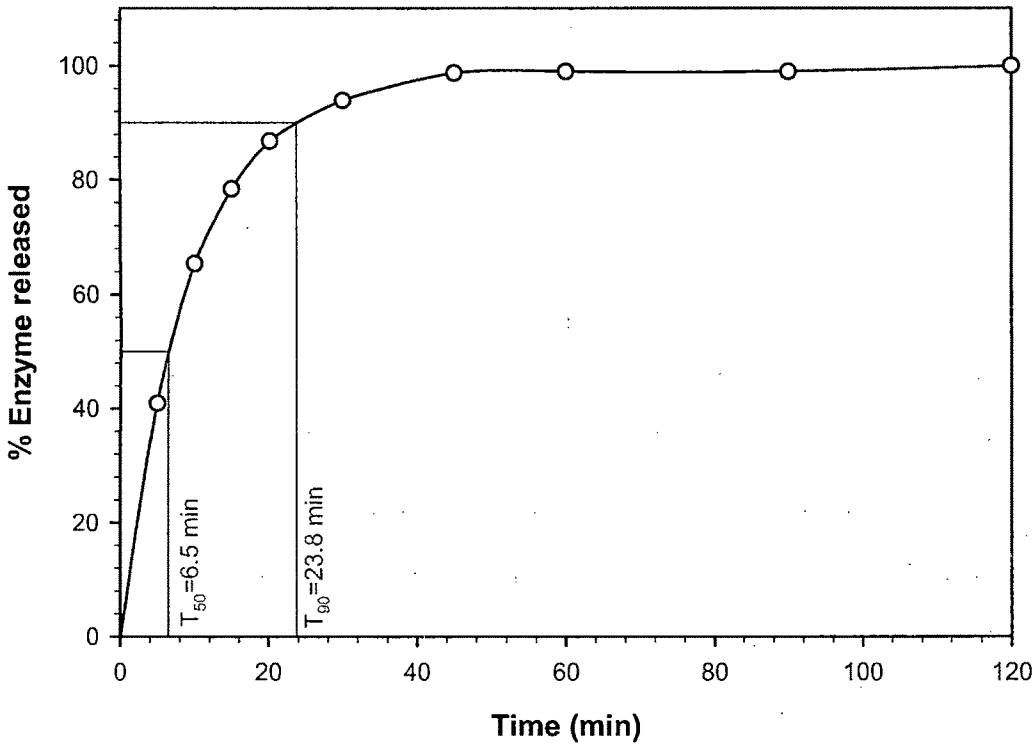

Figure 9.10: Release profile of optimized batch (formulation 1) in simulated intestinal fluid without enzyme.

9.2.2. EFFECT OF THE FACTORS ON RESPONSES

9.2.2.1. % Entrapment

ANOVA results and regression coefficients of response variables are shown in Table 9.7 from which it can be concluded that the effects of all three factors on the % entrapment were statistically significant (P <0.05). The results obtained from the Table 9.6 showed

that the highest % entrapment value was obtained at the high level (2% w/v) of the sodium alginate concentration. Especially the highest % entrapment value was obtained when the high level of the sodium alginate concentration was followed by the low levels of the other two factors (experiment 3).

Table 9.6: Factorial 3^3: matrix of the experiments and results for the measured responses and the desirability.

Factors/ levels				Responses					
ES[a]	Na. Alginate (% w/v)	Calcium chloride (M)	Hardening Time (min)	% Entrapment	T_{50}	T_{90}	Size (μm)	Angle of repose	Overall desirability
1	1.0	0.05	20	91.80	6.50	23.80	211.136	22.62	0.962
10	1.0	0.05	25	89.00	8.30	25.70	207.319	22.88	0.913
19	1.0	0.05	30	86.20	9.35	28.40	202.628	23.27	0.868
4	1.0	0.10	20	85.00	7.80	27.50	184.327	23.39	0.878
13	1.0	0.10	25	82.60	9.10	30.55	181.059	23.75	0.831
22	1.0	0.10	30	80.71	10.70	34.00	178.289	24.15	0.781
7	1.0	0.15	20	68.80	8.60	34.60	175.983	24.07	0.599
16	1.0	0.15	25	67.79	10.30	39.00	171.384	24.94	0.533
25	1.0	0.15	30	65.28	12.05	59.25	169.737	26.33	0.000
2	1.5	0.05	20	93.40	13.35	48.00	297.039	19.50	0.815
11	1.5	0.05	25	90.80	14.45	57.40	291.606	19.76	0.747
20	1.5	0.05	30	88.00	16.30	57.40	285.497	20.02	0.694
5	1.5	0.10	20	87.70	14.35	75.00	266.941	20.27	0.648
29	1.5	0.10	25	87.01	15.30	82.50	261.453	20.56	0.579
32	1.5	0.10	25	86.29	15.90	82.90	259.825	20.20	0.563
31	1.5	0.10	25	85.06	15.20	82.40	260.348	20.98	0.569
28	1.5	0.10	25	84.35	15.80	81.90	261.874	20.44	0.561
14	1.5	0.10	25	86.78	15.70	82.30	262.013	20.89	0.572
30	1.5	0.10	25	85.80	15.50	82.60	261.265	20.58	0.568
23	1.5	0.10	30	83.50	16.80	87.65	255.367	20.97	0.489
8	1.5	0.15	20	77.30	15.55	80.55	258.163	21.20	0.522
17	1.5	0.15	25	75.30	16.90	83.50	252.709	21.84	0.464
26	1.5	0.15	30	72.00	19.30	86.50	246.003	22.20	0.366
3	2.0	0.05	20	94.40	15.90	83.80	715.268	16.14	0.599
12	2.0	0.05	25	91.39	17.05	91.50	708.007	16.49	0.476
21	2.0	0.05	30	88.50	18.60	95.60	701.294	16.87	0.339
6	2.0	0.10	20	88.40	17.70	90.80	682.689	17.00	0.464
15	2.0	0.10	25	86.00	18.60	94.20	677.136	17.26	0.375
24	2.0	0.10	30	84.00	20.20	96.15	671.935	17.77	0.270
9	2.0	0.15	20	79.50	19.40	95.60	673.543	18.03	0.293
18	2.0	0.15	25	76.60	20.40	96.30	668.162	18.56	0.233
27	2.0	0.15	30	73.70	22.80	97.20	662.736	18.89	0.000

[a] ES, experimental sequence.

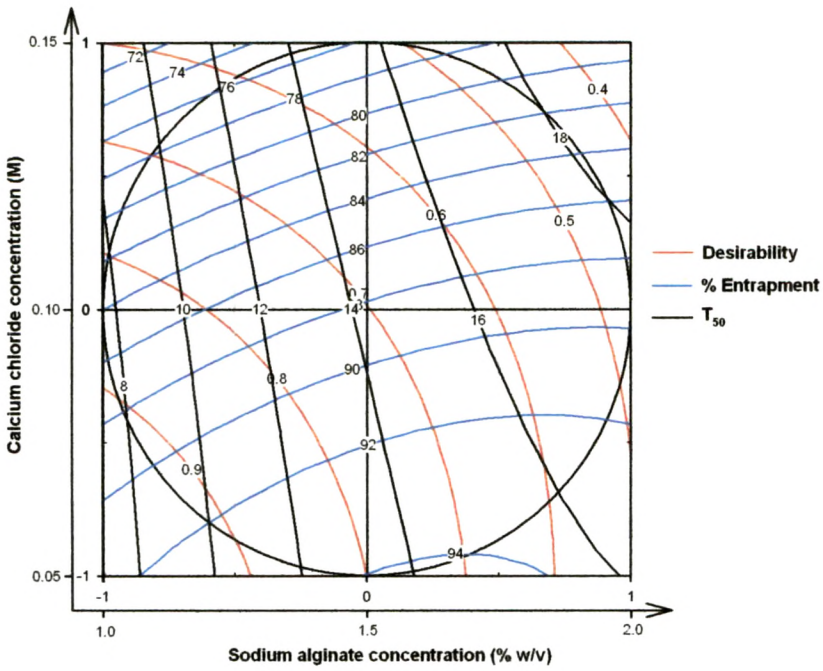

Figure 9.11: Contour plots of desirability, % entrapment and T_{50} as function of sodium alginate concentration and calcium chloride concentration, with fixed hardening time of 20 min ($C = -1$).

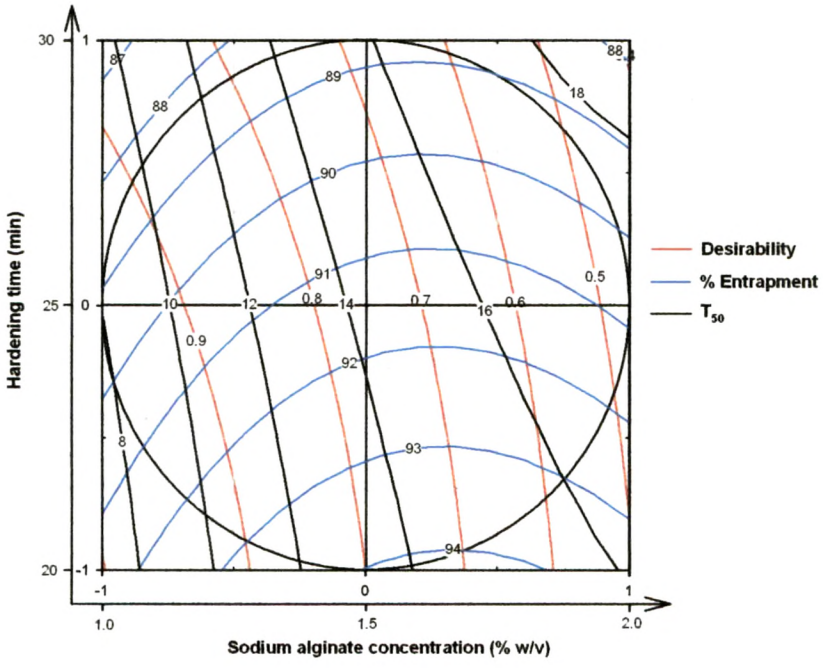

Figure 9.12: Contour plots of desirability, % entrapment and T_{50} as function of sodium alginate concentration and hardening time, with fixed calcium chloride concentration of 0.05 M ($B = -1$).

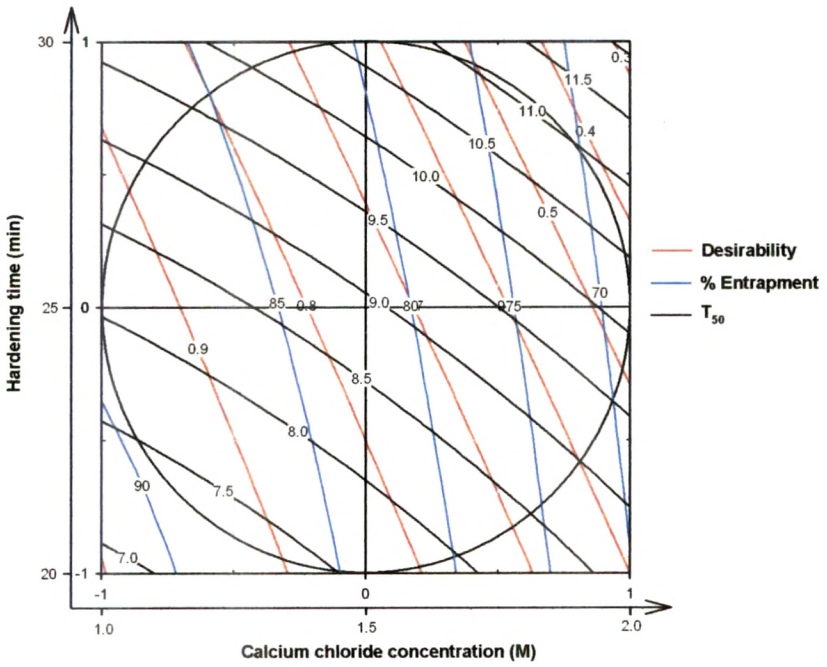

Figure 9.13: Contour plots of desirability, % entrapment and T_{50} as function of calcium chloride concentration and hardening time, with fixed sodium alginate concentration of 1.0 % w/v ($A = -1$).

On addition of sodium alginate solution to a calcium solution, instantaneous interfacial crosslinking took place with precipitation of calcium alginate followed by a more gradual gelation of the interior which caused loss of enzyme from the surface of the beads. Loss of surface enzyme was proportional to the degree of crosslinking. Increased viscosity at higher sodium alginate concentration retarded penetration of calcium to the interior of the bead. This resulted in decrease of crosslinking and increased entrapment efficiency which was further supported by the positive coefficient of factor A (Table 9.7). Degree of crosslinking increased with increase in calcium chloride concentration and hardening time(Lee and Min, 1996) and resulted in decreased entrapent(Wang and He, 2002) which correspond to negative coefficient for factor B and C in Table 9.7. Calcium chloride concentration was the most influential (42.23%) factor amongst all three factors.

Table 9.7: ANOVA results (*P* values): effect of the variables on % entrapment, T_{50}, T_{90}, particle size and angle of repose.

	% Entrapment		T_{50}		T_{90}		Particle size		Angle of repose	
Factors	Coefficient	*P*	Coefficient	*P*	Coefficient	*P*	Coefficient	*P*	Coefficient	*P*
A	2.517	<0.0001*	4.886	<0.0001*	29.908	<0.0001*	248.828	<0.0001*	-3.244	<0.0001*
B	-8.734	<0.0001*	1.417	<0.0001*	8.939	<0.0001*	-18.965	<0.0001*	1.028	<0.0001*
C	-2.467	<0.0001*	1.497	<0.0001*	4.583	0.0071*	-5.089	<0.0001*	0.458	<0.0001*
A^2	-1.532	0.0003*	-1.766	<0.0001*	-11.39	0.0001*	167.526	<0.0001*	-0.028	0.7433
B^2	-3.184	<0.0001*	0.193	0.0764	-4.694	0.0682	10.123	<0.0001*	0.172	0.0485*
C^2	-0.112	0.7569	0.218	0.0474*	-1.744	0.4836	0.183	0.6531	0.019	0.8450
AB	1.720	<0.0001*	0.354	0.0002*	-3.063	0.1194	-1.346	0.0003*	-0.049	0.4462
AC	-0.2245	0.4249	-0.050	0.5386	-1.417	0.4614	-1.229	0.0007*	-0.109	0.0987
BC	0.190	0.4981	0.175	0.0397*	0.533	0.7804	0.401	0.2106	0.185	0.0078*
Constant	85.933	-	15.567	-	79.231	-	261.305	-	20.590	-
$r^2_{adj.}$	0.968	-	0.996	-	0.935	-	0.999	-	0.993	-

Regression coefficients and in coded values. *, Statistically significant ($P < 0.05$)

9.2.2.2. T_{50}

The time required for 50 % of enzyme release (T_{50}) was used to evaluate the onset of action of the formulations. As shown in Table 9.7, all three factors had significant positive effect on response value (i.e. response value increase with increase in factor level). The concentration of alginate (factor A) had the most significant (46.26%) effect on T_{50}. However, immediate release of enzyme for quicker on set of action and hence shorter T_{50} was the desirable criteria for the optimum formulation. Release of papain from beads was inversely proportional to the degree of crosslinking. Higher calcium concentration and hardening time also resulted in higher T_{50} due to higher degree of crosslinking(Wang and He, 2002).

9.2.2.3. T_{90}

90% of enzyme should be released in minimum time to exert maximum action at the site of release. All three factors had positive effect on response value which can be seen in Table 9.7. The concentration of alginate (factor A) was the most influencing (45.14%) factor. T_{90} was inversely proportional to the degree of crosslinking and particle size. Higher concentration of alginate yielded larger beads with high T_{90} values. Higher calcium concentration and hardening time resulted in higher T_{90} due to higher degree of crosslinking(Wang and He, 2002).

9.2.2.4. Particle Size

As shown in Table 9.7, all three parameters were significant for particle size amongst which sodium alginate concentration was the most affecting (54.84%) factor. The sizes of the beads are influenced by the size of the opening through which the alginate solution is allowed to pass (which was kept constant) and viscosity of the alginate solution. Viscosity increased with concentration of sodium alginate which resulted in larger particles. Calcium chloride concentration and hardening time had the negative effect (i.e. response decreases with increase in factor levels) on the particle size. Higher degree of crosskinking due to higher calcium chloride concentration and hardening time caused shrinkage of beads and resulted in smaller particle size(Wang and He, 2002).

9.2.2.5. Angle of Repose

Angle of repose was measured for estimating flowability of the beads. If the angle exceeds 50°, the material will not flow satisfactorily while materials having values near the minimum, flow easily and well(Carter, 1986). The rougher and more irregular the surface of the particles, the higher will be the angle of repose. The angle also increases with decrease in particle size.

Here, too, all three factors exhibited significant effect on angle of repose. Particle size increased with increase in sodium alginate concentration and resulted in decreased angle. This was further confirmed by a negative coefficient of factor A in Table 9.7. Higher calcium chloride concentration and hardening time resulted in smaller beads with irregular surface due to shrinkage and showed increased angle. Concentration of sodium alginate concentration was the most influencing (61.33%) factor amongst all three.

9.2.3. INTERACTIONS BETWEEN THE FACTORS

An interaction is the failure of a factor to produce the same effect on the response at the different levels of the other factor(Montgomery, 2001). The ANOVA results (Table 9.7) showed that the interaction AB had significant influence on the % entrapment, T_{50} and particle size. The interaction AC had significant influence only on particle size while interaction BC was also found to influence significantly on T_{50} and angle of repose.

The analysis of the results of the Table 9.6 by multiple regression leads to equations that adequately describe the influence of the selected factors on % entrapment, T_{50}, T_{90}, particle size and angle of repose. In Table 9.7 regression coefficients of these equations are presented.

9.2.4. OPTIMIZATION OF THE PROCESS USING THE DESIRABILITY FUNCTION

Generally the aim of the optimization of pharmaceutical formulations is to find the optimum levels of the variables, which affect a process, where a product of good characteristics could be produced. Using the desirability function, all the selected responses were combined in one overall response, the overall desirability. As it has been already discussed, the overall desirability response was calculated from the individual desirability of each of the responses using the Eqs. (3)–(11). The results of each of these overall desirability responses are included in the optimization procedure and the equation found out was as follow (coded factors):

Eq. 9.3

$$D = 0.609 - 0.184A - 0.189B - 0.110C - 0.046A^2 - 0.044B^2 - 0.016C^2 + 0.060AB + 0.004AC - 0.048BC \; (r^2_{adj.} = 0.8530, P < 0.0001)$$

In Figure 9.11, Figure 9.12, and Figure 9.13 the contour plots that describe the influence of the factors on the overall desirability, % entrapment and T_{50} are presented. The study of these plots showed that the highest values of the desirability could be obtained at low values of all three process variables. Especially the analysis of the Eq. 9.3 resulted to the optimum combination of the independent variables where a product of desired characteristics may occur and results of this analysis are shown in Table 9.8.

Table 9.8: Optimum levels for the independent process variables.

Independent variables	Optimum values
Sodium alginate concentration	1% w/v
Calcium chloride concentration	0.05 M
Hardening time	20 min
Overall desirability	0.952

9.2.5. EVALUATION OF MODEL

In order to assess the reliability of the model, five experiments were conducted by the varying the process variables at values other than that of the model. For each of these test experiments the responses were estimated by using the equations and experimental procedure. In Table 9.9 the comparison between the experimental and predicted values of the response for these additional experiments is presented. Bios was calculated by the following equation:

Eq. 9.4

$$\text{Bias} = \left[\frac{(\text{predicted value} - \text{edperimental value})}{\text{predicted value}}\right] \times 100$$

It can be seen that in all cases there was a reasonable agreement between the predicted and the experimental value, since low value of the bias were found. For this reason it can be concluded that the equations describe adequately the influence of the selected process variables on the responses under study.

Table 9.9: Comparison between predicted and experimental values for the test formulations.

Responses	Test	Factors/levels			Predicted values	Experimental values	Bias%
		A	B	C			
% Entrapment	1	-1	-0.6	-0.6	88.38	90.72	2.6
	2	-0.6	0	0.4	82.92	81.15	2.1
	3	-0.4	0.6	0	77.88	76.01	2.4
	4	0	-0.4	0.6	87.35	84.58	3.2
	5	0.4	0.4	-0.4	83.94	86.06	2.5
T_{50}	1	-1	-0.6	-0.6	7.56	7.41	1.9
	2	-0.6	0	0.4	12.65	12.83	1.5
	3	-0.4	0.6	0	14.16	14.47	2.1
	4	0	-0.4	0.6	15.97	16.23	1.7
	5	0.4	0.4	-0.4	17.31	17.09	1.2
T_{90}	1	-1	-0.6	-0.6	25.01	24.68	1.3
	2	-0.6	0	0.4	59.08	60.33	2.1
	3	-0.4	0.6	0	69.85	72.15	3.3
	4	0	-0.4	0.6	76.90	75.61	1.7
	5	0.4	0.4	-0.4	89.74	88.63	1.2
Particle size	1	-1	-0.6	-0.6	196.74	181.71	7.6
	2	-0.6	0	0.4	170.61	180.72	5.9
	3	-0.4	0.6	0	181.17	172.76	4.6
	4	0	-0.4	0.6	267.43	285.91	6.9
	5	0.4	0.4	-0.4	383.66	414.58	8.1
Angle of repose	1	-1	-0.6	-0.6	22.95	22.29	2.9
	2	-0.6	0	0.4	22.74	21.95	3.5
	3	-0.4	0.6	0	22.57	23.56	4.4
	4	0	-0.4	0.6	20.44	19.89	2.7
	5	0.4	0.4	-0.4	19.53	18.90	3.2
Overall desirability	1	-1	-0.6	-0.6	0.93	0.94	1.8
	2	-0.6	0	0.4	0.66	0.69	4.9
	3	-0.4	0.6	0	0.53	0.56	5.9
	4	0	-0.4	0.6	0.62	0.60	3.5
	5	0.4	0.4	-0.4	0.50	0.49	2.7

9.2.6. DIFFERENTIAL SCANNING CALORIMETRY (DSC)

The DSC thermograms a, b, c, d and e which represent calcium chloride dihydrate, papain, sodium alginate, blank calcium alginate beads and papain-loaded beads,

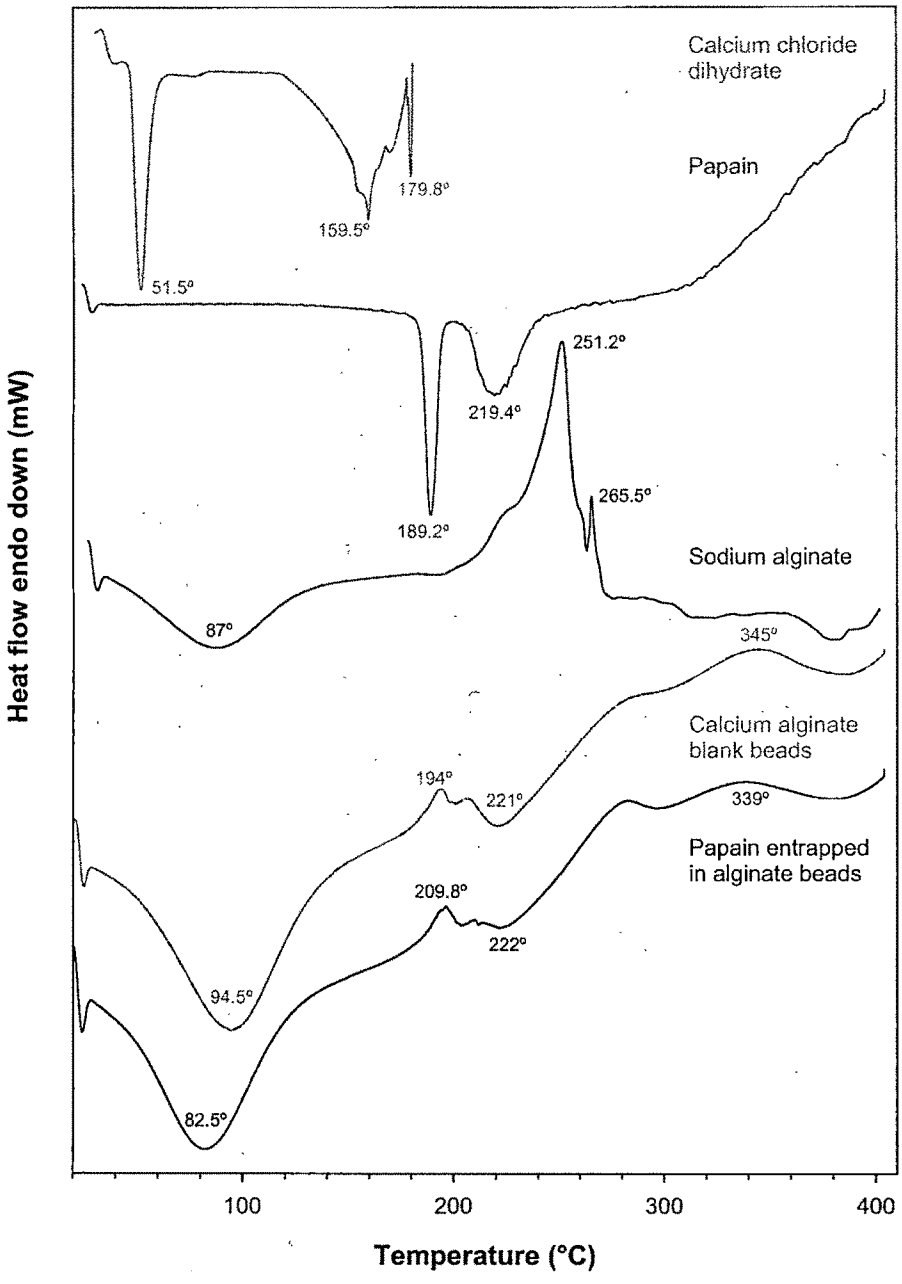

Figure 9.14: The DSC thermograms of (a) calcium chloride hexahydrate, (b) papain, (c) sodium alginate, (d) blank calcium alginate beads and (e) papain-loaded alginate beads made at the same analytical conditions.

respectively, made at the same analytical conditions are shown in Figure 9.14. The degradation exotherm of sodium alginate at ≈ 252°C was absent in blank calcium alginate bead and at ≈ 221°C, an endotherm corresponding to alginate-calcium interaction was observed. The melting peak shape of papain-loaded alginate beads appeared to be similar to the one of blank beads except it contained extra peak of papain. This indicated that papain was entrapped in the lattice structure of alginate beads.

9.2.7. MORPHOLOGY OF THE BEADS

The spherical shape of beads in wet state was usually lost after drying especially those beads prepared with low alginate concentration. In 1.0% (w/v) alginate, the dried beads were very irregular and tend to agglomerate due to low mechanical strength. With the increasing of alginate concentration (2.0% w/v), the shape of beads changed to a spherical disc with a collapsed center. Normally the spherical shape was retained when the alginate concentration was as high as 5.0% (w/v)(Shu and Zhu, 2002), but viscosity of 5.0% w/v solution was too high for complete batch preparation under experimental conditions so it was not studied. These results indicated that the shape of calcium alginate beads was seriously destroyed in the drying process, and the spherical shape of dried beads improved with the increase of alginate concentration. It was reported by Skjåk-Bræk et al.(Skjak-Brae et al., 1989) that calcium alginate beads usually have a heterogeneous structure with dense surface layer and loose core due to the heterogeneous gelation mechanism, which resulted in the collapse of beads during the drying process(Polk et al., 1994).

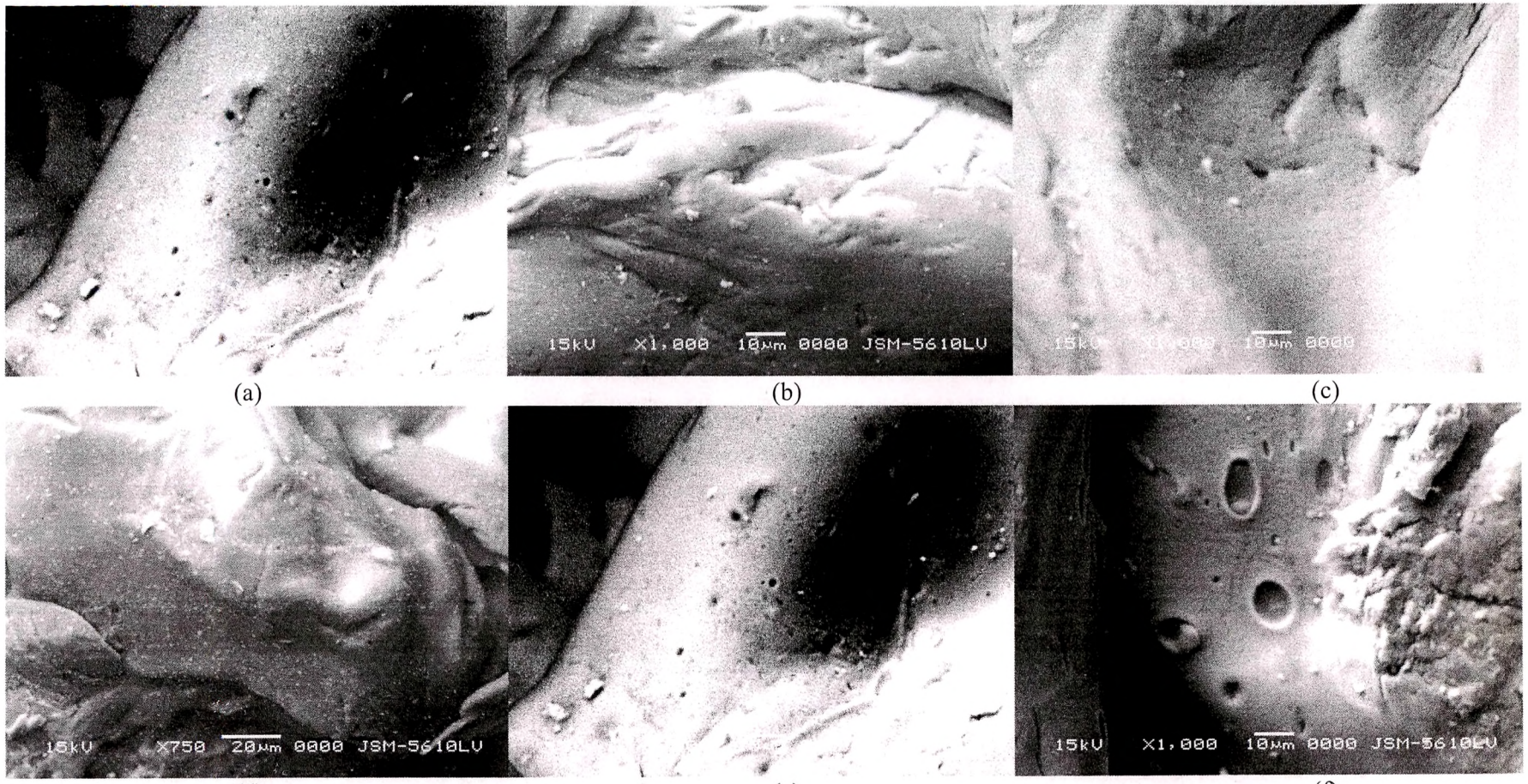

(a) (b) (c)

(d) (e) (f)

Figure 9.15: SEM micrographs and surface morphology of calcium alginate beads: (a–c) Effect of sodium alginate concentration on surface morphology (calcium chloride concentration 0.15 M) (a) 1.0% w/v; (b) 1.5% w/v and (c) 2.0% w/v sodium alginate concentration. (d–f) Effect of calcium chloride concentration on surface morphology (sodium alginate concentration 1.5 % w/v) (d) 0.10 M; (e) 0.15 M and (f) 0.20 M calcium chloride concentration.

One noticeable characteristic of the beads surface is its high porosity when the concentration of calcium chloride increased (Figure 9.15; d–f). This suggested that the water-soluble macromolecule created pores both because it affected the calcium alginate network formation during the unit preparation and because it was leached from the membrane into the medium (Iannuccelli et al., 1998). Further, the surface morphology was improved (i.e. decrease in roughness) with increase in sodium alginate concentration (Figure 9.15; a–c) (Shu and Zhu, 2002) due to the high viscosity of the sodium alginate solution.

9.2.8. CONCLUSIONS

It was found that the drug entrapment capacity of papain was significantly enhanced by decreasing calcium chloride concentration and hardening time as well as by increasing in sodium alginate concentration. Sodium alginate concentration, calcium chloride concentration and hardening time affect % entrapment, T_{50}, T_{90}, particle size and angle of repose of the beads significantly. Interaction terms were also found to be statistically significant. Furthermore, texture analysis of the beads formulations illustrated that the higher concentration of sodium alginate and calcium chloride affect the surface morphology as well as shape of the beads. Enzyme entrapment was confirmed with the help of differential scanning calorimetry. The optimization of the process using the desirability function resulted to the optimum values of the factors at which the goal of the production of beads with acceptable characteristics could be fulfilled. Dissolution studies over a pH range similar to the human gastrointestinal tract demonstrated that the rate of drug release from the different beads in simulated small intestinal environments depends mainly on sodium alginate concentration and particle size. Based on the provided

methodologies and depending on the site of action for papain within the gastrointestinal tract, desirable beads can be easily and reproducibly manufactured. The application of a single polymer (as used traditionally) for the formation of beads allows the formulator to predict and produce pH-sensitive beads of different geometries, strengths and release characteristics. More specifically, some of the formulation problems encountered for the delivery of gastric-irritating or acid-labile enzyme or drugs can be overcome by the application of multiple unit crosslinked pH-responsive beads. The results of this study may be of value to those pharmaceutical scientists who are engaged in site-specific delivery, as well as the oral delivery of enzymes, peptides, proteins and ulcerogenic agents.

9.3. Alginate-Papain Beads (Neu.Net.)

9.3.1. OPTIMIZATION OF NEURAL NETWORK

Optimization of various parameters like number of neuron in hidden layer, step size and momentum of hidden and output layer was carried out. For optimization, the training was carried out three times and the minimum of average MSE was the optimization criteria. Results of various run are summarized in Figure 9.16. Optimum number of neurons in hidden layer was found to be 15, while optimum step size for hidden layer and output layer was

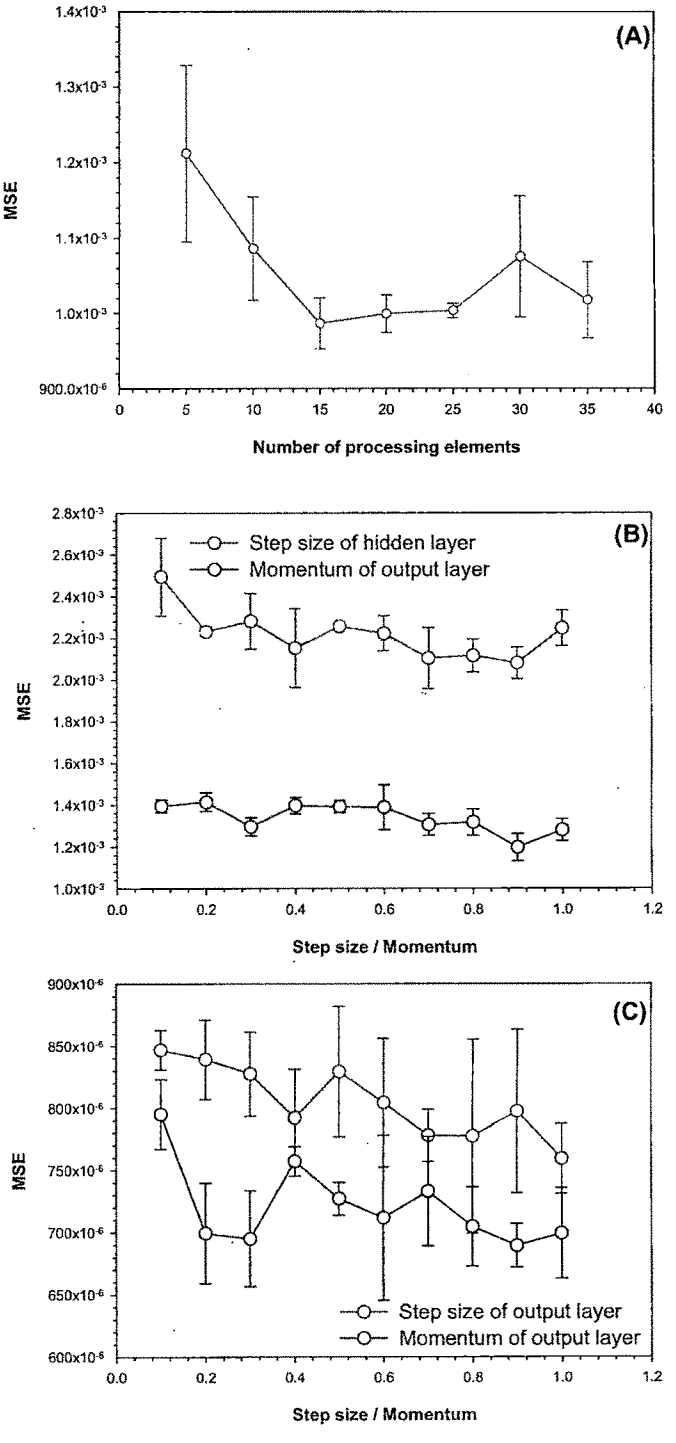

Figure 9.16: Optimization of neural network: (A) Optimization of number of neurons in hidden layer, (B) optimization of step size and momentum of hidden layer, and (C) optimization of step size and momentum of output layer.

0.9 and 1.0 respectively (out of 0.1 to 1.0). Optimum momentum for hidden layer and output layer was found to be 0.9 (out of 0.1 to 1.0). For prediction purpose, the neural network was constructed using the optimum conditions and trained (n=3) along with cross validation data set. The predicted responses were plotted to generate the response surfaces for interpreting the effect of various process factors.

9.3.2. EFFECT OF THE FACTORS ON RESPONSES

9.3.2.1. % Entrapment

Contour plots of response surface for % entrapment are shown in Figure 9.17 (A, C, E) from which it can be concluded that the more than 90% entrapment value was obtained at the high level (2% w/v) of the sodium alginate concentration especially when the high level of the sodium alginate concentration was followed by the low levels of the other two factors (94.4% entrapment, experiment 3; Table 9.10). Whilst, the calcium chloride concentration and hardening time were affecting negatively (i.e. response decreases with increase in factor level) in significant amount and their interaction was synergistic at higher levels (experiment 25, 26, and 27; Table 9.10).

On addition of sodium alginate solution to a calcium chloride solution, instantaneous interfacial crosslinking takes place with precipitation of calcium alginate followed by a more gradual gelation of the interior which causes loss of enzyme from the surface of the beads. This can be noticed from the pores on the bead surface (Figure 9.18) created due to the water-soluble macromolecules both because it affected the calcium alginate network formation during the unit preparation and because it was leached from the membrane into the medium. (Iannuccelli et al., 1998) Loss of surface enzyme was found to be

proportional to the degree of crosslinking. Increase in viscosity with increase in sodium alginate concentration retarded penetration of calcium to the interior of the bead, resulted in decreased crosslinking (also decreased surface roughness and porosity; Figure 9.18a-c) and increased entrapment efficiency. Degree of crosslinking increases with increase in calcium concentration and contact time, (Wang and He, 2002) hence entrapment efficiency decreased.

Table 9.10: Matrix of the experiments and results for the measured responses.

Factors/ levels				Responses				
ES[a]	Na. Alg. (% w/v)	$CaCl_2$ (M)	Hard. Time (min)	% Entrap-ment	T_{50}	T_{90}	Size (μm)	Angle of repose
1	1.0	0.05	20	91.80	6.50	23.80	211.1	22.62
10	1.0	0.05	25	89.00	8.30	25.70	207.3	22.88
19	1.0	0.05	30	86.20	9.35	28.40	202.6	23.27
4	1.0	0.10	20	85.00	7.80	27.50	184.3	23.39
13	1.0	0.10	25	82.60	9.10	30.55	181.1	23.75
22	1.0	0.10	30	80.71	10.70	34.00	178.3	24.15
7	1.0	0.15	20	68.80	8.60	34.60	176.0	24.07
16	1.0	0.15	25	67.79	10.30	39.00	171.4	24.94
25	1.0	0.15	30	65.28	12.05	59.25	169.7	26.33
2	1.5	0.05	20	93.40	13.35	48.00	297.0	19.50
11	1.5	0.05	25	90.80	14.45	57.40	291.6	19.76
20	1.5	0.05	30	88.00	16.30	57.40	285.5	20.02
5	1.5	0.10	20	87.70	14.35	75.00	266.9	20.27
29	1.5	0.10	25	87.01	15.30	82.50	261.5	20.56
32	1.5	0.10	25	86.29	15.90	82.90	259.8	20.20
31	1.5	0.10	25	85.06	15.20	82.40	260.3	20.98
28	1.5	0.10	25	84.35	15.80	81.90	261.9	20.44
14	1.5	0.10	25	86.78	15.70	82.30	262.0	20.89
30	1.5	0.10	25	85.80	15.50	82.60	261.3	20.58
23	1.5	0.10	30	83.50	16.80	87.65	255.4	20.97
8	1.5	0.15	20	77.30	15.55	80.55	258.2	21.20
17	1.5	0.15	25	75.30	16.90	83.50	252.7	21.84
26	1.5	0.15	30	72.00	19.30	86.50	246.0	22.20
3	2.0	0.05	20	94.40	15.90	83.80	715.3	16.14
12	2.0	0.05	25	91.39	17.05	91.50	708.0	16.49
21	2.0	0.05	30	88.50	18.60	95.60	701.3	16.87
6	2.0	0.10	20	88.40	17.70	90.80	682.7	17.00
15	2.0	0.10	25	86.00	18.60	94.20	677.1	17.26
24	2.0	0.10	30	84.00	20.20	96.15	671.9	17.77
9	2.0	0.15	20	79.50	19.40	95.60	673.5	18.03
18	2.0	0.15	25	76.60	20.40	96.30	668.2	18.56
27	2.0	0.15	30	73.70	22.80	97.20	662.7	18.89

[a] ES, experimental sequence.

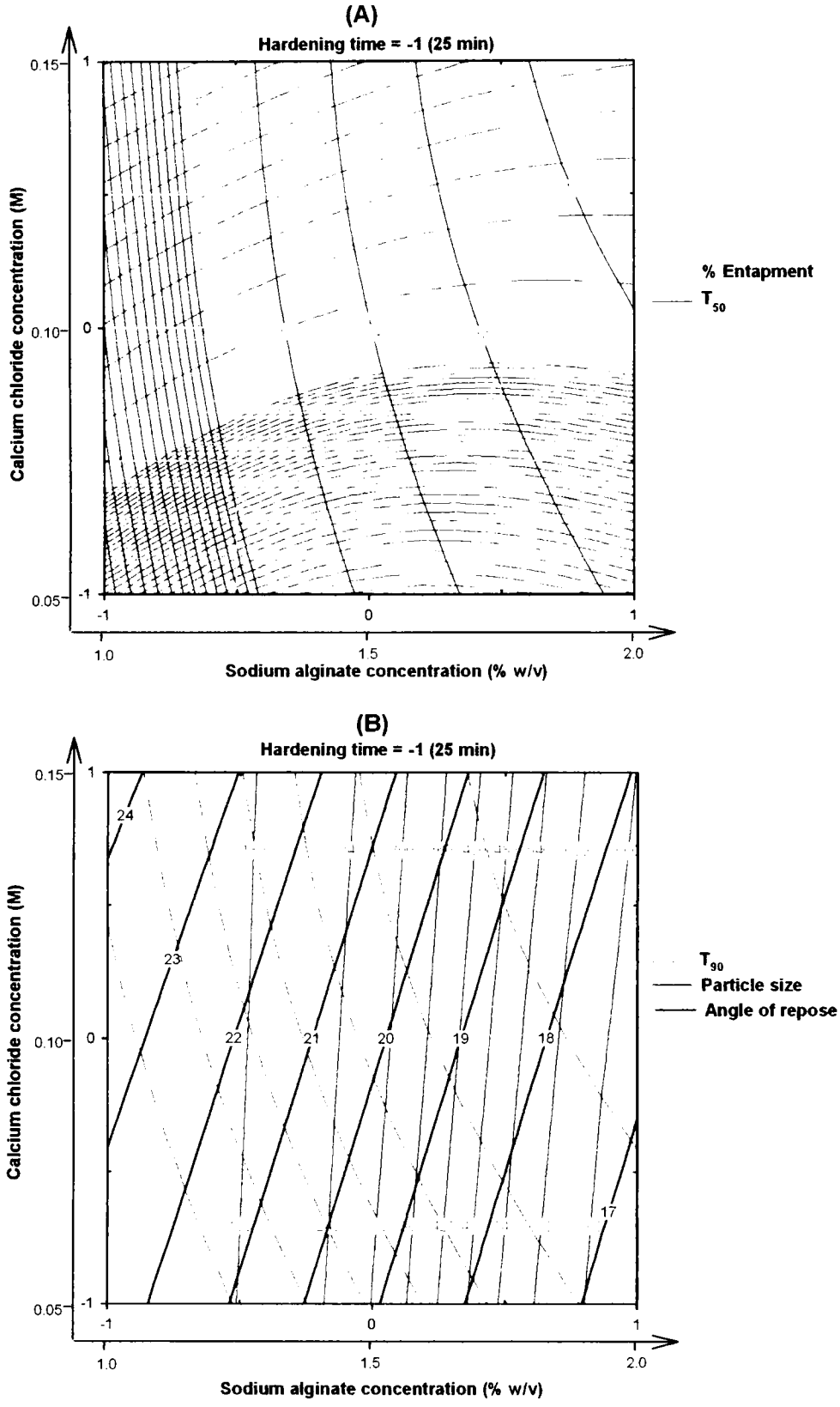
(A)
Hardening time = -1 (25 min)
Calcium chloride concentration (M)
0.15
0.10
0.05
1
0
-1
-1
0
1
1.0
1.5
2.0
Sodium alginate concentration (% w/v)
% Entapment
T_{50}
(B)
Hardening time = -1 (25 min)
Calcium chloride concentration (M)
24
23
22
21
20
19
18
17
Sodium alginate concentration (% w/v)
T_{90}
Particle size
Angle of repose

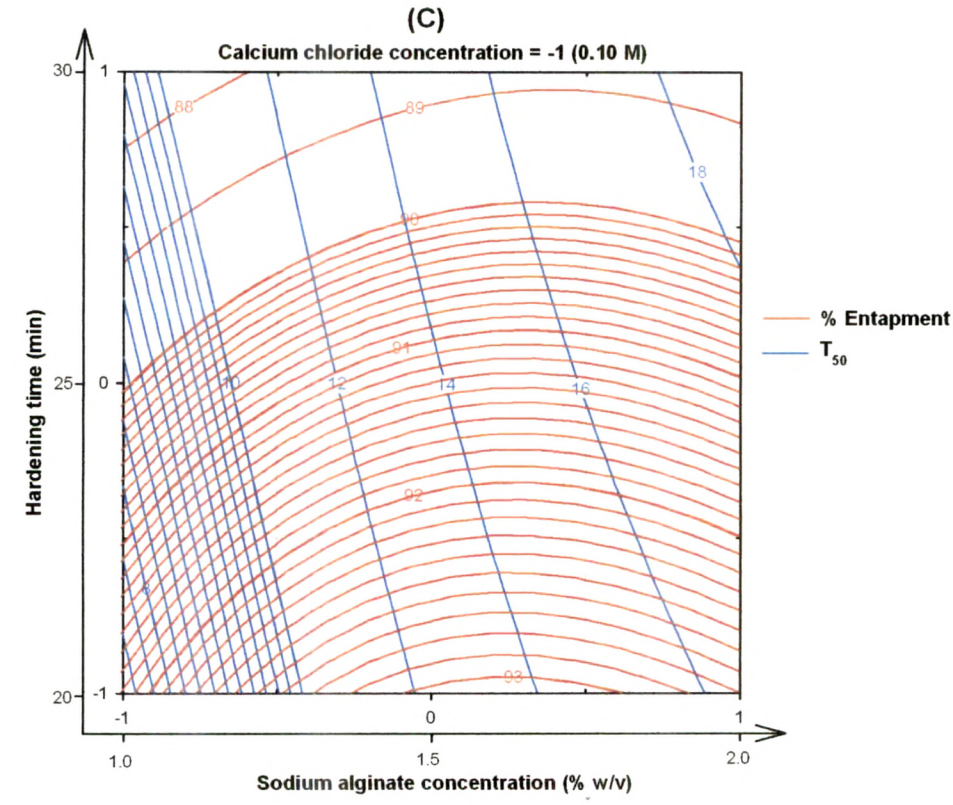
(C)
Calcium chloride concentration = -1 (0.10 M)
Hardening time (min)
30
25
20
1
0
-1
88
89
18
90
91
12
14
16
92
93
1.0
1.5
2.0
Sodium alginate concentration (% w/v)
% Entapment
T50

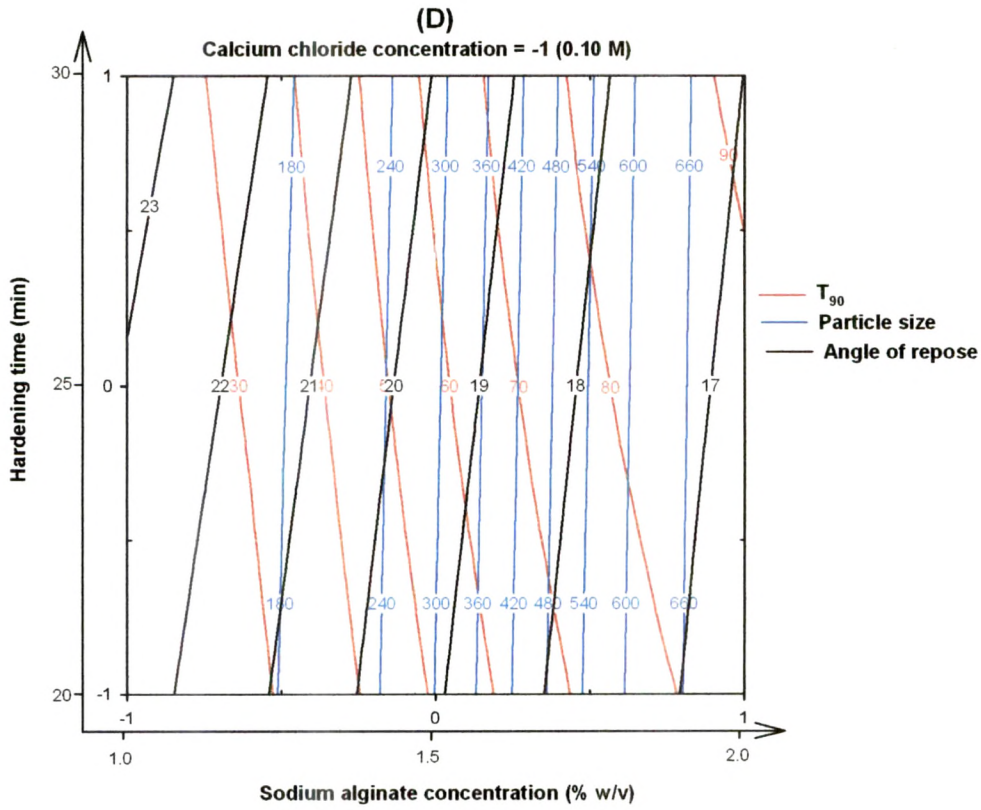
(D)
Calcium chloride concentration = -1 (0.10 M)
Hardening time (min)
30
25
20
1
0
-1
180
240
300
360
420
480
540
600
660
90
23
22
21
20
19
18
17
1.0
1.5
2.0
Sodium alginate concentration (% w/v)
T90
Particle size
Angle of repose

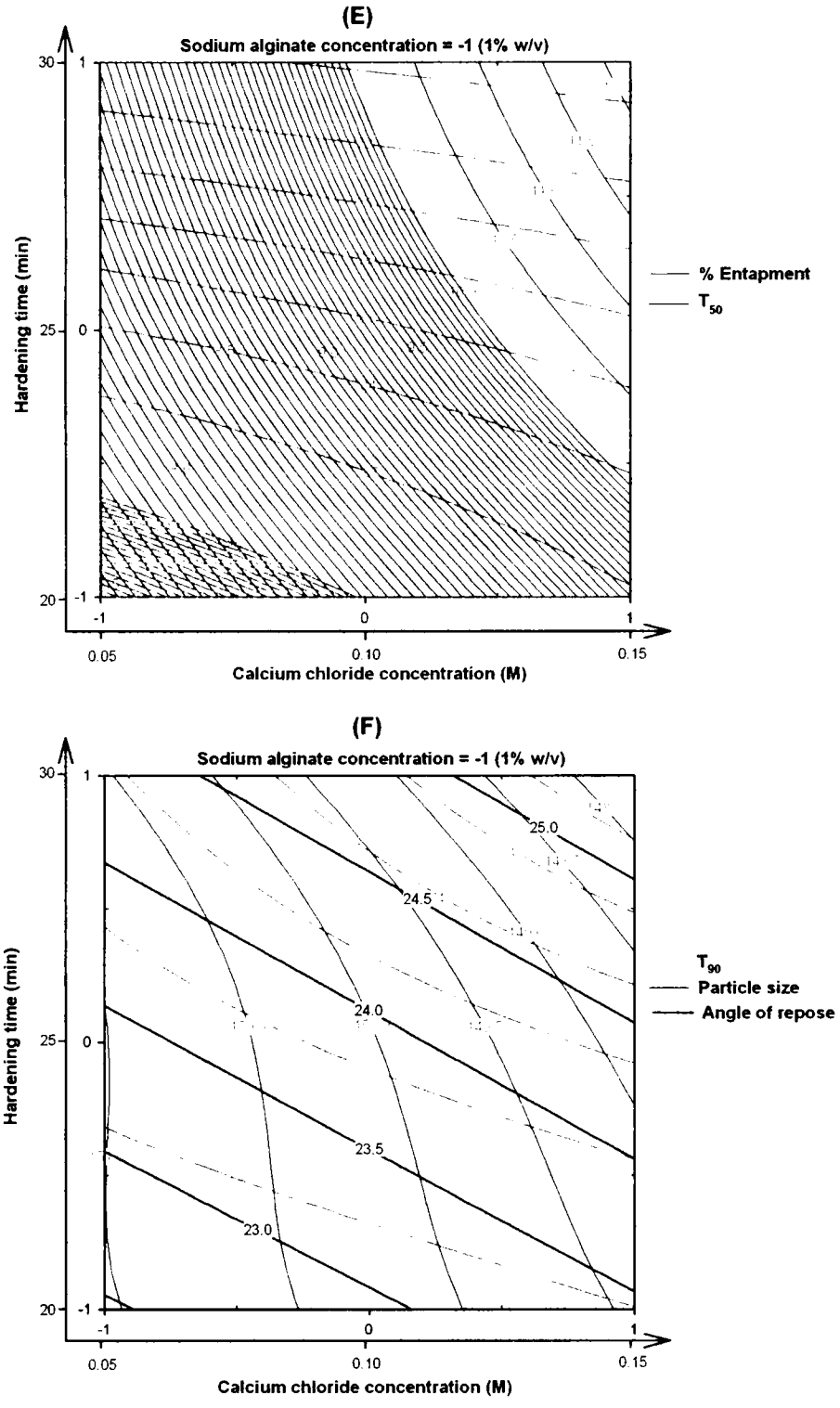

Figure 9.17: Contour plots of % entrapment, T50, T90, particle size and angle of repose as a function of sodium alginate concentration, calcium chloride concentration, and hardening time.

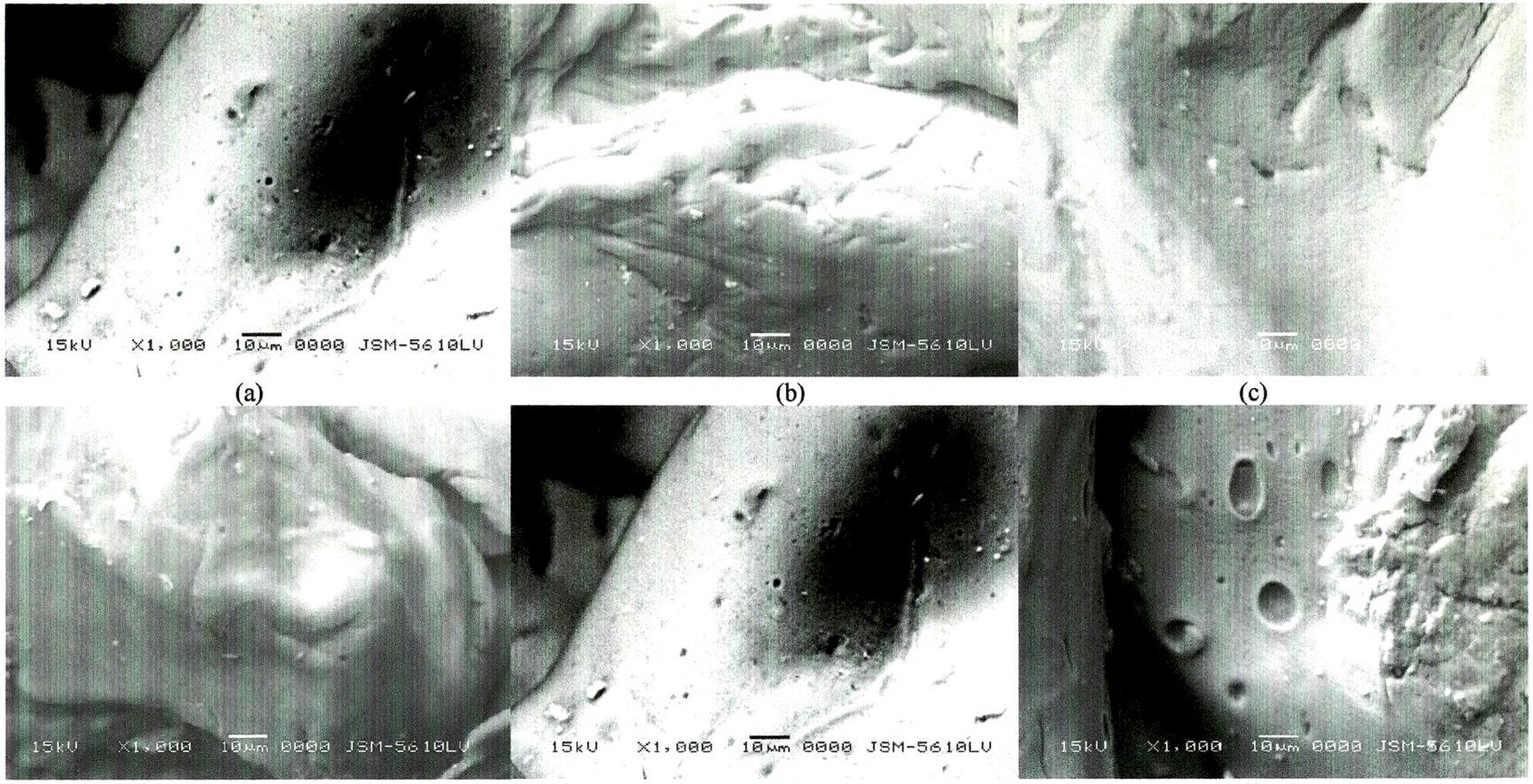

Figure 9.18: SEM micrographs and surface morphology of calcium alginate beads: (a–c) Effect of sodium alginate concentration on surface morphology (calcium chloride concentration 0.15 M) (a) 1.0% w/v, (b) 1.5% w/v and (c) 2.0% w/v sodium alginate concentration. (d–f) Effect of calcium chloride concentration on surface morphology (sodium alginate concentration 1.5 % w/v) (d) 0.10 M, (e) 0.15 M and (f) 0.20 M calcium chloride concentration.

Table 9.11: Matrix of the experiments and neural network predicted responses.

Factors/ levels				Responses				
Sr. No.	Na. Alginate (% w/v)	Calcium chloride (M)	Harde-ning Time (min)	% Entrap-ment	T_{50}	T_{90}	Size (μm)	Angle of repose
1	1.0	0.05	20	91.81	7.45	22.09	151.0	22.45
2	1.0	0.05	25	89.93	8.31	23.26	150.3	22.92
3	1.0	0.05	30	87.28	9.44	24.94	149.4	23.43
4	1.0	0.10	20	84.23	8.00	26.94	151.0	23.37
5	1.0	0.10	25	81.61	9.28	31.09	150.0	23.89
6	1.0	0.10	30	78.63	10.87	36.27	148.8	24.43
7	1.0	0.15	20	69.87	8.46	34.30	150.5	24.31
8	1.0	0.15	25	68.70	10.14	43.54	149.2	24.84
9	1.0	0.15	30	67.78	12.21	54.11	147.7	25.33
10	1.5	0.05	20	93.04	12.29	51.25	300.2	19.10
11	1.5	0.05	25	91.31	13.77	57.76	292.1	19.50
12	1.5	0.05	30	88.69	15.11	62.82	283.9	19.94
13	1.5	0.10	20	88.81	13.96	72.34	275.5	20.18
14	1.5	0.10	25	86.17	15.89	80.51	269.5	20.65
15	1.5	0.10	30	82.90	17.49	85.84	262.6	21.17
16	1.5	0.15	20	76.07	14.94	81.70	257.0	21.32
17	1.5	0.15	25	74.14	17.20	89.34	250.9	21.86
18	1.5	0.15	30	72.35	18.94	93.72	242.5	22.48
19	2.0	0.05	20	92.80	16.31	84.32	699.8	16.67
20	2.0	0.05	25	91.04	17.59	88.50	698.5	16.82
21	2.0	0.05	30	88.54	18.64	91.26	696.6	16.99
22	2.0	0.10	20	89.04	17.89	92.74	684.8	17.18
23	2.0	0.10	25	86.16	19.16	95.39	682.1	17.40
24	2.0	0.10	30	82.77	20.13	97.03	678.6	17.67
25	2.0	0.15	20	79.81	19.23	96.34	661.9	17.93
26	2.0	0.15	25	76.91	20.38	98.09	657.4	18.25
27	2.0	0.15	30	74.28	21.20	99.10	651.5	18.63

9.3.2.2. T_{50}

As shown in Figure 9.17 (A, C, E), all three factors had significant positive (i.e. response increases with increase in factor level) effect on response value. However, immediate release of enzyme for quicker on set of action and hence shorter T_{50} was the desirable criteria for the optimum formulation, hence low value of all three variables resulted the beads with T_{50} as low as 6.5 min (experiment 1, Table 9.10). T_{50} was found to be

proportional to the particle size and degree of crosslinking. As the concentration and hence the viscosity of alginate solutions incereases, larger beads (discussed under 'Particle size') with less surface porosity (Figure 9.18a-c) were obtained which took long time for complete dissolution and resulted in higher T_{50} (16-23 min; Table 9.10). Higher calcium concentration and hardening time caused penetration of calcium to the interior of the bead, resulted in increased crosslinking (Wang and He, 2002) (also increased surface roughness and porosity; Figure 9.18d-f), delayed dissolution and hence higher T_{50}.

9.3.2.3. T_{90}

Same as the T_{50}, all three factors had positive effect on this response which can be observed in Figure 9.17(B, D, F). The sodium alginate concentration was the most positively influencing factor amongst all three (higher T_{90} of the magnitude of 83-98 min; Table 9.10). None of the remaining two factors was affecting T_{90} significantly. However, both calcium chloride concentration and hardening time at higher level had synergistic positive action (experiment 25, 26, and 27; Table 9.10). T_{90} was also found to be proportional to the particle size and degree of crosslinking. For further explanation, see '*T_{50}*' above.

9.3.2.4. Particle Size

As shown in Figure 9.17(B, D, F), the sodium alginate concentration was the factor affecting the most. The bead size is influenced by the opening through which the alginate solution is allowed to pass (which was kept constant) and the viscosity of the alginate solution. Increased viscosity at higher concentration of sodium alginate resulted in larger

particles (660-715 μm; Table 9.10). Calcium chloride concentration and hardening time had the negative effect on the particle size. High calcium chloride concentration and hardening time caused shrinkage of beads and resulted in smaller particle size (experiment 25, 26, and 27; Table 9.10) due to high degree of crosslinking. (Wang and He, 2002) Though the negative effect of calcium chloride concentration and hardening time was of less magnitude, they contribute to the morphology of the beads and surface became rougher and porous (Figure 9.18d-f).

9.3.2.5. Angle of Repose

Here, too, the sodium alginate concentration had significant positive effect on angle of repose. However, calcium chloride concentration and hardening time had synergistic positive effect at higher levels (experiment 25, 26, and 27; Table 9.10), their individual effect were negligible. Particle size increased with increase in sodium alginate concentration and resulted in decreased angle (lowest angle of 16.14, experiment 3; Table 9.10). Higher calcium chloride concentration and hardening time resulted in smaller beads with irregular surface due to shrinkage and showed increased angle (from 16.14 to 18.89 in experiments 3 to 27 respectively).

9.3.3. OPTIMIZATION OF THE PROCESS USING THE GRAPHICAL EVALUATION

Generally the aim of the optimization of pharmaceutical formulations is to find the optimum levels of the variables, which affect a process, where a product of good characteristics could be produced. NN can be trained for predicting the response surface

and can be used for optimization within the experimental region. Contour plot of the NN predicted responses affected by two chosen variables are shown in Figure 9.17(A-F). The contours represent different combinations of two variables with the same response. Two responses namely % entrapment and T_{50} were selected for optimization of the process. The criteria for the optimum formulation selection were more than 90% entrapment and T_{50} of less than 10 min. From observing these figures it is clear that the more than 90% entrapment area coincides with the T_{50} area of less than 10 min. The study of these plots showed that the highest values of the entrapment and lowest value of T_{50} could be obtained at low values of all three process variables (i.e. at -1, -1, -1; experiment 1; Table 9.10).

9.3.4. EVALUATION OF MODEL USING CROSS-VALIDATION

In order to assess the reliability of the model, five cross-validation experiments were conducted by varying the process variables at values other than that of the model and responses were predicted using the trained network. A comparison between the experimental and predicted values of the responses for these additional experiments is presented in Table 9.12. Bias was calculated by the following equation:

Eq. 9.5

$$\text{Bias} = \left[\frac{(\text{predicted value} - \text{experimental value})}{\text{predicted value}}\right] \times 100$$

It can be seen that in all cases there was a reasonable agreement between the NN predicted and the experimental value, since low value of the bias were found. For this reason it can be concluded that the NN predicted responses describe adequately the influence of the selected process variables on the responses under study and NN can be used successfully as a predictive and optimizing tool.

Table 9.12: Comparison of responses between predicted and experimental values for the cross-validation set.

Responses	Test	Factors/levels			Experimental values	Predicted values	Bias%
		A	B	C			
% Entrapment	1	-1	-0.6	-0.6	90.72	89.04	1.9
	2	-0.6	0	0.4	81.15	82.98	2.2
	3	-0.4	0.6	0	76.01	77.65	2.1
	4	0	-0.4	0.6	84.58	87.13	2.9
	5	0.4	0.4	-0.4	86.06	84.17	2.2
T_{50}	1	-1	-0.6	-0.6	7.81	8.04	2.9
	2	-0.6	0	0.4	12.83	12.79	0.4
	3	-0.4	0.6	0	14.47	14.31	1.1
	4	0	-0.4	0.6	16.23	16.07	1.0
	5	0.4	0.4	-0.4	17.09	17.58	2.7
T_{90}	1	-1	-0.6	-0.6	24.68	24.27	1.7
	2	-0.6	0	0.4	56.33	54.47	3.4
	3	-0.4	0.6	0	72.15	73.18	1.4
	4	0	-0.4	0.6	75.61	76.88	1.7
	5	0.4	0.4	-0.4	88.63	90.90	2.5
Particle size	1	-1	-0.6	-0.6	161.7	150.7	7.3
	2	-0.6	0	0.4	180.7	166.2	8.8
	3	-0.4	0.6	0	172.8	182.6	5.4
	4	0	-0.4	0.6	285.9	273.8	4.4
	5	0.4	0.4	-0.4	414.6	435.0	4.7
Angle of repose	1	-1	-0.6	-0.6	22.29	23.01	3.1
	2	-0.6	0	0.4	21.95	22.98	4.5
	3	-0.4	0.6	0	23.56	22.78	3.4
	4	0	-0.4	0.6	19.89	20.47	2.8
	5	0.4	0.4	-0.4	18.90	19.44	2.8

9.3.5. CHARACTERIZATION OF OPTIMAL FORMULATION

9.3.5.1. Effect of pH on Release Profile

The effect of pH on the release of papain from calcium alginate beads in different pH (1.2, 4.0, 5.4, 6.8, 7.4, and 8.0) buffers simulating the human gastrointestinal tract is given in Figure 9.19(A). Release profile of optimized batch in simulated intestinal fluid without enzyme is shown in Figure 9.19(B). Generally, higher molecular weight and

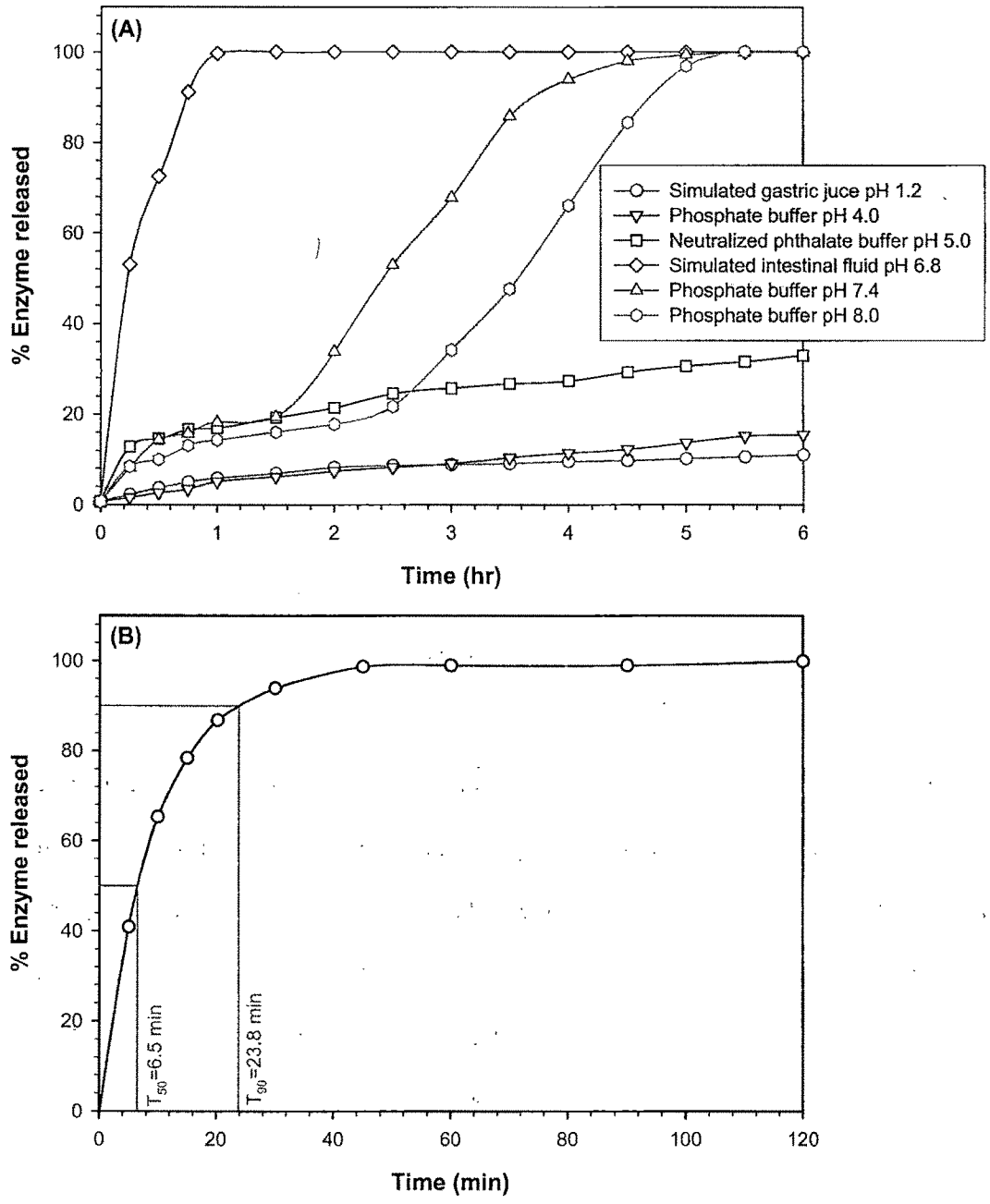

Figure 9.19: (A) The effect of pH on the release profile of papain in different buffers simulating the human gastrointestinal tract (B) *'In vitro'* release profile of optimized batch in simulated intestinal fluid without enzyme.

poorly water-soluble drugs are not released from calcium alginate beads due to stability and non swelling property in acidic environment while swell and disintegrate in intestinal fluid. (Yotsuyanagi et al., 1987; Kim and Lee, 1992) This was further confirmed by very

low amount of papain release in the acidic media (pH 1.2, 4.0, and 5.4) due to higher molecular weight. The swelling and disintegration of calcium alginate beads are dependent on compositions of dissolution medium, e.g. sodium and phosphate, and solubility of drug entrapped into alginate beads. (Ostberg et al., 1994) The swelling and disintegration of alginate beads in intestinal fluid (pH 6.8) were due to the affinity of calcium to phosphate and sodium/calcium exchange. However, the complete release profile was delayed up to 6 hr as the pH increased (7.4 and 8.0) despite the presence of sodium and phosphate. This study confirms the site specific papain delivery to the intestine rather than the stomach.

9.3.5.2. Fourier Transform Infra-red Spectroscopy (FTIR)

FTIR spectra of papain, sodium alginate, calcium alginate blank beads, papain loaded optimized batch, and physical mixture of papain and blank beads are shown in Figure 9.20. FTIR spectrum of sodium alginate powder showed various distinct peaks of alginate: hydroxyl at 3263.33 cm^{-1}, carbonyl at 1600.81 cm^{-1}, and carboxyl and carboxylate at about 1000–1400 cm^{-1} (Figure 9.20b). Crosslinking of alginate by Ca^{2+} was shown by a decrease in the wavenumber of carbonyl peak from 1600.81 to 1579.32 cm^{-1}. The hydroxyl peak of calcium alginate had a higher value of wavenumber than that of the sodium alginate (Figure 9.20c). This was probably due to a negative effect on bond formation involving adjacent hydroxyl groups as a result of conformational changes of alginate after reacting with Ca^{2+}. (Wong et al., 2002) With incorporation of papain, the spectrum of beads (Figure 9.20e) was similar to that of the calcium alginate blank beads (Figure 9.20d). However, the physical mixture of papain and calcium alginate blank

beads showed the peaks due to both papain and calcium alginate. This confirms the papain entrapment into the alginate beads at molecular level.

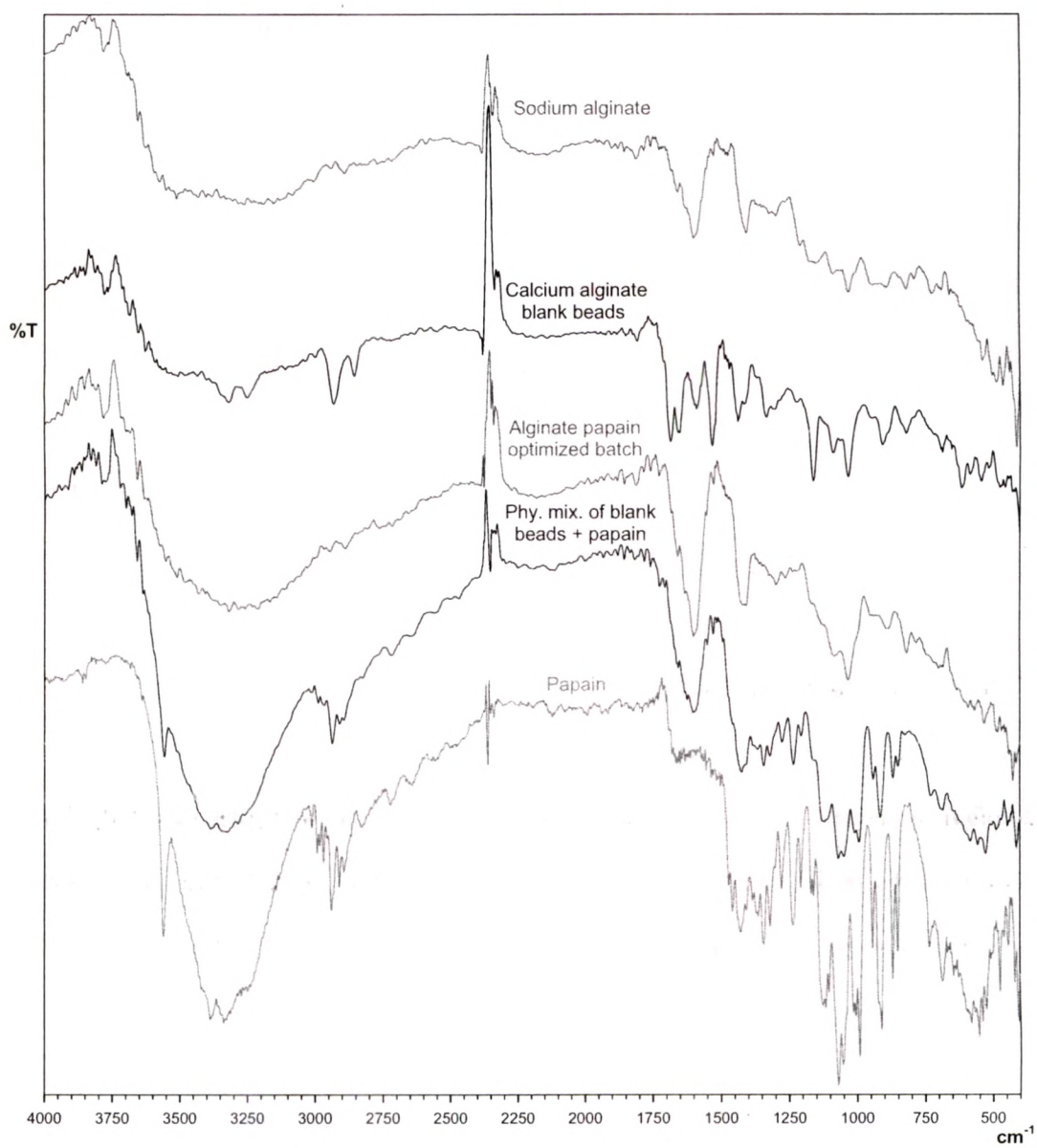

Figure 9.20: The FTIR spectra of papain, sodium alginate, blank calcium alginate beads, papain-loaded alginate beads, and physical mixture of papain and blank calcium alginate beads.

9.3.5.3. Differential Scanning Calorimetry (DSC)

The DSC thermograms of papain, sodium alginate, blank calcium alginate beads and papain-loaded beads are shown in Figure 9.21. The degradation exotherm of sodium alginate at 252°C was absent in blank calcium alginate bead and an additional endothermic peak at 221°C corresponding to alginate-calcium interaction was observed. Similar results were reported by Fernandez-Hervas et al. (Fernandez-Hervas et al., 1998) The papain exhibits sharp endothermic peak at 196°C while the melting peak shape of papain-loaded alginate beads was similar to the blank beads and did not show any peak at 196°C. This confirms that the most of the enzyme was uniformly dispersed at the molecular level in the beads.

9.3.5.4. Morphology of the Beads

The spherical shape of beads in wet state was usually lost after drying especially for beads prepared with low alginate concentration. In 1.0% (w/v) alginate, the dried beads were very irregular and tend to agglomerate due to low mechanical strength. With the increasing of alginate concentration (2.0% w/v), the shape of beads changed to a spherical disc with a collapsed center (Figure 9.22). Normally the spherical shape was retained when the alginate concentration was as high as 5.0% (w/v), but viscosity of 5.0% w/v solution was too high for bead preparation under present experimental conditions so it was not studied. These results indicated that the shape of calcium alginate beads was seriously destroyed in the drying process, and the spherical shape of dried beads improved with the increase of alginate concentration. It was reported by Skjåk-Bræk et al. (Skjak-Brae et al., 1989) that calcium alginate beads usually have a heterogeneous

structure with dense surface layer and loose core due to the heterogeneous gelation mechanism, which resulted in the collapse of beads during the drying process.

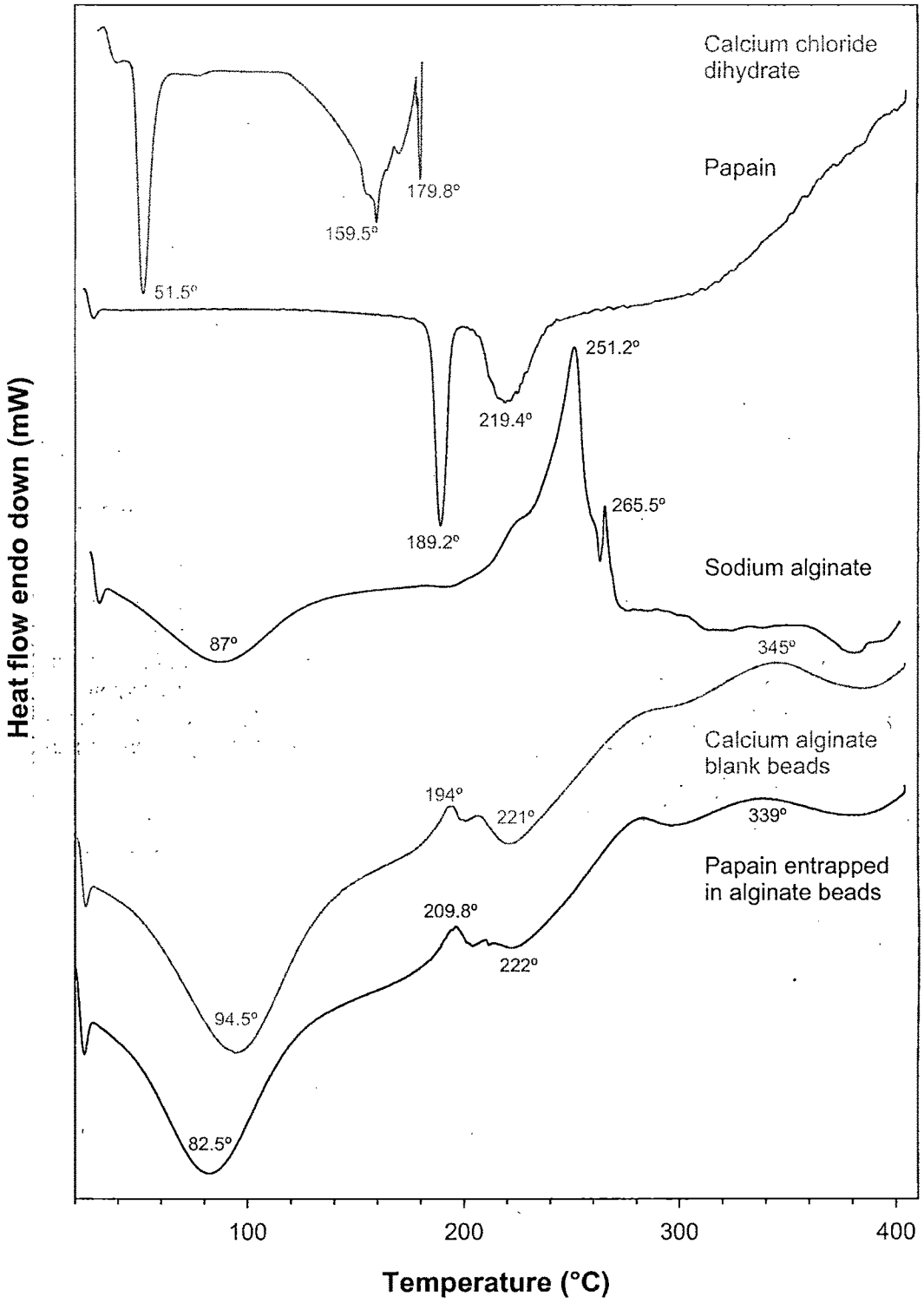

Figure 9.21: The DSC thermograms of papain, sodium alginate, blank calcium alginate beads, and papain-loaded alginate beads made at the same analytical conditions.

Figure 9.22: The scanning electron micrograph of dried alginate bead at 100X magnification (bar at the right bottom is equivalent to 100 μm).

9.3.6. STABILITY STUDY

For the developed formulation, the similarity factor (f_2) was calculated by a comparison of the dissolution profiles at each storage condition with the control at the initial condition. Results of f_2 factors ranged from 76 to 98 or 2 to 5% average difference. In addition to the dissolution profiles, capsule potency results for all stability conditions

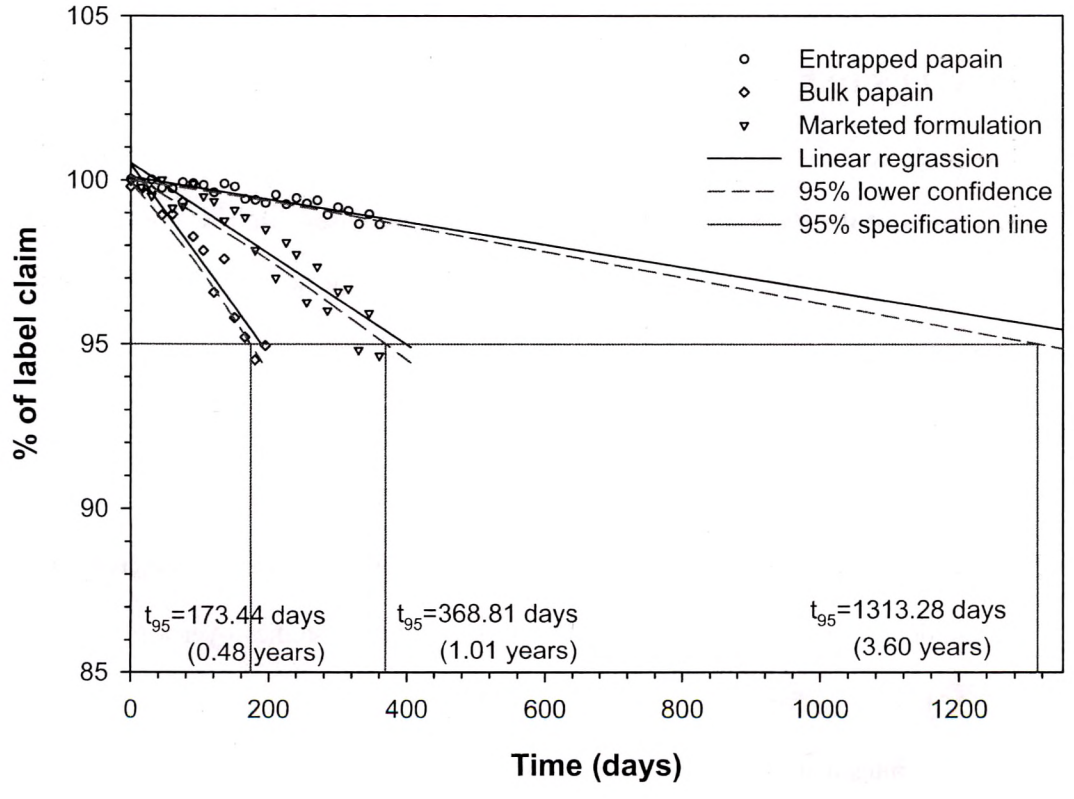

Figure 9.23: Extrapolation of accelerated stability data of developed formulation, marketed formulation and bulk papain for shelf-life calculation.

were within 90–110% of label claim. Overall, results from the stability studies indicated that capsules were physically and chemically stable for at least 12 months at 40±2°C/75±5% relative humidity and for more than 12 months (approximately for double time period) at 30±2°C/65±5% relative humidity.

An approach for analyzing the data on a quantitative attribute that is expected to change with time is to determine the time at which the 95% one-sided confidence limit for the mean curve intersects the acceptance criterion (not more than 5% change in assay from its initial value). The accelerated stability data for prepared formulation, marketed formulation and the bulk papain were extrapolated to calculate the shelf-life (Figure 9.23) and were found be 3.60 years, 1.01 year, and 0.48 year respectively. Hence, the stability of the entrapped papain was significantly improved than the conventional dosage forms.

9.3.7. CONCLUSIONS

The optimization of the process using the NN predicted responses resulted in more than 90% entrapment and les than 10 min of T_{50} at low levels of all three process variables (1.0% sodium alginate, 0.05 M calcium chloride, and 20 min hardening time). Entrapment of papain in alginate beads was confirmed using FTIR and DSC study. Texture analysis of the beads formulations illustrated that the degree of crosslinking decreased with increase in sodium alginate concentration while increased with increase in calcium chloride concentration and hardening time. Dissolution studies over a pH range similar to the human gastrointestinal tract demonstrated that alginate beads can be used for site specific intestinal delivery of papain. Accelerated and long term stability study illustrated considerable improvement in shelf-life of papain entrapped in alginate beads than the conventional dosage form.

9.4. References

CARTER, S.J., 1986. Tutorial Pharmacy, 6th Ed., CBS Publishers & Distributors, New Delhi, India, pp. 225-226.

FERNANDEZ-HERVAS, M.J., HOLGADO, M.A., FINI, A. and FELL, J.T., 1998. In vitro evaluation of alginate beads of a diclofenac salt. Int. J. Pharm. 163, 23-34.

IANNUCCELLI, V., COPPI, G., BERNABEI, M.T. and CAMERONI, R., 1998. Air compartment multiple-unit system for prolonged gastric residence. Part I. Formulation study. Int. J. Pharm. 174, 47-54.

KIM, C.-K. and LEE, E.-J., 1992. The controlled release of blum dextran from alginate beads. Int. J. Pharm. 79, 11-19.

LEE, B.-J. and MIN, G.-H., 1995. Preparation and release characteristics of polymer-reinforced and coated alginate beads. Arch. Pharm. Res. 18, 183-188.

LEE, BEOM-JIN and MIN, GEUN-HONG, 1996. Oral controlled release of melatonin using polymer-reinforced and coated alginate beads. Int. J. Pharm. 144, 37-46.

MONTGOMERY, DOUGLAS C., 2001. Ch 1. Introduction. in: Design and Analysis of Experiments, 5th Ed., John Wiley & Sons, Inc., New York, pp. 1-20.

OSTBERG, T., LUND, E.M. and GRAFFNER, C., 1994. Calcium alginate matrices for oral multiple unit administration. IV Release characteristics in different media. Int. J. Pharm. 112, 241-248.

OSTBERG, T., VESTERHUS, L. and GRAFFNER, C., 1993. Calcium alginate matrices for oral multiple unit administration: II. Effect of process and formulation factors on matrix properties. Int. J. Pharm. 97, 183-193.

POLK, A., AMSDEN, B., YAO, K.D., PENG, T. and GOOSEN, M.F.A., 1994. Controlled release of albumin from chitosan-alginate microcapsules. J. Pharm. Sci. 83, 178-185.

RATSIMBAZAFY, VOAHIRANA, BOURRET, EVELYNE, DUCLOS, ROSELYNE and BROSSARD, CLAUDE, 1999. Rheological behavior of drug suspensions in Gelucire® mixtures and proxyphylline release from matrix hard gelatin capsules. Eur. J Pharm. Biopharm. 48, 247-252.

SHU, X.Z. and ZHU, K.J., 2002. The release behavior of brilliant blue from calcium-alginate gel beads coated by chitosan: the preparation method effect. Eur. J. Pharm. Biopharm. 53, 193-201.

SKJAK-BRAE, G., GRASDALEN, K.H., DRAGET, K.I. and SMIDSROD, O., 1989. Inhomogeneous poysaccharide ionic gels. Carbohydr. Polym. 10, 31-54.

WANG, KANG and HE, ZHIMIN, 2002. Alginate-konjac glucomannan-chitosan beads as controlled release matrix. Int. J. Pharm. 244, 117-126.

WONG, TIN WUI, CHAN, LAI WAH, KHO, SHYAN BIN and HENG, PAUL WAN SIA, 2002. Design of controlled-release solid dosage forms of alginate and chitosan using microwave. J. Controlled Release 84, 99-114.

YOTSUYANAGI, T., OHKUBO, T., OHHASHI, T. and IKEDA, K., 1987. Calcium-induced gelation of alginic acid and pH-sensitive reswelling of dried gels. Chem. Pharm. Bull. 35, 1555-1563.

10. CARRAGEENAN BEADS

10.1. Carrageenan-Amylase Beads

10.1.1. EFFECT OF THE FACTORS ON RESPONSES

10.1.1.1. % Entrapment

ANOVA results and regression coefficients of response variables are shown in Table 10.2. All three process variables were statistically significant (P <0.05). From the contour plots of response surface for % entrapment (Figure 10.1;A-C) and Table 10.1, it can be concluded that concentration of κ-carrageenan was the most influencing factor (45.53%) and affecting positively (positive coefficient; Table 10.2; i.e. response increases with increase in factor level). However, potassium chloride concentration and hardening time were affecting negatively (negative coefficient; Table 10.2; i.e. response decreases with increase in factor level) in significant amount. More than 84% entrapment (experiment 4) was obtained at the high level of the κ-carrageenan concentration especially when it was followed by the low levels of the other two factors.

On addition of κ-carrageenan solution to a potassium chloride solution, instantaneous interfacial crosslinking takes place followed by a more gradual gelation of the interior and causes loss of enzyme from the beads, which was found to be proportional to the degree of crosslinking. Increase in viscosity with increase in κ-carrageenan concentration may retard penetration of potassium to the interior of the bead, resulted in decreased crosslinking (also decreased surface roughness and porosity; Figure 10.2;D-E) and hence

increased entrapment efficiency. Degree of crosslinking increased with increase in potassium concentration and contact time, and so entrapment efficiency decreased. The entrapment efficiency of the α-amylase containing beads prepared with calcium alginate

Table 10.1: Factorial 3^3: matrix of the experiments and results for the measured responses and the composite index.

ES[a]	Factors/levels			Responses				Transformed		Comp-osite Index (CI)
	Carrag-eenan (% w/v)	KCl (M)	Harde-ning Time (min)	% Immobi-lization	T_{50}	T_{90}	Particle Size ± SD[b] (mm)	% Immobi-lization	T_{90}	
9	-1	-1	-1	65.34	17.15	25.50	1.83±0.19	19.85	50.00	19.85
13	-1	-1	0	62.40	19.20	29.70	1.80±0.17	15.28	45.71	19.57
2	-1	-1	1	60.29	22.10	33.65	1.76±0.18	11.99	41.67	20.32
24	-1	0	-1	62.11	22.30	32.50	1.68±0.20	14.82	42.84	21.98
17	-1	0	0	59.25	25.45	38.60	1.65±0.19	10.37	36.61	23.77
6	-1	0	1	57.24	29.10	44.10	1.61±0.20	7.24	30.98	26.26
1	-1	1	-1	57.27	28.86	42.35	1.63±0.19	7.29	32.77	24.52
27	-1	1	0	54.49	32.65	46.10	1.60±0.20	2.96	28.94	24.02
10	-1	1	1	52.59	36.40	49.70	1.56±0.17	0.00	25.26	24.74
23	0	-1	-1	78.79	24.50	35.30	2.09±0.20	40.80	39.98	50.82
8	0	-1	0	75.97	28.75	41.10	2.06±0.16	36.41	34.05	52.36
15	0	-1	1	73.96	33.05	46.05	2.02±0.17	33.28	28.99	54.29
12	0	0	-1	76.65	30.75	41.50	1.95±0.20	37.46	33.64	53.82
26	0	0	0	73.92	33.70	44.15	1.92±0.19	33.21	30.93	52.28
19	0	0	1	72.02	37.75	50.90	1.88±0.20	30.26	24.03	56.23
3	0	1	-1	70.68	37.86	50.83	1.90±0.22	28.17	24.10	54.07
18	0	1	0	68.00	42.05	55.20	1.87±0.19	24.00	19.63	54.36
21	0	1	1	66.18	44.60	62.95	1.83±0.18	21.16	11.71	59.45
4	1	-1	-1	84.70	31.50	45.40	2.43±0.19	50.00	29.65	70.35
25	1	-1	0	82.02	35.90	49.30	2.41±0.19	45.83	25.66	70.16
11	1	-1	1	80.13	40.95	56.20	2.38±0.18	42.88	18.61	74.27
22	1	0	-1	82.30	38.47	51.90	2.29±0.17	46.26	23.01	73.26
14	1	0	0	79.79	42.10	56.05	2.27±0.19	42.35	18.76	73.59
7	1	0	1	78.03	45.50	62.00	2.24±0.19	39.61	12.68	76.93
5	1	1	-1	77.80	45.60	60.50	2.26±0.18	39.26	14.21	75.04
16	1	1	0	75.42	48.30	67.80	2.24±0.18	35.55	6.75	78.80
20	**1**	**1**	**1**	**73.79**	**51.40**	**74.40**	**2.21**±0.18	**33.01**	**0.00**	**83.01**

[a] ES, experimental sequence.
[b] SD, standard deviation (n=50).

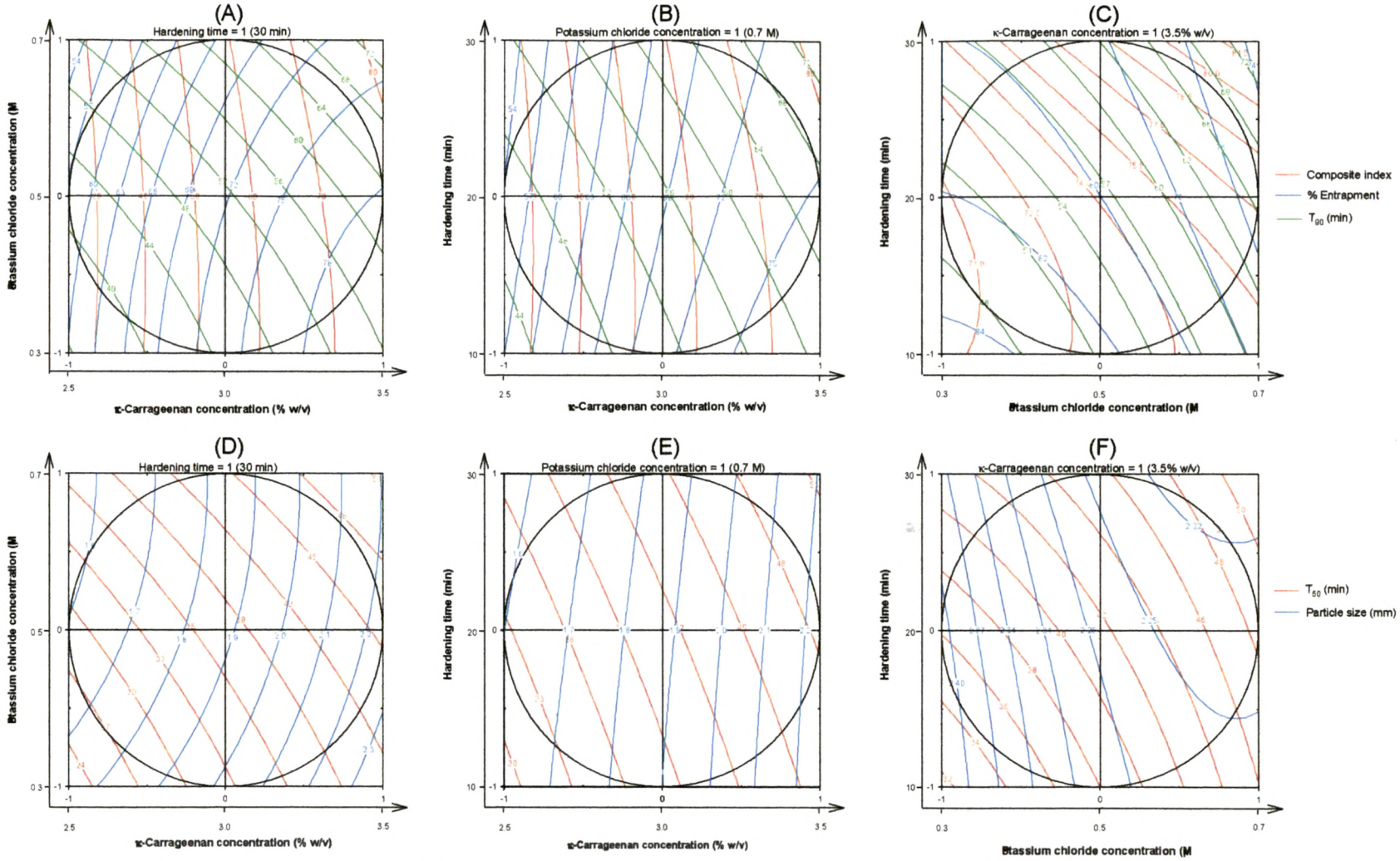

Figure 10.1: Contour plots of composite index, % entrapment, T_{90}, T_{50}, and particle size as a function of sodium carrageenan concentration, potassium chloride concentration, and hardening time.

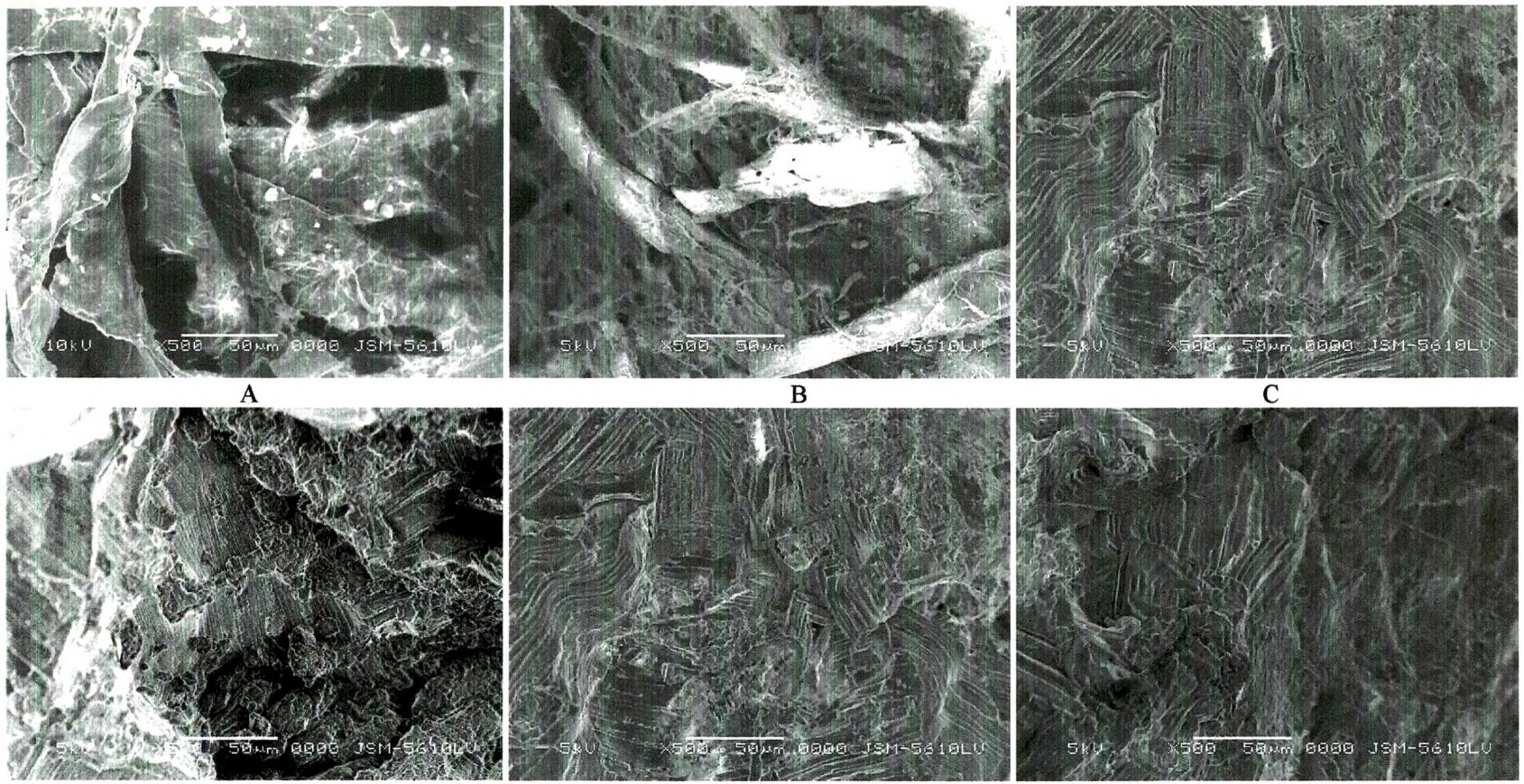

Figure 10.2: SEM micrographs and surface morphology of carrageenan beads: (A–C) Effect of potassium chloride concentration (κ-carrageenan concentration 3.0% w/v) (A) 0.3 M, (B) 0.5 M, and (C) 0.7 M potassium chloride concentration. (D–F) Effect of κ-carrageenan concentration (potassium chloride concentration 0.7 M) (D) 2.5% w/v, (E) 3.0% w/v, and (F) 3.5% w/v κ-carrageenan concentration.

Table 10.2: ANOVA results (*P* values): Effect of the variables on % entrapment, T_{50}, T_{90}, particle size and composite index.

Factors	% Entrapment		T_{50}		T_{90}		Particle size		Composite index	
	Coefficient	*P*	Coefficient	*P*	Coefficient	*P*	Coefficient	*P*	Coefficient	*P*
Intercept	73.73	<0.0001*	33.97	<0.0001*	45.10	<0.0001*	1.92	<0.0001*	52.96	<0.0001*
A	10.17	<0.0001*	8.14	<0.0001*	10.08	<0.0001*	0.31	<0.0001*	26.13	<0.0001*
B	-3.74	<0.0001*	6.37	<0.0001*	8.20	<0.0001*	-0.09	<0.0001*	2.56	<0.0001*
C	-2.30	<0.0001*	3.55	<0.0001*	5.23	<0.0001*	-0.03	<0.0001*	1.77	<0.0001*
A^2	-3.85	<0.0001*	-0.58	0.0068*	0.98	0.0929	0.04	<0.0001*	-4.99	<0.0001*
B^2	-1.37	<0.0001*	0.74	0.0009*	2.03	0.0016*	0.05	<0.0001*	-0.06	0.8971
C^2	0.30	0.0609	0.24	0.2173	0.98	0.0939	-0.005	0.0126*	1.47	0.0060*
AB	0.32	0.0120*	-0.21	0.1672	0.21	0.6308	0.008	<0.0001*	0.71	0.0664
AC	0.15	0.2228	0.25	0.1032	0.64	0.1484	0.005	0.0025*	0.88	0.0256*
BC	0.10	0.3757	-0.24	0.1169	0.30	0.4820	0.000	1.0000	0.48	0.2083
ABC	0.02	0.8688	-0.78	0.0003*	0.49	0.3622	0.000	1.0000	0.54	0.2466
$r^2_{adj.}$	0.9979	-	0.9965	-	0.9820	-	0.9996	-	0.9962	-

Regression coefficients are in coded values.

* Statistically significant (*P* <0.05)

(sodium alginate and calcium chloride) and chitosan-alginate was 91% and 90% respectively, using κ-carrageenan the α-amylase entrapment efficiency in our study did not exceed 85%, although the same method was used. So with chitosan or alginate more efficient entrapment was achieved (Bodmeier and Wang, 1993).

10.1.1.2. T_{50} and T_{90}

As shown in Figure 10.1 and Table 10.2, all three factors had significant positive effect on both response values. The concentration of κ-carrageenan concentration (factor A) had the most significant effect. For maximum activity of enzyme in the intestine longer T_{50} and T_{90} were the desired criteria for the optimum formulation. Thus, extreme level of all three variables resulted the beads with T_{50} and T_{90} as high as 51.4 and 74.4 min respectively (experiment 20, Table 10.1). T_{50} and T_{90} were found to be proportional to particle size and degree of crosslinking. As the concentration and hence the viscosity of κ-carrageenan incereases, larger beads (discussed under 'Particle size') were obtained which took long time for complete dissolution and resulted in higher T_{50} and T_{90}. The increase of the in vitro release rates of α-amylase from carrageenan beads prepared with low concentrations of potassium chloride solutions may be due to the less crosslinked structure of the beads which may result in a more porous matrix (Figure 10.2;A-C) and higher drug release (Garcia and Ghaly, 1996; Sipahigil and Dortunc, 2001). Higher hardening time caused penetration of potassium to the interior of the bead, resulted in increased crosslinking, and hence higher T_{50} and T_{90}.

10.1.1.3. Particle Size

As depicted in Table 10.2, the κ-carrageenan concentration (factor A; most influential; 56.77%) had positive coefficient, while potassium chloride concentration and hardening time had negative coefficient. In contrast to the finding of Sipahigil (Sipahigil and Dortunc, 2001) and Bhardwaj (Bhardwaj et al., 1995), all three process variables were statistically significant ($P<0.05$). Freely water soluble drug always entrapped in higher ratio and results in bigger particles. (Sipahigil and Dortunc, 2001) The bead size is influenced by the opening through which the κ-carrageenan is allowed to pass (which was kept constant) and the viscosity of the carrageenan solution. Increased viscosity at higher concentration of κ-carrageenan resulted in larger particles. High potassium chloride concentration and hardening time resulted in smaller particle size due to high degree of crosslinking. Though the negative effect of potassium chloride concentration and hardening time was of less magnitude, they contribute to the morphology of the beads (Figure 10.2;A-C).

10.1.2. INTERACTIONS BETWEEN THE FACTORS

An interaction is the failure of a factor to produce the same effect on the response at the different levels of the other factor. The ANOVA results (Table 10.2) showed that interaction AB had significant influence on % entrapment, ABC had significant influence on T_{50}, while AB and AC had significant influence on particle size. The analysis of the results by multiple regression (Table 10.2) leads to equations that adequately describe the influence of the selected factors on % entrapment, T_{50}, T_{90}, particle size, and composite index.

10.1.3. OPTIMIZATION OF THE PROCESS USING THE COMPOSITE INDEX

Generally the aim of the optimization is to find the optimum levels of the variables, which affect a process, where a product of desired characteristics could be produced easily and reproducibly. Using the composite index, both selected responses (% entrapment and T_{90}) were combined in one response. As it has been already discussed, the composite index was calculated from the individually calculated transformed value of each of the responses using the Eq. 7.1–7.2. The equation found out using multiple regression was as follow (coded factors):

Eq. 10.1 $$CI = 62.87 + 5.53A - 14.22B - 8.93C - 7.00A^2 - 4.22B^2 - 0.53C^2 + 0.28AB - 0.43AC - 0.15BC - 0.46ABC \quad (r^2_{adj.} = 0.9822,\ P < 0.0001)$$

In Figure 10.1;A-C the contour plots that describe the influence of the independent factors on the composite index is presented. The study of these plots and Table 10.1 showed that the highest values of the CI (83.01) could be obtained at high level of all three independent factors (experiment 20) and was considered as a batch fulfilling all the constraints favorable for the bead preparation.

10.1.4. EVALUATION OF MODEL USING CROSS-VALIDATION

In order to assess the reliability of the model, five experiments were conducted by varying the process variables at values other than that of the model. For each of these test experiments the responses were estimated by using the multiple regression equations and experimental procedure for comparison between both responses (Table 10.3). Bias was calculated by the following equation:

Eq. 10.2

$$\text{Bias} = \left[\frac{(\text{predicted value} - \text{experimental value})}{\text{predicted value}}\right] \times 100$$

It can be seen that in all cases there was a reasonable agreement between the predicted and the experimental value, since low value of the bias were found. For this reason it can be concluded that the equations describe adequately the influence of the selected process variables on the responses under study.

Table 10.3: Comparison of responses between predicted and experimental values for the cross-validation set.

Responses	Test	Factors/levels			Experimental values	Predicted values	Bias%
		A	B	C			
% Entrapment	1	-1	-0.6	-0.6	63.26	62.50	1.2
	2	-0.6	0	0.4	65.34	63.70	2.5
	3	-0.4	0.6	0	66.23	68.08	-2.8
	4	0	-0.4	0.6	73.71	71.79	2.6
	5	0.4	0.4	-0.4	76.44	78.28	-2.4
T_{50}	1	-1	-0.6	-0.6	19.88	20.44	-2.8
	2	-0.6	0	0.4	30.28	31.10	-2.7
	3	-0.4	0.6	0	34.76	33.68	3.1
	4	0	-0.4	0.6	33.82	34.66	-2.5
	5	0.4	0.4	-0.4	38.44	37.96	1.2
T_{90}	1	-1	-0.6	-0.6	29.48	29.22	0.9
	2	-0.6	0	0.4	41.51	42.39	-2.1
	3	-0.4	0.6	0	46.83	46.09	1.6
	4	0	-0.4	0.6	45.57	46.66	-2.4
	5	0.4	0.4	-0.4	50.81	51.37	-1.1
Particle size	1	-1	-0.6	-0.6	1.75	1.71	2.1
	2	-0.6	0	0.4	1.73	1.76	-1.8
	3	-0.4	0.6	0	1.76	1.74	1.3
	4	0	-0.4	0.6	1.94	1.98	-2.2
	5	0.4	0.4	-0.4	2.03	2.06	-1.6
Composite index	1	-1	-0.6	-0.6	20.69	19.24	7.0
	2	-0.6	0	0.4	36.22	34.58	4.5
	3	-0.4	0.6	0	43.05	45.19	-4.9
	4	0	-0.4	0.6	53.41	51.54	3.5
	5	0.4	0.4	-0.4	63.02	66.45	-5.4

10.1.5. CURVE FITTING AND RELEASE MECHANISM

'In vitro' dissolution profile of the optimized batch is shown in Figure 10.3A. Release of α-amylase from κ-carrageenan beads in simulated gastric fluid is conceivably attributed to the presence of strongly acidic sulphate groups in the carrageenan molecule, that allow a certain degree of ionization to be maintained also at low pH (Bonferoni et al., 1994). Values of release exponent (n) and kinetic constant (K) were derived using Eq. 7.3 to 7.7 and are presented in Table 10.4. The enzyme release data show a good fit to the Korsmeyer-Peppas' power law release kinetics (Eq. 7.6) which can be confirmed by comparing the values of correlation coefficient (r) with that of the other models. The values of Korsmeyer-Peppas' release exponent (n) determined for the various formulations studied ranged from 1.29 to 2.42 suggesting the probable release by super case-II transport. The K_k values ranged from 0.0033 to 1.22 where low K_k value may suggest near to zero release from the beads initially. If one considers the correlation coefficient (r) values of zero-order and Korsemeyer-Peppas release models, both models describe the dissolution data reasonably well. Where there are competing models (with similar r values), residuals analysis can be used to distinguish between the models (Pather et al., 1998). Figure 10.3B is the residual plot for optimized formulation. The residuals are high for the zero-order, first-order, Higuchi, and Hixson-Crowell models (and least for the Korsemeyer-Peppas model) which also shows systematic deviation: the models overpredict initially and underpredict at the later stages of the dissolution process. This indicates that Korsemeyer-Peppes' power low is the best fit model in describing the dissolution behavior of α-amylase from κ-carrageenan beads.

Finally, in order to know whether the enzyme release was due to erosion or diffusion, the release data of the optimized formulation was fitted to Kopcha model (Eq. 7.8) and

parameters like A and B at different time intervals were determined (Figure 10.4). Throughout the release profile, A was <0 and B was >0, and expressed the predominance of erosion relative to diffusion. This probably may be due to the lower gel strength of carrageenan gels. During dissolution study carrageenan gel swell but is unable to maintain the gel matrix due to low gel strength and start to erode. However, the rate of hydration initially was found to be the rate limiting step of erosion rate and explain the biphasic nature of release profile (plateau initially followed by steep rise in erosion rate). The erosion term B increases with time because erosion of the hydrated layer is easier.

Table 10.4: Comparison of different dissolution kinetics models.

ES[a]	Release model										
	Zero-order		First-Order		Higuchi matrix		Korsmeyer-Peppas			Hixson-Crowell	
	K_o	r_0	K_1	r_1	K_H	r_H	n	K_k	r_k	K_s	r_s
9	3.19	0.97	-0.11	0.74	14.13	0.87	1.30	1.22	0.98	-0.02	0.87
13	2.53	0.96	-0.08	0.90	13.06	0.87	1.33	0.83	0.97	-0.02	0.94
2	2.31	0.96	-0.07	0.85	11.91	0.84	1.62	0.27	0.98	-0.01	0.92
24	2.33	0.96	*	*	12.04	0.85	1.38	0.61	0.97	-0.02	0.87
17	2.08	0.96	*	*	10.87	0.82	1.56	0.27	0.98	-0.02	0.82
6	1.75	0.95	*	*	10.30	0.83	1.71	0.12	0.97	-0.01	0.90
1	1.79	0.96	-0.06	0.86	10.60	0.84	1.50	0.27	0.97	-0.01	0.92
27	1.65	0.94	-0.05	0.83	9.68	0.81	1.94	0.04	0.98	-0.01	0.90
10	1.51	0.93	-0.05	0.79	8.93	0.78	2.21	0.01	0.96	-0.01	0.87
23	2.18	0.97	*	*	11.38	0.85	1.29	0.76	0.98	-0.02	0.84
8	1.93	0.95	-0.06	0.76	10.18	0.81	1.50	0.29	0.98	-0.01	0.86
15	1.65	0.95	-0.05	0.83	9.74	0.81	1.81	0.07	0.99	-0.01	0.90
12	1.86	0.94	-0.06	0.72	9.83	0.79	1.47	0.30	0.97	-0.01	0.83
26	1.66	0.94	-0.05	0.85	9.78	0.81	2.00	0.04	0.99	-0.01	0.90
19	1.32	0.92	-0.04	0.90	9.15	0.83	2.03	0.02	0.97	-0.01	0.92
3	1.50	0.94	*	*	8.90	0.79	1.81	0.06	0.97	-0.01	0.80
18	1.24	0.93	-0.05	0.86	8.59	0.81	2.04	0.02	0.97	-0.01	0.91
21	1.16	0.94	-0.04	0.84	8.09	0.80	2.14	0.01	0.94	-0.01	0.91
4	1.70	0.96	*	*	10.10	0.84	1.40	0.35	0.97	-0.01	0.89
25	1.55	0.95	-0.05	0.80	9.24	0.81	1.64	0.12	0.97	-0.01	0.88
11	1.25	0.94	*	*	8.73	0.82	1.77	0.05	0.96	-0.01	0.91
22	1.47	0.94	-0.05	0.71	8.83	0.80	1.69	0.09	0.98	-0.01	0.85
14	1.24	0.94	-0.04	0.88	8.61	0.82	2.01	0.02	0.98	-0.01	0.92
7	1.16	0.93	-0.04	0.86	8.02	0.80	2.42	0.00	0.98	-0.01	0.91
5	1.17	0.94	-0.04	0.82	8.17	0.81	1.61	0.08	0.96	-0.01	0.91
16	1.09	0.93	-0.04	0.79	7.58	0.79	2.22	0.01	0.97	-0.01	0.89
20	1.02	0.93	-0.03	0.80	7.13	0.78	2.23	0.00	0.95	-0.01	0.88

[a] ES, experimental sequence. * Not possible.

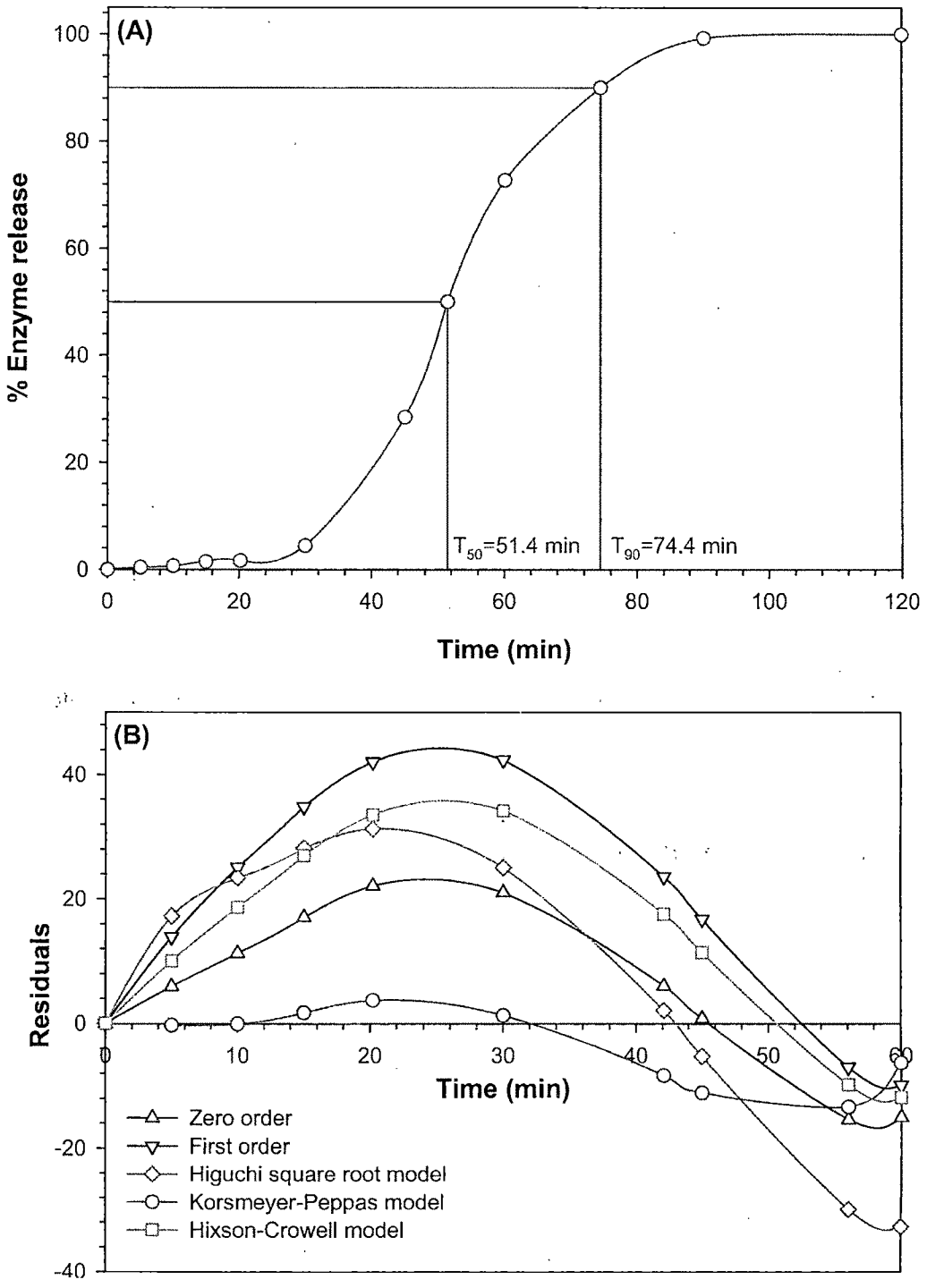

Figure 10.3: (A) 'In vitro' release profile of optimized formulation (experiment 20) in SGF without enzyme. (B) Residual plot of different release models for the same formulation.

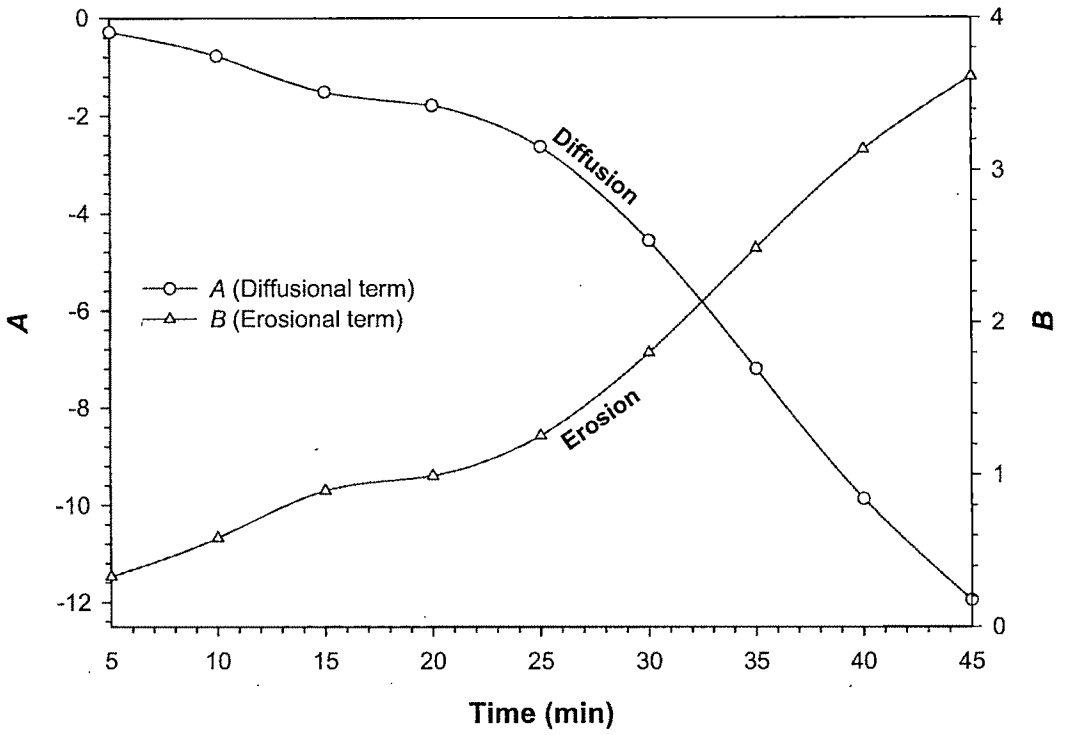

Figure 10.4: Kopcha model parameters (*A* and *B*) versus time profile for optimized batch (experiment 20).

10.1.6. CHARACTERIZATION OF OPTIMAL FORMULATION

10.1.6.1. Fourier transform infra-red spectroscopy (FTIR)

FTIR spectra of κ-carrageenan powder, carrageenan blank beads, α-amylase loaded carrageenan beads, physical mixture of α-amylase and blank beads, and α-amylase are shown in Figure 10.5. FTIR spectrum of κ-carrageenan powder showed various distinct peaks: very broad band spreading 3150-3600 cm^{-1} (strong; s) due to polyhydroxy $(-OH)_n$ group; 2968 cm^{-1} (s), 2920 cm^{-1} (s), and 2850 cm^{-1} (medium; m) due to C-H stretch; 1425 cm^{-1} (s) and 1375 cm^{-1} (s) due to C-H deformation; 1225 cm^{-1} (s) due to S=O stretch of sulfate ester salt; 1070 cm^{-1} due to C-O stretch of cyclic ethers; 925 cm^{-1} (s) due to C-O

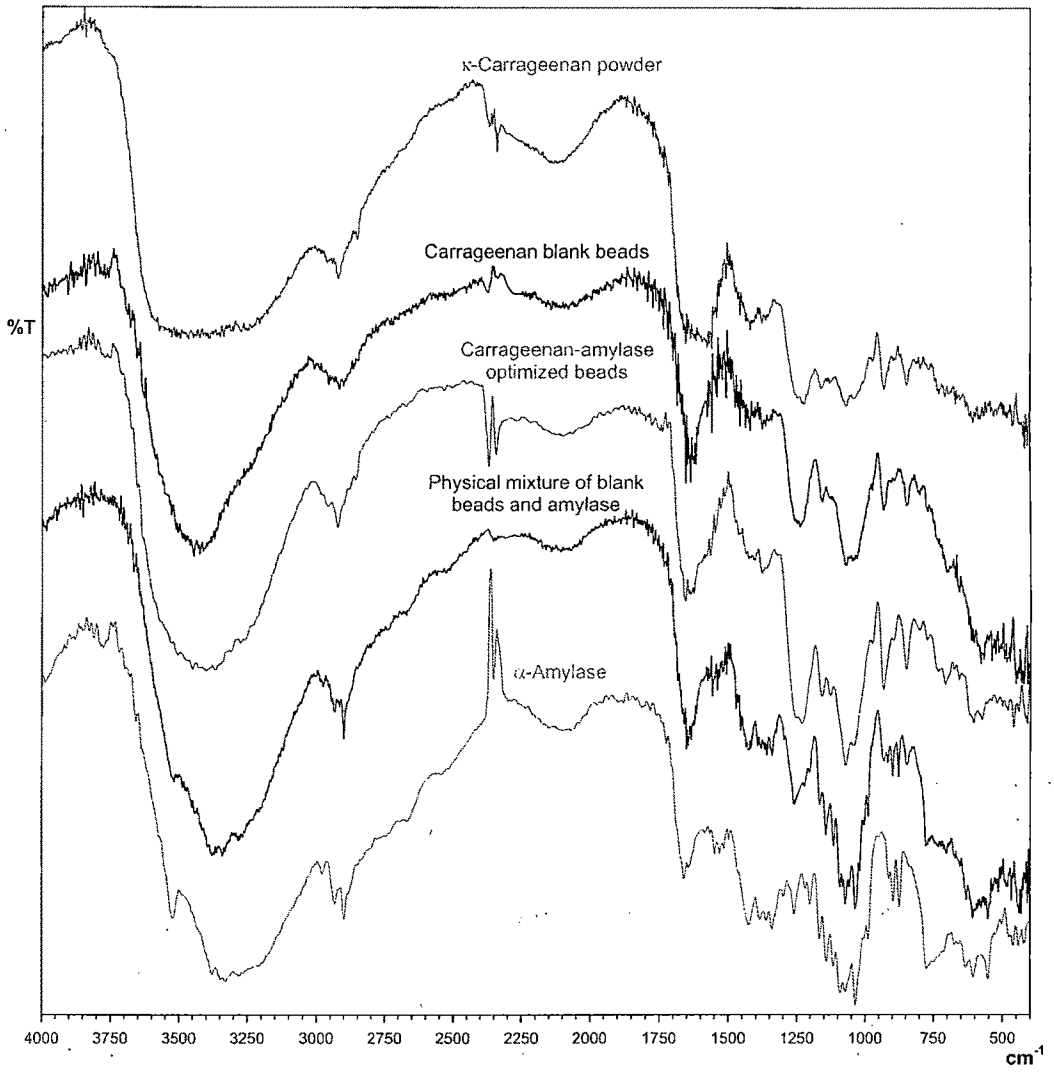

Figure 10.5: The FTIR spectra of κ-carrageenan powder, carrageenan blank beads, α-amylase loaded carrageenan beads, physical mixture of α-amylase and blank beads, and α-amylase.

stretch of polyhydroxy groups attached to carbons; etc. Crosslinking of carrageenan by K^+ was shown by a decrease in the intensity of S=O stretch (1225 cm^{-1}) of sulfate ester group which was same as C-O stretch (1070 cm^{-1}) of cyclic ethers in intensity for the κ-carrageenan powder. This was probably because of some negatively charged sulfate ester reacted with positively charged K^+ and resulted in physicochemical changes of carrageenan. α-Amylase also showed various distinct peaks: one predominant band at

3190-3380 cm^{-1} (s) due to N-H stretch of secondary N-substituted amides; 2980 cm^{-1} (weak; w) due to C-H stretch, medium bands at 1500-1650 cm^{-1} due to C...C, while 898 cm^{-1} (s) and 875 cm^{-1} (s) due to *p*-substituted aromatic out of plane C-H deformation of aromatic residue of tryptophan or tyrosine; 2931 cm^{-1} (s) and 2898 cm^{-1} (s) due to C-H stretch, while 1425 cm^{-1} (s), 1382 cm^{-1} (m), 1361 cm^{-1} (m), and 1340 cm^{-1} (m) due to C-H deformation of alkyl chain of amino acids; 1670 cm^{-1} due to C=O stretch of carboxylate anion and amide group; strong peaks between 1050-1200 cm^{-1}, weak bands at 550-600 cm^{-1}, and 400-450 cm^{-1} due to C-S stretch of sulfides and disulfides. With incorporation of α-amylase, the spectrum of beads was similar to that of the κ-carrageenan blank beads. However, the physical mixture of α-amylase and blank beads showed the peaks due to both α-amylase and κ-carrageenan. This confirms the amylase entrapment into the κ-carrageenan beads at molecular level.

10.1.6.2. Differential scanning calorimetry (DSC)

The DSC thermograms of potassium chloride, α-amylase, κ-carrageenan, blank beads, and α-amylase-loaded beads are shown in Figure 10.6. Potassium chloride showed two non significant exothermic peaks at 323° and 374°C. α-Amylase exhibited three endothermic peaks at 148.5°, 215.5°, and 226.8°C and one minor exothermic peak at 358°C. Broad endothermic peak at 85°C in the thermogram of κ-carrageenan was observed due to the presence of water molecules. Two minor peaks at 259° and 266°C in the degradation exotherm of κ-carrageenan were absent in blank beads and α-amylase loaded beads, while major exothermic peak at 344°C was found to be shifted towards higher temperature (355°C) in blank beads. This showed that, κ-carrageenan-KCl beads are more stable than κ-carrageenan. However, additional two peaks (one endothermic at

207° and one exothermic at 226.5°C) were observed in the thermogram of blank beads due to the potassium-κ-carrageenan interaction. DSC thermogram of enzyme loaded beads was similar to that of blank beads except all corresponding peaks were shifted to lower temperature, might be due to the presence of α-amylase. However, it did not showed any peak analogous to α-amylase. This confirms that most of the enzyme was uniformly dispersed at the molecular level in the beads.

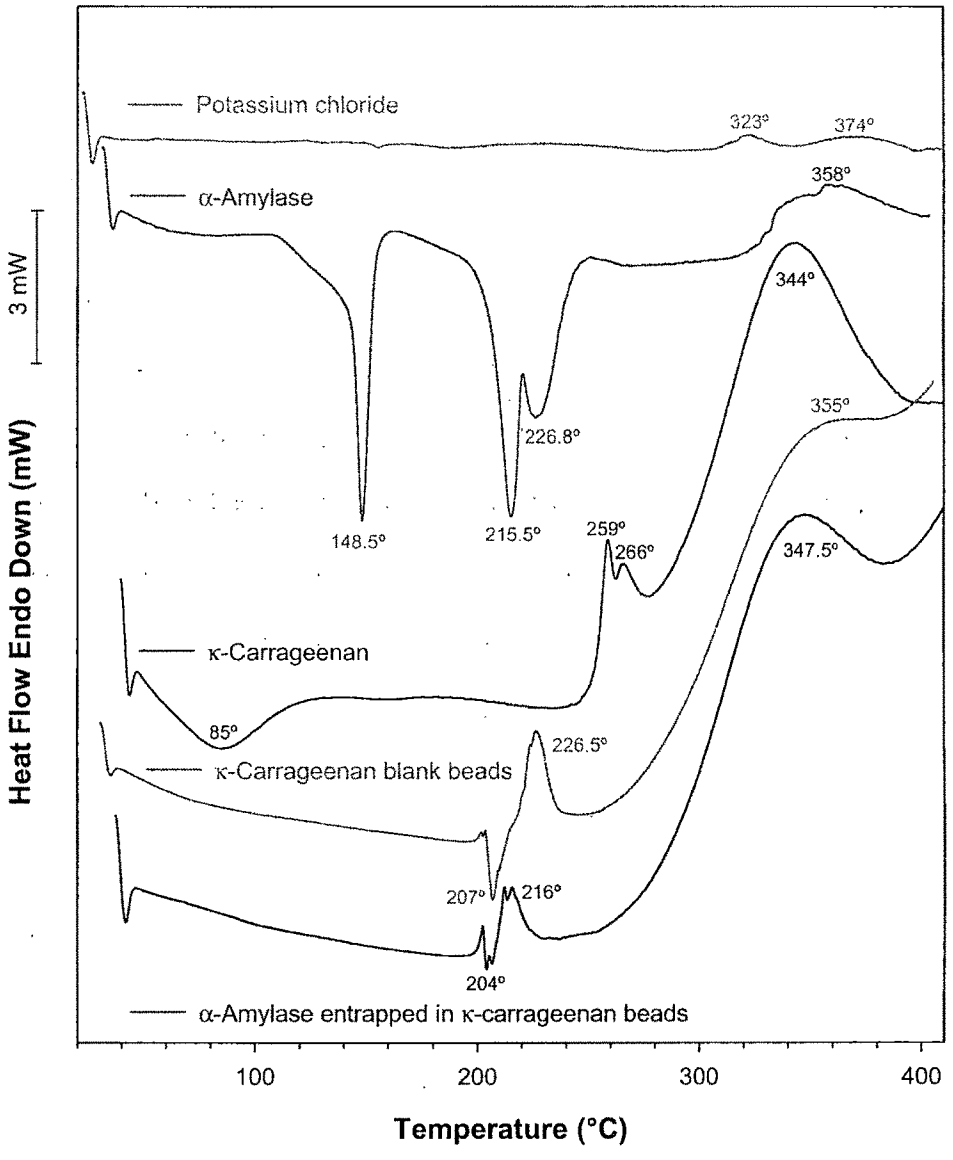

Figure 10.6: The DSC thermograms of potassium chloride, α-amylase, κ-carrageenan powder, blank beads, and α-amylase loaded carrageenan beads made at the same analytical conditions.

10.1.6.3. Morphology of the beads

The spherical shape of beads in wet state was usually lost after drying especially for beads prepared with low carrageenan concentration. In 2.5% w/v carrageenan, the dried beads were very irregular and tend to agglomerate due to low mechanical strength. With the increase of κ-carrageenan concentration (3.5% w/v), the shape of beads retained considerably. However, the shape of beads changed to disc with a collapsed center (Figure 10.7) during drying process due to aggregation of the helical fibers into bundles and the squeezing out of some water from the gel (Iborra et al., 1997). Normally the spherical shape was retained when the carrageenan concentration was as high as 5.0% (w/v), but viscosity of 5.0% w/v solution was too high for bead preparation under present experimental conditions so it was not studied. Crosslinked hydrogels reach an equilibrium swelling level in aqueous solutions which depends mainly on the crosslink density. In some cases, depending on the solvent composition, temperature and solids concentration during gel formation, phase separation can occur, and water-filled 'voids' or 'macropores' can form which can be observed Figure 10.2. One noticeable characteristic of the beads' surface is high degree of crosslinking when the concentration of potassium chloride increased (Figure 10.2;A-C). Further, the surface morphology was improved (i.e. decrease in roughness) with increase in κ-carrageenan concentration (Figure 10.2;D-F) due to the high viscosity of the κ-carrageenan solution.

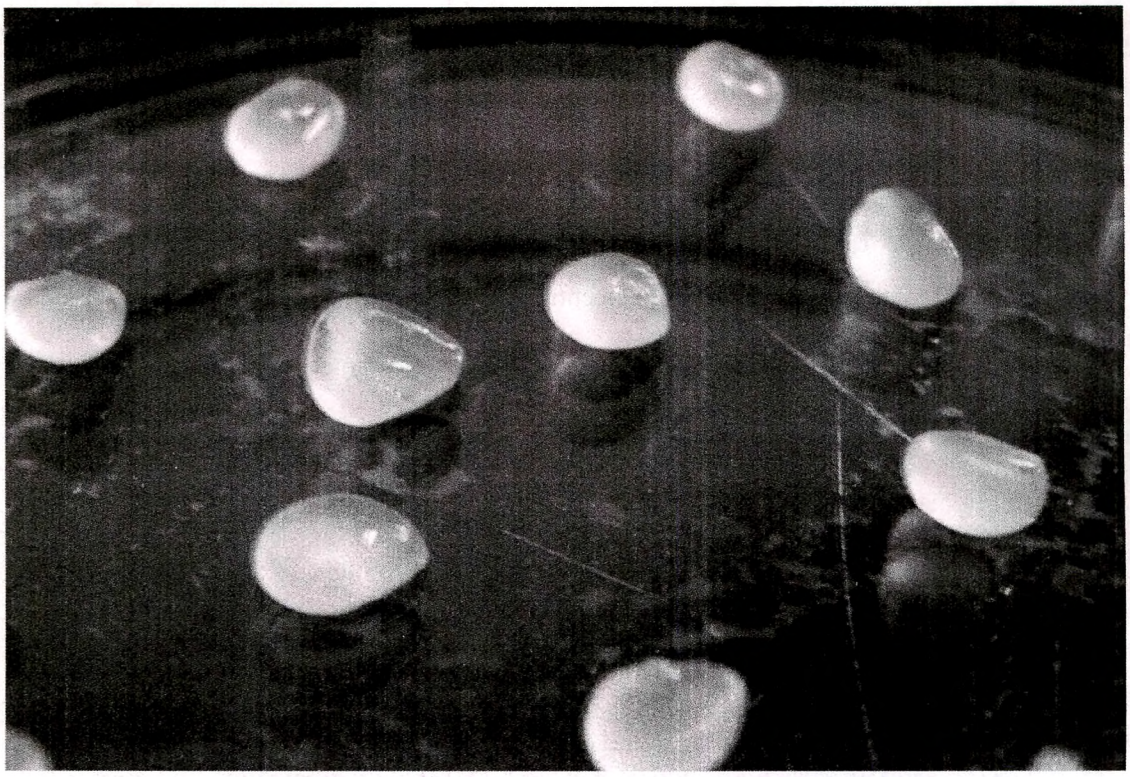

Figure 10.7: Photograph of wet κ-carrageenan beads showing spherical disk shape with collapsed centre during drying process.

10.1.7. STABILITY STUDY

For the formulation developed, the similarity factor (f_2) was calculated by a comparison of the dissolution profiles at each storage condition with the control at the initial condition. Results of f_2 factors ranged from 73 to 97 with 2 to 5% average difference. Overall, results from the stability studies indicated that capsules were physically and chemically stable for at least 12 months at 40±2°C/75±5% relative humidity and for more than 12 months (approximately for double time period) at 30±2°C/65±5% relative humidity.

An approach for analyzing the data on a quantitative attribute that is expected to change with time is to determine the time at which the 95% one-sided confidence limit for the

mean curve intersects the acceptance criterion (not more than 5% change in assay from its initial value). The accelerated stability data for prepared formulation, marketed formulation and the bulk α-amylase were extrapolated to calculate the shelf-life (Figure 10.8) and were found be 3.53 years, 0.99 year, and 0.41 year respectively. Hence, the stability of the entrapped α-amylase was significantly improved than that of the conventional dosage forms.

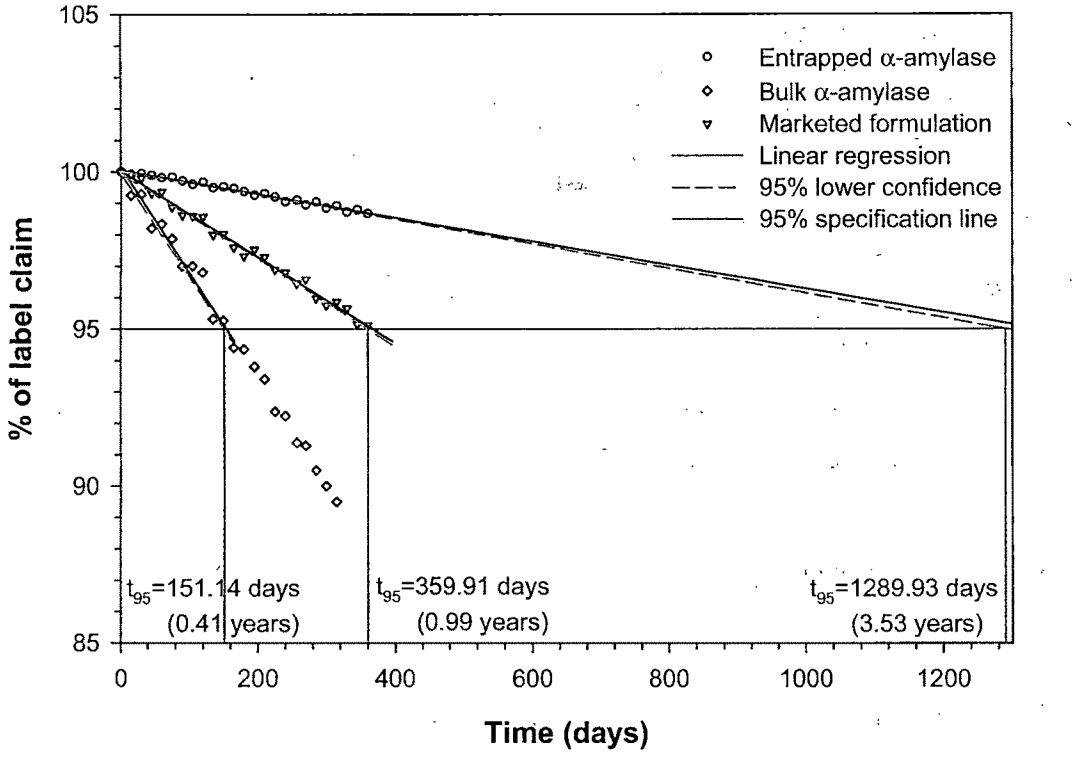

Figure 10.8: Extrapolation of accelerated stability data for shelf-life calculation.

10.1.8. CONCLUSIONS

Ionotropically corsslinked κ-carrageenan beads exhibit promising stability improvement of entrapped α-amylase and can find a place in the design of multiparticulate drug delivery systems. The optimization of the process using the composite index resulted in more than 73% entrapment and more than 74 min of T_{90} at high levels of all three process

variables. T_{50} and T_{90} were increased with increase in all three process variables. Percentage entrapment and particle size were found to be directly proportional to κ-carrageenan concentration and inversely proportional to potassium chloride concentration and hardening time. Mathematical analysis of the different drug release modalities has evidenced that enzyme release from carrageenan beads follows Korsmeyer-Peppas' power law equation with super case-II transport mechanism. Furthermore, investigation of release profile by Kopcha model revealed that enzyme release is due to erosion and not by diffusion. FTIR and DSC study showed uniform dispersion of α-amylase at molecular level in the carrageenan beads. Texture analysis discovered directly proportional relation of degree of crosslinking with potassium chloride concentration. In addition, the surface roughness decreased with increase in κ-carrageenan concentration. Accelerated and long term stability study illustrated considerably improved shelf-life of α-amylase entrapped in carrageenan than the conventional dosage form. The application of a single polymer (as used traditionally) for the formation of beads allows the formulator to predict and produce beads of different geometries, strengths and release characteristics. Results of presented experiments seem to be of value for the pharmaceutical industries associated with digestive enzymes formulations.

10.2. Carrageenan-Papain Beads

10.2.1. EFFECT OF THE FACTORS ON RESPONSES

10.2.1.1. % Entrapment

ANOVA results and regression coefficients of response variables are shown in Table 10.6. All three process variables were statistically significant (P <0.05). From the contour plots of response surface for % entrapment (Figure 10.9) and Table 10.5, it can be concluded that concentration of κ-carrageenan was the most influencing factor (37.68%) and affecting positively (positive coefficient; Table 10.6; i.e. response increases with increase in factor level). However, potassium chloride concentration and hardening time were affecting negatively (negative coefficient; Table 10.6; i.e. response decreases with increase in factor level) to a significant level. More than 82% entrapment (formulation 2 and 11) was obtained at the high level of the κ-carrageenan concentration especially when it was followed by the low levels of the other two factors. Sipahigil et al. observed that, freely water-soluble drug always entrapped in higher ratio and results in bigger particles.(Sipahigil and Dortunc, 2001) This probably may be the reason for getting the high entrapment values in our study because papain is a freely water-soluble drug and probably may be due to higher molecular weight of papain which make it difficult to diffuse out of the pores of the carrageenan matrix.

On addition of κ-carrageenan solution to a potassium chloride solution, instantaneous interfacial cross-linking takes place followed by a more gradual gelation of the interior which causes loss of enzyme from the beads. Loss of enzyme was found to be proportional to the degree of cross-linking. Increase in viscosity with increase in κ-

Table 10.5: Distribution of Doehlert shell design experiments in the space of three process variables and results for the measured responses.

Sr. No.	Factors/ levels			Responses				Transformed value		Comp-osite index	Papain in beads	Papain in filtrate	
	κ-carra-geenan (% w/v)	Potassium chloride (M)	Hardening time (min)	% Entrap-ment[a]	T_{50}	T_{90}	Particle size (mm)±SD[b]	% Entrap-ment	T_{90}		Inactive	Active	Inactive
1	0	0	0	76.23	34.05	46.30	1.95±0.19	31.97	23.30	55.26	16.88	5.70	0.52
2	**1**	**0**	**0**	**82.75**	**41.24**	**55.36**	**2.23±0.18**	**48.09**	**40.45**	**88.55**	11.21	4.14	0.35
3	0.5	0.866	0	76.92	43.38	60.40	2.09±0.15	33.67	50.00	83.67	15.47	5.31	0.67
4	-0.5	0.866	0	65.87	36.32	47.15	1.70±0.16	6.34	24.90	31.23	23.89	8.87	0.85
5	-1	0	0	63.31	25.36	35.21	1.68±0.12	0.00	2.29	2.29	25.31	9.54	0.99
6	-0.5	-0.866	0	73.23	24.51	36.12	1.92±0.16	24.55	4.02	28.57	18.74	5.89	0.80
7	0.5	-0.866	0	82.82	33.53	43.32	2.25±0.17	48.28	17.64	65.92	11.68	3.78	0.43
8	0.5	0.289	0.816	78.61	42.58	57.17	1.99±0.12	37.86	43.88	81.74	14.76	4.71	0.51
9	-0.5	0.289	0.816	67.33	34.28	48.55	1.74±0.19	9.93	27.56	37.49	23.20	7.51	0.85
10	0	-0.577	0.816	76.91	34.21	46.73	1.99±0.14	33.64	24.10	57.74	16.40	5.31	0.69
11	0.5	-0.289	-0.816	83.52	32.87	45.81	2.09±0.16	50.00	22.36	72.36	11.70	4.12	0.45
12	-0.5	-0.289	-0.816	73.46	24.85	34.00	1.80±0.14	25.10	0.00	25.10	18.05	6.90	0.56
13	0	0.577	-0.816	76.44	35.67	47.65	1.94±0.13	32.49	25.85	58.34	16.73	5.18	0.64
14	0	0	0	76.93	34.07	43.40	1.89±0.17	33.70	17.80	51.50	15.46	5.08	0.65
15	0	0	0	76.63	33.79	43.90	1.95±0.16	32.96	18.75	51.71	15.66	5.37	0.65
16	0	0	0	77.43	34.12	46.40	1.89±0.19	34.94	23.49	58.42	14.90	5.87	0.68

[a] % Entrapment is the percent active papain in the beads.

[b] SD, standard deviation (n=50).

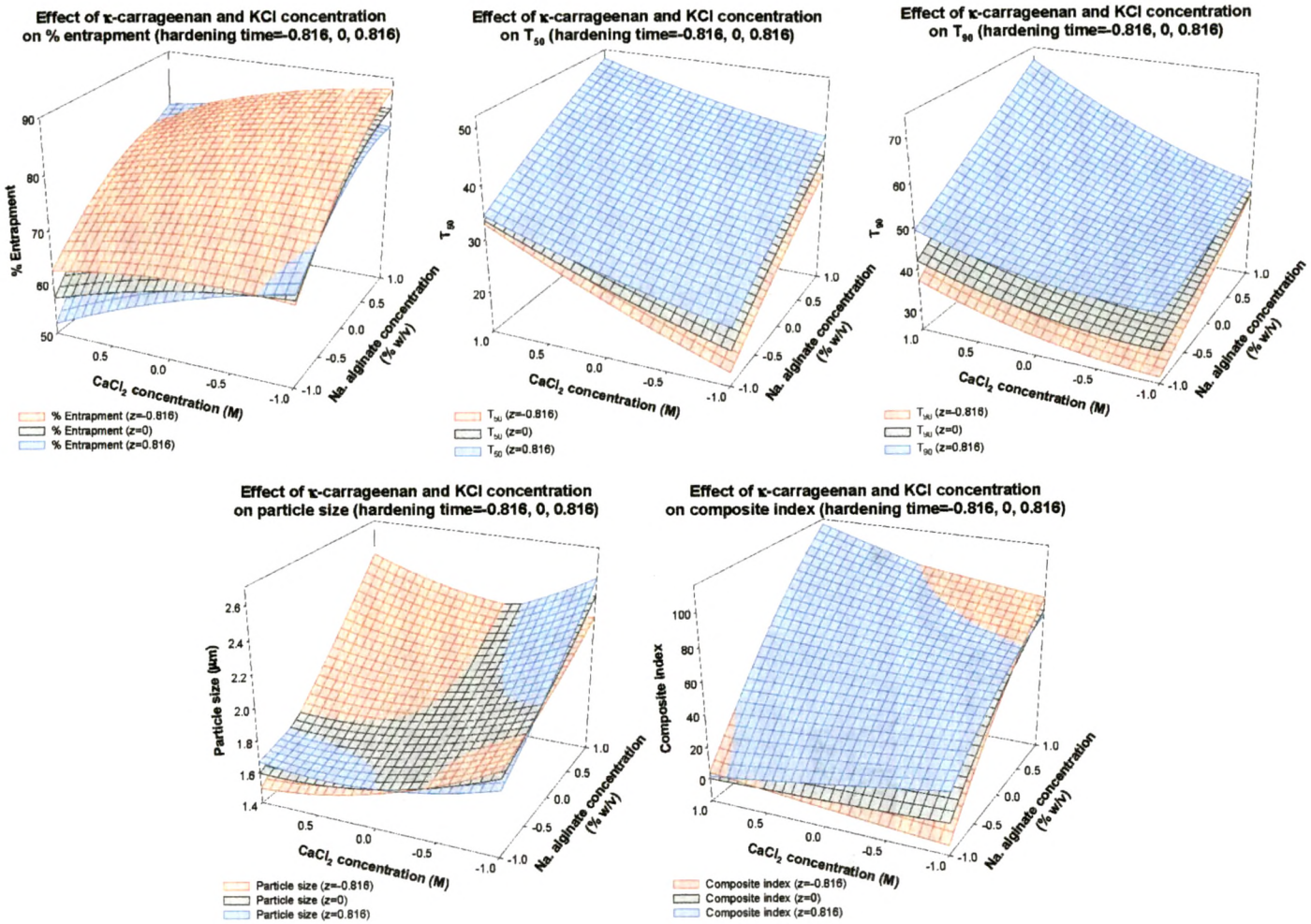

Figure 10.9: Surface plots of composite index, % entrapment, T_{90}, T_{50}, and particle size as a function of κ-carrageenan concentration, potassium chloride concentration, and hardening time.

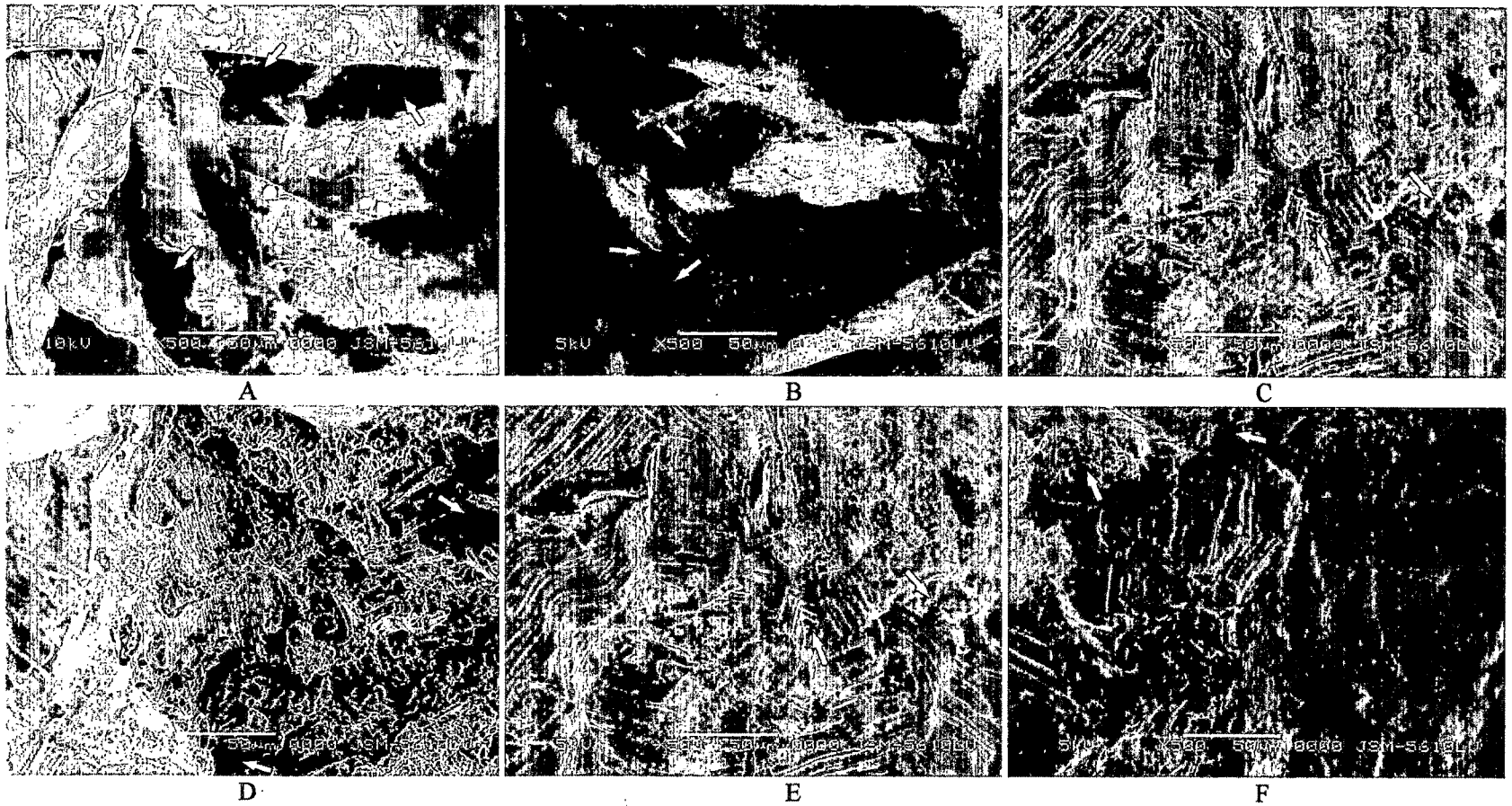

Figure 10.10: SEM micrographs and surface morphology of carrageenan beads: (A–C) Effect of potassium chloride concentration (κ-carrageenan concentration 3.0% w/v; *A*=0) (A) 0.33 M (*B*=-0.866), (B) 0.5 M (*B*=0), and (C) 0.67 M (*B*=0.866) potassium chloride concentration. (D–F) Effect of κ-carrageenan concentration (potassium chloride concentration 0.67 M; *B*=0.866) (D) 2.5% w/v (*A*=-1), (E) 3.0% w/v (*A*=-0), and (F) 3.5% w/v (*A*=1) κ-carrageenan concentration.

Table 10.6: ANOVA results (*P* values): effect of the variables on % entrapment, T_{50}, T_{90}, particle size, and composite index.

Factors	% Entrapment		T_{50}		T_{90}		Particle size		Composite index	
	Coefficient[a]	*P*	Coefficient[a]	*P*	Coefficient[a]	*P*	Coefficient[a]	*P*	Coefficient[a]	*P*
Intercept	76.81	<0.0001*	34.01	<0.0001*	45.00	<0.0001*	1.92	<0.0001*	54.22	<0.0001*
A	9.92	<0.0001*	7.97	<0.0001*	10.13	<0.0001*	0.30	0.0001*	43.72	<0.0001*
B	-3.74	<0.0001*	6.28	<0.0001*	8.09	<0.0001*	-0.10	0.0053*	6.08	0.0059*
C	-2.16	0.0003*	3.61	<0.0001*	5.10	0.0004*	-0.02	0.3506	4.32	0.0223*
A^2	-3.78	0.0002*	-0.71	0.0014*	0.29	0.7981	0.03	0.4191	-8.80	0.0120*
B^2	-1.54	0.0131*	0.81	0.0008*	2.24	0.0880	0.09	0.0746	0.43	0.8571
C^2	0.19	0.6448	0.08	0.4826	1.85	0.1229	-0.02	0.5880	3.95	0.1268
AB	0.84	0.1820	-1.13	0.0006*	3.49	0.0559	0.04	0.4866	8.71	0.0357*
AC	0.45	0.4950	0.57	0.0181*	-3.20	0.0985	-0.04	0.5077	-4.94	0.2079
BC	-0.54	0.4134	-1.30	0.0005*	-0.46	0.7839	-0.06	0.3219	-2.20	0.5472
ABC	3.18	0.2265	0.79	0.2634	0.38	0.9515	-0.15	0.5174	8.63	0.5345
$r^2_{adj.}$	0.9935	-	0.9995	-	0.9723	-	0.9317		0.9874	-

[a] Regression coefficients are in coded values.

* Statistically significant ($P < 0.05$)

carrageenan concentration may retard penetration of potassium to the interior of the bead, resulting in decreased cross-linking (also decreased surface roughness; Figure 10.10;D-E) and hence increased entrapment efficiency. Degree of cross-linking increased with increase in potassium concentration and contact time, and so entrapment efficiency decreased. The entrapment efficiency of the papain containing beads prepared with calcium alginate (sodium alginate and calcium chloride)(Sankalia et al., 2004; 2005) and chitosan-alginate was 91% and 90% respectively, using κ-carrageenan the papain entrapment efficiency in our study did not exceed 84%, although the same method was used. So with chitosan or alginate more efficient entrapment was achieved.(Bodmeier and Wang, 1993; Sipahigil and Dortunc, 2001)

Active and total fraction of papain entrapped in beads as well as in filtrate (un-entrapped) were analyzed using modified method of An et al.(An et al., 1994) and fluorescence method respectively, and the results are enumerated in Table 10.5. The response surface of the inactive fraction of papain in the beads (not shown) is completely opposite to that of the active fraction of papain in the beads (i.e. inactivation decreases with increase in κ-carrageenan concentration, inactivation increases with increase in potassium chloride concentration and hardening time). Appearance of papain in the filtrate may be due to its loss from the surface of the beads. However, the inactive fraction in the filtrate was of very less magnitude suggesting that the enzyme might have inactivated due to the interaction with polymer in the beads.

10.2.1.2. T_{50} and T_{90}

As shown in Figure 10.9 and Table 10.6, all three factors had significant a positive effect on both response values. The κ-carrageenan concentration (factor *A*) had the most

significant effect. For maximum activity of enzyme in the intestine longer T_{50} and T_{90} were the desired criteria for the optimum formulation. Thus, formulation 3 and 2 (extreme level points of DSD) resulted in beads with T_{90} as high as 60.40 and 55.36 min respectively (Table 10.5). T_{50} and T_{90} were found to be proportional to particle size and degree of cross-linking. As the concentration and hence the viscosity of κ-carrageenan incereases, larger beads (discussed under 'Particle size') were obtained which took a long time for complete dissolution and resulted in higher T_{50} and T_{90}. The increase of the in vitro release rates of papain from carrageenan beads prepared with low concentrations of potassium chloride solutions may be due to the less cross-linked structure of the beads which may result in a more porous matrix (Figure 10.10;A-C) and higher drug release.(Garcia and Ghaly, 1996; Sipahigil and Dortunc, 2001) Longer hardening time caused penetration of potassium to the interior of the bead, resulted in increased cross-linking, and hence higher T_{50} and T_{90}.(Sipahigil and Dortunc, 2001)

10.2.1.3. Particle Size

As depicted in Table 10.6, the κ-carrageenan concentration (factor A; most influential; 35.34%) had a positive coeficient, while potassium chloride concentration and hardening time had negative coefficients. In contrast to the finding of Sipahigil(Sipahigil and Dortunc, 2001) and Bhardwaj,(Bhardwaj et al., 1995) two process variables, namely, κ-carrageenan and potassium chloride concentration were statistically significant ($P<0.05$). The bead size is influenced by the orifice of the needle through which the κ-carrageenan is allowed to pass, addition of surfactant, extrusion rate, (which were kept constant) surface tension and the viscosity of the carrageenan solution. Increased viscosity at higher concentration of κ-carrageenan resulted in larger particles. High potassium chloride

concentration and hardening time resulted in smaller particle size due to high degree of cross-linking. Though the negative effect of potassium chloride concentration was of less magnitude, it contributed to the morphology of the beads (Figure 10.10;A-C).

10.2.2. INTERACTIONS BETWEEN THE FACTORS

An interaction is the failure of a factor to produce the same effect on the response at the different levels of the other factor. The ANOVA results (Table 10.6) showed that interaction AB, AC and BC had significant influence on T_{50}, AB had significant influence on composite index, while non-significant for other responses. The analysis of the results by multiple regression (Table 10.6) leads to equations that adequately describe the influence of the selected factors on % entrapment, T_{50}, T_{90}, particle size, and composite index.

10.2.3. OPTIMIZATION OF THE PROCESS USING THE COMPOSITE INDEX

Generally the aim of the optimization is to find the optimum levels of the variables, which affect a process, where a product of desired characteristics could be produced easily and reproducibly. Using the composite index, both selected responses (% entrapment and T_{90}) were combined in one response. As it has been already discussed, the composite index was calculated from the individually calculated transformed value of each of the responses using the Eq. 7.11–7.12. The equation found out using multiple regression was as follow (coded factors):

Eq. 10.3 $$CI = 54.22 + 43.72A + 6.08B + 4.32C - 8.80A^2 + 0.43B^2 + 3.95C^2 + 8.71AB - 4.94AC - 2.02BC + 8.63ABC \quad (r^2_{adj.} = 0.9874, P < 0.0001)$$

In Figure 10.9 the contour plots that describe the influence of the independent factors on the composite index is presented. The study of these plots and Table 10.5 showed that the highest values of the CI (88.55) could be obtained at formulation 2 and was considered as a batch fulfilling all the constraints favorable for the bead preparation.

10.2.4. EVALUATION OF MODEL USING CROSS-VALIDATION

In order to assess the reliability of the model, five experiments were conducted (one optimized and another with second highest composite index value and rest were tested at

Table 10.7: Comparison of responses between predicted and experimental values for the cross-validation set.

Responses	Test	Factors/levels			Experimental values	Predicted values	Bias%
		A	B	C			
% Entrapment	1	1	0	0	82.95	85.27	-2.8
	2	0.5	0.866	0	76.80	78.72	-2.5
	3	0.3	0.2	0.4	77.94	75.60	3.0
	4	-0.3	-0.2	-0.4	75.05	77.45	-3.2
	5	0	-0.4	0.4	77.31	75.53	2.3
T_{50}	1	1	0	0	41.27	39.95	3.2
	2	0.5	0.866	0	43.37	42.16	2.8
	3	0.3	0.2	0.4	39.00	39.83	-2.1
	4	-0.3	-0.2	-0.4	28.78	27.68	3.8
	5	0	-0.4	0.4	33.29	34.65	-4.1
T_{90}	1	1	0	0	55.41	53.91	2.7
	2	0.5	0.866	0	60.33	61.65	-2.2
	3	0.3	0.2	0.4	51.91	53.15	-2.4
	4	-0.3	-0.2	-0.4	38.50	37.23	3.3
	5	0	-0.4	0.4	44.53	44.04	1.1
Particle size	1	1	0	0	2.26	2.38	-5.4
	2	0.5	0.866	0	2.07	1.99	3.9
	3	0.3	0.2	0.4	1.97	2.09	-5.8
	4	-0.3	-0.2	-0.4	1.86	1.99	-7.1
	5	0	-0.4	0.4	1.97	2.11	-6.9
Composite index	1	1	0	0	89.14	92.05	-3.3
	2	0.5	0.866	0	83.24	90.50	-8.7
	3	0.3	0.2	0.4	70.10	66.67	4.9
	4	-0.3	-0.2	-0.4	37.57	41.10	-9.4
	5	0	-0.4	0.4	54.58	49.24	9.8

the process variables of values other than that of the model). For each of these test experiments the responses were estimated by using the multiple regression equations and experimental procedure for comparison between both responses (Table 10.7). Bias was calculated by the following equation:

Eq. 10.4

$$\text{Bias} = \left[\frac{\text{predicted value} - \text{experimental value}}{\text{predicted value}} \right] \times 100$$

It can be seen that in all cases there was a reasonable agreement between the predicted and the experimental value, since low values of the bias were found. For this reason it can be concluded that the equations describe adequately the influence of the selected process variables on the responses under study.

10.2.5. CURVE FITTING AND RELEASE MECHANISM

Release profile of the active and inactive fraction of papain are shown in Figure 10.11A. As can be seen, the release profiles are similar for both the fractions. Total papain released from the beads did not sum to a 100 percent because some quantity of papain was un-entrapped and lost in the filtrate. However, for simplicity in the calculation the active papain in the beads were assumed to be 100 percent for the label claim as only the active fraction will be available for the therapeutic activity.

An *'in vitro'* dissolution profile of the optimized batch is shown in Figure 10.11B. Release of papain from κ-carrageenan beads in simulated gastric fluid is conceivably attributed to the presence in the carrageenan molecule of strongly acidic sulphate groups that allow a certain degree of ionization to be mantained also at low pH.(Bonferoni et al., 1994) Values of release exponent (n) and kinetic constant (K) were derived using zero-order kinetics, first-order kinetics, Higuchi's square root of time equation, Korsmeyer-

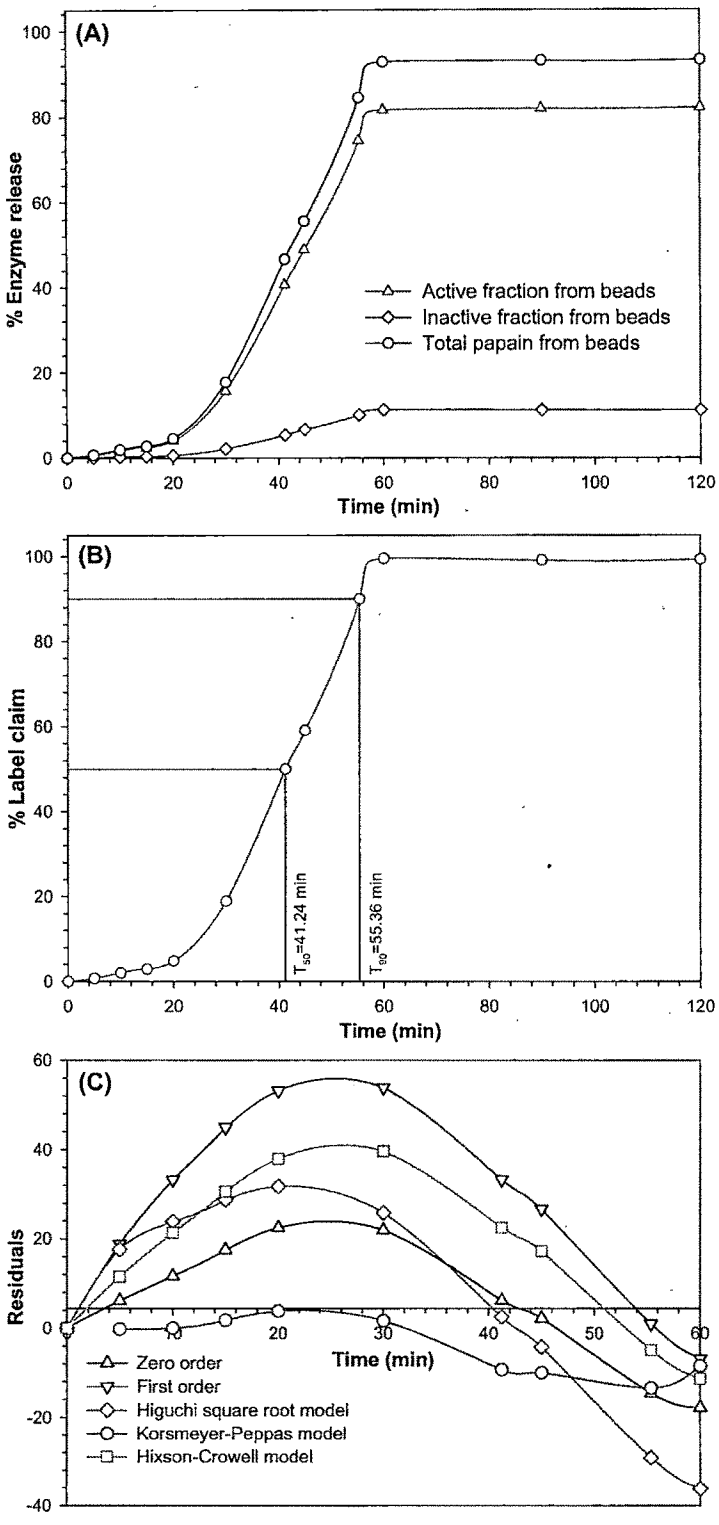

Figure 10.11: 'In vitro' release profile of optimized formulation (experiment 2) in SGF without enzyme (A) in terms of active, inactive and total fraction of papain from the beads; (B) in terms of active fraction of papain as % label claim. (C) Residual plot of different release models for the same formulation.

Peppas' power law equation and Hixson-Crowell's cube root of time equation and presented in Table 10.8. The enzyme release data show a good fit to the Korsmeyer-Peppas' power law release kinetics (Eq. 7.16) which can be confirmed by comparing the values of the correlation coefficient (r) with that of the other models. The values of Korsmeyer-Peppas' release exponent (n) determined for the various formulations studied ranged from 1.49 to 2.15 suggesting the probable release by super case-II transport. The K_k values ranged from 0.01 to 0.36 where a low K_k value may suggest near to zero release from the beads initially. If one considers the correlation coefficient (r) values of zero-order and Korsemeyer-Peppas release models, both models describe the dissolution data reasonably well. Where there are competing models (with similar r values), residuals analysis can be used to distinguish between the models.(Pather et al., 1998) Figure 10.11C is the residual plot for optimized formulation. The residuals are high for the zero-order, first-order, Higuchi, and Hixson-Crowell models (and least for the Korsemeyer-Peppas model) which also shows systematic deviation: the models overpredict initially and underpredict at the later stages of the dissolution process. This indicates that Korsemeyer-Peppes' power low is the best fit model in describing the dissolution behavior of papain from κ-carrageenan beads.

Finally, in order to know weather the enzyme release was due to erosion or diffusion, the release data of the optimized formulation was fitted to Kopcha model (Eq. 7.18) and parameters like A, and B at different time intervals were determined (Figure 10.12A). Throughout the release profile, A was <0 and B was >0, and expressed the predominance of erosion relative to diffusion. This probably may be due to the lower gel strength of carrageenan gels. During the dissolution study carrageenan gels swell but are unable to maintain the gel matrix due to low gel strength and start to erode. However, the rate of hydration initially was found to be the rate limiting step of erosion rate and explains the

biphasic nature of the release profile (plateau initially followed by steep rise in erosion rate). The erosion term B increases with time because erosion through the hydrated layer is easier.

Table 10.8: Comparison of different dissolution kinetics models.

Sr. No.	Release model										
	Zero-order		First-Order		Higuchi matrix		Korsmeyer-Peppas			Hixson-Crowell	
	K_o	r_0	K_1	r_1	K_H	r_H	n	K_k	r_k	K_s	r_s
1	1.62	0.93	-0.03	0.84	8.73	0.78	2.05	0.03	1.00	-0.01	0.87
2	1.36	0.92	-0.04	0.76	8.15	0.77	2.15	0.01	0.98	-0.01	0.84
3	1.25	0.93	-0.03	0.85	7.64	0.78	2.03	0.02	0.96	-0.01	0.88
4	1.52	0.91	-0.03	0.82	8.24	0.76	1.57	0.15	0.93	-0.01	0.85
5	2.06	0.93	-0.04	0.81	9.67	0.78	1.61	0.24	0.97	-0.01	0.86
6	2.12	0.94	-0.04	0.84	10.00	0.79	1.49	0.36	0.95	-0.01	0.88
7	1.70	0.92	-0.04	0.81	9.00	0.76	1.78	0.08	0.97	-0.01	0.85
8	1.33	0.93	-0.03	0.80	8.06	0.78	1.73	0.06	0.97	-0.01	0.86
9	1.58	0.95	*	*	9.41	0.81	1.64	0.12	0.98	-0.01	0.83
10	1.64	0.94	-0.03	0.84	8.87	0.79	1.76	0.10	0.99	-0.01	0.88
11	1.66	0.94	-0.04	0.85	8.96	0.79	1.71	0.12	0.98	-0.01	0.88
12	2.18	0.93	-0.04	0.82	10.16	0.79	1.60	0.27	0.98	-0.01	0.87
13	1.54	0.92	-0.03	0.83	8.33	0.77	2.07	0.03	0.98	-0.01	0.87

* Not possible.

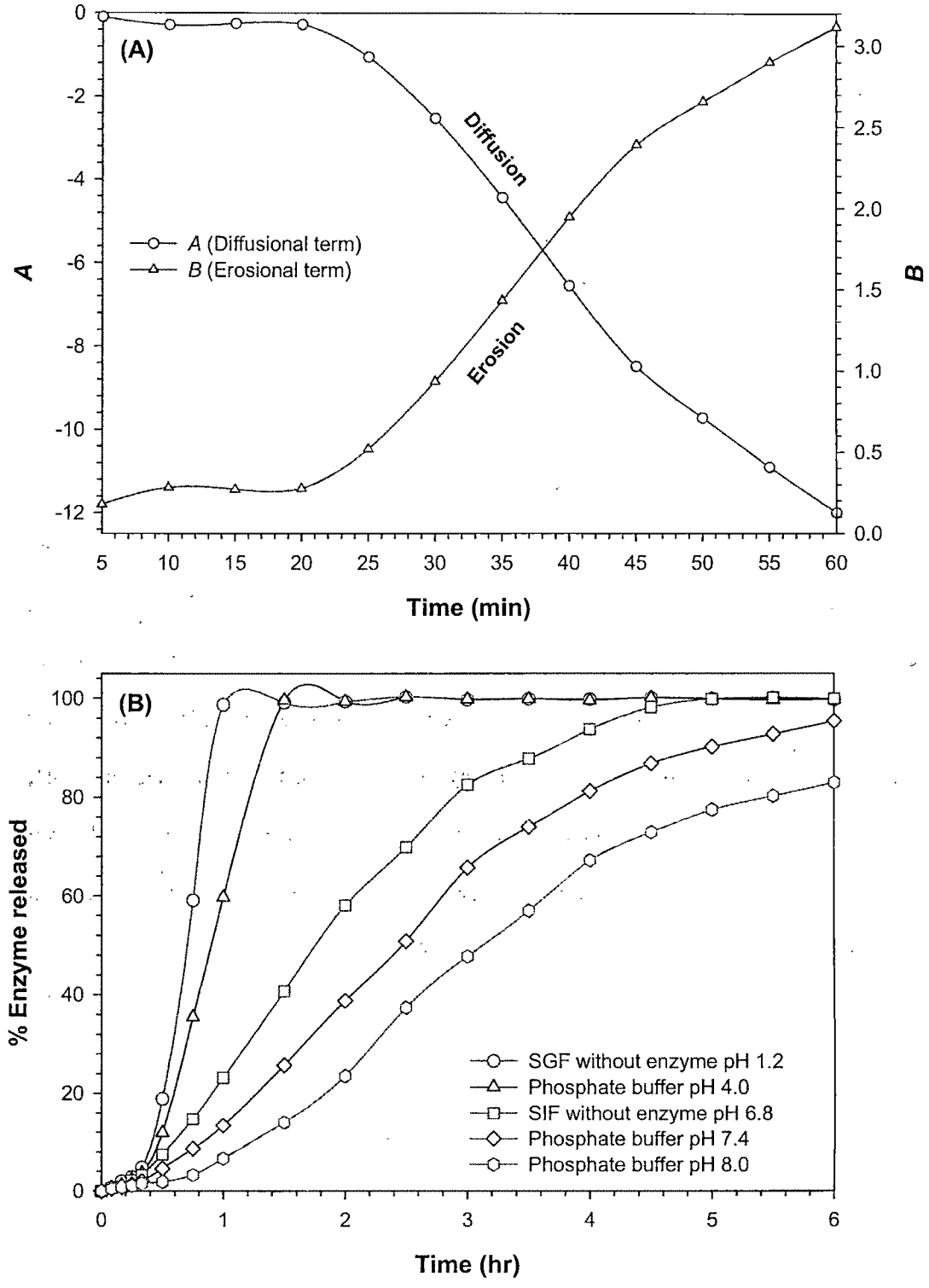

Figure 10.12: (A) Kopcha model parameters (*A* and *B*) versus time profile for optimized batch (formulation 2). (B) Effect of pH on release profile of papain entrapped in κ-carrageenan beads.

10.2.6. CHARACTERIZATION OF OPTIMAL FORMULATION

10.2.6.1. Effect of pH on Release Profile

The effect of pH on the release of papain from κ-carrageenan beads in different pH (1.2, 4.0, 6.8, 7.4, and 8.0) buffers simulating the human gastrointestinal tract is given in Figure 10.12B. Release of papain from κ-carrageenan beads in SGF is conceivably attributed to the presence in the carrageenan molecule of strongly acidic sulphate groups that allow a certain degree of ionization to be maintained also at low pH.(Bonferoni et al., 1994) The swelling and disintegration of κ-carrageenan beads are dependent on compositions of dissolution medium, ionic strength, pH, temperature, solubility of drug entrapped into beads, application of stress, or addition of specific solutes that compete with the polymeric ligand for the affinity site on the protein. As the pH increases, the degree of ionization of the κ-carrageenan hydrogel decreases. At the elevated pH, equilibrium-swelling level is delayed and the sustained-release profile was achieved subsequent to the diffusion. Thus, acid resistant but alkaline susceptible material coated κ-carrageenan beads can be used for sustained-delivery of the drugs (i) that are locally active in the small intense, (ii) that have an absorption window in the small intestine, (iii) that are unstable in the acidic or stomach environment, and / or (iv) have low solubility at low pH values.

10.2.6.2. Fourier Transform Infra-Red Spectroscopy (FTIR)

FTIR spectra of κ-carrageenan powder, carrageenan blank beads, papain loaded optimized beads, physical mixture of papain and blank beads (in the ratio of 1:6.21, same

as that of the optimized batch), and papain are shown in Figure 10.13. FTIR spectrum of κ-carrageenan powder showed various distinct peaks: very broad band spreading 3150-3600 cm^{-1} (strong; s) due to polyhydroxy $(-OH)_n$ group; 2964 cm^{-1} (s), 2920 cm^{-1} (s), and 2852 cm^{-1} (medium; m) due to C-H stretch; 1419 cm^{-1} (s) and 1375 cm^{-1} (s) due to C-H deformation; 1222 cm^{-1} (s) due to S=O stretch of sulfate ester salt; 1070 cm^{-1} due to C-O stretch of cyclic ethers; 929 cm^{-1} (s) due to C-O stretch of polyhydroxy groups attached to carbons; etc. Cross-linking of carrageenan by K^+ was shown by a decrease in the intensity of S=O stretch (1222 cm^{-1}) of sulfate ester group which was same as C-O stretch (1070 cm^{-1}) of cyclic ethers in intensity for the κ-carrageenan powder. Moreover, the peak of sulfate ester group was displaced by 14 cm^{-1}, from 1222 cm^{-1} to 1236 cm^{-1}. This was probably because of some negatively charged sulfate ester reacted with positively charged K^+ and resulted in physicochemical changes of carrageenan. Papain also showed various distinct peaks: one predominant band at 3225-3425 cm^{-1} (s) due to N-H stretch of secondary N-substituted amides; 2981 cm^{-1} (weak; w) due to C-H stretch, medium bands at 1500-1600 cm^{-1} due to C=C, while 868 cm^{-1} (s) and 850 cm^{-1} (s) due to *p*-substituted aromatic out of plane C-H deformation of aromatic residue of tryptophan or tyrosine; 2912 cm^{-1} (s) and 2939 cm^{-1} (s) due to C-H stretch, while 1429 cm^{-1} (m) and 1321 cm^{-1} (m) due to C-H deformation of alkyl chain of amino acids; 1660 cm^{-1} (w) due to C=O stretch of carboxylate anion and amide group; strong peaks between 1050-1150 cm^{-1}, weak bands at 525-600 cm^{-1}, and 472 cm^{-1} (s) due to C-S stretch of sulfides and disulfides. With incorporation of papain, the spectrum of beads was similar to that of the κ-carrageenan blank beads. However, the physical mixture of papain and blank beads showed the peaks due to both papain and κ-carrageenan. The difference spectrum of the optimized beads and the blank beads is shown in Figure 10.13(f). The difference

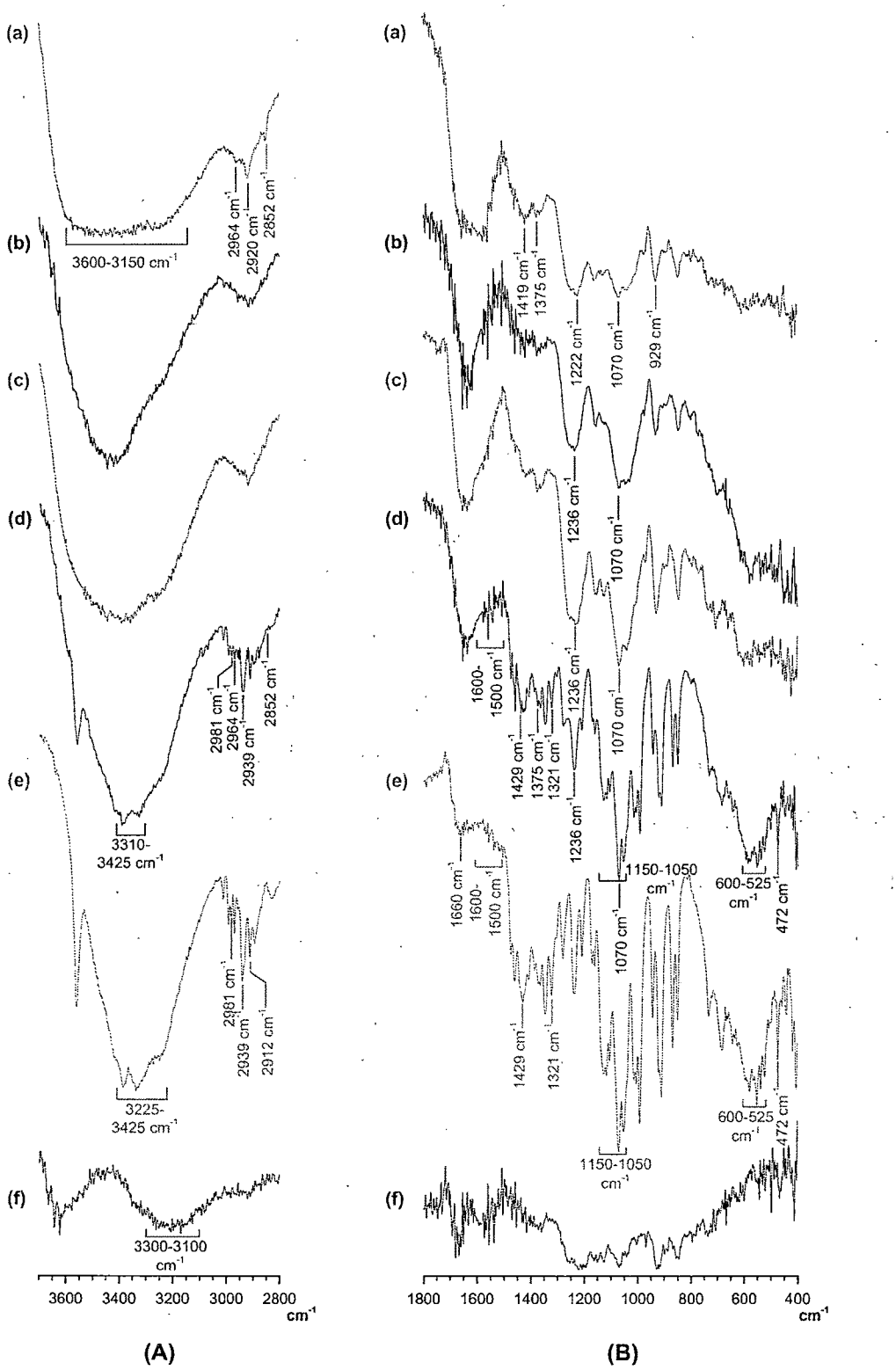

Figure 10.13: The FTIR spectra of (a) κ-carrageenan powder, (b) carrageenan blank beads, (c) papain-loaded optimized beads, (d) physical mixture of papain: blank beads (1:6.21, same as that of the optimized formulation), (e) papain, and (f) difference spectra of blank beads and optimized beads.

spectrum showed protein band in the wavelength range of 3100-3300 cm^{-1}. This confirms the papain entrapment into the κ-carrageenan beads at molecular level.

10.2.6.3. Differential Scanning Calorimetry (DSC)

The DSC thermograms of potassium chloride, papain, κ-carrageenan, blank beads, and papain-loaded beads are shown in Figure 10.14. Potassium chloride showed two non-significant exothermic peaks at 323°C and 374°C. Papain exhibited two endothermic peaks at 189.2°C and 219.4°C followed by a broad degradation exotherm. A broad endothermic peak at 85°C in the thermogram of κ-carrageenan was observed due to the presence of water molecules. Two minor peaks at 259°C and 266°C in the degradation exotherm of κ-carrageenan were absent in blank beads and papain loaded beads, while a major exothermic peak at 344°C was found to be shifted towards a higher temperature (358°C) in blank beads. However, additional two peaks (one endothermic at 207°C and one exothermic at 226.5°C) were observed in the thermogram of blank beads due to the potassium-κ-carrageenan interaction. A DSC thermogram of enzyme-loaded beads was similar to that of blank beads except that all corresponding peaks were shifted to a lower temperature, which might be due to the presence of papain. However, it did not show any peak analogous to papain. Moreover, the physical mixture of papain: blank beads (in the ration of 1: 6.21, same as that of the optimized batch) showed the endothermic peak at 189.2°C corresponding to papain and other peaks (endothermic at 207°C, exothermic at 226.5°C and 358°C) corresponding to blank beads. This confirms that most of the enzyme was dispersed at the molecular level in the beads.

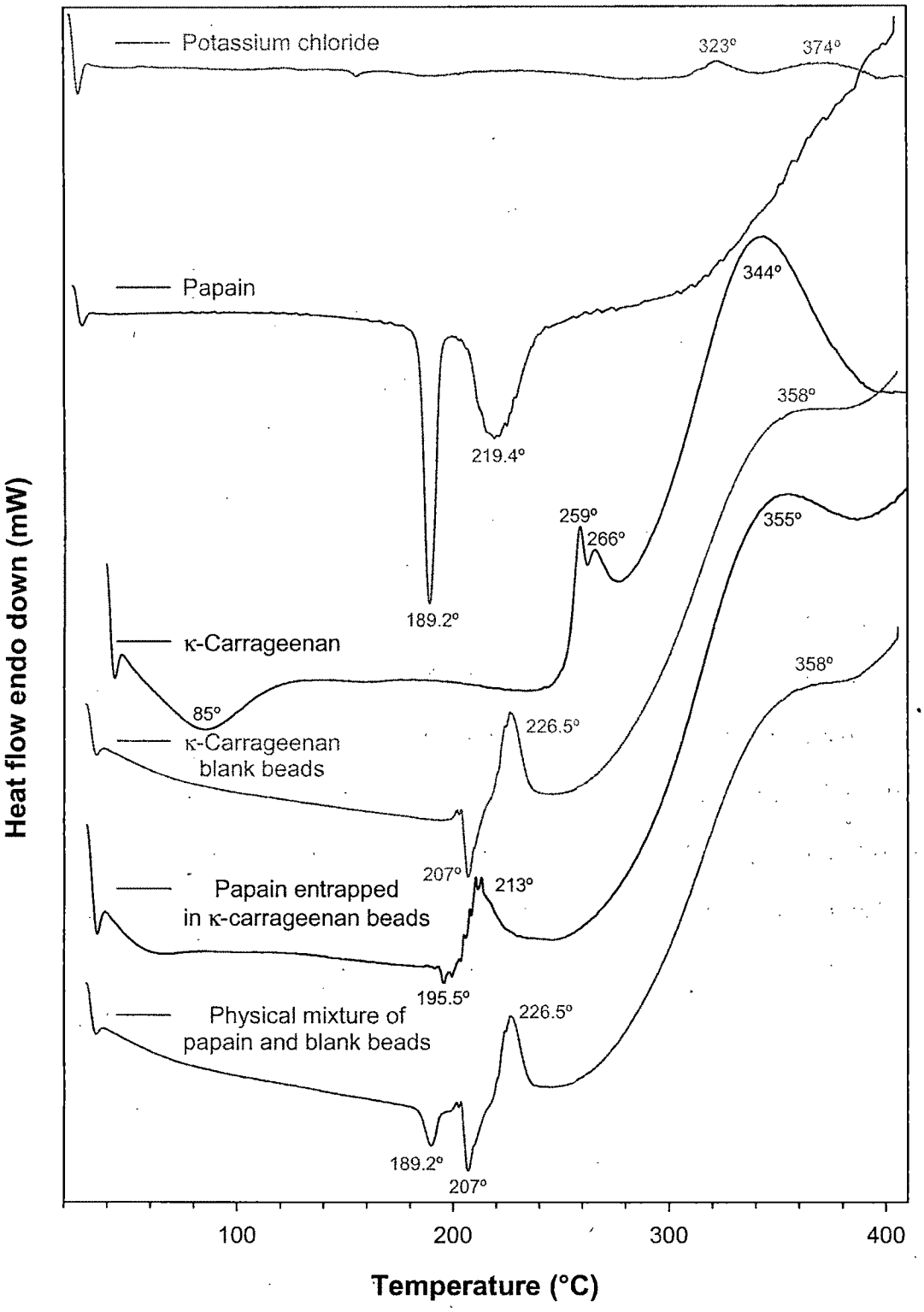

Figure 10.14: The DSC thermograms of potassium chloride, papain, κ-carrageenan powder, blank beads, papain loaded carrageenan beads and physical mixture of papapin: blank beads (1:6.21, same as that of the optimized beads) made at the same analytical conditions.

10.2.6.4. Morphology of the Beads

The spherical shape of beads in the wet state was usually lost after drying, especially for beads prepared with low carrageenan concentrations. As the degree of cross-linking of the beads prepared with 2.5% w/v carrageenan is low, outer surface is not as hard as the beads prepared with 3.5% w/v carrageenan and show much irregular surface with tendency to agglomerate. With an increase of κ-carrageenan concentration (3.5% w/v), the shape of beads was retained considerably. However, the shape of the optimized beads (formulation 2; κ-carrageenan 3.5% w/v) changed to spherical discs with a collapsed center (Figure 10.15) during the drying process The beads prepared with 2.5 % w/v κ-carrageenan showed much deeper collapsed centre or in some cases more than one collapsed centre. The tendency of developing the collapsed centre may be possibly because of mass- and heat-transfer phenomena and/or aggregation of the helical fibers into bundles and the squeezing out of some water from the gel.(Iborra et al., 1997) Normally the spherical shape was retained when the carrageenan concentration was as high as 5.0% (w/v), but the viscosity of a 5.0% w/v solution was too high for bead preparation under the present experimental conditions so it was not studied. Cross-linked hydrogels reach an equilibrium swelling level in aqueous solutions which depends mainly on the cross-link density. In some cases, depending on the solvent composition, temperature and solids concentration during gel formation, phase separation can occur, and water-filled 'voids' or 'macropores' can form which can be observed Figure 10.10. One noticeable characteristic of the bead surface is the high degree of cross-linking when the concentration of potassium chloride increased (Figure 10.10;A-C). Further, the surface morphology was improved (i.e. decrease in roughness) with increase in κ-

carrageenan concentration (Figure 10.10;D-F) due to the high viscosity of the κ-carrageenan solution.

Figure 10.15: Photograph of wet κ-carrageenan beads (optimized formulation 2, Table 10.5, κ-carrageenan 3.5% w/v, potassium chloride 0.5M, and hardening time 20 min) showing spherical disk-shape with collapsed centre during drying process.

10.2.7. STABILITY STUDY

For the developed formulation, the similarity factor (f_2) was calculated by a comparison of the dissolution profiles at each storage condition with the control at the initial condition. Results of f_2 factors ranged from 73 to 97 with 2 to 5% average difference. Evaluation of shelf-life was carried out as per the ICH Q1EStep4 (Evaluation of Stability Data) guidelines for the drug substances intended for room temperature storage. Long-term and accelerated stability data showed little change over time, so the shelf-life up to

twice the length of available long-term data (i.e. 24 months) can be proposed. Extrapolation of the shelf-life beyond the length of available long-term data can be proposed. For this an approach for analyzing the data on a quantitative attribute that is expected to change with time is to determine the time at which the 95% one-sided confidence limit for the mean curve intersects the acceptance criterion (not more than 5% change in assay from its initial value) can be accepted. The long-term stability data of the developed formulation, marketed formulation and the bulk papain were linearly extrapolated (zero-order kinetics) to calculate the shelf-life (Figure 10.16) and were found be 3.63 years, 1.01 years, and 0.48 year respectively. Hence, the stability of the entrapped papain was significantly improved compared to the conventional dosage forms.

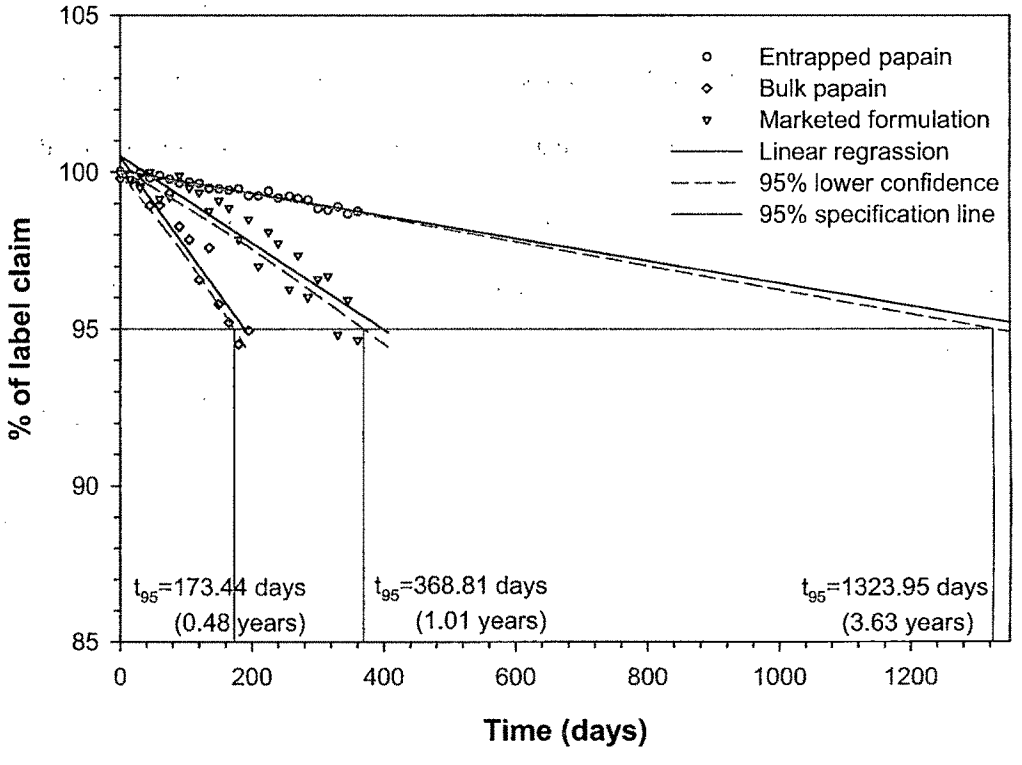

Figure 10.16: Extrapolation of long-term stability data for shelf-life calculation.

Dumitriu and Chornet observed that, hydrogels, formed through interaction of a polyanion with a cation (i.e. papain), have the advantage of creating an ionic micro-system which favors the stabilization of a protein polymer (i.e. enzyme in this case) by interacting with the free acid and base functions.(Severian and Esteban, 1998) Moreover, protein–polyelectrolyte complexes also have the ability to improve the operational stability of the enzyme activity during catalysis.(Severian and Esteban, 1998) This probably may be the reason of improved stability of papain entrapped in the ionotropically cross-linked κ-carrageenan gel beads.

CONCLUSIONS

Ionotropically cross-linked κ-carrageenan beads are a promising method for improving the stability of entrapped papain and can find a place in the design of multiparticulate drug delivery systems. The optimization of the process using the composite index resulted in more than 82% entrapment and more than 55 min of T_{90} at optimized process variables. T_{50} and T_{90} were increased with increase in all three process variables. Percentage entrapment and particle size were found to be directly proportional to κ-carrageenan concentration and inversely proportional to potassium chloride concentration and hardening time. Mathematical analysis of the different drug release modalities has evidenced that enzyme release from carrageenan beads follows the Korsmeyer-Peppas' power law equation with super case-II transport mechanism. Furthermore, investigation of release profiles using the Kopcha model revealed that enzyme release is due to erosion and not by diffusion. FTIR and DSC studies indicated uniform dispersion of papain, at the molecular level, in the carrageenan beads. Texture analysis indicated a direct proportionality between degree of cross-linking and potassium chloride concentration,

and an inverse relationship between surface roughness with increase in κ-carrageenan concentration. Accelerated and long term stability studies illustrated considerably improved shelf-life of papain entrapped in carrageenan compared to conventional dosage forms. Based on the provided methodologies, desirable beads of different geometries, strength and release characteristics can be easily manufactured. Results of presented experiments seem to be of value for the pharmaceutical industries associated with digestive enzyme formulations.

10.3. Carrageenan-Pepsin Beads

10.3.1. EFFECT OF THE FACTORS ON RESPONSES

10.3.1.1. % Entrapment

ANOVA results and regression coefficients of response variables are shown in Table 10.10. All three process variables were statistically significant (P <0.05). From the contour plots of response surface for % entrapment (Figure 10.17) and Table 10.10, it can be concluded that concentration of κ-carrageenan was the most influencing factor and affecting positively (i.e. response increases with increase in factor level). However, potassium chloride concentration and hardening time were affecting negatively (i.e. response decreases with increase in factor level) in significant amount. More than 80% entrapment (experiment 11, 9, 12, and 3) was obtained at the high level of the κ-carrageenan concentration especially when it was followed by the low levels of the other two factors.

On addition of κ-carrageenan solution to a potassium chloride solution, instantaneous interfacial crosslinking takes place followed by a more gradual gelation of the interior which causes loss of enzyme from the beads. Loss of enzyme was found to be proportional to the degree of crosslinking. Increase in viscosity with increase in κ-carrageenan concentration may retard penetration of potassium to the interior of the bead, resulted in decreased crosslinking (also decreased surface roughness; Figure 10.18D-E) and hence increased entrapment efficiency. Degree of crosslinking increased with

increase in potassium concentration and contact time, and so entrapment efficiency decreased.

Table 10.9: Matrix of Box-Behnken design and results for the measured responses.

Factors/ levels				Responses			
ES[a]	κ-carrageenan (% w/v)	Potassium chloride (M)	Hardening time (min)	% Entrapment	T_{50} (min)	T_{90} (min)	Particle size (mm)
5	-1	-1	0	64.90	19.20	29.70	1.833
11	1	-1	0	84.80	35.90	49.30	2.363
2	-1	1	0	57.48	32.65	46.10	1.646
14	1	1	0	77.85	48.30	67.80	2.209
7	-1	0	-1	66.06	22.30	32.50	1.708
9	1	0	-1	85.70	38.47	51.90	2.325
1	-1	0	1	60.47	29.10	44.10	1.661
12	1	0	1	81.69	45.50	62.00	2.195
3	**0**	**-1**	**-1**	**81.41**	**24.50**	**35.30**	**2.111**
6	0	-1	1	77.20	33.05	46.05	2.054
15	0	1	-1	73.81	37.86	50.83	1.857
8	0	1	1	69.32	44.60	62.95	1.809
13	0	0	0	77.03	33.70	44.15	1.951
4	0	0	0	76.93	34.07	43.74	1.888
10	0	0	0	76.63	33.69	44.38	1.948

[a] ES, experimental sequence.

Table 10.10: ANOVA results (*P* Values): effect of the variables on % entrapment, t_{50}, t_{90}, and particle size.

Factors	% Entrapment		T_{50}		T_{90}		Particle size	
	Coefficient[a]	*P*	Coefficient[a]	*P*	Coefficient[a]	*P*	Coefficient[a]	*P*
Intercept	76.86	<0.0001*	33.82	<0.0001*	44.09	<0.0001*	1.93	<0.0001*
A	10.14	<0.0001*	8.12	<0.0001*	9.83	<0.0001*	0.28	<0.0001*
B	-3.73	<0.0001*	6.35	<0.0001*	8.42	<0.0001*	-0.11	0.0005*
C	-2.29	<0.0001*	3.64	<0.0001*	5.57	<0.0001*	-0.04	0.0421*
A^2	-3.78	<0.0001*	-0.48	0.0297*	1.49	0.0154*	0.05	0.0499*
B^2	-1.83	0.0001*	0.68	0.0084*	2.65	0.0014*	0.03	0.1296
C^2	0.40	0.0403*	0.51	0.0254*	2.05	0.0043*	-0.01	0.7683
AB	0.12	0.4262	-0.26	0.1498	0.53	0.2428	0.01	0.6806
AC	0.40	0.0356*	0.06	0.7248	-0.38	0.3877	-0.02	0.3036
BC	-0.07	0.6350	-0.45	0.0326*	0.34	0.4272	0.00	0.9173
$r^2_{adj.}$	0.9990	-	0.9986	-	0.9946	-	0.9749	-

[a] Regression coefficients are in coded values.
* Statistically significant ($P < 0.05$)

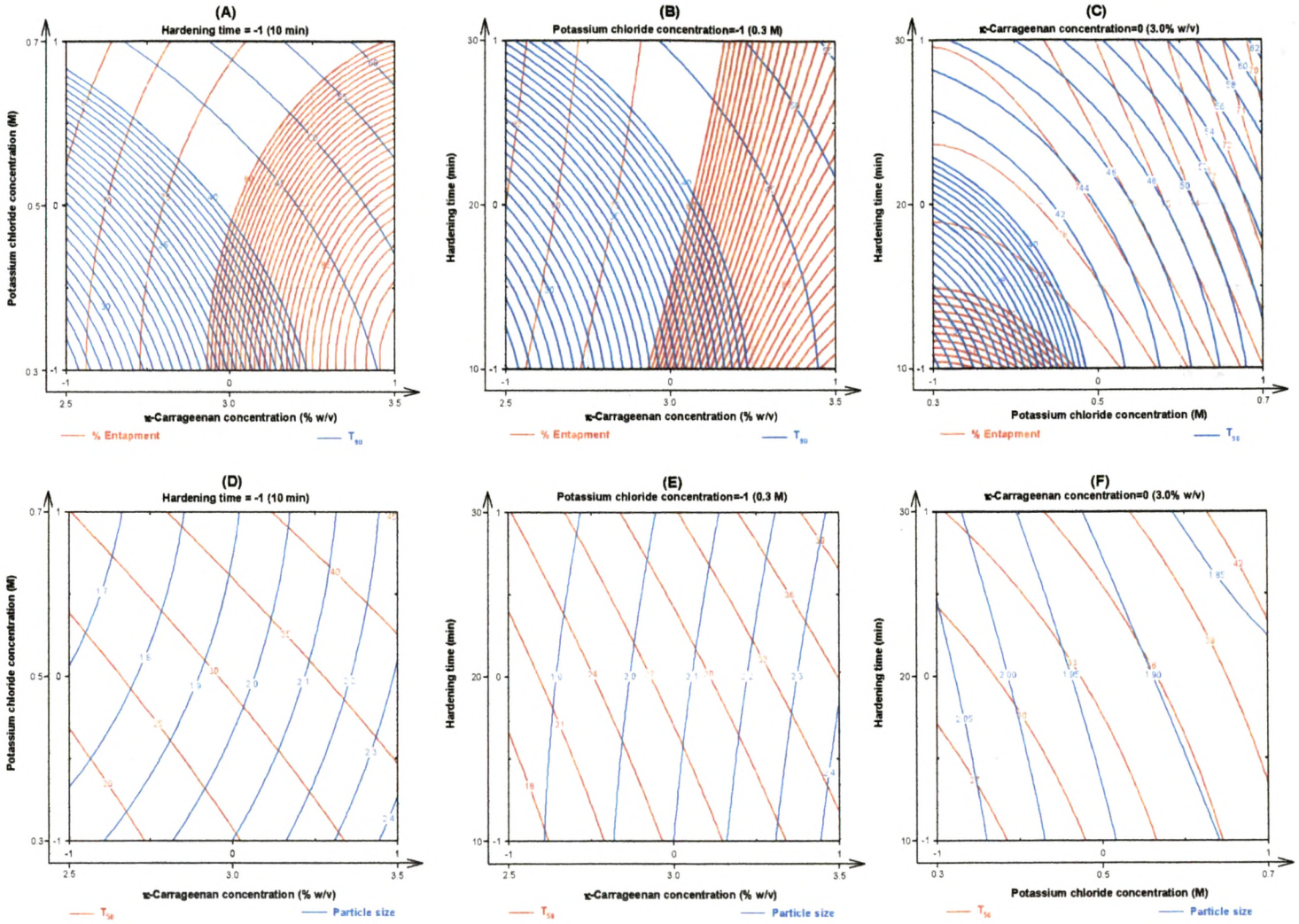

Figure 10.17: Contour plots of % entrapment, T_{90}, T_{50}, and particle size as a function of κ-carrageenan concentration, potassium chloride concentration, and hardening time.

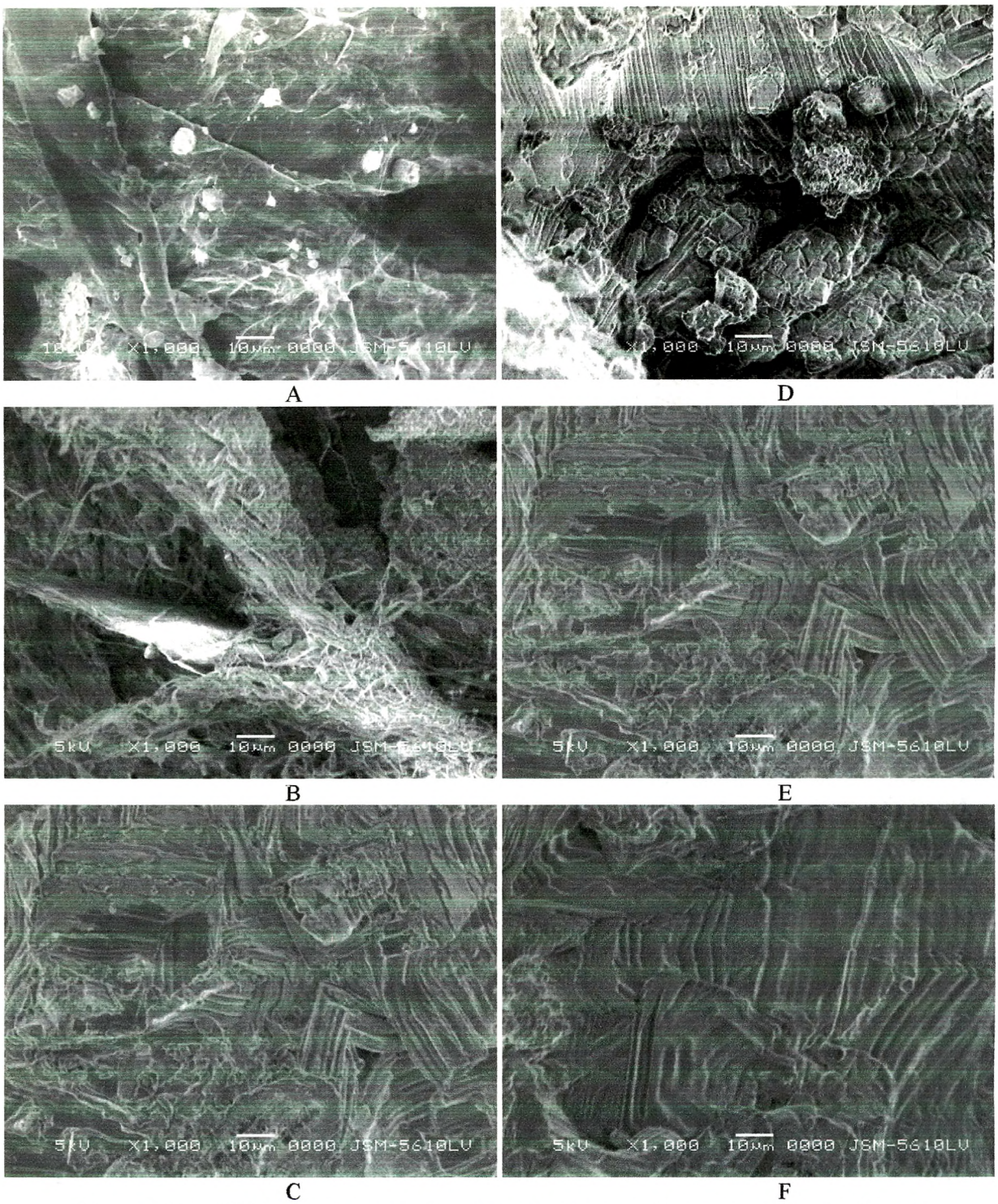

Figure 10.18: SEM micrographs and surface morphology of carrageenan beads: (A–C) Effect of potassium chloride concentration (κ-carrageenan concentration 3.0% w/v; *A*=0) (A) 0.3 M (*B*=-1), (B) 0.5 M (*B*=0), and (C) 0.7 M (*B*=1) potassium chloride concentration. (D–F) Effect of κ-carrageenan concentration (potassium chloride concentration 0.7 M; *B*=1) (D) 2.5% w/v (*A*=-1), (E) 3.0% w/v (*A*=-0), and (F) 3.5% w/v (*A*=1) κ-carrageenan concentration.

10.3.1.2. T_{50} and T_{90}

As shown in Figure 10.17 and Table 10.9, all three factors had significant positive effect on both response values. The κ-carrageenan concentration (factor *A*) was found to be most influencing factor. For pepsin to be functional after release, immediate and complete release of enzyme in the stomach, hence shorter T_{50} and T_{90} was the desired criteria for the optimum formulation. Thus, experiment 5 (least level points of BBD) resulted the beads with T_{90} as low as 29.70 min (Table 10.9). T_{50} and T_{90} were found to be proportional to particle size and degree of crosslinking. As the concentration and hence the viscosity of κ-carrageenan incereases, larger beads (discussed under 'Particle size') were obtained which took long time for complete dissolution and resulted in higher T_{50} and T_{90}. The increase in release rates of pepsin from carrageenan beads prepared with low concentrations of potassium chloride solutions may be due to the less crosslinked structure of the beads which may result in a more porous matrix (Figure 10.18A-C) and higher drug release(Garcia and Ghaly, 1996; Sipahigil and Bortunc, 2001). Longer hardening time caused penetration of potassium to the interior of the bead, resulted in increased crosslinking, and hence higher T_{50} and T_{90}.(Sipahigil and Bortunc, 2001)

10.3.1.3. Particle Size

As depicted in Table 10.10, the κ-carrageenan concentration (factor A; most influential) had positive coeficient, while potassium chloride concentration and hardening time had negative coefficient. In contrast to the finding of Sipahigil(Sipahigil and Bortunc, 2001) and Bhardwaj(Bhardwaj et al., 1995), all three process variables were statistically

significant (P<0.05). Freely water soluble drug always entrapped in higher ratio and results in bigger particles(Sipahigil and Bortunc, 2001). The bead size is influenced by the opening through which the κ-carrageenan is allowed to pass (which was kept constant) and the viscosity of the carrageenan solution. Increased viscosity at higher concentration of κ-carrageenan resulted in larger particles. High potassium chloride concentration and hardening time resulted in smaller particle size due to high degree of crosslinking. Though the negative effect of potassium chloride concentration was of less magnitude, it contributed to the morphology of the beads (Figure 10.18A-C).

10.3.2. INTERACTIONS BETWEEN THE FACTORS

An interaction is the failure of a factor to produce the same effect on the response at the different levels of the other factor. The ANOVA results (Table 10.10) showed that interaction AC and BC had significant influence on % entrapment and T_{50}, respectively. However, other interaction terms were non-significant statistically. The analysis of the results by multiple regression (Table 10.10) leads to equations that adequately describe the influence of the selected factors on % entrapment, T_{50}, T_{90}, and particle size.

10.3.3. OPTIMIZATION OF THE PROCESS USING THE RESPONSE SURFACES

Generally, the aim of the optimization is to find the optimum levels of the variables, which affect a process, where a product of desired characteristics could be produced easily and reproducibly. Using the response surface of selected responses with constraint (% entrapment > 80% and T_{90} < 40 min), it was possible to identify the optimum region.

In Figure 10.17;A-C the contour plots that describe the influence of the independent factors on the % entrapment and T_{90} have been presented. The study of these plots showed that the beads with desired characteristic could be produced at medium level (0) of κ-carrageenan concentration and lowest levels (-1) of both potassium chloride concentration and hardening time. Experiment 3 was the batch with the same experimental condition and was fulfilling all the constraints favorable for the beads preparation, hence was considered as the optimum batch.

10.3.4. EVALUATION OF MODEL USING CROSS-VALIDATION

In order to assess the reliability of the model, five experiments were conducted by varying the process variables at values other than that of the model. For each of these test experiments the responses were estimated by using derived quadratic polynomial equations and experimental procedure for comparison between both responses (Table 10.11). % Relative error was calculated by the following equation:

Eq. 10.5

$$\% \text{ Relative error} = \left[\frac{\text{predicted value} - \text{experimental value}}{\text{predicted value}} \right]$$

It can be seen that in all cases there was a reasonable agreement between the predicted and the experimental value, since low value of the bias were found. For this reason it can be concluded that the equations describe adequately the influence of the selected process variables on the responses under study.

Table 10.11: Comparison of responses between predicted and experimental values for the cross-validation set.

Responses	Test	Factors/levels			Experimental values	Predicted values	% Relative error
		A	B	C			
% Entrapment	1	-0.7	-1	-0.7	71.84	74.35	-3.5
	2	0.3	0	-0.7	81.28	79.33	2.4
	3	0.3	0	-0.3	80.25	82.74	-3.1
	4	0	-0.3	0.7	76.43	74.74	2.2
	5	1	0.7	0.7	78.64	76.04	3.3
T_{50}	1	-0.7	-1	-0.7	19.46	18.78	3.5
	2	0.3	0	-0.7	33.90	34.71	-2.4
	3	0.3	0	-0.3	35.16	36.28	-3.2
	4	0	-0.3	0.7	34.87	33.89	2.8
	5	1	0.7	0.7	48.65	49.92	-2.6
T_{90}	1	-0.7	-1	-0.7	29.70	30.68	-3.3
	2	0.3	0	-0.7	44.35	43.33	2.3
	3	0.3	0	-0.3	45.72	47.14	-3.1
	4	0	-0.3	0.7	46.63	47.85	-2.6
	5	1	0.7	0.7	67.77	66.75	1.5
Particle size	1	-0.7	-1	-0.7	1.91	1.94	-1.2
	2	0.3	0	-0.7	2.04	2.00	1.9
	3	0.3	0	-0.3	2.03	2.05	-1.1
	4	0	-0.3	0.7	1.94	1.90	1.8
	5	1	0.7	0.7	2.17	2.14	1.4

10.3.5. CURVE FITTING AND RELEASE MECHANISM

'In vitro' dissolution profile of the optimized batch is shown in Figure 10.19A. Values of release exponent (n) and kinetic constant (K) were derived using zero-order kinetics, first-order kinetics, Higuchi's square root of time equation, Korsmeyer-Peppas' power law equation and Hixson-Crowell's cube root of time equation and presented in Table 10.12. The enzyme release data show a good fit to the Korsmeyer-Peppas' power law release kinetics (Eq. 7.23) which can be confirmed by comparing the values of correlation coefficient (r) with that of the other models. The values of Korsmeyer-Peppas' release exponent (n) determined for the various formulations studied ranged from 1.30 to 2.42 suggesting the probable release by super case-II transport. The K_k values ranged from 0.003 to 0.83 where low K_k value may suggest near to zero release from the beads

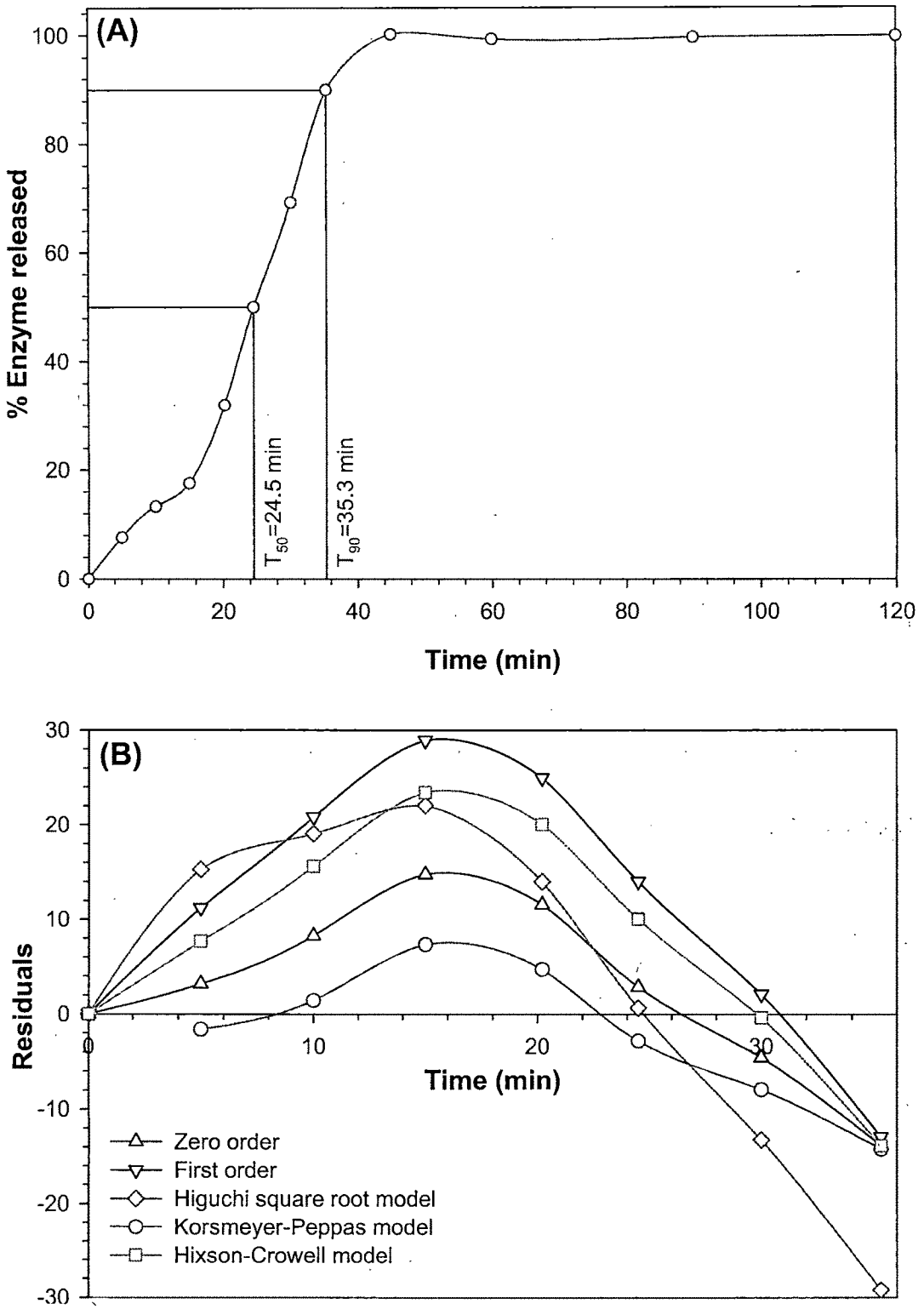

Figure 10.19: (A) 'In vitro' release profile of optimized formulation (experiment 3) in SGF without enzyme. (B) Residual plot of different release models for the same formulation.

Table 10.12: Comparison of different dissolution kinetics models.

ES[a]	Release model										
	Zero-order		First-Order		Higuchi matrix		Korsmeyer-Peppas			Hixson-Crowell	
	K_o	r_0	K_1	r_1	K_H	r_H	n	K_k	r_k	K_s	r_s
5	2.53	0.96	-0.08	0.90	13.06	0.87	1.33	0.83	0.97	-0.02	0.94
11	1.55	0.95	-0.05	0.80	9.24	0.81	1.64	0.12	0.97	-0.01	0.88
2	1.65	0.94	-0.05	0.83	9.68	0.81	1.94	0.04	0.98	-0.01	0.90
14	1.09	0.93	-0.04	0.79	7.58	0.79	2.22	0.01	0.97	-0.01	0.89
7	2.40	0.94	-0.05	0.85	11.05	0.81	1.43	0.54	0.97	-0.01	0.89
9	1.47	0.94	-0.05	0.71	8.83	0.80	1.69	0.09	0.98	-0.01	0.85
1	1.79	0.94	-0.04	0.86	9.51	0.79	1.77	0.10	0.97	-0.01	0.89
12	1.16	0.93	-0.04	0.86	8.02	0.80	2.42	0.00	0.98	-0.01	0.91
3	2.16	0.95	-0.04	0.84	10.23	0.82	1.30	0.74	0.97	-0.01	0.89
6	1.65	0.95	-0.05	0.83	9.74	0.81	1.81	0.07	0.99	-0.01	0.90
15	1.41	0.91	-0.03	0.82	7.75	0.76	1.80	0.06	0.97	-0.01	0.86
8	1.16	0.94	-0.04	0.84	8.09	0.80	2.14	0.01	0.94	-0.01	0.91
13	1.66	0.94	-0.05	0.85	9.78	0.81	2.00	0.04	0.99	-0.01	0.90

[a] ES, experimental sequence.

initially. If one considers the correlation coefficient (r) values of zero-order and Korsemeyer-Peppas release models, both models describe the dissolution data reasonably well. Where there are competing models (with similar r values), residuals analysis can be used to distinguish between the models(Pather et al., 1998). Figure 10.19B is the residual plot for optimized formulation. The residuals are high for the zero-order, first-order, Higuchi, and Hixson-Crowell models (and least for the Korsemeyer-Peppas model) which also shows systematic deviation: the models overpredict initially and underpredict at the later stages of the dissolution process. This indicates that Korsemeyer-Peppes' power low is the best-fit model in describing the dissolution behavior of pepsin from κ-carrageenan beads.

Finally, in order to know weather the enzyme release was due to erosion or diffusion, the release data of the optimized formulation was fitted to Kopcha model (Eq. 7.25) and parameters like A, B, and A/B at different time intervals were determined (Figure 10.20A). During dissolution study carrageenan gel swell but unable to maintain the gel

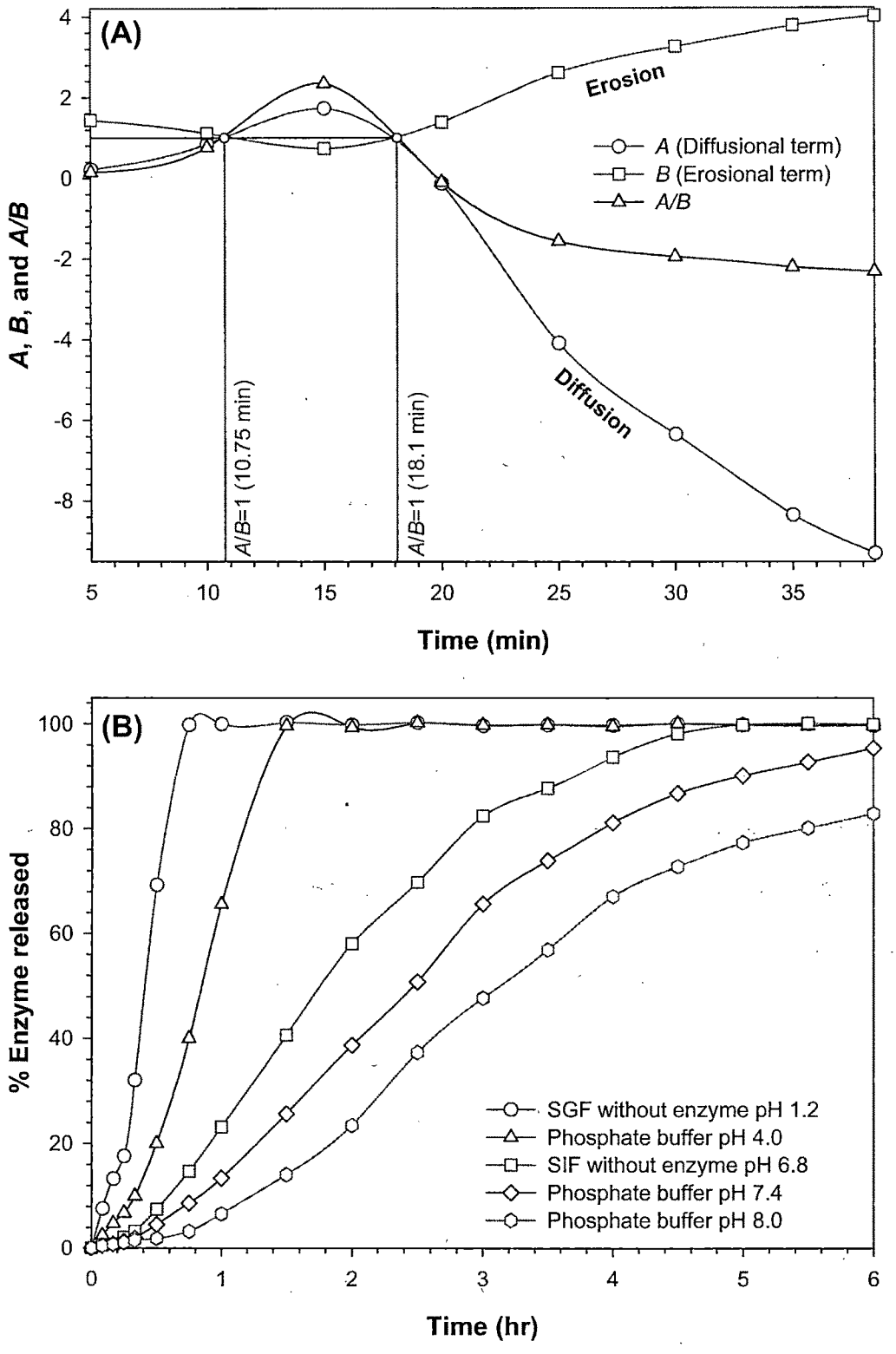

Figure 10.20: (A) Kopcha model parameters (*A*, *B*, and *A/B*) versus time profile for optimized batch (experiment 3). (B) Effect of pH on release profile of pepsin entrapped in κ-carrageenan beads.

matrix due to low gel strength and start to erode. Initially, up to 15 min, the diffusion term *A* increased and was predominant. However, erosion term *B* increased in the course of time, as erosion appeared latter. The corresponding Kopcha profile showed that after 15 min drug release was subsequent to predominant matrix erosion. This explains the biphasic nature (diffusional first and erosional latter) of the '*in vitro*' release profile of the optimized batch (Figure 10.20A). The erosion term *B* increases with time because erosion though the hydrated particles or the layer in process of diffusion is easier. The diffusion and erosion phenomena of the κ-carrageenan hydrogel can be explained as follows.

When a dry hydrogel begins to absorb water, the first water molecules entering the matrix will hydrate the most polar, hydrophilic groups. As the polar groups are hydrated, the network swells, and exposes hydrophobic groups, which also interact with water molecules. After the polar and hydrophobic sites have interacted with and bound water molecules, the network will imbibe additional water, due to the osmotic driving force of the network chains towards infinite dilution. This additional swelling is opposed by the covalent or physical crosslinks, leading to an elastic network retraction force. As the network swells, if the network chains or crosslinks are degradable, the gel will begin to disintegrate at a rate depending on its composition(Hoffman, 2002).

10.3.6. CHARACTERIZATION OF OPTIMAL FORMULATION

10.3.6.1. Effect of pH on Release Profile

The effect of pH on the release of pepsin from κ-carrageenan beads in different pH (1.2, 4.0, 6.8, 7.4, and 8.0) buffers simulating the human gastrointestinal tract is given in Figure 10.20B. Release of pepsin from κ-carrageenan beads in simulated gastric fluid is

conceivably attributed to the presence in the carrageenan molecule of strongly acidic sulphate groups that allow a certain degree of ionization to be maintained also at low pH(Bonferoni et al., 1994). The swelling and disintegration of κ-carrageenan beads are dependent on compositions of dissolution medium, ionic strength, pH, temperature, solubility of drug entrapped into beads, application of stress, or addition of specific solutes that compete with the polymeric ligand for the affinity site on the protein. As the pH increases, the degree of ionization of the κ-carrageenan hydrogel decreases. At the elevated pH, equilibrium-swelling level is delayed and the sustained-release profile was achieved subsequent to the diffusion. This study confirms the site-specific pepsin delivery to the stomach. Thus, κ-carrageenan beads are highly desirable for delivery of the drugs (i) that are locally active in the stomach, (ii) that have an absorption window in the stomach or in the upper small intestine, (iii) that are unstable in the intestinal or colonic environment, and / or (iv) have low solubility at high pH values. Alternatively, acid resistant but alkaline susceptible material coated κ-carrageenan beads can be used for sustained-delivery of the drugs (i) that are locally active in the small intense, (ii) that have an absorption window in the small intestine, (iii) that are unstable in the acidic or stomach environment, and / or (iv) have low solubility at low pH values.

10.3.6.2. Fourier Transform Infra-Red Spectroscopy (FTIR)

FTIR spectra of κ-carrageenan powder, carrageenan blank beads, pepsin loaded carrageenan beads, physical mixture of pepsin and blank beads, and pepsin are shown in Figure 10.21. FTIR spectrum of κ-carrageenan powder showed various distinct peaks: very broad band spreading 3150-3600 cm^{-1} (strong; s) due to polyhydroxy $(-OH)_n$ group; 2964 cm^{-1} (s), 2920 cm^{-1} (s), and 2852 cm^{-1} (medium; m) due to C-H stretch; 1425 cm^{-1}

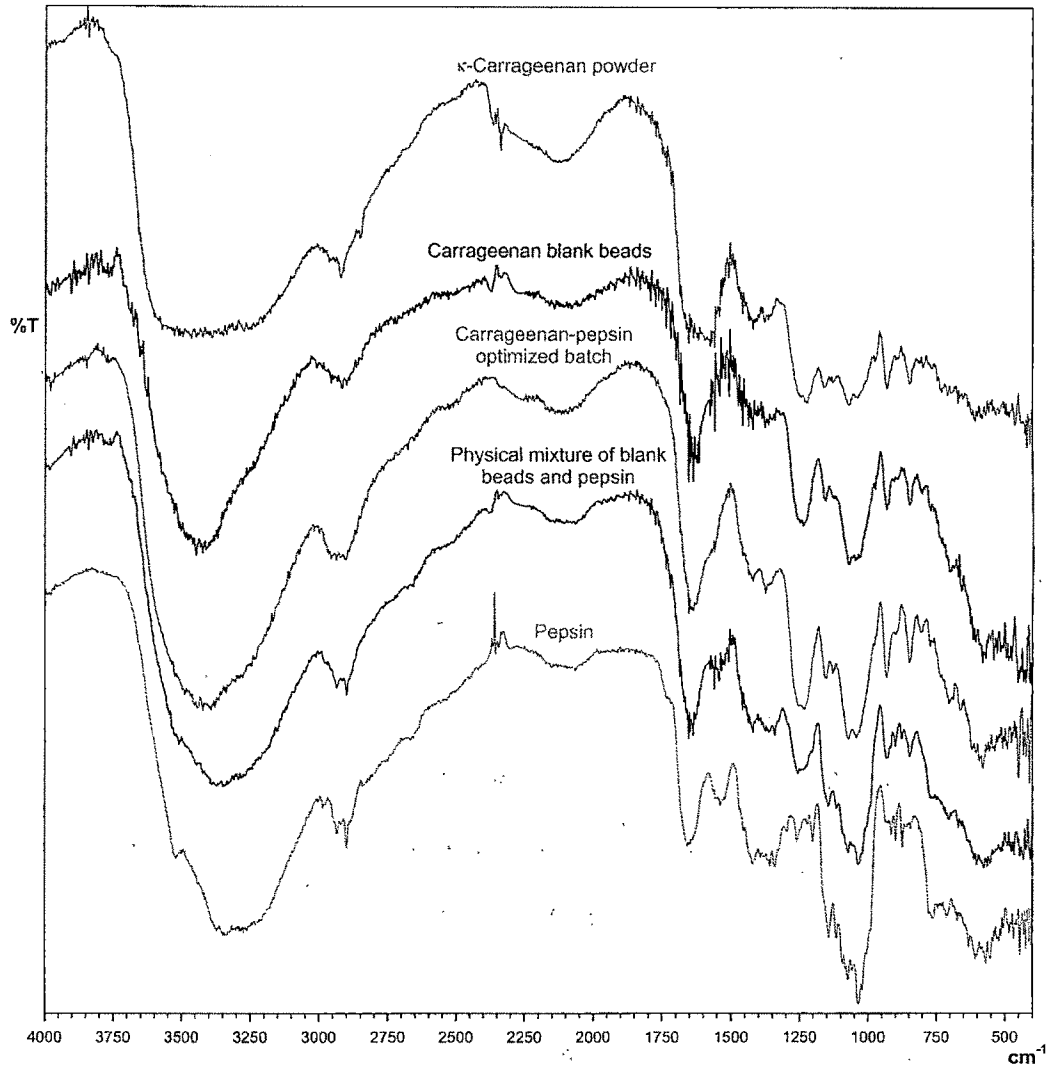

Figure 10.21: The FTIR spectra of κ-carrageenan powder, carrageenan blank beads, pepsin loaded carrageenan beads, physical mixture of pepsin and blank beads, and pepsin.

(s) and 1375 cm^{-1} (s) due to C-H deformation; 1222 cm^{-1} (s) due to S=O stretch of sulfate ester salt; 1070 cm^{-1} due to C-O stretch of cyclic ethers; 929 cm^{-1} (s) due to C-O stretch of polyhydroxy groups attached to carbons; etc. Crosslinking of carrageenan by K^+ was shown by a decrease in the intensity of S=O stretch (1222 cm^{-1}) of sulfate ester group which was same as C-O stretch (1070 cm^{-1}) of cyclic ethers in intensity for the κ-carrageenan powder. Moreover, the peak of sulfate ester group was displaced by 14 cm^{-1}, from 1222 cm^{-1} to 1236 cm^{-1}.This was probably because of some negatively charged

sulfate ester reacted with positively charged K^+ and resulted in physicochemical changes of carrageenan. Pepsin also showed various distinct peaks: one predominant band at 3220-3380 cm^{-1} (s) due to N-H stretch of secondary N-substituted amides; 2980 cm^{-1} (weak; w) due to C-H stretch, medium bands at 1550 cm^{-1} due to C=C, while 880 cm^{-1} (s) and 875 cm^{-1} (s) due to *p*-substituted aromatic out of plane C-H deformation of aromatic residue of tryptophan or tyrosine; 2895 cm^{-1} (s) and 2938 cm^{-1} (s) due to C-H stretch, while 1418 cm^{-1} (m), 1327 cm^{-1} (m), and 1337 cm^{-1} (m) due to C-H deformation of alkyl chain of amino acids (particularly of isopropyl group of leucine); 1662 cm^{-1} (w) due to C=O stretch of carboxylate anion and amide group; strong peaks between 1030-1150 cm^{-1}, weak bands at 545-615 cm^{-1}, and 400-450 cm^{-1} due to C-S stretch of sulfides and disulfides. With incorporation of pepsin, the spectrum of beads was similar to that of the κ-carrageenan blank beads. However, the physical mixture of pepsin and blank beads showed the peaks due to both pepsin and κ-carrageenan. This confirms the pepsin entrapment into the κ-carrageenan beads at molecular level.

10.3.6.3. Differential Scanning Calorimetry (DSC)

The DSC thermograms of potassium chloride, pepsin, κ-carrageenan, blank beads, and pepsin-loaded beads are shown in Figure 10.22. Potassium chloride showed two non-significant exothermic peaks at 323° and 374°. Pepsin exhibited 4 endothermic peaks at 146°, 204.7°, 219.5°, and 255.4° followed by a broad degradation exotherm at 347°. Broad endothermic peak at 85°C in the thermogram of κ-carrageenan was observed due to the presence of water molecules. Two minor peaks at 259° and 266°C in the degradation exotherm of κ-carrageenan were absent in blank beads and pepsin loaded beads, while

major exothermic peak at 344°C was found to be shifted towards higher temperature (358°C) in blank beads. This showed that, κ-carrageenan-KCl beads are more stable than

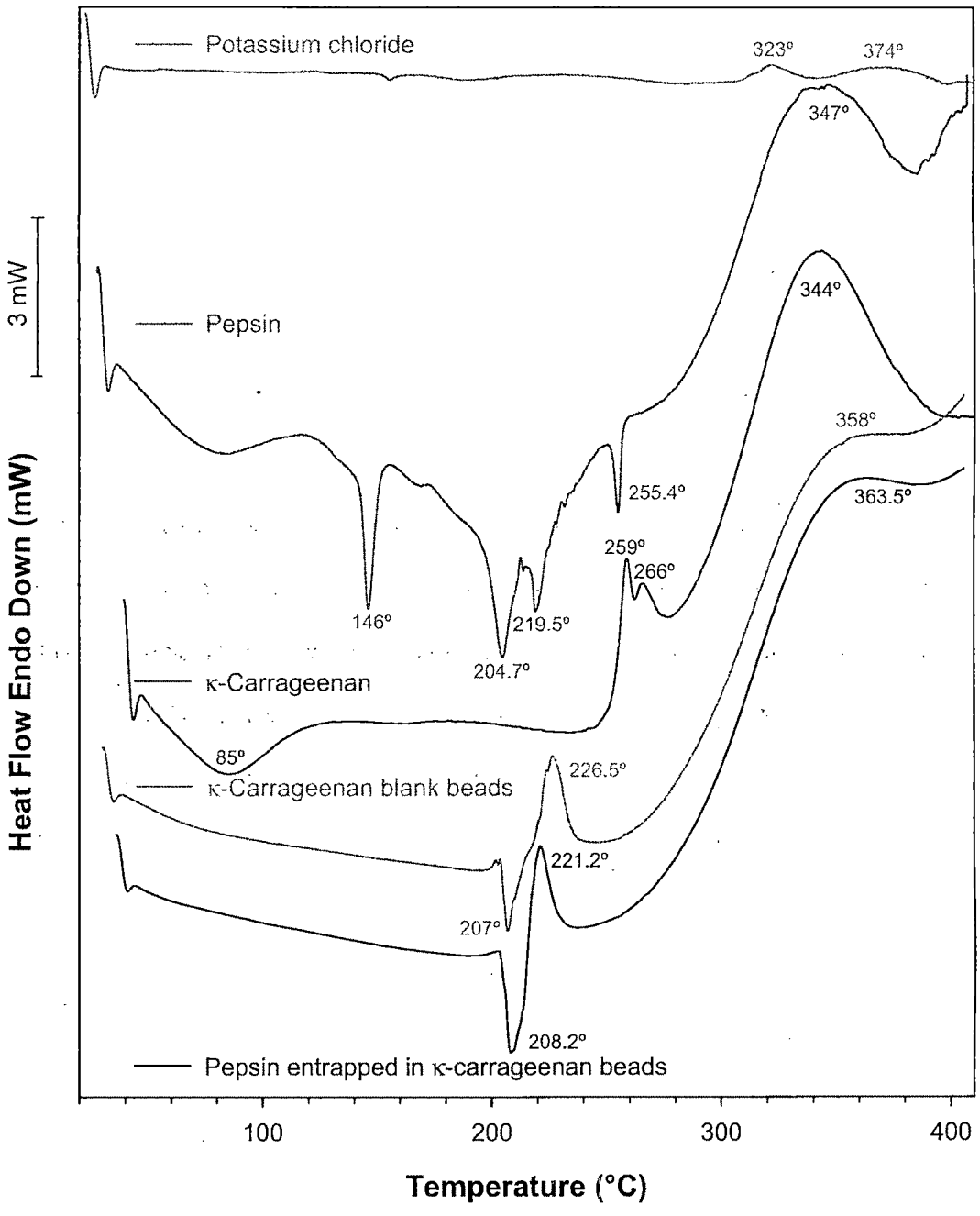

Figure 10.22: The DSC thermograms of potassium chloride, pepsin, κ-carrageenan powder, blank beads, and pepsin loaded carrageenan beads made at the same analytical conditions.

κ-carrageenan. However, additional two peaks (one endothermic at 207° and one exothermic at 226.5°C) were observed in the thermogram of blank beads due to the potassium- κ-carrageenan interaction. DSC thermogram of enzyme loaded beads was similar to that of blank beads except all corresponding peaks were shifted to higher temperature, might be due to the presence of pepsin. However, it did not showed any peak analogous to pepsin. This confirms that most of the enzyme was uniformly dispersed at the molecular level in the beads.

10.3.6.4. Morphology of the Beads

The spherical shape of beads in wet state was usually lost after drying especially for beads prepared with low carrageenan concentration. In 2.5% w/v carrageenan, the dried beads were very irregular and tend to agglomerate due to low mechanical strength. With the increase of κ-carrageenan concentration (3.5% w/v), the shape of beads retained considerably. However, the shape of beads changed to spherical disc with a collapsed center (Figure 10.23) during drying process due to aggregation of the helical fibers into bundles and the squeezing out of some water from the gel (Iborra et al., 1997). Normally the spherical shape was retained when the carrageenan concentration was as high as 5.0% (w/v), but viscosity of 5.0% w/v solution was too high for bead preparation under present experimental conditions so it was not studied. Crosslinked hydrogels reach an equilibrium swelling level in aqueous solutions which depends mainly on the crosslink density. In some cases, depending on the solvent composition, temperature and solids concentration during gel formation, phase separation can occur, and water-filled 'voids' or 'macropores' can form which can be observed Figure 10.18. One noticeable characteristic

of the beads surface is high degree of crosslinking when the concentration of potassium chloride increased (Figure 10.18A-C). Further, the surface morphology was improved (i.e. decrease in roughness) with increase in κ-carrageenan concentration (Figure 10.18D-F) due to the high viscosity of the κ-carrageenan solution.

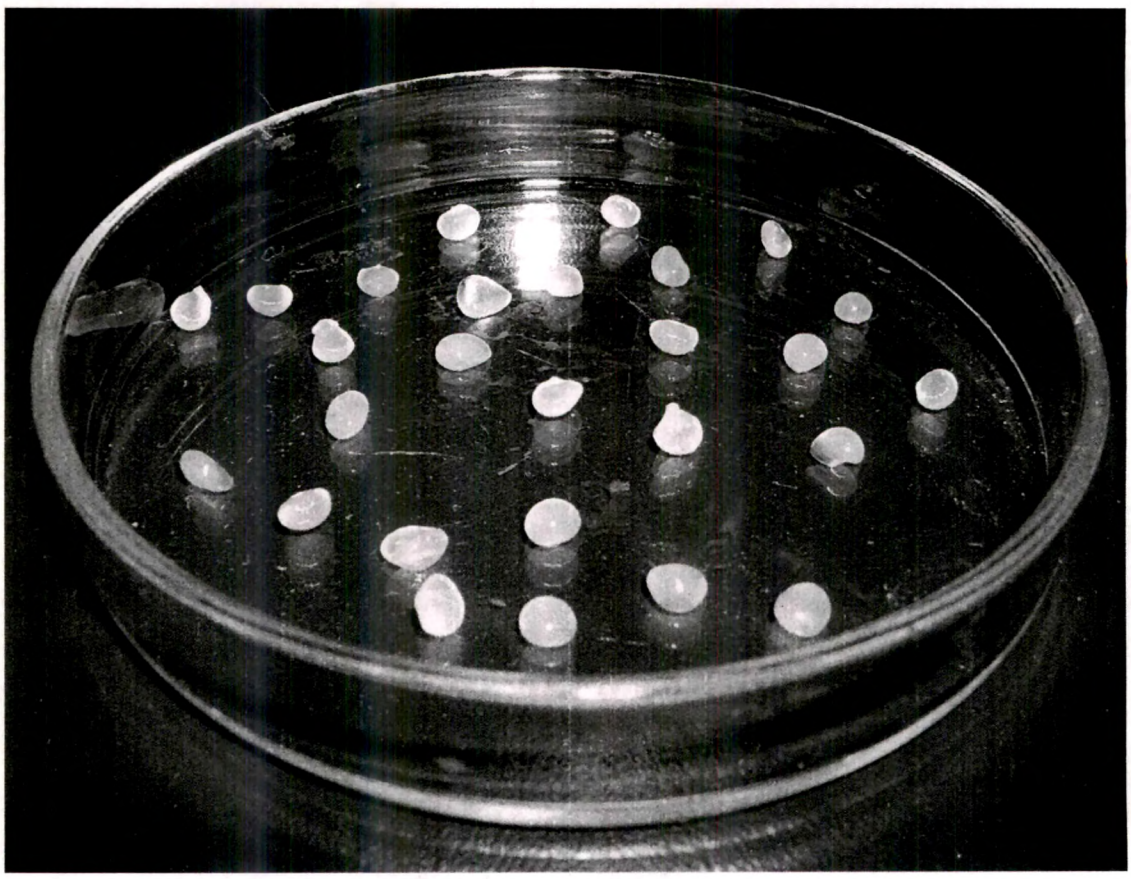

Figure 10.23: Photograph of wet κ-carrageenan beads showing spherical disk shape with collapsed centre during drying process.

10.3.7. STABILITY STUDY

For the developed formulation, the similarity factor (f_2) was calculated by a comparison of the dissolution profiles at each storage condition with the control at the initial condition. Results of f_2 factors ranged from 67 to 95 with 2 to 5% average difference.

Overall, results from the stability studies indicated that capsules were physically and chemically stable for at least 12 months at 40±2°C/75±5% relative humidity and for more than 12 months (approximately for double time period) at 30±2°C/65±5% relative humidity. An approach for analyzing the data on a quantitative attribute that is expected to change with time is to determine the time at which the 95% one-sided confidence limit for the mean curve intersects the acceptance criterion (not more than 5% change in assay from its initial value). The accelerated stability data for prepared formulation, marketed formulation and the bulk pepsin were extrapolated to calculate the shelf-life (Figure 10.24) and were found be 3.24 years, 0.97 year, and 0.40 year respectively. Hence, the stability of the entrapped pepsin was significantly improved than the conventional dosage forms.

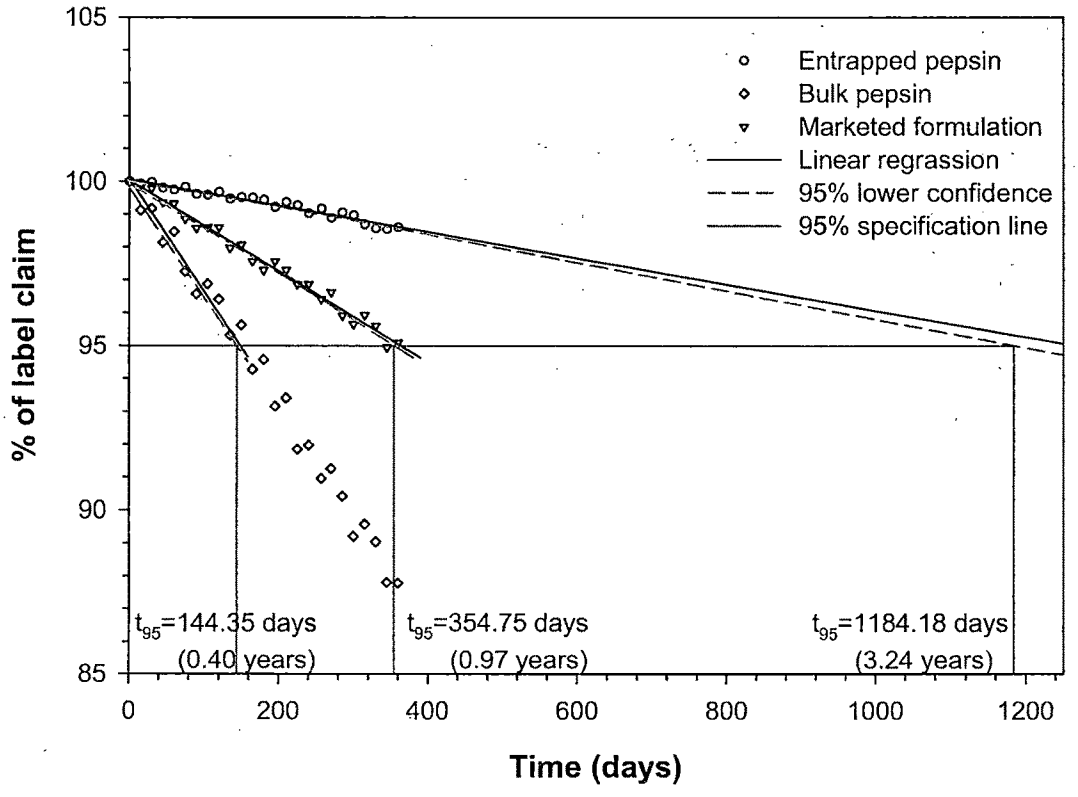

Figure 10.24: Extrapolation of accelerated stability data for shelf-life calculation.

10.3.8. CONCLUSIONS

Ionotropically corsslinked κ-carrageenan beads exhibited promising stability improvement of entrapped pepsin and can find a place in the design of multiparticulate drug delivery systems. The optimization of the process using the response surfaces resulted in more than 81% entrapment and less than 36 min of T_{90} at optimized process variables (experiment 3). T_{50} and T_{90} were increased with increase in all three process variables. Percentage entrapment and particle size were found to be directly proportional to κ-carrageenan concentration and inversely proportional to potassium chloride concentration and hardening time. Mathematical analysis of the different drug release modalities has evidenced that enzyme release from carrageenan beads follows Korsmeyer-Peppas' power law equation with super case-II transport mechanism. Further, the investigation of release profile by Kopcha model revealed that enzyme release up to 15 min was due to diffusion followed by erosion. FTIR and DSC study showed uniform dispersion of pepsin at molecular level in the carrageenan beads. Texture analysis discovered directly proportional relation of degree of crosslinking with potassium chloride concentration. Also the surface roughness decreased with increase in κ-carrageenan concentration. Accelerated and long term stability study illustrated considerably improved shelf-life of pepsin entrapped in carrageenan than the conventional dosage form. Results of presented experiments seem to be of value for the pharmaceutical industries associated with digestive enzymes formulations.

10.4. References

AN, H., SEYMOUR, T. A., WU, J. W. and MORRISSEY, M. T., 1994. Assay systems and characterization of Pacific whiting (*Merluccius productus*) protease. J. Food Sci. 59, 277-281.

BHARDWAJ, S. B., SHUKIA, A. J. and COLLINS, C. C., 1995. Effect of varying drug loading on particle size distribution and drug release kinetics of verapamil hydrochloride microspheres prepared with cellulose esters. J. Microencapsul. 12, 71-81.

BODMEIER, R. and WANG, J., 1993. Microencapsulation of drugs with aqueous colloidal polymer dispersions. J. Pharm. Sci. 82, 191-194.

BONFERONI, M. C., ROSSI, S., TAMAYO, M., PEDRAZ, J. L., DOMINGUEZ GIL, A. and CARAMELLA, C., 1994. On the employment of λ carrageenan in a matrix system. II: λ carrageenan and hydroxypropylmethylcellulose mixtures. J. Controlled Release 30, 175–182.

GARCIA, A. M. and GHALY, E. S., 1996. Preliminary spherical agglomerates of water soluble drug using natural polymer and cross-linking technique. J. Controlled Release 40, 179-186.

HOFFMAN, ALLAN S., 2002. Hydrogels for biomedical applications. Advanced Drug Delivery Reviews 43, 3-12.

IBORRA, JOSE L., MANJON, ARTURO and CANOVAS, MANUEL, 1997. Immobilization in carrageenans. in: BICKERSTAFF, G. F. (Ed.) Immobilization of Enzymes and Cells, Methods in Biotechnology, Vol. 1, Humana Press, Totowa, New Jersey, pp. 53-60.

PATHER, S. INDIRAN, RUSSELL, IRINA, SYCE, JAMES A. and NEAU, STEVEN H., 1998. Sustained release theophylline tablets by direct compression Part 1: formulation and in vitro testing. Int. J. Pharm. 164, 1-10.

SANKALIA, MAYUR G., MASHRU, RAJASHREE C., SANKALIA, JOLLY M. and SUTARIYA, VIJAY B., 2004. Evaluation and simultaneous optimization of papain entrapped in crosslinked alginate beads using 3^3 factorial design and the desirability function. ARS Pharmaceutica 45, 253-279.

SANKALIA, MAYUR G., MASHRU, RAJASHREE C., SANKALIA, JOLLY M. and SUTARIYA, VIJAY B., 2005. Papain Entrapment in Alginate Beads for Stability Improvement and Site Specific Delivery: Physicochemical Characterization and Factorial Optimization using Neural Network Modeling. AAPS PharmSciTech 7, Article xx (in press).

SEVERIAN, DUMITRIU and ESTEBAN, CHORNET, 1998. Inclusion and release of proteins from polysaccharide-based polyion complexs. Advanced Drug Delivery Reviews 31, 223-246.

SIPAHIGIL, O. and BORTUNC, B., 2001. Preparation and in vitro evaluation of verapamil HCl and ibuprofen containing carrageenan beads. Int. J. Pharm. 228, 119-128.

SIPAHIGIL, O. and DORTUNC, B., 2001. Preparation and in vitro evaluation of verapamil HCl and ibuprofen containing carrageenan beads. Int. J. Pharm. 228, 119-128.

11. CHITOSAN-ALGINATE BEADS

11.1. Chitosan-Alginate Amylase Beads

11.1.1. PRINCIPLE OF PEC FORMATION

The electrostatic attraction between the cationic amino groups of chitosan (the macro pKa is about 6.5) (Lee et al., 1999) and the anionic carboxyl groups of the alginate is the main interaction leading to the formation of the PEC. It is stronger than most secondary binding interactions (Lee et al., 1999). In order to prepare the beads with reverse engineering, the formation of good mechanical strength membrane (precipitate) at the interface of both the polymer is essential. This is required to avoid the homogenous mixing of chitosan and alginate solution and also to maintain the geometry of the bead, which may otherwise easily distorted even under the mild shear stress of the stirring. Table 11.1 depicts the effect of chitosan and alginate solution pH on the beads properties. As can be seen, the M-2 condition resulted in the spherical beads with no aggregates. Moreover, the membrane was thin but the mechanical strength was good enough. At acidic environment chitosan is highly protonated and at neutral or alkaline environment alginate is decidedly anionic. Under such circumstances, maximum interaction between amino and carboxyl group takes place (see Figure 8.3) and results in compact membrane. Moreover, chitolytic activity of α-amylase can be suppressed almost entirely at the acidic

range of chitosan solution (α-amylase is functionally inactive at acidic pH) to prevent the digestion of chitosan.

Table 11.1: Effect of chitosan and alginate solution ph on beads properties[a].

Sr. No.	pH		Mechanical strength of membrane[b]	Membrane thickness	Comments
	Chitosan solution	Alginate solution			
M-1	2	3.5	– + –	thick	alginate viscosity very high, bead shape distorted, beads aggregated
M-2	2	6.5	+ + +	thin	spherical beads, no aggregate
M-3	5.4	3.5	– – –	very thin	lump of chitosan after few minutes, chitosan and alginate viscosity very high
M-4	5.4	6.5	– + –	thin	chitosan viscosity very high, beads aggregated

[a] results are comparative for 2% w/v chitosan, 2% w/v alginate, and 30 min hardening time.
[b] + + +, excellent; – + –, good; – – –, poor.

11.1.2. EFFECT OF THE FACTORS ON RESPONSES

11.1.2.1. % Entrapment

ANOVA results and regression coefficients of response variables are shown in Table 11.3. All three process variables were statistically significant (P <0.05). From the contour plots of the response surface for % entrapment (Figure 11.1) and Table 11.3, it can be concluded that concentration of alginate was the most influencing factor and affecting positively (i.e. response increases with increase in factor level). However, hardening time was affecting negatively (i.e. response decreases with increase in factor level) in significant amount. More than 90% entrapment (experiment 28, 8, and 12; Table 11.2) was obtained at the high level of the all three process variables.

Table 11.2: Matrix of 3^3 full factorial design and results for the measured responses.

	Factrors/Levels			Responses			
ES[a]	Chitosan (% w/v)	Sodium alginate (% w/v)	Hardening time (min)	% Immobilization	T_{50}	T_{90}	Particle Size (mm)
19	-1	-1	-1	82.21	29.20	33.50	1.020
11	-1	-1	0	81.48	33.30	38.40	1.013
24	-1	-1	1	81.18	36.40	43.70	1.011
31	-1	0	-1	85.22	34.70	40.50	0.960
23	-1	0	0	84.57	38.80	44.60	0.953
20	-1	0	1	84.26	42.40	49.20	0.950
7	-1	1	-1	88.55	40.50	46.50	0.910
16	-1	1	0	87.97	44.05	51.60	0.909
4	-1	1	1	87.61	48.10	55.60	0.909
29	0	-1	-1	83.66	27.20	33.50	1.530
5	0	-1	0	83.00	31.50	38.55	1.524
17	0	-1	1	82.71	34.40	40.40	1.522
25	0	0	-1	86.85	33.30	38.30	1.440
21	0	0	0	85.99	37.06	43.61	1.438
22	0	0	0	86.28	36.84	42.53	1.431
10	0	0	0	86.27	37.00	43.20	1.434
26	0	0	0	86.65	37.68	43.19	1.436
18	0	0	0	86.37	36.74	42.94	1.432
6	0	0	1	85.94	40.15	47.20	1.431
13	0	1	-1	90.38	38.70	44.20	1.380
27	0	1	0	89.88	43.20	49.50	1.375
1	0	1	1	89.51	46.55	52.95	1.370
15	1	-1	-1	85.35	26.30	31.30	1.940
3	1	-1	0	84.74	30.30	36.10	1.935
2	1	-1	1	84.46	33.05	38.50	1.933
9	1	0	-1	88.93	31.80	37.30	1.810
30	1	0	0	88.42	35.40	41.50	1.805
14	1	0	1	88.11	38.80	44.30	1.802
28	1	1	-1	92.64	37.20	42.85	1.728
8	1	1	0	92.24	40.40	46.80	1.723
12	**1**	**1**	**1**	**91.91**	**44.15**	**49.90**	**1.719**

[a] ES, experimental sequence.

On addition of chitosan solution to the alginate solution, instantaneous interfacial cross-linking takes place which is proportional to the charge density of the solutions. Higher concentration of the polymers and pH values corresponding to their ionized state results in increased charge density of both the polymers and will lead to intense cross-linking with small micropores. This probably might be the cause of minimized loss of enzyme

from the PEC beads and higher % entrapment values at higher polymer concentrations. However, longer hardening time may cause the deeper penetration of the alginate into the chitosan solution; probably inactivate the greater proportion of the enzyme and may results in less % entrapment values.

Table 11.3: ANOVA results (*P* values): effect of the variables on % entrapment, t_{50}, t_{90}, and particle size.

Factors	% Entrapment		T_{50}		T_{90}		Particle size	
	Coefficient[a]	*P*	Coefficient[a]	*P*	Coefficient[a]	*P*	Coefficient[a]	*P*
Intercept	86.31	<0.0001*	37.08	<0.0001*	43.24	<0.0001*	1.43	<0.0001*
A	1.88	<0.0001*	-1.67	<0.0001*	-1.95	<0.0001*	0.43	<0.0001*
B	3.44	<0.0001*	5.62	<0.0001*	5.89	<0.0001*	-0.08	<0.0001*
C	-0.45	<0.0001*	3.62	<0.0001*	4.10	<0.0001*	0.00	0.0013*
A^2	0.19	0.0004*	0.05	0.7052	-0.11	0.5555	-0.05	<0.0001*
B^2	0.12	0.0102*	-0.01	0.9315	0.17	0.3772	0.02	<0.0001*
C^2	0.12	0.0101*	-0.28	0.0366*	-0.52	0.0119*	0.00	0.5583
AB	0.25	<0.0001*	-0.14	0.1623	-0.37	0.0182*	-0.03	<0.0001*
AC	0.04	0.2355	-0.15	0.1291	-0.56	0.0009*	0.00	0.8014
BC	0.03	0.4198	0.10	0.2847	0.05	0.7324	0.00	0.7243
ABC	0.01	0.8327	-0.02	0.8316	0.12	0.5091	0.00	0.4377
$r^2_{adj.}$	0.9986		0.9962		0.9926		0.9998	

11.1.2.2. T_{50} and T_{90}

As shown in Table 11.3 and Figure 11.1, all three factors had significant positive effect on both response values. The alginate concentration (factor *B*) was found to be most influencing factor. For maximum activity of enzyme in the intestine longer T_{50} and T_{90} were the desired criteria for the optimum formulation. Thus, extreme level of all three variables were resulted the beads with T_{50} and T_{90} as high as 44.15 and 49.9 min respectively (experiment 12, Table 11.2). T_{50} and T_{90} were found to be proportional to the alginate concentration and hardening time while inversely proportional to the chitosan concentration. This may explained as follows:

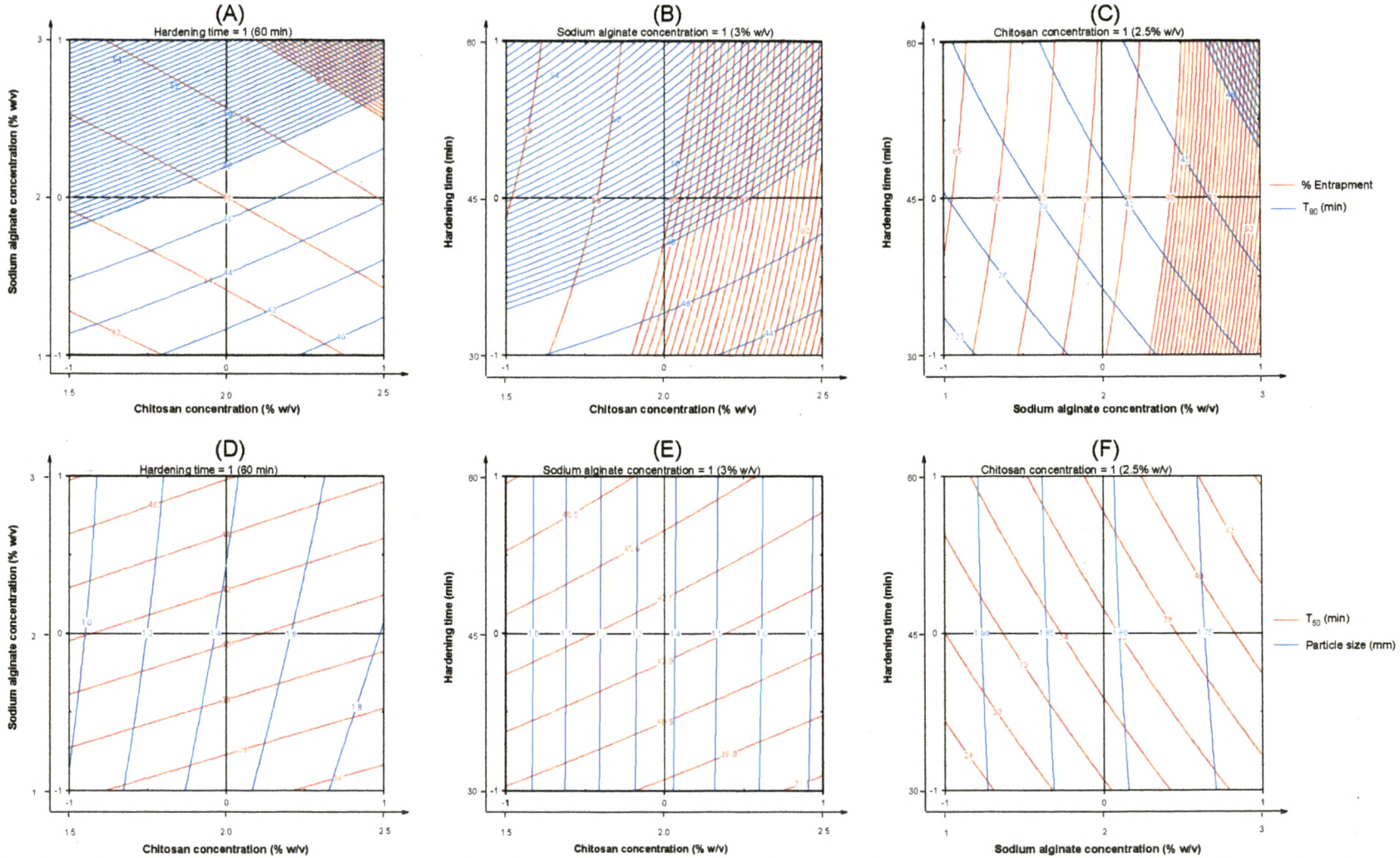

Figure 11.1: Contour plots of % entrapment, T_{90}, T_{50}, and particle size as a function of chitosan concentration, sodium alginate concentration, and hardening time.

Alginate prepares the outer layer of the beads. Thus higher concentration of alginate avails higher charge density of alginate carboxyl group and results in higher cross-linking of the PEC thus it prepare stronger PEC membrane with less thickness and small micropores. Alginate, upon exposure to the acidic dissolution media, might be converted to alginic acid, which is more viscous than alginate and results in delayed dissolution of the beads. Similarly, as mentioned above, longer hardening time may cause the deeper penetration of the alginate into the chitosan and prepare the thick PEC at the surface which will require longer time for complete dissolution. The release of enzyme from the beads is due to burst of the PEC membrane (see 'Curve Fitting and Release Mechanism' below). In the core of the beads, chitosan is not complexed with alginate and thus provides a good hypertonic environment for osmosis to occur. As the chitosan concentration increases, the hypertonicity also increases and exert greater amount of osmotic pressure against the mechanical strength of the PEC membrane. Thus, higher concentration of chitosan cause early busts effect and short T_{50} and T_{90}.

11.1.2.3. Particle Size

As depicted in Table 11.3, the chitosan concentration (factor A; most influential) and hardening time had positive coefficient, while alginate concentration had negative coefficient. All three process variables were statistically significant ($P<0.05$). The bead size is influenced by the orifice of the needle through which the chitosan is allowed to pass, addition of surfactant, extrusion rate, (which were kept constant) surface tension and the viscosity of the chitosan solution. Increased viscosity at higher concentration of chitosan resulted in larger particles. As before, the higher concentration of alginate provides the higher charge density and results in stronger but thin membrane with small

micropores. Thus, increased alginate concentration cause decrease in the particle size. The effect hardening time seems to be negligible indicating that the interaction of chitosan-alginate is instantaneous and the membrane formed upon first exposure is hard enough to restrict the expansion or constriction due to longer hardening time.

11.1.3. INTERACTIONS BETWEEN THE FACTORS

An interaction is the failure of a factor to produce the same effect on the response at the different levels of the other factor. The ANOVA results (Table 11.3) showed that interaction *AB* had significant influence on % entrapment, T_{90}, and particle size; while interaction *AC* had significant effect on only T_{90}. However, other interaction terms were non-significant statistically. The analysis of the results by multiple regression (Table 11.3) leads to equations that adequately describe the influence of the selected factors on % entrapment, T_{50}, T_{90}, and particle size.

11.1.4. OPTIMIZATION OF THE PROCESS USING THE RESPONSE SURFACES

Generally the aim of the optimization is to find the optimum levels of the variables, which affect a process, where a product of desired characteristics could be produced easily and reproducibly. Using the response surface of selected responses with constraint (% entrapment > 90% and T_{90} > 48 min), it was possible to identify the optimum region. In Figure 11.1;A-C the contour plots that describe the influence of the independent factors on the % entrapment and T_{90} have been presented. The study of these plots showed that the beads with desired characteristic could be produced at extreme levels (+1) of all three

process variables. Experiment 12 was the batch with the same experimental condition and was fulfilling both the constraints favorable for the beads preparation, hence was considered the optimum batch.

11.1.5. EVALUATION OF MODEL USING CROSS-VALIDATION

In order to assess the reliability of the model, five experiments were conducted by varying the process variables at values other than that of the model. For each of these test experiments the responses were estimated by using derived quadratic polynomial equations and experimental procedure for comparison between both responses (Table 11.4).

Table 11.4: Comparison of responses between predicted and experimental values for the cross-validation set.

Responses	Test	Factors/levels			Experimental values	Predicted values	% Relative error
		A	B	C			
% Entrapment	1	-1	-0.6	-0.6	63.26	62.50	1.2
	2	-0.6	0	0.4	65.34	63.70	2.5
	3	-0.4	0.6	0	66.23	68.08	-2.8
	4	0	-0.4	0.6	73.71	71.79	2.6
	5	0.4	0.4	-0.4	76.44	78.28	-2.4
T_{50}	1	-1	-0.6	-0.6	19.88	20.44	-2.8
	2	-0.6	0	0.4	30.28	31.10	-2.7
	3	-0.4	0.6	0	34.76	33.68	3.1
	4	0	-0.4	0.6	33.82	34.66	-2.5
	5	0.4	0.4	-0.4	38.44	37.96	1.2
T_{90}	1	-1	-0.6	-0.6	29.48	29.22	0.9
	2	-0.6	0	0.4	41.51	42.39	-2.1
	3	-0.4	0.6	0	46.83	46.09	1.6
	4	0	-0.4	0.6	45.57	46.66	-2.4
	5	0.4	0.4	-0.4	50.81	51.37	-1.1
Particle size	1	-1	-0.6	-0.6	1.75	1.71	2.1
	2	-0.6	0	0.4	1.73	1.76	-1.8
	3	-0.4	0.6	0	1.76	1.74	1.3
	4	0	-0.4	0.6	1.94	1.98	-2.2
	5	0.4	0.4	-0.4	2.03	2.06	-1.6

% Relative error was calculated by the following equation:

Eq. 11.1

$$\% \text{ Relative error} = \left[\frac{\text{predicted value} - \text{experimental value}}{\text{predicted value}} \right]$$

It can be seen that in all cases there was a reasonable agreement between the predicted and the experimental value, since low value of the % relative error were found. For this reason it can be concluded that the equations describe adequately the influence of the selected process variables on the responses under study.

11.1.6. CURVE FITTING AND RELEASE MECHANISM

'In vitro' dissolution profile of the optimized batch is shown in Figure 11.2A. Values of release exponent (n) and kinetic constant (K) were derived using zero-order kinetics, first-order kinetics, Higuchi's square root of time equation, Korsmeyer-Peppas' power law equation and Hixson-Crowell's cube root of time equation and presented in Table 11.5. The enzyme release data show a good fit to the Korsmeyer-Peppas' power law release kinetics (Eq. 8.5) which can be confirmed by comparing the values of correlation coefficient (r) with that of the other models. The values of Korsmeyer-Peppas' release exponent (n) determined for the various formulations studied ranged from 2.08 to 2.72 suggesting the probable release by super case-II transport. The K_k values ranged from 0.003 to 0.93 where low K_k value may suggest near to zero release from the beads initially. If one considers the correlation coefficient (r) values of zero-order and Korsemeyer-Peppas release models, both models describe the dissolution data reasonably well. Where there are competing models (with similar r values), residuals analysis can be used to distinguish between the models (Pather et al., 1998). Figure 11.2B is the residual plot for optimized formulation. The residuals are high for the zero-order, first-order,

Higuchi, and Hixson-Crowell models (and least for the Korsemeyer-Peppas model) which also shows systematic deviation: the models overpredict initially and underpredict at the later stages of the dissolution process. This indicates that Korsemeyer-Peppes' power low is the best-fit model in describing the dissolution behavior of α-amylase from chitosan-alginate PEC.

Table 11.5: Comparison of different dissolution kinetics models.

ES[a]	Release model										
	Zero-order		First-Order		Higuchi matrix		Korsmeyer-Peppas			Hixson-Crowell	
	K_o	r_0	K_1	r_1	K_H	r_H	n	K_k	r_k	K_s	r_s
19	1.88	0.80	-0.06	0.61	9.03	0.66	2.37	0.01	0.86	-0.01	0.70
11	1.62	0.80	-0.05	0.61	8.22	0.65	2.28	0.01	0.88	-0.01	0.70
24	1.46	0.81	-0.04	0.59	7.82	0.65	2.08	0.02	0.85	-0.01	0.70
31	1.59	0.81	-0.04	0.68	8.43	0.66	2.32	0.01	0.84	-0.01	0.74
23	1.42	0.81	-0.04	0.67	7.88	0.65	2.31	0.01	0.87	-0.01	0.74
20	1.17	0.78	-0.03	0.67	6.57	0.62	2.11	0.01	0.85	-0.01	0.71
7	1.30	0.78	-0.04	0.57	7.19	0.62	2.33	0.00	0.82	-0.01	0.69
16	1.06	0.75	-0.02	0.67	5.90	0.60	2.33	0.00	0.84	-0.01	0.70
4	0.96	0.75	-0.02	0.66	5.60	0.60	2.20	0.00	0.85	0.00	0.70
29	1.98	0.83	-0.05	0.72	9.48	0.68	2.49	0.01	0.90	-0.01	0.77
5	1.73	0.82	-0.06	0.57	8.79	0.67	2.34	0.01	0.89	-0.01	0.71
17	1.47	0.79	-0.03	0.70	7.49	0.64	2.15	0.01	0.85	-0.01	0.73
25	1.60	0.79	-0.04	0.63	8.10	0.64	2.37	0.01	0.86	-0.01	0.70
10	1.41	0.79	-0.04	0.62	7.53	0.64	2.21	0.01	0.87	-0.01	0.70
6	1.31	0.79	-0.04	0.56	7.29	0.64	2.17	0.01	0.87	-0.01	0.69
13	1.29	0.76	-0.03	0.66	6.85	0.61	2.38	0.00	0.84	-0.01	0.70
27	1.13	0.76	-0.02	0.66	6.30	0.61	2.21	0.01	0.85	-0.01	0.70
1	1.06	0.75	*	*	6.16	0.60	2.19	0.01	0.85	-0.01	0.61
15	1.98	0.81	-0.04	0.72	8.97	0.67	2.72	0.00	0.93	-0.01	0.76
3	1.67	0.80	-0.03	0.71	8.06	0.65	2.40	0.01	0.89	-0.01	0.75
2	1.62	0.80	-0.04	0.65	8.20	0.65	2.37	0.01	0.87	-0.01	0.72
9	1.52	0.79	-0.03	0.69	7.39	0.63	2.46	0.01	0.89	-0.01	0.73
30	1.37	0.78	-0.03	0.69	6.98	0.63	2.27	0.01	0.87	-0.01	0.72
14	1.29	0.77	-0.03	0.67	6.90	0.62	2.29	0.01	0.87	-0.01	0.71
28	1.41	0.78	-0.04	0.62	7.47	0.63	2.43	0.00	0.87	-0.01	0.70
8	1.14	0.75	-0.02	0.67	6.10	0.60	2.28	0.01	0.85	-0.01	0.70
12	**1.07**	**0.74**	**-0.02**	**0.65**	**5.94**	**0.59**	**2.21**	**0.01**	**0.83**	**-0.01**	**0.68**

[a] ES, experimental sequence.
* Not possible.

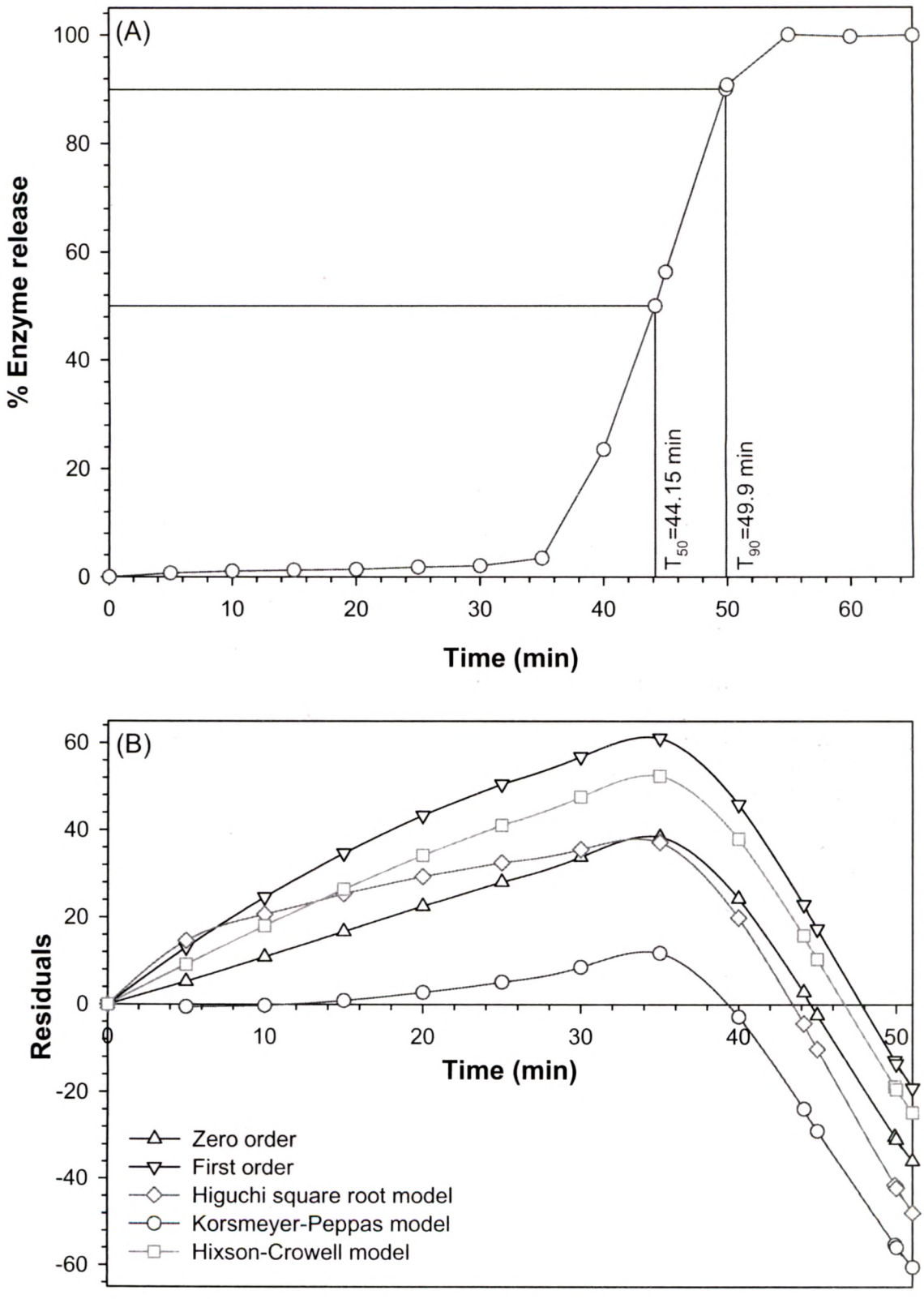

Figure 11.2: (A) 'In vitro' release profile of optimized formulation (experiment 12) in SGF without enzyme. (B) Residual plot for different release models (experiment 12).

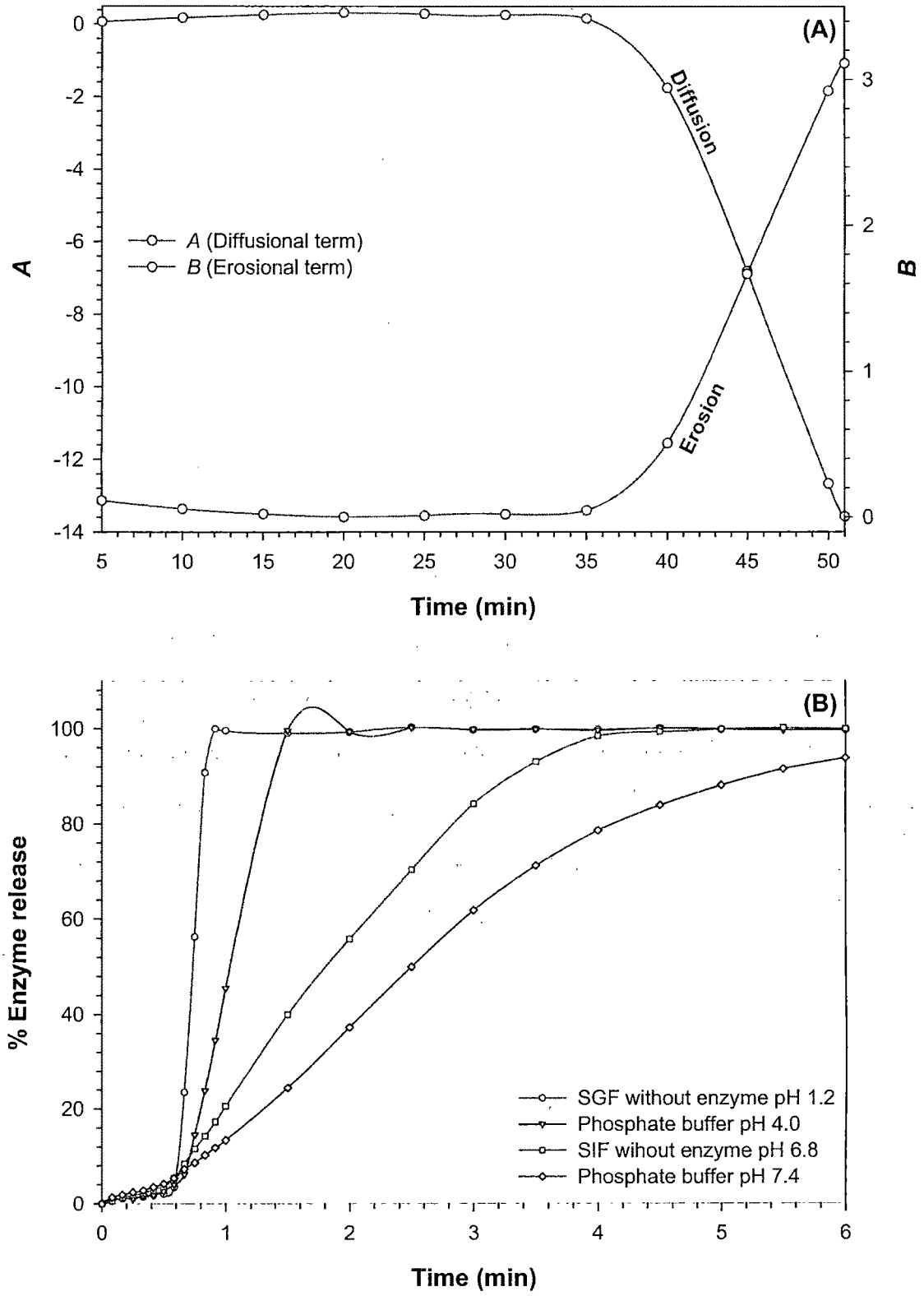

Figure 11.3: (A) Kopcha model parameters (*A* and *B*) versus time profile for optimized batch (experiment 12). (B) Effect of pH on release profile of α-amylase entrapped in chitosan-alginate beads.

Finally, in order to know weather the enzyme release was due to erosion or diffusion, the release data of the optimized formulation was fitted to Kopcha model (Eq. 8.7) and parameters like *A* and *B* at different time intervals were determined (Figure 11.3A). Initially, up to 35 min, though the diffusion term *A* was predominant, was almost constant near to zero. This suggests lack of α-amylase diffusion from the PEC and diffusion of dissolution media in side the PEC to hydrate it. However, erosion term *B* increased in the course of time, as erosion appeared latter and increased linearly afterwards to express the predominance of erosion relative to diffusion. The rate of hydration (depends on the cross-link density, chitosan and alginate concentration, hardening time, degree of deacetylation of chitosan, molecular mass of chitosan and alginate, pH, presence of salt-counter ions, etc.) initially was found to be the rate-limiting step for erosion and explains the biphasic nature of the release profile: plateau initially followed by steep rise in erosion rate. This indicates the burst of the PEC membrane which can be explained as follows.

When a dry hydrogel begins to absorb water, the first water molecules entering the matrix will hydrate the most polar, hydrophilic groups. As the polar groups are hydrated, the network swells, and exposes hydrophobic groups, which also interact with water molecules. After the polar and hydrophobic sites have interacted with and bound water molecules, the network will imbibe additional water, due to the osmotic driving force of the network chains towards infinite dilution. This additional swelling is opposed by the physical cross-links, leading to an elastic network retraction force. As the network swells, network chains or cross-links begin to disintegrate at a rate depending on its composition, rate of solvent intake, and equilibrium between the osmotic pressure and the mechanical strength of the PEC membrane (Hoffman, 2002).

11.1.7. CHARACTERIZATION OF OPTIMAL FORMULATION

11.1.7.1. Effect of pH on Release Profile

The effect of pH on the release of α-amylase from chitosan-alginate beads in different pH (1.2, 4.0, 6.8, and 7.4) buffers simulating the human gastrointestinal tract is given in Figure 11.3B. As with ionically cross-linked hydrogels, PEC exhibit pH-sensitive swelling not only in acidic but also in basic conditions (Berger et al., 2004). As pH changes, the charge balance inside the gel and therefore the degree of interaction between the two polymers is modified and swelling occurs because of the dissociation of the complex. In acidic medium, the polyacid (carboxylate $-COO^-$ of alginate) is neutralized and due to the free ammonium ($-NH_3^+$) groups of chitosan, free positive charges appear inside the bead. Their mutual repulsion and the entry of water together with counterions to neutralize these charges cause swelling. In basic medium, the mechanism is the same but swelling is induced by the free negative charges of the polyacid (Chu et al., 1995; Sakiyama et al., 1999). According to Cárdenas et al., the chitosan-alginate PEC in acidic conditions reaches a degree of swelling five times higher than in neutral conditions (Cárdenas et al., 2003). Similar reslts were obtained in the present study and can be explained by the schematic presentation of the ionic interactions between chitosan and alginate shown in Figure 11.4. As can be seen in Figure 11.4A, at pH 2.0, the ionic interaction between chitosan and alginate is very less and there is a folding of alginate with increased 'micropores' size which allow greater portion of dissolution media to enter with counterions. However, at pH 6.8, chitosan is still protonated and form much stronger network with alginate with small micropore size which restricts the entry of larger counterions. Moreover, osmotic pressure and electrostatic repulsion responsible for

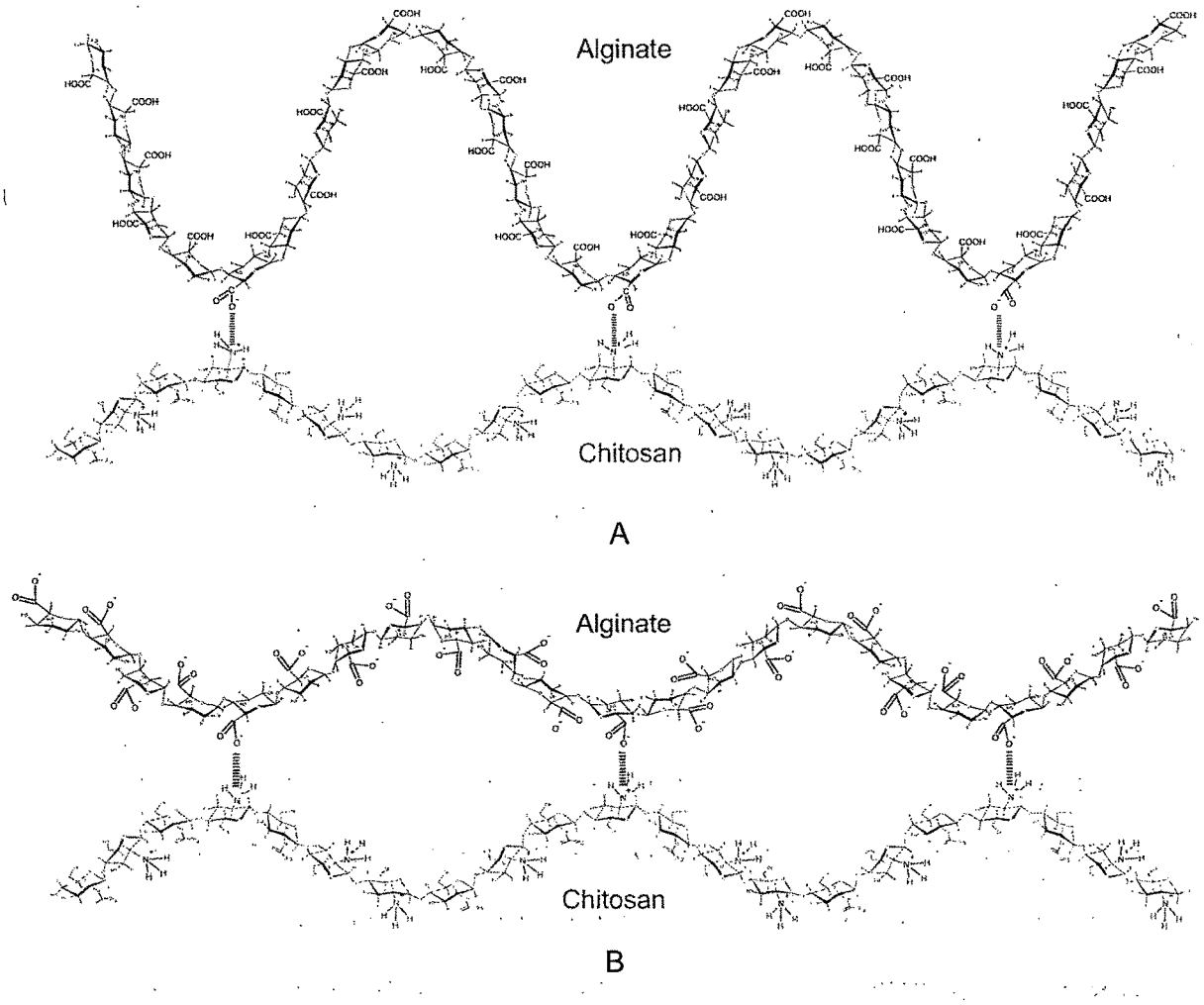

Figure 11.4: Schematic representation of the ionic interactions between alginate and chitosan at (A) pH 2.0 and (B) pH 6.8.

swelling are balanced by the contractile force of the network, which depends on elasticity (Sakiyama et al., 1999) and determines the maximum degree of swelling. If pH values is such that the global charge density of one of the polymer is no longer sufficiently high to ensure complexation, swelling becomes too significant and dissolution of the complex may observed (Chavasit et al., 1988). Burst effect for the optimized formulation in SGF without enzyme thus can be explained by the rapid swelling and lack of significant ionic interaction between chitosan-alginate at pH 1.2. As the pH increases, the swelling tend to decrease due to progressively increasing carboxyl groups. Further, solubility of chitosan

decreases at higher pH and act as a sustained-release matrix. Thus, the release of α-amylase is delayed at higher pH.

11.1.7.2. Fourier Transform Infra-Red Spectroscopy (FTIR)

FTIR spectra of chitosan, sodium alginate, chitosan-alginate blank beads, α-amylase loaded chitosan-alginate beads, physical mixture of α-amylase and blank beads (in the ratio same as that of the optimized batch), and α-amylase are shown in Figure 11.5. FTIR spectrum of chitosan powder showed, absorption bands at 3500–3100 cm^{-1} ascribed to combined peaks of O–H stretching (polyhydroxy $(–OH)_n$ carbohydrate) and intermolecular hydrogen bonding. The N–H stretching from primary amines are overlapped in the same region (Borges et al., 2005). Also it showed a weak band at 2875 cm^{-1} due to C–H stretching, the bridge oxygen C–O–C (cyclic ether) stretching band at 1151 cm^{-1}, and the C–O stretching bands 1070, 1031, and 893 cm^{-1} (Khor, 2001). The carbonyl (C=O) stretching of secondary amide (amide I band) absorption bands at 1655 cm^{-1}; N–H bending vibration of non-acylated 2-aminoglucose primary amines band at 1570 cm^{-1}, and N–H bending vibrations of (*N*-acetylated residues) amide II band at 1558 cm^{-1} were observed as well (Le-Tien et al., 2004). The peaks at 1419 cm^{-1} and 1321 cm^{-1} belongs to the N–H stretching of the amide and ether bonds and N–H stretching (amide III band) respectively. Sodium alginate showed various distinct peaks: broad strong band at around 3600–3000 cm^{-1} due to O–H stretching and strong peak at 1029 cm^{-1} due to C–O stretch of polyhydroxy $(OH)_n$ carbohydrate; strong peak at 1085 cm^{-1} due to C–O–C stretch of cyclic ether (carbohydrate). Sodium alginate as a carboxyl salt showed strong absorption bands at 1601 and 1407 cm^{-1} due to carboxyl anions (asymmetric and

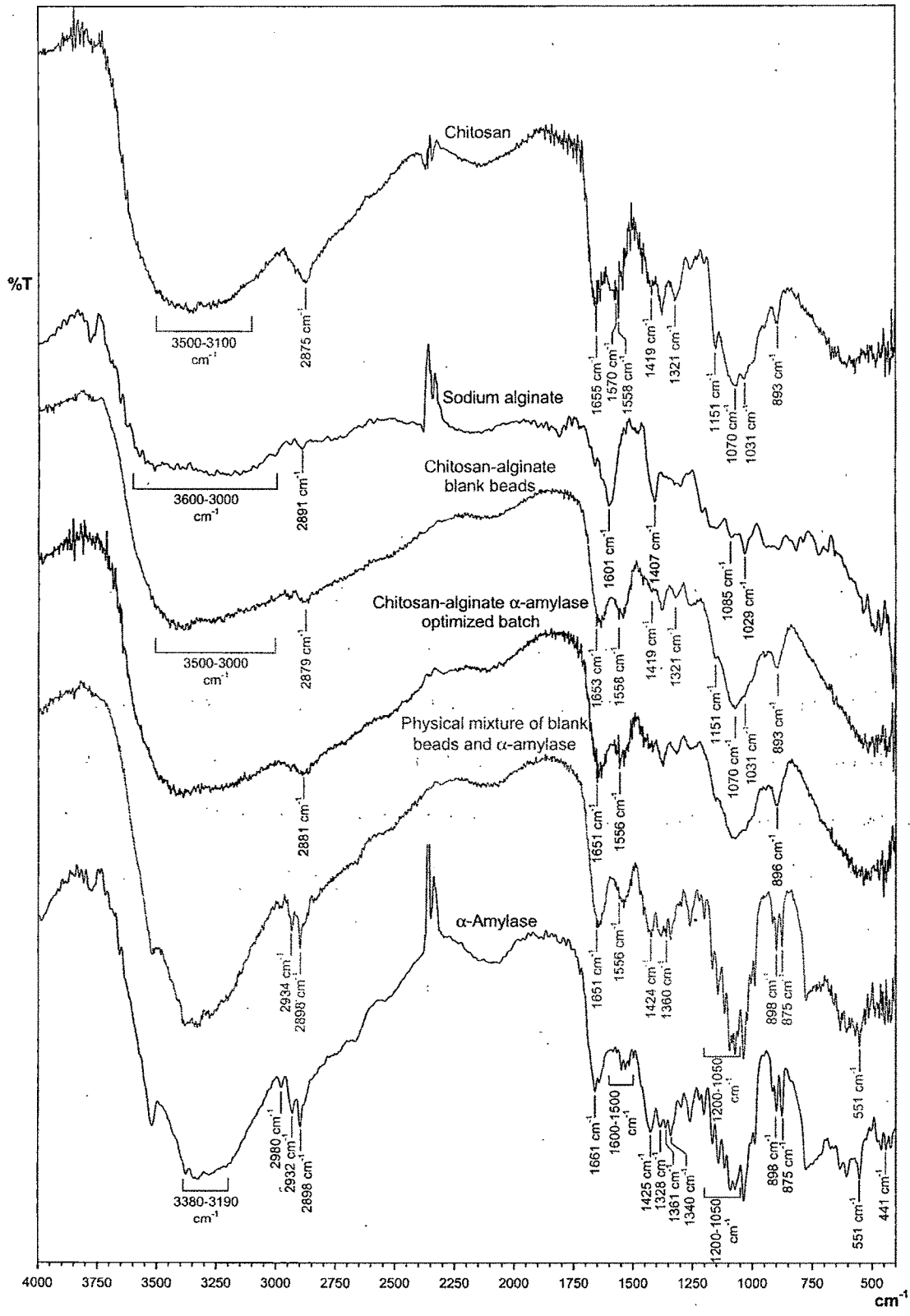

Figure 11.5: The FTIR spectra of chitosan, sodium alginate, chitosan-alginate blank beads, α-amylase loaded optimized beads, physical mixture (in the ratio same as that of the optimized batch) of α-amylase and blank beads, and α-amylase.

symmetric stretching vibrations). The frequency of carbonyl absorption is lowered compared to the value found for the parent carboxylic acid due to a resonance phenomenon. α-Amylase also showed various distinct peaks: one predominant band at 3190-3380 cm^{-1} (strong; s) due to N-H stretch of secondary N-substituted amides; 2980 cm^{-1} (weak; w) due to C-H stretch, medium bands at 1500-1600 cm^{-1} due to C⁻⁻C, while 898 cm^{-1} (s) and 875 cm^{-1} (s) due to *p*-substituted aromatic out of plane C-H deformation of aromatic residue of tryptophan or tyrosine; 2931 cm^{-1} (s) and 2898 cm^{-1} (s) due to C-H stretch, while 1425 cm^{-1} (s), 1382 cm^{-1} (medium; m), 1361 cm^{-1} (m), and 1340 cm^{-1} (m) due to C-H deformation of alkyl chain of amino acids; 1661 cm^{-1} due to C=O stretch of carboxyl anion and amide group; strong peaks between 1050-1200 cm^{-1}, weak bands at 550-600 cm^{-1}, and 400-450 cm^{-1} due to C-S stretch of sulfides and disulfides.

For chitosan-alginate blank beads, the band around 3500–3100 cm^{-1} becames broader, this indicates hydrogen bonding is enhanced (Yu et al., 1999). Moreover, N–H bending vibration of non-acylated 2-aminoglucose primary amines band at 1570 cm^{-1} and asymmetric and symmetric –C⁻⁻O stretching at 1601 and 1407 cm^{-1} respectively disappeared indicating that–NH_3^+ of chitosan has reacted with $-COO^-$ of alginate. Distinct peaks correspond to the alginate are absent. This is probably due to very less alginate concentration compared to chitosan and also alginate is present at the interface. Some peaks disappeared or became weak due to interaction or superposition between groups of chitosan and alginate. One reason is that more chitosan was contained within beads and other one may be multi-interaction (hydrogen binding and electrostatics interaction) among chitosan and alginate. With incorporation of α-amylase, the spectrum of beads was similar to that of the chitosan-alginate blank beads, except the shift in the C–H stretch by 2 units from 2879 cm^{-1} to 2881 cm^{-1} and shift in the carbonyl (C=O) stretching of secondary amide (amide I band) by 2 units from 1651 cm^{-1} to 1653 cm^{-1}.

This may be because of interaction of α-amylase with chitosan. However, the physical mixture of α-amylase and blank beads showed the peaks due to both α-amylase and blank beads. This confirms the amylase entrapment into the chitosan-alginate beads at molecular level.

11.1.7.3. Differential Scanning Calorimetry (DSC)

The DSC thermograms of α-amylase, chitosan, sodium alginate, chitosan-alginate blank beads, α-amylase loaded optimized batch, and physical mixture of α-amylase and blank beads are shown in Figure 11.6. α-Amylase exhibited three endothermic peaks at 148.5°, 215.5°, and 226.8°C followed by a broad degradation exotherm at 358°C. The thermogram of the chitosan polymer exhibited an endothermic peak at about 94°C that has been attributed to the evaporation of absorbed water. The exothermic baseline deviation beginning around 250°C indicates the onset of chitosan degradation (Khalid et al., 2002; Borges et al., 2005). A broad endothermic peak at 87°C in the thermogram of sodium alginate was similarly attributed to the presence of water molecules in the sample. It also showed two exothermic peaks at 251.2°C and 265.5°C. The chitosan-alginate reaction can be characterized by disappearance of degradation exothermic peaks of chitosan at 317.5°C and alginate at 251.2°C. The analysis of the DSC curves for chitosan-alginate beads showed two additional exothermic peaks at about 230°C and 266°C. The peak at 230°C is probably related to the breakdown of weak unspecific electrostatic interactions. The second peak is probably related to the cleavage of the electrostatic interactions between the chitosan and alginate polymers. DSC thermogram of enzyme loaded beads was similar to that of blank beads except all corresponding peaks were shifted to lower temperature, which might be due to the electrostatic interaction between

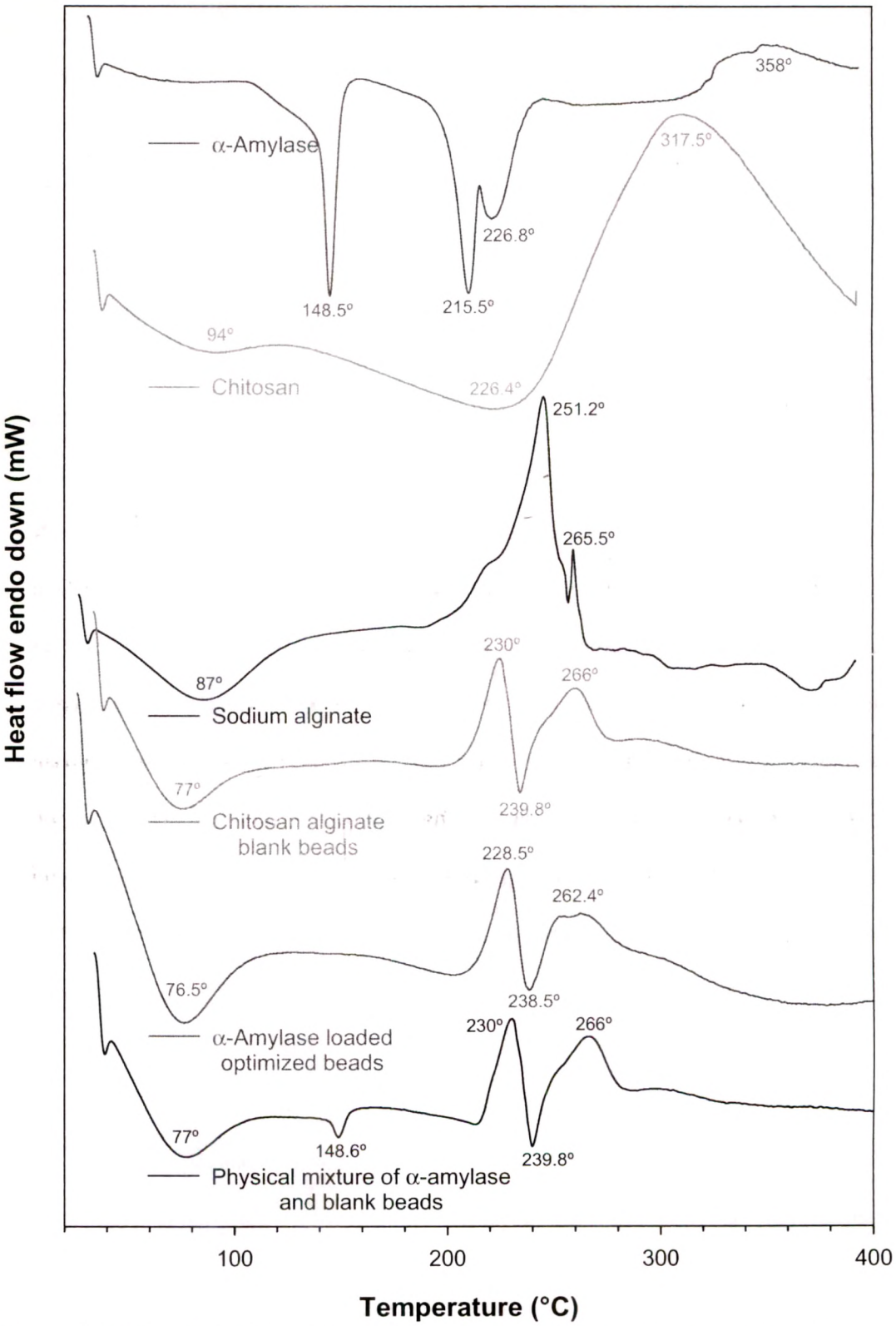

Figure 11.6: The DSC thermograms of α-amylase, chitosan, sodium alginate, chitosan-alginate blank beads, α-amylase loaded optimized beads, and physical mixture of α-amylase and blank beads made at the same analytical conditions.

α-amylase and biopolymers. However, it did not showed any peak analogous to α-amylase. Moreover, the physical mixture of α-amylase and blank beads (in the ratio same as that of the optimized batch) showed the endothermic peak at 148.6°C corresponding to α-amylase and other peaks (230°C, 239.8°C and 266°C) corresponding to blank beads. This confirms that most of the enzyme was uniformly dispersed at the molecular level in the beads.

11.1.7.4. Morphology of the Beads

The spherical shape of beads in the wet state was usually lost after drying, especially for beads prepared with low chitosan concentrations. With an increase of chitosan concentration, the shape of beads was retained considerably. However, the shape of the optimized beads (experiment 12) changed to spherical discs with a collapsed center (Figure 11.7) during the drying process. The beads prepared with 1.5 % w/v chitosan showed much deeper collapsed centre or in some cases more than one collapsed centre. The tendency of developing the collapsed centre may be possibly because of mass- and heat-transfer phenomena and/or aggregation of chitosan helical fibers into bundles and the squeezing out of some water from the gel (Iborra et al., 1997). Further, keen observation of Figure 11.8A-D showed the presence of fracture on the surface of the beads developed during the drying process through which the dissolution media enter first. Very fine mesh-like structure observed in Figure 11.8E-F was due to polyelectrolyte reaction and is quite comparable with many other PEC micrographs (Cruz et al., 2004; Lee et al., 2004).

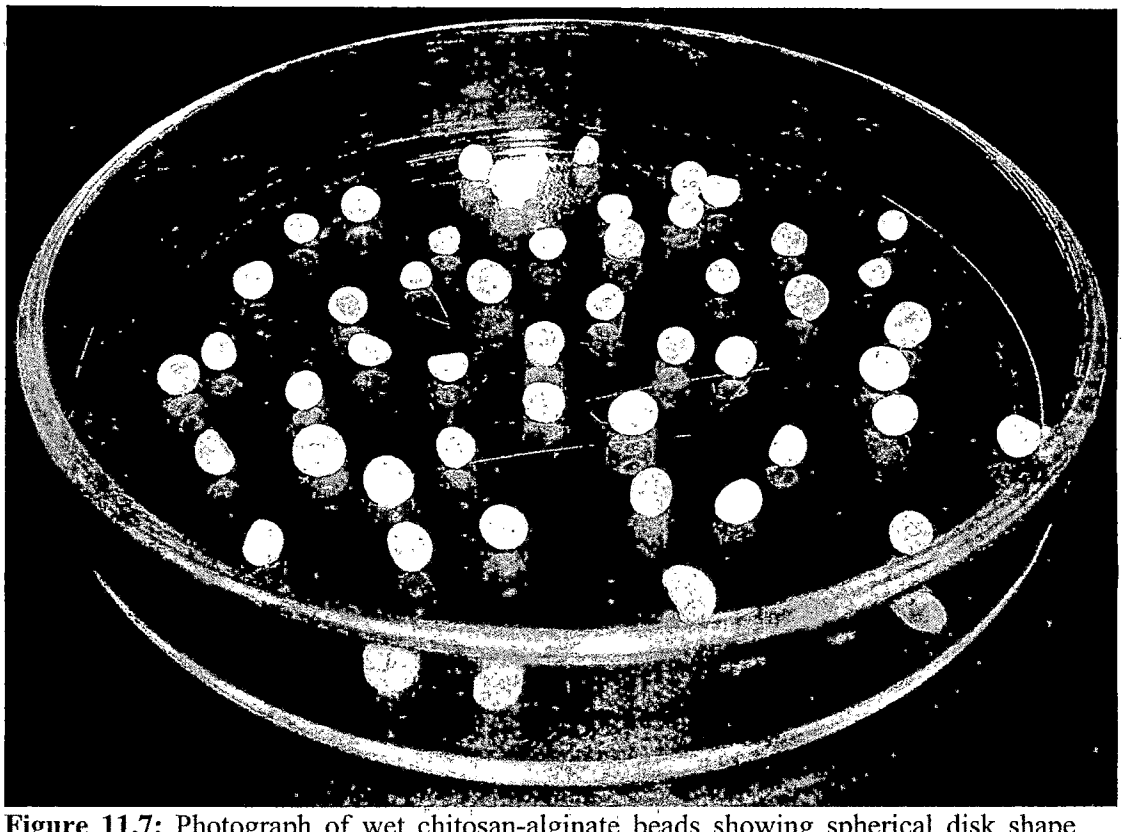

Figure 11.7: Photograph of wet chitosan-alginate beads showing spherical disk shape with collapsed centre during drying process.

11.1.8. STABILITY STUDY

For the developed formulation, the similarity factor (f_2) was calculated by a comparison of the dissolution profiles at each storage condition with the control at the initial condition. Results of f_2 factors ranged from 78 to 98 with 2 to 4% average difference. Evaluation of shelf-life was carried out as per the ICH Q1E Step4 (Evaluation of Stability Data) guidelines for the drug substances intended for room temperature storage. Long-term and accelerated stability data showed little change over time, so the shelf-life up to twice the length of available long-term data (i.e. 24 months) can be proposed. Extrapolation of the shelf-life beyond the length of available long-term data can be proposed. For this, an approach for

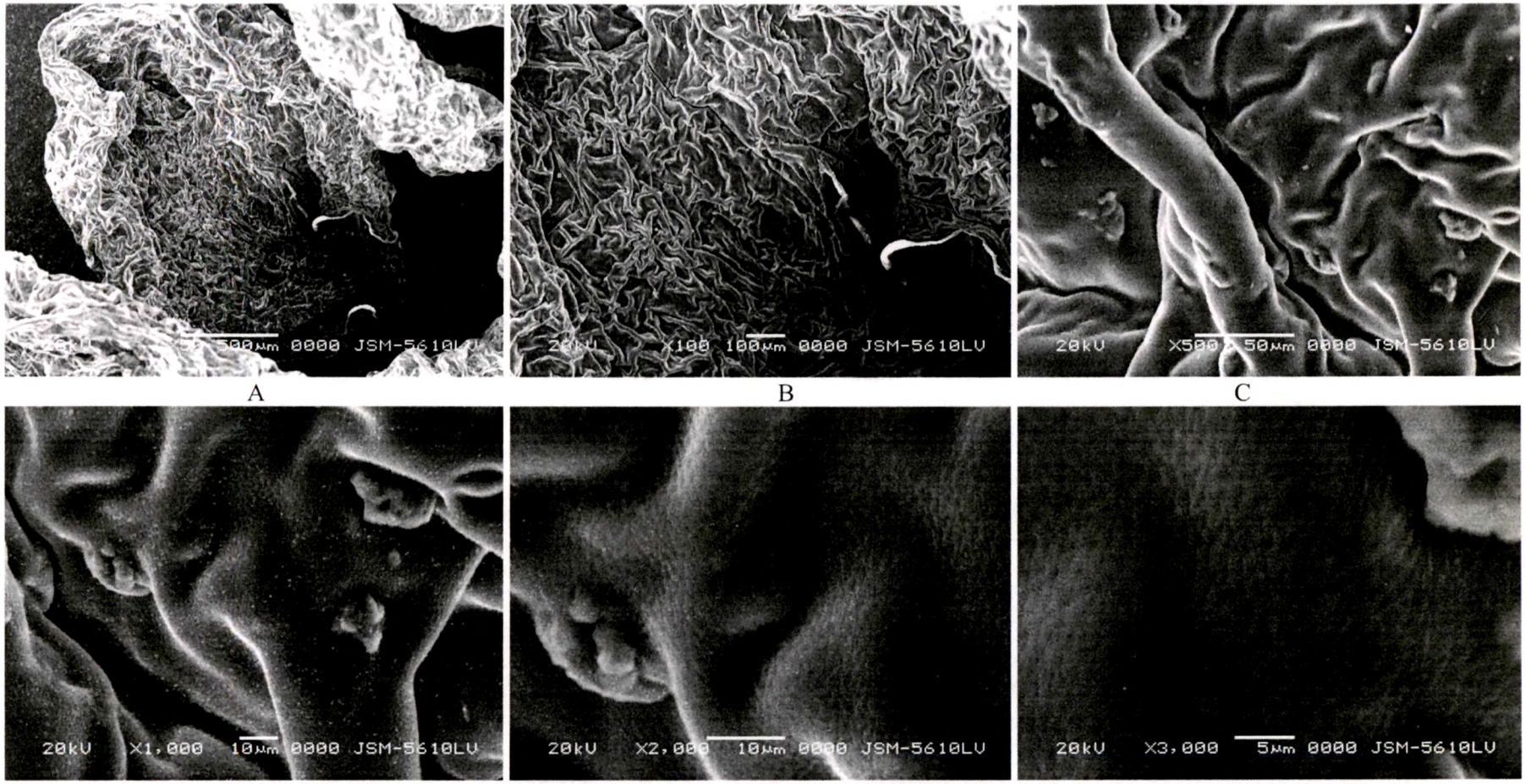

A B C

D E F

Figure 11.8: SEM micrographs and surface morphology of optimized chitosan-alginate beads (formulation 12) at different magnification.

analyzing the data on a quantitative attribute that is expected to change with time is to determine the time at which the 95% one-sided confidence limit for the mean curve intersects the acceptance criterion (not more than 5% change in assay from its initial value) can be accepted. The long-term stability data of the developed formulation, marketed formulation and the bulk papain were linearly extrapolated (zero-order kinetics) to calculate the shelf-life (Figure 11.9) and were found be 3.68 years, 0.99 year, and 0.41 year respectively. Hence, the stability of the entrapped α-amylase was significantly improved compared to the conventional dosage forms.

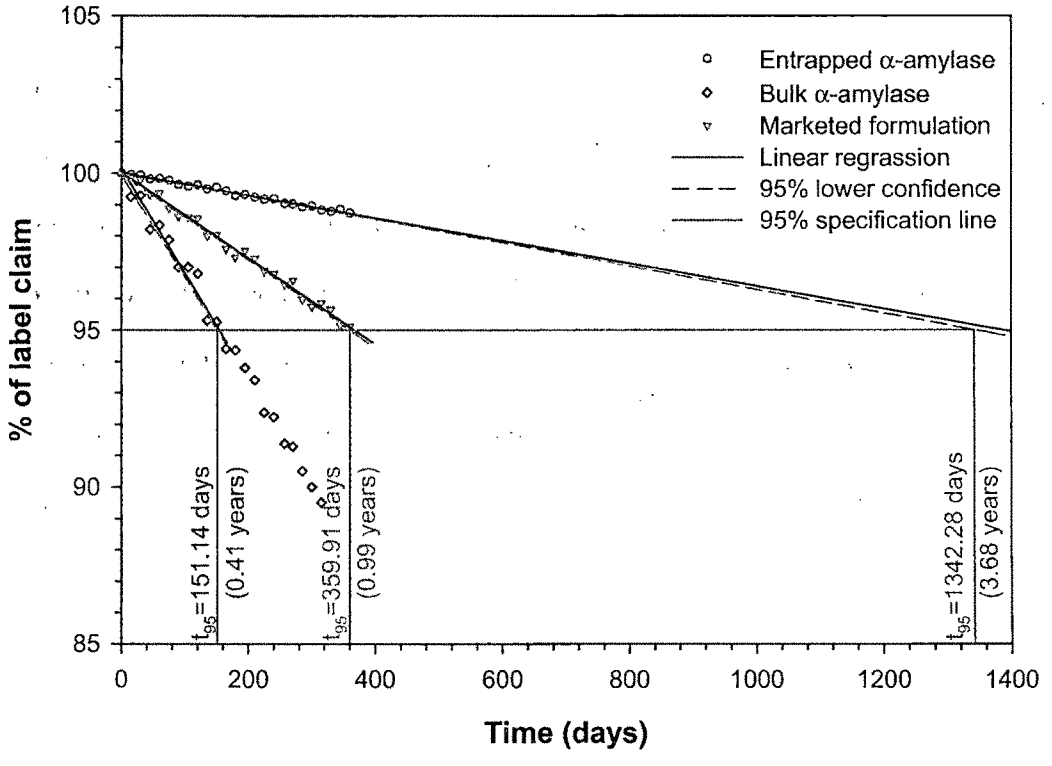

Figure 11.9: Extrapolation of long-term stability data for shelf-life calculation.

Dumitriu and Chornet observed that, hydrogels, formed through interaction of a polycation with a protein (i.e. α-amylase in this case), have the advantage of creating an ionic micro-system which favors the stabilization of a protein polymer (i.e. enzyme) by

interacting with the free acid and base functions (Severian and Esteban, 1998). Moreover, protein–polyelectrolyte complexes also have the ability to improve the operational stability of the enzyme activity during catalysis (Severian and Esteban, 1998). This probably may be the reason of improved stability of α-amylase entrapped in the chitosan-alginate PEC beads.

11.1.9. CONCLUSIONS

Reversed chitosan-alginate PEC beads exhibited promising stability improvement of entrapped α-amylase and can find a place in the design of multiparticulate drug delivery systems. The optimization of the process using the response surfaces resulted in > 90% entrapment and > 48 min of T_{90} (experiment 12). T_{50} and T_{90} were increased with increase in alginate concentration and hardening time while decreased with increase in chitosan concentration. Percentage entrapment was found to be directly proportional to chitosan and alginate concentration while inversely proportional to the hardening time. Mathematical analysis of the different drug release modalities and Kopcha model revealed that after 35 min the enzyme was released due to the burst effect. FTIR and DSC study confirmed the entrapment of α-amylase in the chitosan-alginate beads. Texture analysis demonstrated the mesh-like fine structure due to the PEC reaction in absence of added salt. Accelerated and long term stability study illustrated considerably improved shelf-life of α-amylase entrapped in chitosan-alginate beads than the conventional dosage form. Results of present study seem to be of value for the pharmaceutical industries associated with digestive enzymes formulations, also the reversed chitosan-alginate PEC can be employed for number of application due to short time of reaction, simplicity and reactivity in salt-free condition.

11.2. Chitosan-Alginate Papain Beads

11.2.1. PRINCIPLE OF PEC FORMATION

The electrostatic attraction between the cationic amino groups of chitosan (the macro pKa is about 6.5) (Lee et al., 1999) and the anionic carboxyl groups of the alginate is the main interaction leading to the formation of the PEC. It is stronger than most secondary binding interactions (Lee et al., 1999). In order to prepare the beads with reverse engineering, the formation of good mechanical strength membrane (precipitate) at the interface of both the polymer is essential. This is required to avoid the homogenous mixing of chitosan and alginate solution and also to maintain the geometry of the bead, which may otherwise easily distorted even under the mild shear stress of the stirring. Table 11.6 depicts the effect of chitosan and alginate solution pH on the beads properties. As can be seen, the M-2 condition resulted in the spherical beads with no aggregates. Though the membrane was thin, mechanical strength was good enough. At acidic environment chitosan is highly protonated and at neutral or alkaline environment alginate is decidedly anionic. Under such circumstances, maximum interaction between amino and carboxyl group takes place (see Figure 11.10) and results in compact membrane.

Table 11.6: Effect of chitosan and alginate solution pH on beads properties[a].

Sr. No.	pH		Mechanical strength of membrane[b]	Membrane thickness	Comments
	Chitosan solution	Alginate solution			
M-1	2	3.5	– + –	thick	alginate viscosity very high, bead shape distorted, beads aggregated
M-2	2	6.5	+ + +	thin	spherical beads, no aggregate
M-3	5.4	3.5	– – –	very thin	lump of chitosan after few minutes, chitosan and alginate viscosity very high
M-4	5.4	6.5	– + –	thin	chitosan viscosity very high, beads aggregated

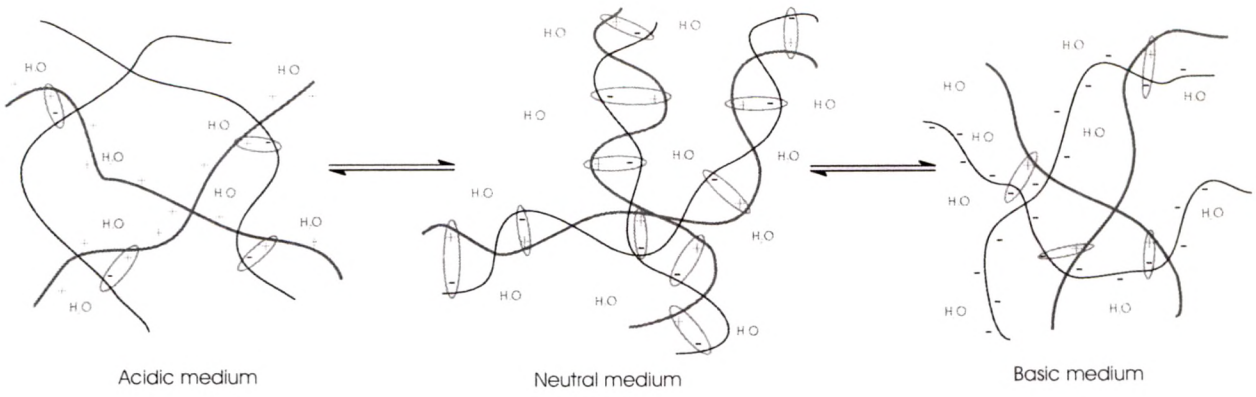

Figure 11.10: Structure of a chitosan-alginate PEC; +, positive charge of chitosan; –, negative charge of the alginate; ○, ionic interaction; + + +, chitosan; – – –, alginate.

11.2.2. EFFECT OF THE FACTORS ON RESPONSES

11.2.2.1. % Entrapment

ANOVA results and regression coefficients of response variables are shown in Table 11.8. Chitosan- and alginate concentration were statistically significant (P <0.05), while hardening time was not. From the contour plots of the response surface for % entrapment (Figure 11.11) and Table 11.8, it can be concluded that concentration of alginate was the most influencing factor and affecting positively (i.e. response increases with increase in factor level). More than 90% entrapment (experiment J-7, J-8, and J-12; Table 11.7) was obtained at the high level of alginate concentration. On addition of chitosan solution to the alginate solution, instantaneous interfacial cross-linking takes place which is proportional to the charge density of the solutions. Higher concentration of the polymers and pH values corresponding to their ionized state results in increased charge density of both the polymers and will lead to intense cross-linking with small micropores. This probably might be the cause of minimized loss of enzyme from the PEC beads and higher % entrapment values at higher polymer concentrations.

Table 11.7: Matrix of central composite design and results for the measured responses.

Sr. No.	Factors/Levels			Responses				Transformed		Composite index
	Chitosan (% w/v)	Sodium alginate (% w/v)	Hardening time (min)	% Immobilization	T_{50}	T_{90}	Particle Size (mm)	% Immobilization	T_{90}	
J-1	-1	-1	-1	80.48	29.31	33.94	1.09	6.87	3.79	10.66
J-2	-1	-1	1	78.77	36.59	43.30	1.21	0.00	23.60	23.60
J-3	-1	1	-1	87.23	40.47	46.49	0.92	33.82	30.35	64.17
J-4	-1	1	1	86.08	48.17	55.78	0.99	29.25	50.00	79.25
J-5	1	-1	-1	83.08	26.00	32.15	1.96	17.23	0.00	17.23
J-6	1	-1	1	83.09	32.67	38.79	1.91	17.27	14.05	31.31
J-7	1	1	-1	91.28	37.11	42.34	1.71	50.00	21.57	71.57
J-8	1	1	1	90.73	44.40	50.35	1.67	47.82	38.52	86.34
J-9	-1.73	0	0	81.01	40.21	46.18	0.71	8.99	29.69	38.68
J-10	1.73	0	0	88.71	34.03	39.43	2.04	39.76	15.41	55.17
J-11	0	-1.73	0	79.42	27.11	33.16	1.68	2.63	2.14	4.77
J-12	**0**	**1.73**	**0**	**90.43**	**46.69**	**53.85**	**1.29**	**46.64**	**45.92**	**92.56**
J-13	0	0	-1.73	85.66	29.88	34.48	1.42	27.55	4.93	32.48
J-14	0	0	1.73	84.50	42.81	49.08	1.48	22.92	35.83	58.75
J-15	0	0	0	83.61	36.97	43.22	1.36	19.35	23.43	42.79
J-16	0	0	0	83.21	37.09	43.30	1.39	17.76	23.59	41.34
J-17	0	0	0	85.11	37.21	43.14	1.36	25.35	23.27	10.66

11.2.2.2. T_{50} and T_{90}

As shown in Table 11.8 and Figure 11.11, all three factors had significant positive effect on both response values. The alginate concentration (factor *B*) was found to be most influencing factor. For maximum activity of enzyme in the intestine longer T_{50} and T_{90} were the desired criteria for the optimum formulation. T_{50} and T_{90} were found to be proportional to the alginate concentration and hardening time while inversely proportional to the chitosan concentration. Thus, high level of alginate and hardening time and low level of chitosan resulted to the beads with T_{50} and T_{90} as high as 48.17 and 55.78 min respectively (experiment J-4, Table 11.7). This may explained as follows:

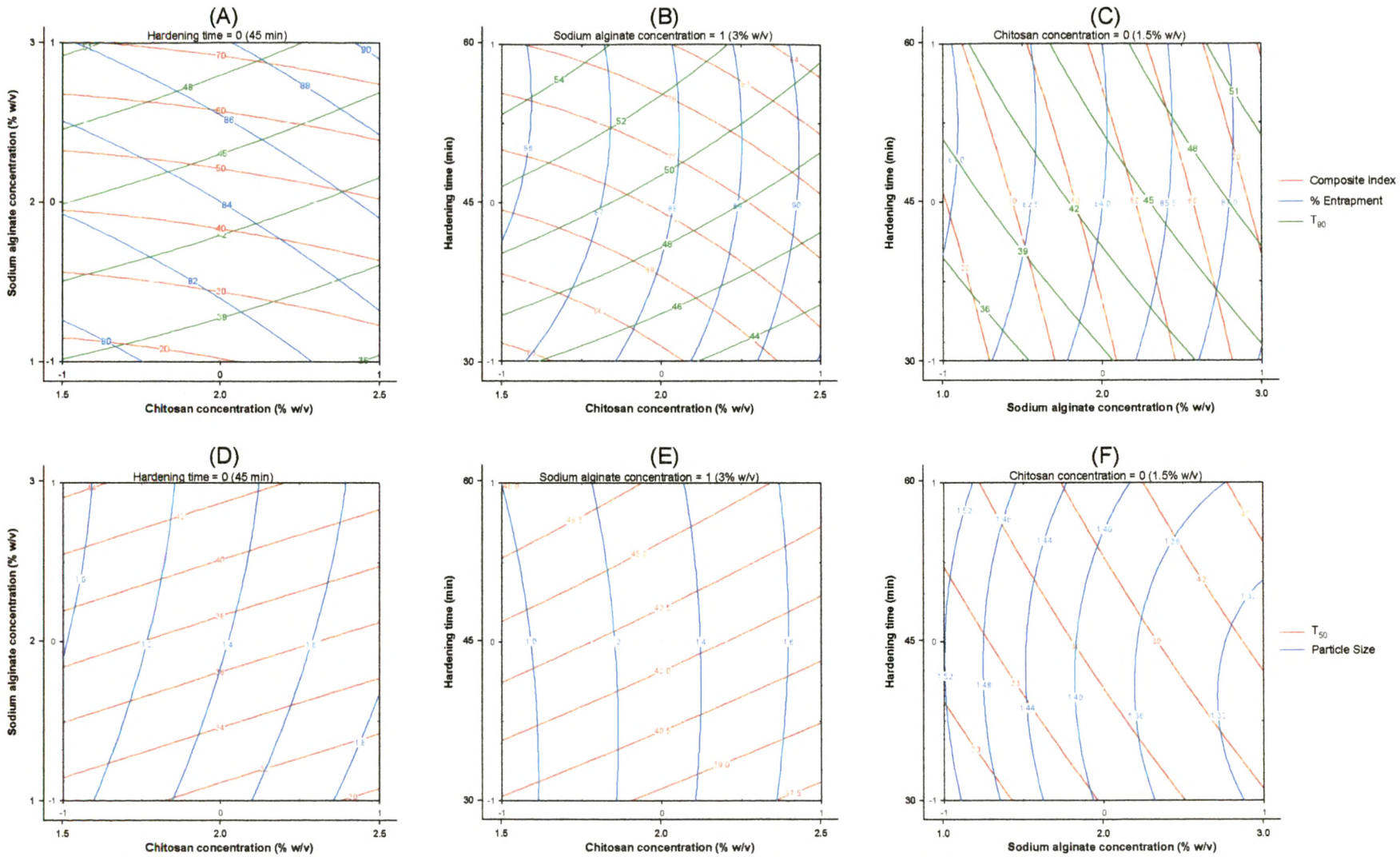

Figure 11.11: Contour plots of composite index, % entrapment, T_{90}, T_{50}, and particle size as a function of chitosan concentration, sodium alginate concentration, and hardening time.

Table 11.8: ANOVA results (*P* values): effect of the variables on % entrapment, T_{50}, T_{90}, particle size, and composite index.

Factors	% Entrapment		T_{50}		T_{90}		Particle size		Composite index	
	Coefficient[a]	*P*	Coefficient[a]	*P*	Coefficient[a]	*P*	Coefficient[a]	*P*	Coefficient[a]	*P*
Interce										
pt	83.97	<0.0001*	37.09	<0.0001*	43.22	<0.0001*	1.37	<0.0001*	44.30	<0.0001*
A	2.07	<0.0001*	-1.79	<0.0001*	-1.97	<0.0001*	0.38	<0.0001*	4.10	0.0019*
B	3.50	<0.0001*	5.68	<0.0001*	5.90	<0.0001*	-0.11	<0.0001*	26.47	<0.0001*
C	-0.39	0.1042	3.67	<0.0001*	4.19	<0.0001*	0.02	0.0038*	7.31	<0.0001*
A^2	0.32	0.1874	0.02	0.5864	-0.10	0.1072	0.00	0.9461	1.06	0.2523
B^2	0.34	0.1632	-0.05	0.1693	0.13	0.0492*	0.04	<0.0001*	1.64	0.0972
C^2	0.39	0.1185	-0.24	0.0005*	-0.44	0.0002*	0.02	0.0006*	0.62	0.4849
AB	0.22	0.4358	0.01	0.7827	-0.41	0.0008*	-0.01	0.0463*	0.03	0.9799
AC	0.29	0.3179	-0.12	0.0279*	-0.50	0.0003*	-0.04	0.0002*	0.10	0.9225
BC	0.00	0.9928	0.13	0.0246*	0.16	0.0495*	0.00	0.3632	0.35	0.7426
ABC	-0.14	0.6158	0.03	0.5850	0.18	0.0338*	0.01	0.0817	-0.18	0.8661
$r^2_{adj.}$	0.9621	–	0.9996	–	0.9993	–	0.9989	–	0.9876	–

[a] Regression coefficients are in coded values.

* Statistically significant ($P < 0.05$).

Alginate prepares the outer layer of the beads. Thus higher concentration of alginate avails higher charge density of alginate carboxyl group and results in higher cross-linking of the PEC thus it prepare stronger PEC membrane with less thickness and small micropores. Alginate, upon exposure to the acidic dissolution media, might be converted to alginic acid, which is more viscous than alginate and results in delayed dissolution of the beads. Similarly, as mentioned above, longer hardening time may cause the deeper penetration of the alginate into the chitosan and prepare the thick PEC at the surface which will require longer time for complete dissolution. The release of enzyme from the beads is due to burst of the PEC membrane (see 'Curve fitting and release mechanism' below). In the core of the beads, chitosan is not complexed with alginate and thus provides a good hypertonic environment for osmosis to occur. As the chitosan concentration increases, the hypertonicity also increases and exert greater amount of osmotic pressure against the mechanical strength of the PEC membrane. Thus, higher concentration of chitosan cause early busts effect and short T_{50} and T_{90}.

11.2.2.3. Particle Size

As depicted in Table 11.8, the chitosan concentration (factor A; most influential) and hardening time had positive coefficient, while alginate concentration had negative coefficient. All three process variables were statistically significant ($P<0.05$). The bead size is influenced by the orifice of the needle through which the chitosan is allowed to pass, addition of surfactant, extrusion rate, (which were kept constant) surface tension and the viscosity of the chitosan solution. Increased viscosity at higher concentration of chitosan resulted in larger particles. As before, the higher concentration of alginate provides the higher charge density and results in stronger but thin membrane with small

micropores. Thus, increased alginate concentration caused decrease in the particle size of PEC. The effect hardening time seems to be negligible indicating that the interaction of chitosan-alginate is instantaneous and the membrane formed upon first exposure is hard enough to restrict the expansion or constriction due to longer hardening time.

11.2.3. INTERACTIONS BETWEEN THE FACTORS

An interaction is the failure of a factor to produce the same effect on the response at the different levels of the other factor. The ANOVA results (Table 11.8) showed that following interaction terms were statistically significant: *AC* and *BC* for T_{50}; *AB*, *AC*, *BC*, and *ABC* for T_{90}; and *AB* and *AC* for particle size. However, other interaction terms were non-significant statistically. The analysis of the results by multiple regression (Table 11.8) leads to equations that adequately describe the influence of the selected factors on % entrapment, T_{50}, T_{90}, and particle size.

11.2.4. OPTIMIZATION OF THE PROCESS USING THE COMPOSITE INDEX

Generally the aim of the optimization is to find the optimum levels of the variables, which affect a process, where a product of desired characteristics could be produced easily and reproducibly. Using the composite index, both selected responses (% entrapment and T_{90}) were combined in one response. As it has been already discussed, the composite index was calculated from the individually calculated transformed value of each of the responses using the Eqs. (8.11)–(8.12). In Figure 11.11 the contour plots that describe the influence of the independent factors on the composite index is presented. The study of these plots and Table 11.7 showed that the highest values of the composite index (92.56)

could be obtained at formulation J-12 and was considered as a batch fulfilling all the constraints favorable for the bead preparation.

11.2.5. EVALUATION OF MODEL USING CROSS-VALIDATION

In order to assess the reliability of the model, five experiments were conducted by varying the process variables at values other than that of the model. For each of these test experiments the responses were estimated by using derived quadratic polynomial equations and experimental procedure for comparison between both responses (Table 11.10). % Relative error was calculated by the following equation:

Eq. 11.2

$$\% \text{ Relative error} = \left[\frac{\text{predicted value} - \text{experimental value}}{\text{predicted value}} \right]$$

It can be seen that in all cases there was a reasonable agreement between the predicted and the experimental value, since low value of the % relative error were found. For this reason it can be concluded that the equations describe adequately the influence of the selected process variables on the responses under study.

Table 11.9: Comparison of responses between predicted and experimental values for the cross-validation set.

Responses	Test	Factors/levels			Experimental values	Predicted values	% Relative error
		A	B	C			
% Entrapment	1	-0.7	0.5	0	84.44	85.79	-1.6
	2	0	0	1.4	84.21	83.53	0.8
	3	1.6	0	0	88.11	87.66	0.5
	4	0	1.5	0	89.99	89.00	1.1
	5	0.3	0.8	0.2	87.64	89.57	-2.2
T_{50}	1	-0.7	0.5	0	41.18	41.71	-1.3
	2	0	0	1.4	41.76	42.80	-2.5
	3	1.6	0	0	34.28	33.49	2.3
	4	0	1.5	0	45.48	45.03	1.0
	5	0.3	0.8	0.2	41.80	42.56	-1.8
T_{90}	1	-0.7	0.5	0	47.68	46.96	1.5
	2	0	0	1.4	48.21	49.51	-2.7
	3	1.6	0	0	39.81	38.78	2.6
	4	0	1.5	0	52.37	53.47	-2.1
	5	0.3	0.8	0.2	48.15	47.38	1.6
Particle size	1	-0.7	0.5	0	1.06	1.05	1.7
	2	0	0	1.4	1.44	1.47	-2.1
	3	1.6	0	0	1.99	1.95	1.8
	4	0	1.5	0	1.29	1.32	-2.4
	5	0.3	0.8	0.2	1.42	1.39	2.1
Composite index	1	-0.7	0.5	0	55.58	59.43	-6.9
	2	0	0	1.4	55.75	55.80	-0.1
	3	1.6	0	0	53.55	49.59	7.4
	4	0	1.5	0	87.68	86.04	1.9
	5	0.3	0.8	0.2	69.39	75.43	-8.7

11.2.6. CURVE FITTING AND RELEASE MECHANISM

'In vitro' dissolution profile of the optimized batch is shown in Figure 11.12A. Values of release exponent (n) and kinetic constant (K) were derived using zero-order kinetics, first-order kinetics, Higuchi's square root of time equation, Korsmeyer-Peppas' power law equation and Hixson-Crowell's cube root of time equation and presented in Table 11.10. The enzyme release data show a good fit to the Korsmeyer-Peppas' power law release kinetics (Eq. 8.16) which can be confirmed by comparing the values of correlation coefficient (r) with that of the other models. The values of Korsmeyer-Peppas' release

exponent (n) determined for the various formulations studied ranged from 2.07 to 2.77 suggesting the probable release by super case-II transport. The K_k values ranged from 0.004 to 0.018 where low K_k value may suggest near to zero release from the beads initially. If one considers the correlation coefficient (r) values of zero-order and Korsemeyer-Peppas release models, both models describe the dissolution data reasonably well. Where there are competing models (with similar r values), residuals analysis can be used to distinguish between the models (Pather et al., 1998). Figure 11.12B is the residual plot for optimized formulation. The residuals are high for the zero-order, first-order,

Table 11.10: Comparison of responses between predicted and experimental values for the cross-validation set.

Responses	Test	Factors/levels			Experimental values	Predicted values	% Relative error
		A	B	C			
% Entrapment	1	-0.7	0.5	0	84.44	85.79	-1.6
	2	0	0	1.4	84.21	83.53	0.8
	3	1.6	0	0	88.11	87.66	0.5
	4	0	1.5	0	89.99	89.00	1.1
	5	0.3	0.8	0.2	87.64	89.57	-2.2
T_{50}	1	-0.7	0.5	0	41.18	41.71	-1.3
	2	0	0	1.4	41.76	42.80	-2.5
	3	1.6	0	0	34.28	33.49	2.3
	4	0	1.5	0	45.48	45.03	1.0
	5	0.3	0.8	0.2	41.80	42.56	-1.8
T_{90}	1	-0.7	0.5	0	47.68	46.96	1.5
	2	0	0	1.4	48.21	49.51	-2.7
	3	1.6	0	0	39.81	38.78	2.6
	4	0	1.5	0	52.37	53.47	-2.1
	5	0.3	0.8	0.2	48.15	47.38	1.6
Particle size	1	-0.7	0.5	0	1.06	1.05	1.7
	2	0	0	1.4	1.44	1.47	-2.1
	3	1.6	0	0	1.99	1.95	1.8
	4	0	1.5	0	1.29	1.32	-2.4
	5	0.3	0.8	0.2	1.42	1.39	2.1
Composite index	1	-0.7	0.5	0	55.58	59.43	-6.9
	2	0	0	1.4	55.75	55.80	-0.1
	3	1.6	0	0	53.55	49.59	7.4
	4	0	1.5	0	87.68	86.04	1.9
	5	0.3	0.8	0.2	69.39	75.43	-8.7

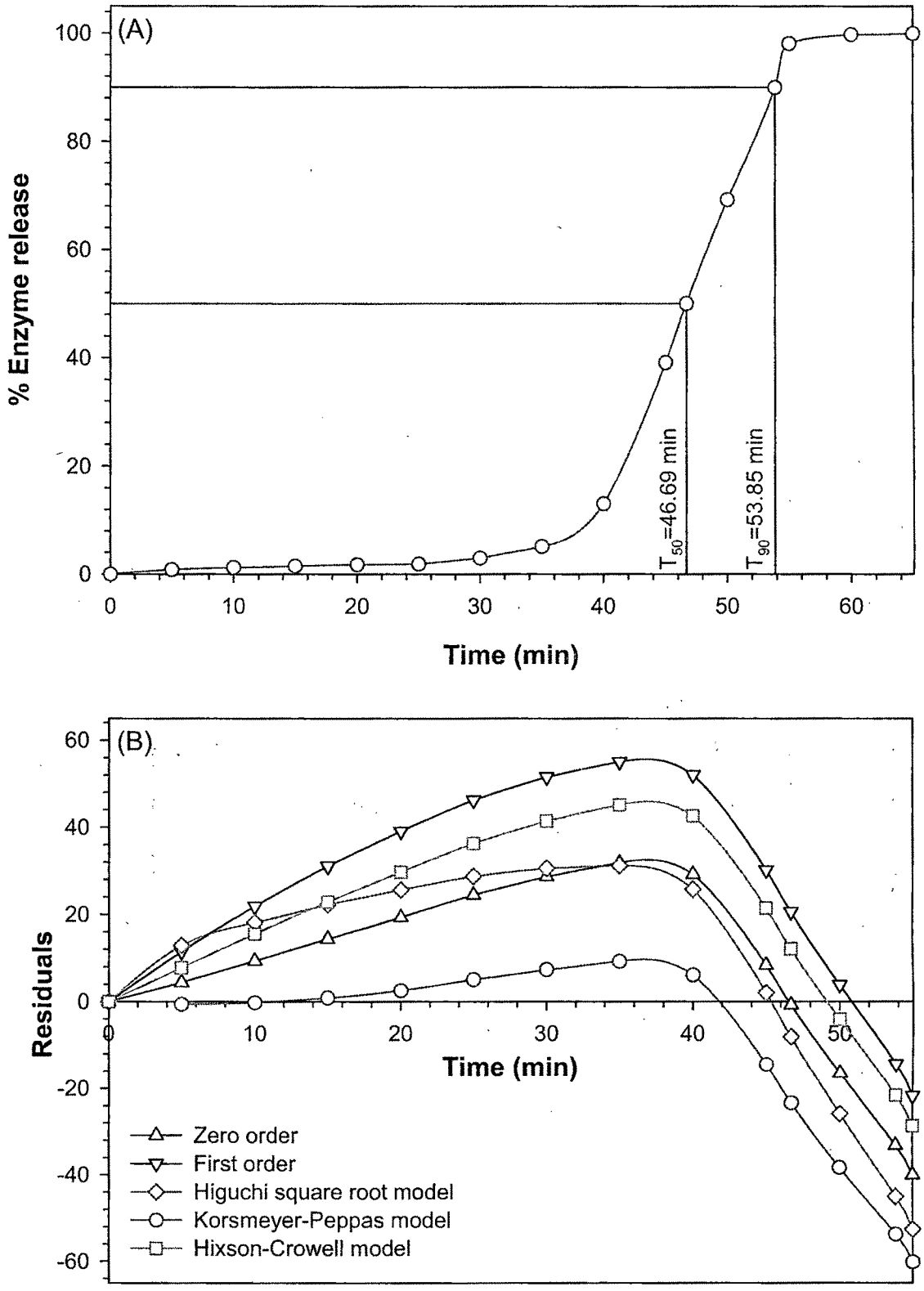

Figure 11.12: (A) 'In vitro' release profile of optimized formulation (experiment J-12) in SGF without enzyme USP XXVI pH 1.2. (B) Residual plot for different release models (experiment J-12).

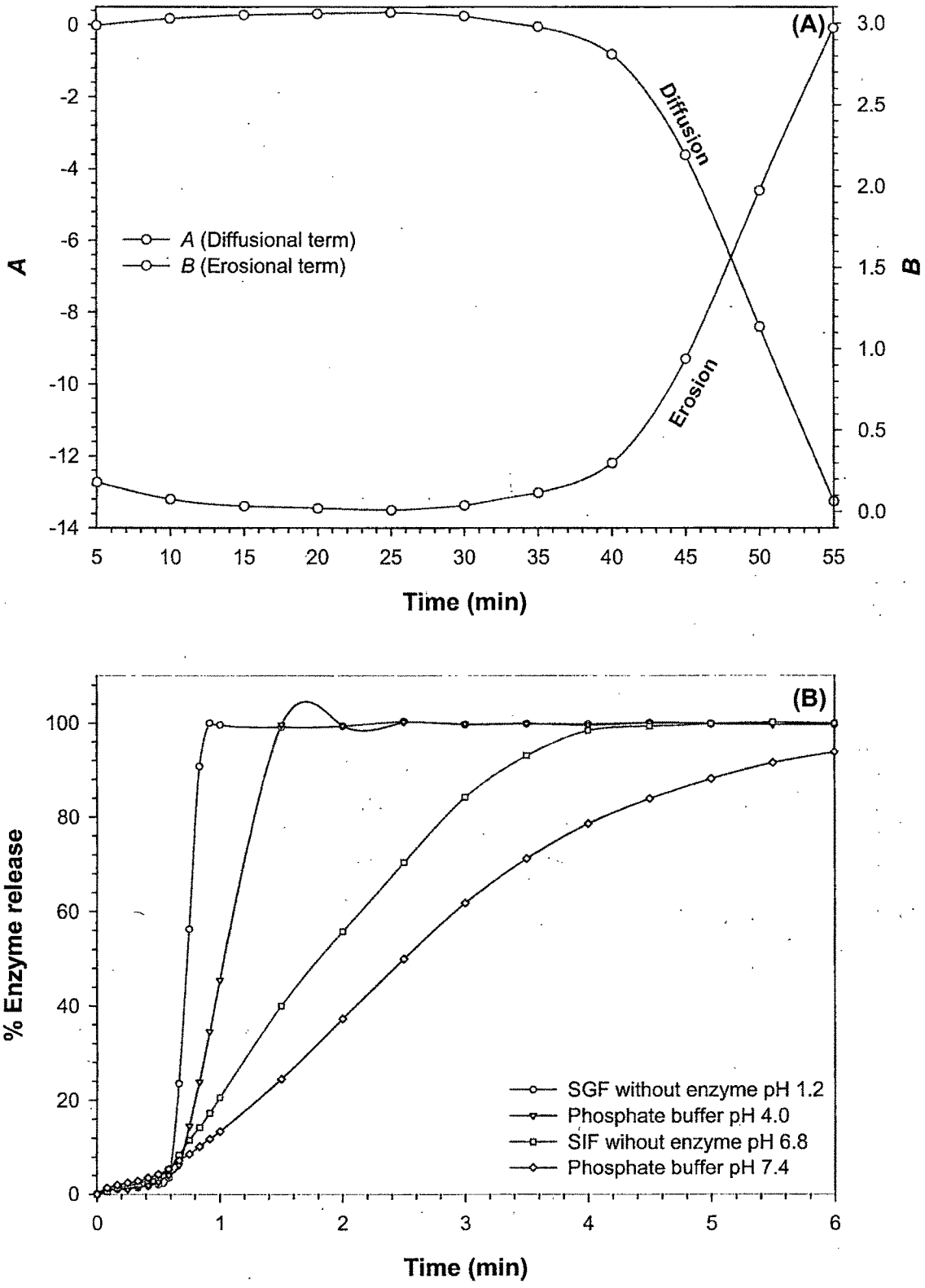

Figure 11.13: (A) Kopcha model parameters (*A* and *B*) versus time profile for optimized batch (experiment J-12). (B) Effect of pH on release profile of papain entrapped in chitosan-alginate beads.

Higuchi, and Hixson-Crowell models (and least for the Korsemeyer-Peppas model) which also shows systematic deviation: the models over-predict initially and under-predict at the later stages of the dissolution process. This indicates that Korsemeyer-Peppes' power low is the best-fit model in describing the dissolution behavior of papain from chitosan-alginate PEC.

Finally, in order to know weather the enzyme release was due to erosion or diffusion, the release data of the optimized formulation was fitted to Kopcha model (Eq. 8.18) and parameters like A and B at different time intervals were determined (Figure 11.1A). Initially, up to 40 min, though the diffusion term A was predominant, was almost constant near to zero. This suggests lack of papain diffusion from the PEC and diffusion of dissolution media in side the PEC to hydrate it. However, erosion term B increased in the course of time, as erosion appeared latter and increased linearly afterwards to express the predominance of erosion relative to diffusion. The rate of hydration (depends on the cross-link density, chitosan and alginate concentration, hardening time, degree of deacetylation of chitosan, molecular mass of chitosan and alginate, pH, presence of salt-counter ions, etc.) initially was found to be the rate-limiting step for erosion and explains the biphasic nature of the release profile: plateau initially followed by steep rise in erosion rate. This indicates the burst of the PEC membrane which can be explained as follows.

When a dry hydrogel begins to absorb water, the first water molecules entering the matrix will hydrate the most polar, hydrophilic groups. As the polar groups are hydrated, the network swells, and exposes hydrophobic groups, which also interact with water molecules. After the polar and hydrophobic sites have interacted with and bound water molecules, the network will imbibe additional water, due to the osmotic driving force of the network chains towards infinite dilution. This additional swelling is opposed by the physical cross-links, leading to an elastic network retraction force. As the network swells,

network chains or cross-links begin to disintegrate at a rate depending on its composition, rate of solvent intake, and equilibrium between the osmotic pressure and the mechanical strength of the PEC membrane (Hoffman, 2002).

11.2.7. CHARACTERIZATION OF OPTIMAL FORMULATION

11.2.7.1. Effect of pH on Release Profile

The effect of pH on the release of papain from chitosan-alginate beads in different pH (1.2, 4.0, 6.8, and 7.4) buffers simulating the human gastrointestinal tract is given in Figure 11.13B. As with ionically cross-linked hydrogels, PEC exhibit pH-sensitive swelling not only in acidic but also in basic conditions (Berger et al., 2004). As pH changes, the charge balance inside the gel and therefore the degree of interaction between the two polymers is modified and swelling occurs because of the dissociation of the complex. In acidic medium, the polyacid (carboxylate $-COO^-$ of alginate) is neutralized and due to the free ammonium ($-NH_3^+$) groups of chitosan, free positive charges appear inside the bead. Their mutual repulsion and the entry of water together with counterions to neutralize these charges cause swelling. In basic medium, the mechanism is the same but swelling is induced by the free negative charges of the polyacid (Chu et al., 1995; Sakiyama et al., 1999). According to Cárdenas et al., the chitosan-alginate PEC in acidic conditions reaches a degree of swelling five times higher than in neutral conditions (Cárdenas et al., 2003). Similar reslts were obtained in the present study and can be explained by the schematic presentation of the ionic interactions between chitosan and alginate shown in Figure 11.14. As can be seen in Figure 11.14A, at pH 2.0, the ionic interaction between chitosan and alginate is very less and there is a folding of alginate

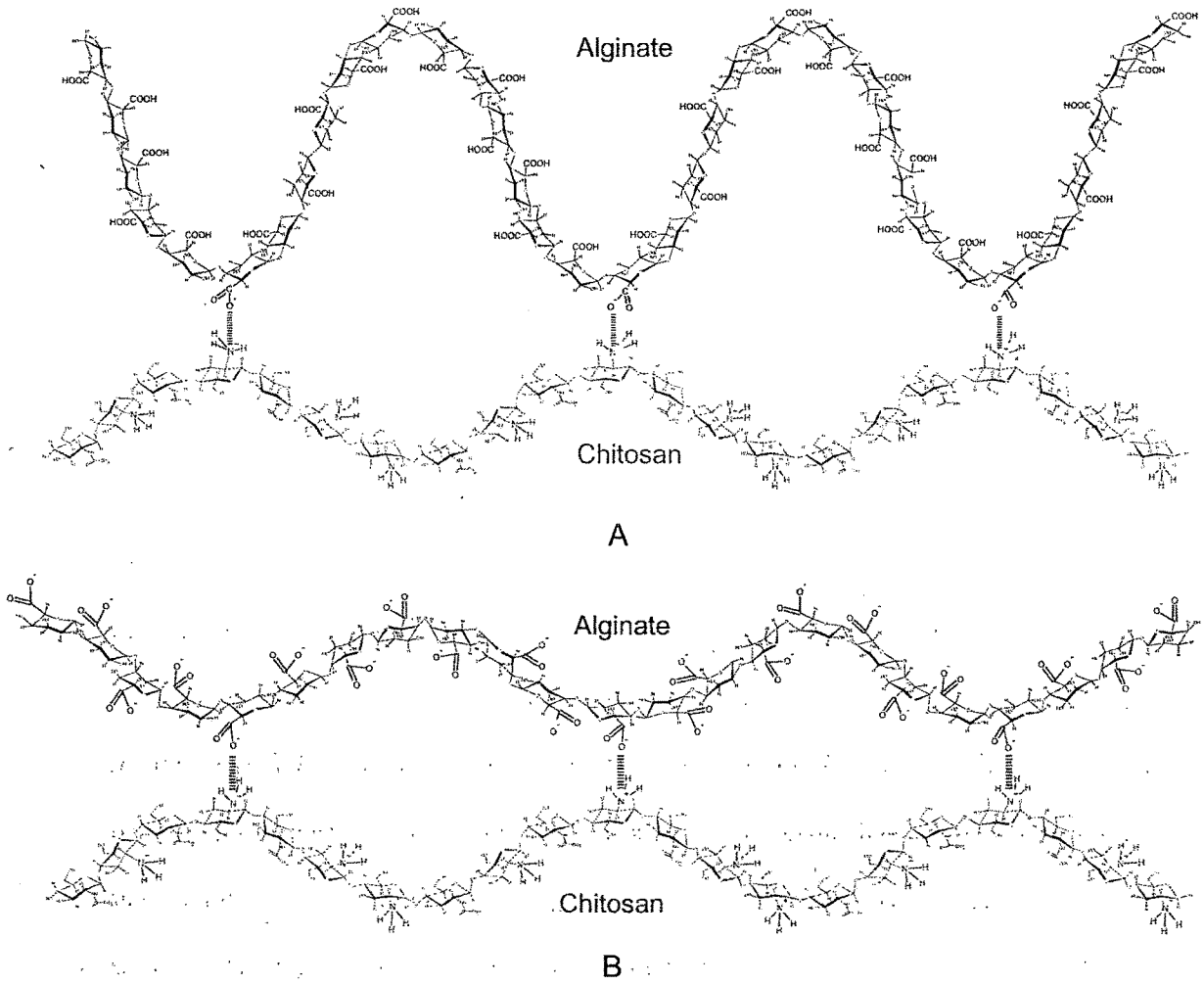

Figure 11.14: Schematic representation of the ionic interactions between alginate and chitosan at (A) pH 2.0 and (B) pH 6.8.

with increased 'micropores' size which allow greater portion of dissolution media to enter with counterions. However, at pH 6.8, chitosan is still protonated and form much stronger network with alginate with small micropore size which restricts the entry of larger counterions. Moreover, osmotic pressure and electrostatic repulsion responsible for swelling are balanced by the contractile force of the network, which depends on elasticity (Sakiyama et al., 1999) and determines the maximum degree of swelling. If pH values is such that the global charge density of one of the polymer is no longer sufficiently high to

ensure complexation, swelling becomes too significant and dissolution of the complex may observed (Chavasit et al., 1988). Burst effect for the optimized formulation in SGF without enzyme thus can be explained by the rapid swelling and lack of significant ionic interaction between chitosan-alginate at pH 1.2. As the pH increases, the swelling tend to decrease due to progressively increasing carboxyl groups. Further, solubility of chitosan decreases at higher pH and it act as a sustained-release matrix. Thus, the release of papain is delayed at higher pH.

11.2.7.2. Fourier Transform Infra-Red Spectroscopy (FTIR)

FTIR spectra of chitosan, sodium alginate, chitosan-alginate blank beads, papain loaded chitosan-alginate beads, physical mixture of papain and blank beads (in the ratio same as that of the optimized batch), and papain are shown in Figure 11.15. FTIR spectrum of chitosan powder showed, absorption bands at 3500–3100 cm^{-1} ascribed to combined peaks of O–H stretching (polyhydroxy $(–OH)_n$ carbohydrate) and intermolecular hydrogen bonding. The N–H stretching from primary amines are overlapped in the same region (Borges et al., 2005). Also it showed a weak band at 2875 cm^{-1} due to C–H stretching, the bridge oxygen C–O–C (cyclic ether) stretching band at 1151 cm^{-1}, and the C–O stretching bands 1070, 1031, and 893 cm^{-1}. The carbonyl (C=O) stretching of secondary amide (amide I band) absorption bands at 1655 cm^{-1}, N–H bending vibration of non-acylated 2-aminoglucose primary amines band at 1570 cm^{-1}, and N–H bending vibrations of (*N*-acetylated residues) amide II band at 1558 cm^{-1} were observed as well. The peaks at 1419 cm^{-1} and 1321 cm^{-1} belongs to the N–H stretching of the amide and ether bonds and N–H stretching (amide III band) respectively. Sodium alginate showed various distinct peaks: broad strong band at around 3600–3000 cm^{-1} due to O–H

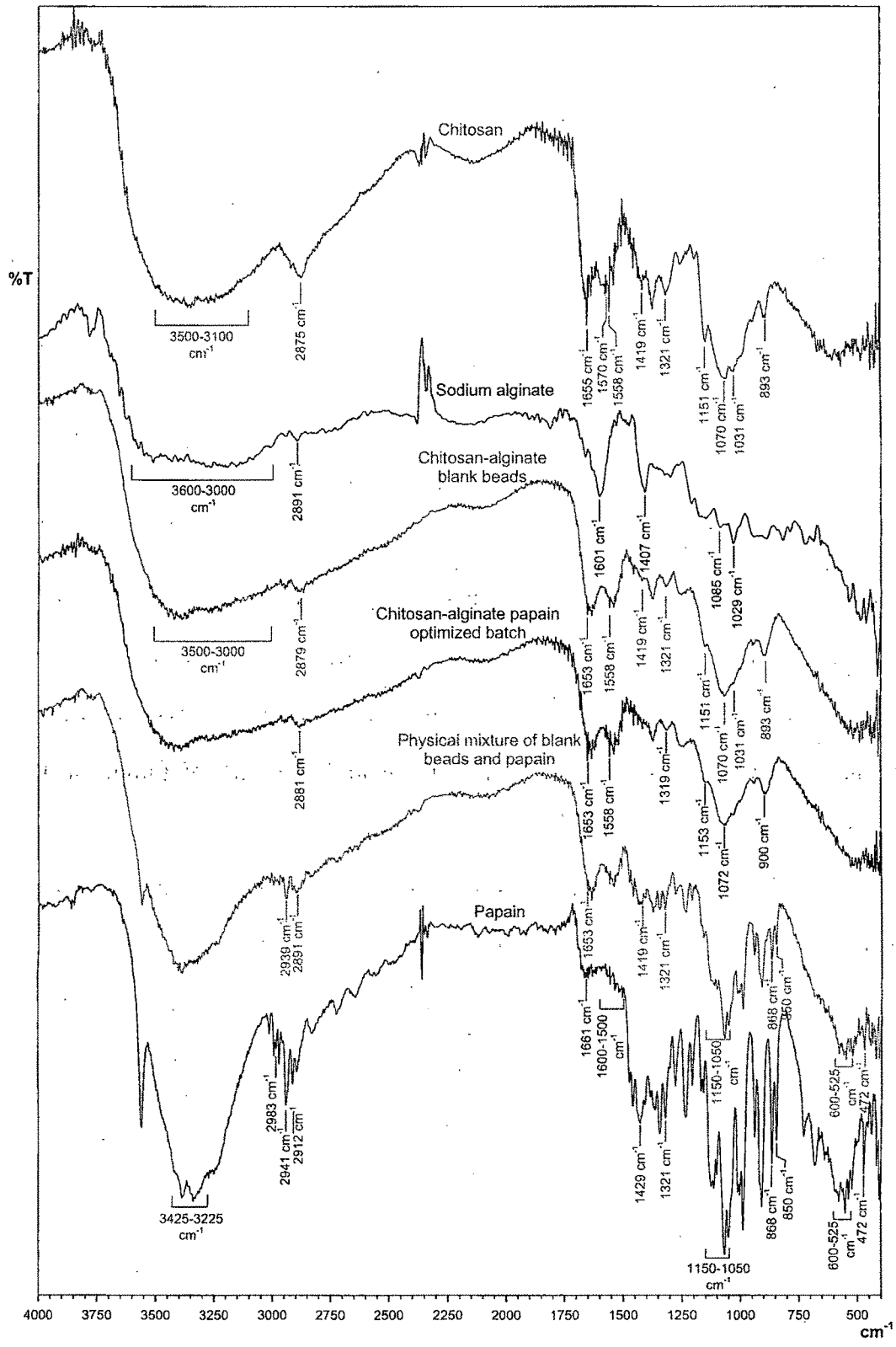

Figure 11.15: The FTIR spectra of chitosan, sodium alginate, chitosan-alginate blank beads, papain loaded optimized beads, physical mixture (in the ratio same as that of the optimized batch) of papain and blank beads, and papain.

stretching and strong peak at 1029 cm^{-1} due to C–O stretch of polyhydroxy $(OH)_n$ carbohydrate; strong peak at 1085 cm^{-1} due to C–O–C stretch of cyclic ether (carbohydrate). Sodium alginate as a carboxyl salt showed strong absorption bands at 1601 and 1407 cm^{-1} due to carboxyl anions (asymmetric and symmetric stretching vibrations). The frequency of carbonyl absorption is lowered compared to the value found for the parent carboxylic acid due to a resonance phenomenon. Papain also showed various distinct peaks: one predominant band at 3225-3425 cm^{-1} (s) due to N-H stretch of secondary N-substituted amides; 2983 cm^{-1} (weak; w) due to C-H stretch, medium bands at 1500-1600 cm^{-1} due to C=C, while 868 cm^{-1} (s) and 850 cm^{-1} (s) due to *p*-substituted aromatic out of plane C-H deformation of aromatic residue of tryptophan or tyrosine; 2912 cm^{-1} (s) and 2941 cm^{-1} (s) due to C-H stretch, while 1429 cm^{-1} (m) and 1321 cm^{-1} (m) due to C-H deformation of alkyl chain of amino acids; 1661 cm^{-1} (w) due to C=O stretch of carboxylate anion and amide group; strong peaks between 1050-1150 cm^{-1}, weak bands at 525-600 cm^{-1}, and 472 cm^{-1} (s) due to C-S stretch of sulfides and disulfides.

For chitosan-alginate blank beads, the band around 3500–3100 cm^{-1} becames broader, this indicates hydrogen bonding is enhanced (Yu et al., 1999). Moreover, N–H bending vibration of non-acylated 2-aminoglucose primary amines band at 1570 cm^{-1} and asymmetric and symmetric –C=O stretching at 1601 and 1407 cm^{-1} respectively disappeared indicating that $-NH_3^+$ of chitosan has reacted with $-COO^-$ of alginate. Distinct peaks correspond to the alginate are absent. This is probably due to very less alginate concentration compared to chitosan and also alginate is present at the interface. Some peaks disappeared or became weak due to interaction or superposition between groups of chitosan and alginate. One reason is that more chitosan was contained within beads and other one may be multi-interaction (hydrogen binding and electrostatics

interaction) among chitosan and alginate. With incorporation of papain, the spectrum of beads was similar to that of the chitosan-alginate blank beads, except the shift in the C–H stretch by 2 units from 2879 cm^{-1} to 2881 cm^{-1} and shift in the ether bonds and N–H stretching (amide III band) by 2 units from 1321 cm^{-1} to 1319 cm^{-1}. This may be because of interaction of papain with chitosan. However, the physical mixture of papain and blank beads showed the peaks due to both papain and blank beads. This confirms the papain entrapment into the chitosan-alginate beads at molecular level.

11.2.7.3. Differential Scanning Calorimetry (DSC)

The DSC thermograms of papain, chitosan, sodium alginate, chitosan-alginate blank beads, papain loaded optimized batch, and physical mixture of papain and blank beads are shown in Figure 11.16. Papain exhibited two endothermic peaks at 189.15° and 219.4°C followed by a broad degradation exotherm. The thermogram of the chitosan polymer exhibited an endothermic peak at about 94°C that has been attributed to the evaporation of absorbed water. The exothermic baseline deviation beginning around 250°C indicates the onset of chitosan degradation (Borges et al., 2005). A broad endothermic peak at 87°C in the thermogram of sodium alginate was similarly attributed to the presence of water molecules in the sample. It also showed two exothermic peaks at 251.2°C and 265.5°C. The chitosan-alginate reaction can be characterized by disappearance of degradation exothermic peaks of chitosan at 317.5°C and alginate at 251.2°C. The analysis of the DSC curves for chitosan-alginate beads showed two additional exothermic peaks at about 230°C and 266°C. The peak at 230°C is probably related to the breakdown of weak unspecific electrostatic interactions. The second peak is probably related to the cleavage of the electrostatic interactions between the chitosan and alginate polymers. DSC

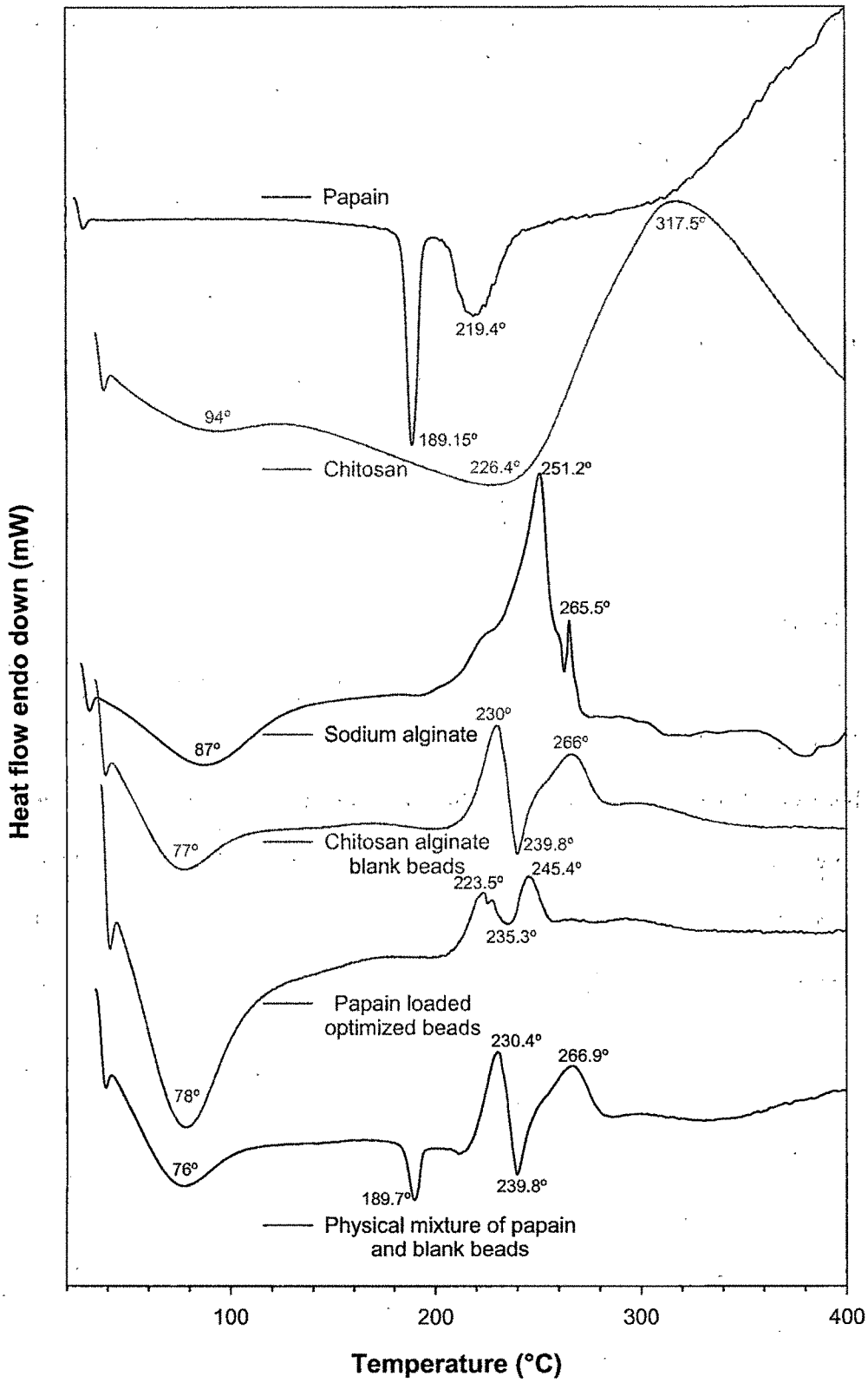

Figure 11.16: The DSC thermograms of papain, chitosan, sodium alginate, chitosan-alginate blank beads, papain loaded optimized beads, and physical mixture of papain and blank beads made at the same analytical conditions.

thermogram of enzyme loaded beads was similar to that of blank beads except all corresponding peaks were shifted to lower temperature, which might be due to the electrostatic interaction between papain and biopolymers. However, it did not showed any peak analogous to papain. Moreover, the physical mixture of papain and blank beads (in the ratio same as that of the optimized batch) showed the endothermic peak at 89.7°C corresponding to papain and other peaks (230.4°C, 239.8°C and 266.9°C) corresponding to blank beads. This confirms that most of the enzyme was uniformly dispersed at the molecular level in the beads.

11.2.7.4. Morphology of the Beads

The spherical shape of beads in the wet state was usually lost after drying, especially for beads prepared with low chitosan concentrations. With an increase of chitosan concentration, the shape of beads was retained considerably. However, the shape of the optimized beads (experiment J-12) changed to spherical discs with a collapsed center (Figure 11.17) during the drying process. The beads prepared with 1.13 % w/v chitosan showed much deeper collapsed centre or in some cases more than one collapsed centre. The tendency of developing the collapsed centre may be possibly because of mass- and heat-transfer phenomena and/or aggregation of chitosan helical fibers into bundles and the squeezing out of some water from the gel. Further, keen observation of Figure 11.18A-D showed the presence of fracture on the surface of the beads developed during the drying process through which the dissolution media enter first. Very fine mesh-like structure observed in Figure 11.18E-F was due to polyelectrolyte reaction and is quite comparable with many other PEC micrographs (Cruz et al., 2004; Lee et al., 2004).

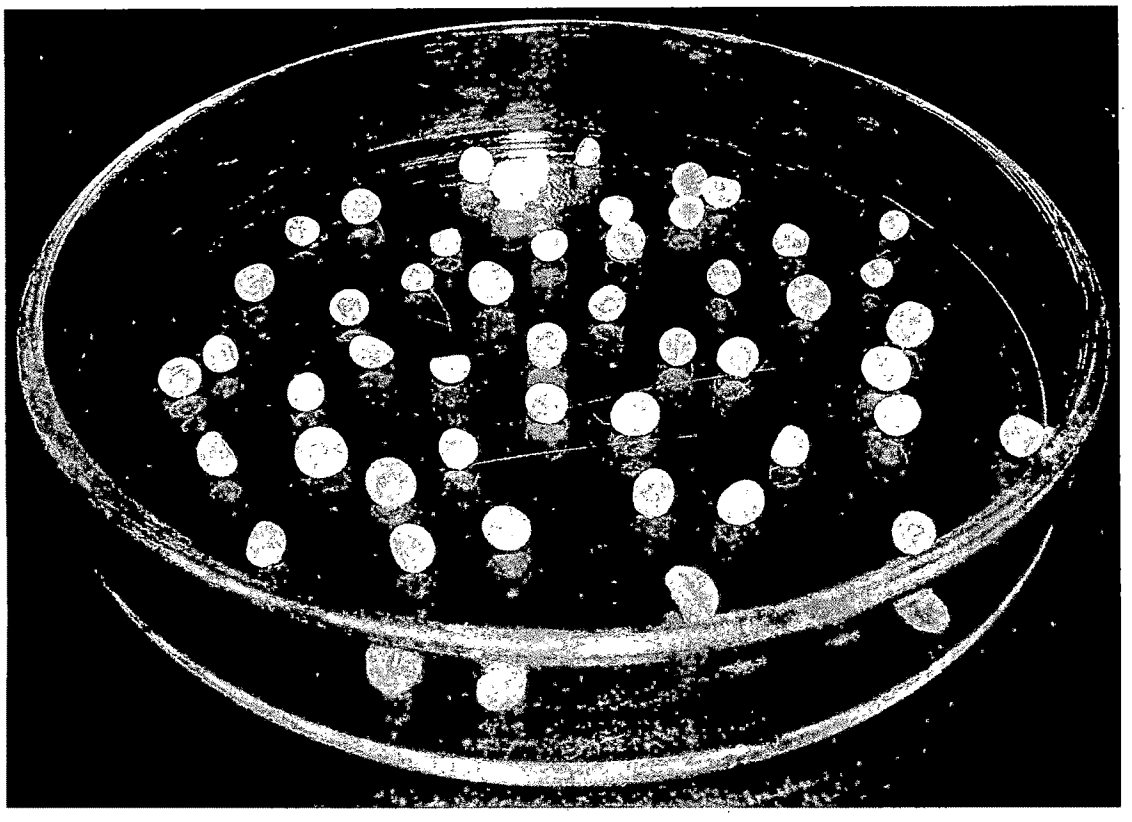

Figure 11.17: Photograph of wet chitosan-alginate beads showing spherical disk shape with collapsed centre during drying process.

11.2.8. STABILITY STUDY

For the developed formulation, the similarity factor (f_2) was calculated by a comparison of the dissolution profiles at each storage condition with the control at the initial condition. Results of f_2 factors ranged from 73 to 96 with 2 to 5% average difference. Evaluation of shelf-life was carried out as per the ICH Q1E Step4 (Evaluation of Stability Data) guidelines for the drug substances intended for room temperature storage. Long-term and accelerated stability data showed little change over time, so the shelf-life up to twice the length of available long-term data (i.e. 24 months) can be proposed. Extrapolation of the shelf-life beyond the length of available long-term data can be

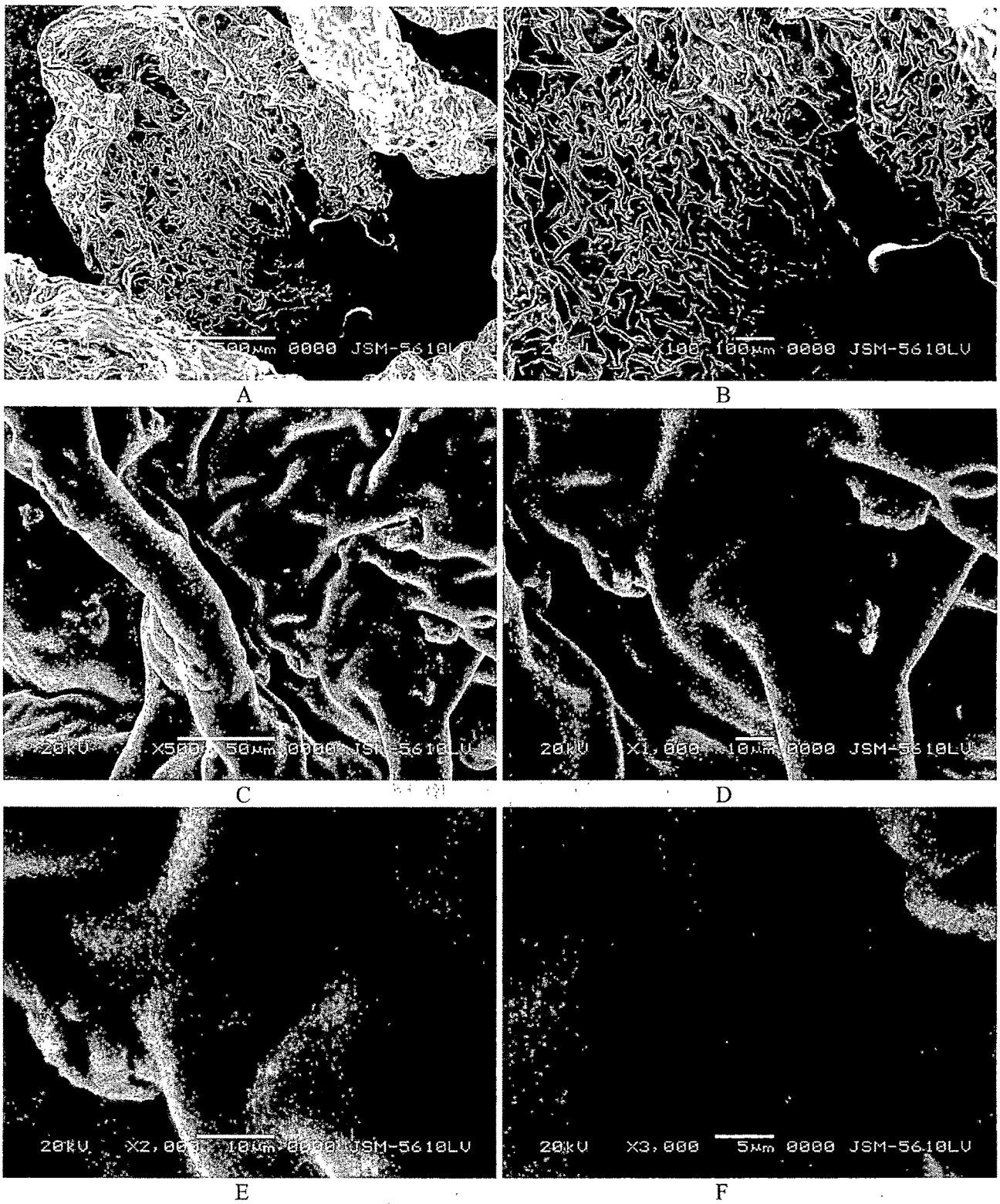

Figure 11.18: SEM micrographs and surface morphology of optimized chitosan-alginate beads (formulation J-12) at different magnification.

proposed. For this, an approach for analyzing the data on a quantitative attribute that is expected to change with time is to determine the time at which the 95% one-sided confidence limit for the mean curve intersects the acceptance criterion (not more than 5% change in assay from its initial value) can be accepted. The long-term stability data of the developed formulation, marketed formulation and the bulk papain were linearly extrapolated (zero-order kinetics) to calculate the shelf-life (Figure 11.19) and were found be 3.75 years, 1.01 year, and 0.48 year respectively. Hence, the stability of the entrapped papain was significantly improved compared to the conventional dosage forms.

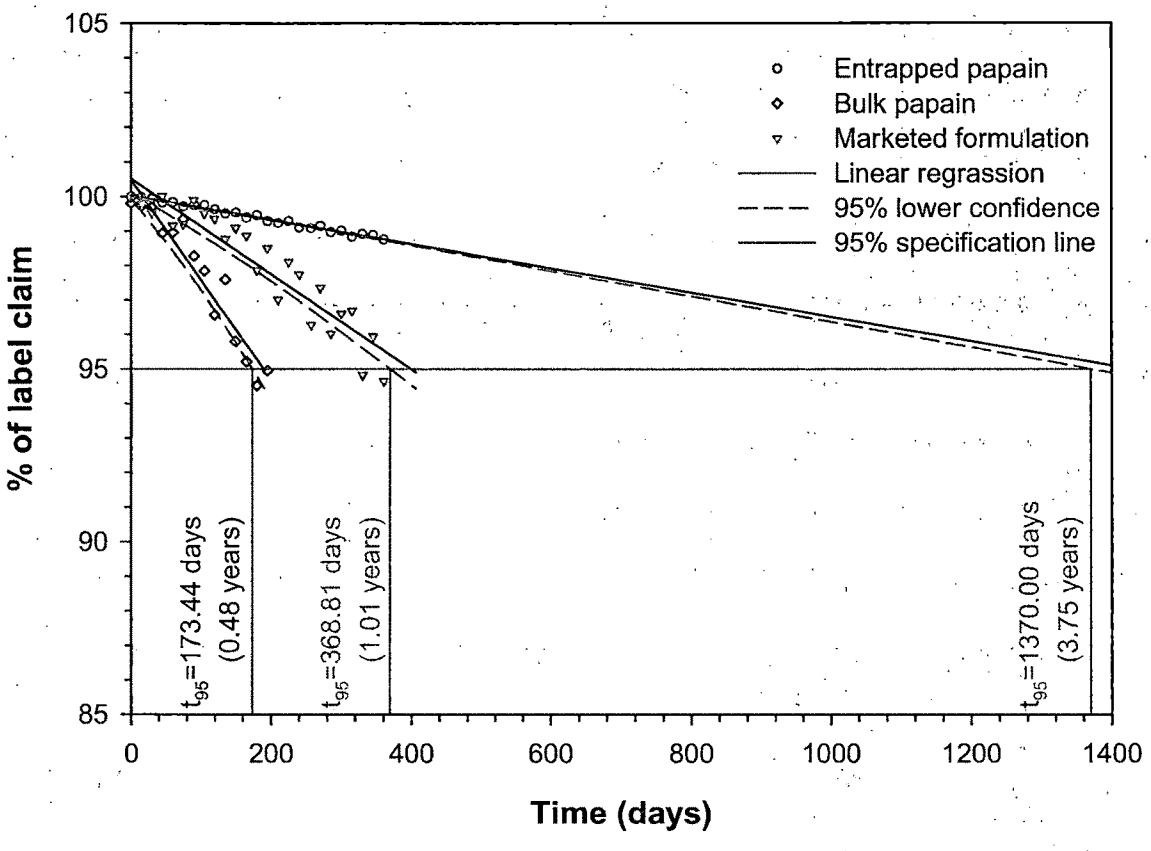

Figure 11.19: Extrapolation of long-term stability data for shelf-life calculation.

Dumitriu and Chornet (Dumitriu and Chornet, 1998) observed that, hydrogels, formed through interaction of a polycation with a protein (i.e. papain in this case), have the

advantage of creating an ionic micro-system which favors the stabilization of a protein polymer (i.e. enzyme) by interacting with the free acid and base functions (Severian and Esteban, 1998). Moreover, protein–polyelectrolyte complexes also have the ability to improve the operational stability of the enzyme activity during catalysis (Severian and Esteban, 1998). This probably may be the reason of improved stability of papain entrapped in the chitosan-alginate PEC beads.

CONCLUSIONS

Reversed chitosan-alginate PEC beads exhibited promising stability improvement of entrapped papain and can find a place in the design of multiparticulate drug delivery systems. The optimization of the process using the response surfaces resulted in > 90% entrapment and > 53 min of T_{90} (experiment J-12). T_{50} and T_{90} were increased with increase in alginate concentration and hardening time while decreased with increase in chitosan concentration. Percentage entrapment was found to be directly proportional to chitosan and alginate concentration. Mathematical analysis of the different drug release modalities and Kopcha model revealed that after 40 min the enzyme was released due to the burst effect. FTIR and DSC study confirmed the entrapment of papain in the chitosan-alginate beads. Texture analysis demonstrated the mesh-like fine structure due to the PEC reaction in absence of added salt. Accelerated and long term stability study illustrated considerably improved shelf-life of papain entrapped in chitosan-alginate beads than the conventional dosage form. Results of present study seem to be of value for the pharmaceutical industries associated with digestive enzymes formulations, also the reversed chitosan-alginate PEC can be employed for number of application due to short time of reaction, simplicity and reactivity in salt-free condition.

11.3. References

BERGER, J., REIST, M., MAYER, J. M., FELT, O. and GURNY, R., 2004. Structure and interactions in chitosan hydrogels formed by complexation or aggregation for biomedical applications. Eur. J. Pharm. Biopharm. 57, 35-52.

BORGES, OLGA, BORCHARD, GERRIT, VERHOEF, J. COOS, SOUSA, ADRIANO DE and JUNGINGER, HANS E., 2005. Preparation of coated nanoparticles for a new mucosal vaccine delivery system. Int. J. Pharm. 299, 155-166.

CÁRDENAS, ADRIANA, ARGÜELLES-MONAL, WALDO, GOYCOOLEA, FRANCISCO M., HIGUERA-CIAPARA, INOCENCIO and PENICHE, CARLOS, 2003. Diffusion through membranes of the polyelectrolyte complex of chitosan and alginate. Macromol. Biosci. 3, 535-539.

CHAVASIT, V., KIENZLE-STERZER, C. A. and TORRES, J. A., 1988. Formation and characterization of an insoluble polyelectrolyte complex: chitosan-polyacrylic acid. Polym. Bull. 19, 223-230.

CHU, C. H., SAKIYAMA, T. and YANO, T., 1995. pH-sensitive swelling of a polyelectrolyte complex gel prepared from xanthan and chitosan. Biosci. Biotech. Biochem. 59, 717-719.

CRUZ, MARIA C. PINTO, RAVAGNANI, SERGIO P., BROGNA, FABIO M. S., CAMPANA, SÉRGIO P., TRIVIÑO, GALO CARDENAS, LUZ LISBOA, ANTONIO C. and MEI, LUCIA H. INNOCENTINI, 2004. Evaluation of the diffusion coefficient for controlled release of oxytetracycline from alginate/chitosan/poly(ethylene glycol) microbeads in simulated gastrointestinal environments. Biotechnol. Appl. Biochem. 40, 243-253.

DUMITRIU, SEVERIAN and CHORNET, ESTEBAN, 1998. Inclusion and release of proteins from polysaccharide-based polyion complexes. Adv. Drug Deliv. Rev. 31, 223-246.

HOFFMAN, ALLAN S., 2002. Hydrogels for biomedical applications. Advanced Drug Delivery Reviews 43, 3-12.

IBORRA, JOSE L., MANJON, ARTURO and CANOVAS, MANUEL, 1997. Immobilization in carrageenans. in: BICKERSTAFF, G. F. (Ed.) Immobilization of Enzymes and Cells, Methods in Biotechnology, Vol. 1, Humana Press, Totowa, New Jersey, pp. 53-60.

KHALID, M. N., AGNELY, F., YAGOUI, N., GROSSIORD, J. L. and COUARRAZE, G., 2002. Water sate characterization, swelling behavior, thermal and mechanical properties of chitosan based networks. Eur. J. Pharm. Sci. 15, 425-432.

KHOR, E., 2001. The structural properties of chitin as it is known today. in: Chitin: Fulfilling a Biomaterials Promise, Elsevier, New York, pp. 73-82.

LEE, J. S., CHA, D. S. and PARK, H. J., 2004. Survival of freeze-dried *Lacrobacillus bulgaricus* KFRI 673 in chitosan-coated calcium alginate microparticles. J. Acric. Food Chem. 52, 7300-7305.

LEE, J. W., KIM, S. Y., KIM, S. S., LEE, Y. M., LEE, K. M. and KIM, S. J., 1999. Synthesis and characteristics of interpenetrating polymer network hydrogel composed of chitosan and poly (acrylic acid). J. Apppl. Polym. Sci. 73, 113-120.

LE-TIEN, CANH, MILLETTE, MATHIEU, MATEESCU, MIRCEA-ALEXANDRU and LACROIX, MONIQUE, 2004. Modified alginate and chitosan for lactic acid bacteria immobilization. Biotechnol. Appl. Biochem. 39, 347-354.

PATHER, S. INDIRAN, RUSSELL, IRINA, SYCE, JAMES A. and NEAU, STEVEN H., 1998. Sustained release theophylline tablets by direct compression Part 1: formulation and in vitro testing. Int. J. Pharm. 164, 1-10.

SAKIYAMA, T., TAKATA, H., KIKUCHI, M. and NAKANISHI, K., 1999. Polyelectrolyte complex gel with high pH-sensitivity prepared from dextran sulfate and chitosan. J. Apppl. Polym. Sci. 73, 2227-2233.

SEVERIAN, DUMITRIU and ESTEBAN, CHORNET, 1998. Inclusion and release of proteins from polysaccharide-based polyion complexs. Advanced Drug Delivery Reviews 31, 223-246.

YU, J. H., DU, Y. M. and ZHENG, H., 1999. Blend films of chitosan-gelation. J. Wuhan Univ. (Nal. Sci. Ed.) 45, 440-444.